



Technische Universität München

Wissenschaftszentrum Weihenstephan für Ernährung, Landnutzung und Umwelt

Lehrstuhl für Waldwachstumskunde

**Detection and definition of forest structure types by means of radar remote sensing (TanDEM-X)**

**Sahra Abdullahi**

Vollständiger Abdruck der von der Fakultät Wissenschaftszentrum Weihenstephan für Ernährung, Landnutzung und Umwelt der Technischen Universität München zur Erlangung des akademischen Grades eines

Doktors der Naturwissenschaften (Dr. rer. nat.)

genehmigten Dissertation.

Vorsitzender: Prof. Dr. Stephan Pauleit

Prüfende der Dissertation: 1. Prof. Dr. Dr. h.c. Hans Pretzsch  
2. Prof. Dr. Mathias Schardt  
3. Prof. Dr. Thomas Knoke

Die Dissertation wurde am 15.01.2018 bei der Technischen Universität München eingereicht und durch die Fakultät Wissenschaftszentrum Weihenstephan für Ernährung, Landnutzung und Umwelt am 24.04.2018 angenommen.



## **Acknowledgements**

At this point, I would like to express my gratitude to everyone who helped and guided me during my dissertation.

First and foremost, I would like to kindly thank my doctoral advisor Prof. Hans Pretzsch for his continuous support and the opportunity to work and graduate at the Chair of Forest Growth and Yield Science of the Technical University of Munich.

Very special thanks go to Prof. Mathias Schardt for his valuable advice and scientific supervision as well as his contribution to my work.

In addition, I would like to thank my former colleagues at the Chair of Forest Growth and Yield Science and the Institute of Forest Management who gave me the opportunity to discuss my work and supported the development of my dissertation. Special mention should be made of Dr. Peter Biber, Michael Heym, Ralf Moshhammer, Dr. Thomas Schneider and Ulrich Kern.

Since this dissertation was part of a cooperate project of the Technical University of Munich and the Microwaves and Radar Institute of the German Aerospace Center (DLR), I also would like to thank Dr. Kostas Papathanassiou and his group for the opportunity to start my dissertation at the Microwaves and Radar Institute in order to gain experience in radar remote sensing and to present my work regularly at DLR. At this point I would like to give special thanks to Dr. Florian Kugler for providing the TanDEM-X data and for his critical and valuable support.

Furthermore, I thank the staff of the Chair of Forest Growth and Yield Science and Gerhard Fischer from the Municipal Forest Traunstein for conducting and providing the field measurements.

I also would like to thank the Federal Ministry for Economic Affairs and Energy, which funded this work under Project 50EE1261.

Moreover, my sincere thanks go to the Technical University of Munich which funded the final year of my Ph.D. by the Laura Bassi-Award.

I am particular grateful to my family for encouragement and scientific support.

Finally, my deep gratitude goes to my husband Tobias Leichtle for his endless patience and his continuous support.

# Contents

Acknowledgements .....	I
Contents .....	II
List of Figures .....	IV
List of Tables .....	VI
List of Abbreviations .....	VII
Abstract .....	VIII
Zusammenfassung .....	IX
1 Introduction .....	1
1.1 Motivation .....	1
1.2 Objectives and Outline .....	5
2 Fundamentals of Radar Remote Sensing and Forest Growth .....	7
2.1 Synthetic Aperture RaDAR (SAR).....	7
2.1.1 Imaging Principles .....	8
2.1.2 Spatial Resolution .....	9
2.1.3 Characteristics of SAR Images .....	12
2.1.4 SAR Interferometry (InSAR).....	15
2.2 Principles of Forest Growth.....	18
2.2.1 Forest Growth Processes .....	18
2.2.2 Forest Stand Structure.....	24
3 Materials.....	26
3.1 Study Area .....	26
3.2 Remote Sensing Data.....	27
3.2.1 Scattering Center Height.....	27
3.2.2 Model-based Top Height .....	28
3.2.3 LiDAR-based Tree Height .....	31
3.3 Forest Inventory Data .....	32
3.3.1 Tree Height .....	33
3.3.2 Stem Volume .....	34
3.3.3 Forest Structure.....	36
4 Methodology and Results.....	37
4.1 Stem Volume Estimation (Publication I).....	37

4.2	Forest Structure Classification (Publication II) .....	38
4.3	Seasonal Effects on Forest Structure Classification (Publication III).....	39
5	Discussion .....	40
6	Conclusion.....	45
7	References .....	46
Appendix.....		53
A	Publication I.....	53
B	Publication II.....	69
C	Publication III .....	83
D	Eidesstattliche Erklärung .....	107
E	Lebenslauf.....	108

## List of Figures

Fig. 1.1: Ecosystem services and their influence on human well-being which in turn are influenced by anthropogenic activities. Based on Assessment Millenium Ecosystem (2005).....	1
Fig. 2.1: The electromagnetic spectrum and the corresponding atmospheric transmittance as well as the ranges of different sensor types. Based on Albertz (2001: p. 11).....	7
Fig. 2.2: Penetration ability into forest according to RaDAR frequency bands. Based on Albertz (2001: p. 64). ....	8
Fig. 2.3: Imaging geometry of a RaDAR system a) oblique view and b) cross-sectional view. Based on Bamler & Hartl (1998).....	8
Fig. 2.4: RaDAR imaging modes. a) StripMap mode, b) ScanSAR mode and c) Spotlight mode. Based on Richards (2009: p. 70).....	9
Fig. 2.5: Spatial Resolution of a RaDAR system. a) slant range direction and b) ground range direction. Based on Richards (2009: p. 85). ....	10
Fig. 2.6: Increase of the spatial resolution of a RaDAR system in azimuth direction by synthesizing a larger antenna. Based on Bamler & Hartl (1998). ....	11
Fig. 2.7: Doppler Effect during a SAR acquisition. Based on Schmitt (2011: p. 24). ....	12
Fig. 2.8: Scattering of microwaves with respect to surface roughness: a) smooth surface, b) slightly rough and c) very rough surface relative to wavelength. From Richards (2009: p. 139). ....	13
Fig. 2.9: Scattering from a volume consisting of many individual scatterers. From Richards (2009: p. 155).....	13
Fig. 2.10: Speckle effect in RaDAR images. From Richards (2009: p. 121).....	14
Fig. 2.11: Geometric effects in SAR imagery: layover, foreshortening and shadowing. Based on Albertz (2001: p. 80). ....	14
Fig. 2.12: Acquisition geometry of an across-track SAR interferometer. Based on Bamler & Hartl (1998). ....	15
Fig. 2.13: Age-dependent non-proportional shape development of a European beech under solitary conditions. Based on Pretzsch (2009: p. 388). ....	19
Fig. 2.14: Positive and negative allometry and isometry between x and y in a) double-logarithmic and b) Cartesian coordinate system. Based on Pretzsch (2009: p. 389). ....	20
Fig. 2.15: Schematic illustration of self-thinning dependent on growth conditions, where A corresponds to a forest stand under optimal growing conditions and B represents a forest stands under suboptimal growing conditions. From Pretzsch & Biber (2005). ....	21

Fig. 2.16: From a) Eichorn's rule (1902) Silver fir stands with moderate thinning to b) common yield levels from Norway spruce stands with medium strong thinning according to Gehrhardt (1923) to c) Special yield levels from Scots pine stands with moderate thinning from Wiedemann (1943) to d) Sub-divided special yield levels in Norway spruce stands with graduated thinning according to Assmann and Franz (1963). From Pretzsch (2009: p. 435).....	23
Fig. 2.17: Feedback system between tree growth and forest stand structure. Based on Pretzsch (2009, p. 226). ..	24
Fig. 2.18: Gap theory (or mosaic-cycle theory) assumes that large-scale ecosystems are composed of individual patches passing through a cyclic succession process of establishment, growth and mortality of individual trees. From Pretzsch (2009: p. 457). .....	25
Fig. 3.1: The study area, a mixed, temperate and highly structured forest, is located east of the city of Traunstein in the South of Germany and covers an area of about 243 ha. Terrestrial measurements of the forest's condition are collected based on 228 permanent circular sampling plots and have been repeated regularly since 1988 on a common cycle of ten years. ....	26
Fig. 3.2: Scattering center height based on HH-polarized TanDEM-X InSAR acquisitions from August 12, 2013.....	28
Fig. 3.3: Schematic illustration of the RVoG model with a) the two-layered representation of the forest, b) its simplified representation and the c) backscatter function along the height of the volume. ....	30
Fig. 3.4: Model-based top height based on HH-polarized TanDEM-X InSAR acquisitions from August 12, 2013, areas of NoData are marked black.....	31
Fig. 3.5: LiDAR-based nDSM from November 18, 2012. ....	32
Fig. 3.6: a) Inventory sampling grid and b) thresholds in diameter measuring. Based on Abdullahi et al. (2016).....	33
Fig. 3.7: Development of stand-height-curves (where h is height and d is diameter) in a Norway spruce-Silver fir-European beech selection forest based on inventory data from 1980, 1987, 1993, 1999 at a forest test site in Bavaria, Germany. From Pretzsch (2009: p. 189). ....	34
Fig. 3.8: Schematic representation of a reference cylinder for stem volume calculation. Based on Pretzsch et al. (2002). ....	35
Fig. 3.9: a) Plan view of an inventory plot with b) the corresponding 3-d representation where light green represents broadleaf tree species and dark green represents coniferous tree species. ....	36

## List of Tables

Tab. 2.1: Commonly used frequency bands for RaDAR systems with the corresponding frequency as well as wavelength range according to Moreira et al. (2013).....	7
Tab. 3.1: Acquisition parameters of the SAR data .....	27
Tab. 3.2: Statistics of forest parameters per plot acquired during forest inventory 2013. Volume is specified as timber harvested (> 7 cm at the smaller end) without bark. From Abdullahi et al. (2016).....	35
Tab. 5.1: Generalized characteristics of the global forest biomes. From Abdullahi et al. (2016) .....	43



## List of Abbreviations

dbh	diameter at breast height
DEM	Digital Elevation Model
DSM	Digital Surface Model
DTM	Digital Terrain Model
FAO	Food and Agriculture Organization of the United Nations
FRA	Forest Resources Assessment
GFOI	Global Forest Observations Initiative
HoA	Height of Ambiguity
InSAR	Interferometric SAR
LiDAR	Light Detection and Ranging
nDSM	normalized DSM
PMVD	Proportional Marginal Variance Decomposition
PRF	Pulse Repetition Frequency
RaDAR	Radio Detection and Ranging
RVoG	Random Volume over Ground
SAR	Synthetic Aperture RaDAR
SDI	Stand Density Index
SLC	Single Look Complex
SNR	Signal-to-Noise-Ratio
SOM	Self-Organizing Map
UN-REDD	United Nations Collaborative Programme on Reducing Emissions from Deforestation and Forest Degradation in Developing Countries

## Abstract

Forests cover about one third of the Earth's land surface and provide essential services which positively affect human well-being in many regards. However, these services are heavily influenced by human activities like changes in land use, harvesting or anthropogenic-induced climatic changes. Especially with regard to ongoing climatic changes, rising population pressure and increasing consumption of resources, sustainable forest management becomes more and more important in order to preserve these services.

Targeted silvicultural activities are required to increase the forests' stability and resilience as adaptation and mitigation strategy. Reliable and up-to-date information on the condition of the world's forests and ongoing trends is a prerequisite for development and adaptation of policy guidelines at global, national and local level. In this regard, remote sensing techniques offer a cost-efficient opportunity for area-wide data collection with high spatial and temporal resolution. Especially Interferometric Synthetic Aperture Radar (InSAR) systems, which facilitate worldwide acquisition of 3-d information independent from weather conditions and illumination, are well suited for forest resources assessment.

This thesis explores the potential of X-band InSAR data acquired by the TanDEM-X mission for detection and definition of forest structure in view of sustainable forest management. First, the applicability of height information derived from interferometric TanDEM-X acquisitions for stem volume estimation was demonstrated. In detail, a linear regression model for stem volume estimation was developed, which also incorporates novel parameters of forest structure. Especially the inclusion of parameters describing forest structure improved stem volume predictions substantially and showed promising results at plot as well as stand level compared to previous studies. Second, classification of forest structure at spatial units of 24 x 24 m<sup>2</sup> according to canopy closure and layering was realized using an unsupervised clustering approach. Compared to in-situ measurements, aerial photos and LiDAR data, the classification approach returned nine meaningful structure classes according to canopy closure and stand layering. The unsupervised classification approach enables easy transferability and offers the opportunity to derive meaningful forest structure classes which may be further adapted to the users' definitions and requirements. Third, the impact of phenology-induced changes on forest structure assessment was investigated for coniferous, broadleaf and mixed temperate forest stands. It was demonstrated that the phenological development stage of trees has a significant impact on X-band InSAR data in broadleaf-dominated forest stands and thus highly influences height estimation, stem volume estimation and forest structure classification. Phenology-based changes of broadleaf trees (i.e., presence and absence of leaves) lead to varied penetration of the X-band SAR signal into the forest canopy and thus causes an increased underestimation of forest height in the leaf-off season compared to the leaf-on season. In contrast, X-band InSAR data over coniferous forest stands is largely unaffected by phenology. Summarizing, this thesis provides an approach for stem volume estimation considering forest stand structure, an easy-transferable and user-adaptive approach for forest structure classification according to vertical as well as horizontal forest structure and essential information for data selection dependent on application and tree species composition.

## Zusammenfassung

Etwa ein Drittel der globalen Landoberfläche ist von Wald bedeckt. Die von Wäldern bereitgestellten Ökosystemdienstleistungen tragen maßgeblich zum menschlichen Wohlbefinden bei. Jedoch werden diese Dienstleistungen durch fortlaufende demographische, ökonomische, soziale, technologische und kulturelle Entwicklungen gefährdet. Vor allem anthropogene Eingriffe wie Landnutzungsänderungen und Steigerung der Holzernte beeinflussen die Wälder zunehmend negativ. Dabei machen der fortschreitende Klimawandel, der steigende Bevölkerungsdruck und der zunehmende Ressourcenbedarf eine nachhaltige Waldbewirtschaftung zum Erhalt der Ökosystemdienstleistungen mehr denn je zwingend notwendig.

Zur Erhöhung der Stabilität und Resilienz von Wäldern müssen gezielte Waldbewirtschaftungsmaßnahmen eingesetzt werden, um eine Anpassung der Wälder an veränderte Rahmenbedingungen zu gewährleisten. Zur Umsetzung dieser Maßnahmen sind aktuelle und verlässliche Informationen über den Zustand und die zeitliche Entwicklung wichtiger Waldparameter unerlässlich. Diese Informationen werden zudem als Grundlage für politische Entscheidungen und Richtlinien auf globaler, nationaler und lokaler Ebene dringend benötigt. Die Fernerkundung stellt dabei eine kosteneffiziente Möglichkeit zur flächendeckenden Erhebung von Informationen mit hoher räumlicher und zeitlicher Auflösung dar. Insbesondere Interferometric Synthetic Aperture Radar (InSAR) Systeme eignen sich für globales Monitoring der Wälder, da sie unabhängig von Wetterbedingungen und Beleuchtungsverhältnissen 3-D Information aufnehmen können.

Die vorliegende Arbeit untersucht das Potential von X-Band InSAR Daten der TanDEM-X Mission für die Erfassung und Definition von Waldstruktur im Hinblick auf eine nachhaltige Waldbewirtschaftung. Zunächst wurde die Anwendbarkeit von Höheninformationen aus interferometrischen TanDEM-X Aufnahmen zur Schätzung des Holzvorrats aufgezeigt. Dabei wurden zusätzliche, neuartige Texturparameter in ein lineares Regressionsmodell integriert, um neben der interferometrischen Höheninformation auch die Bestandesstruktur in die Schätzung zu integrieren. Insbesondere durch die Integration dieser Strukturparameter konnten im Vergleich zu vorherigen Studien vielversprechende Ergebnisse erzielt werden. Die Erfassung der Waldstruktur hinsichtlich ihrer vertikalen und horizontalen Höhenverteilung erfolgte auf räumlichen Einheiten von 24 x 24 m<sup>2</sup>. Dabei wurden Bestände mittels eines unüberwachten Verfahrens in neun Klassen im Sinne des Kronenschlusses und der Bestandesschichtung klassifiziert. Durch die Implementierung im Rahmen eines maschinellen Lernverfahrens ist dieser Klassifikationsansatz leicht übertragbar und kann zudem auf die individuellen Anforderungen der Nutzer angepasst werden. Darüber hinaus wurde der Einfluss phänologischer Änderungen in Nadelholz-dominierten, Laubholz-dominierten und gemischten Waldbeständen untersucht. Dabei zeigte sich, dass das phänologische Entwicklungsstadium des Waldes und damit der Zeitpunkt der interferometrischen Radaraufnahmen einen hohen Einfluss auf die Ableitung von Höheninformation, Vorratsschätzung und Strukturklassifikation in Laubholz-dominierten Waldbeständen hat, wobei Nadelholz-dominierte Waldbestände von diesem Effekt nur wenig beeinflusst werden. Zusammenfassend liefert die vorliegende Arbeit zum einen eine Methode zur Holzvorratsschätzung, die eine Berücksichtigung der Bestandesstruktur ermöglicht sowie ein leicht übertragbares und anwenderspezifisches Klassifikationsverfahren hinsichtlich vertikaler und horizontaler Waldstruktur und zum anderen eine wichtige Grundlage bei der Datenauswahl in Abhängigkeit der Anwendung und der Baumartenzusammensetzung.

# 1 Introduction

## 1.1 Motivation

Forests, covering about one third of the world’s land surface, supply essential services which directly affect human well-being (see Fig. 1.1). These ecosystem services do not only provide a regulating and supporting effect on physical processes like carbon capture, oxygen production and soil formation, but also ensure the provision of natural resources like food and drinkable water. In addition, the forest ecosystem possesses cultural functions as recreation, education and spirituality. Human well-being is positively affected by the forest ecosystem services in many regards. According to the Food and Agriculture Organization of the United Nations (FAO) (2013), forested areas on Earth are a significant source of drinking water for at least one third of the world’s largest cities. Besides the availability of clean water, forests regulate surface as well as groundwater flow and have a preventive function regarding desertification and salinization (Miura et al. 2015). Thus forests contribute to local resilience against natural hazards (e.g., floods, landslides and droughts) and in turn offer the opportunity for mitigation strategies (FAO 2006). Moreover, forests are conducive to protection against erosion caused by rain, wind and coastal waves (Hamilton 2008). Furthermore, they play a crucial role in the global carbon cycle because of their important function as terrestrial sinks of carbon dioxide (Miura et al. 2015). Due to provision of food and habitat, forests are signifying in combating rural poverty, ensuring food security and livelihoods (FAO 2016).

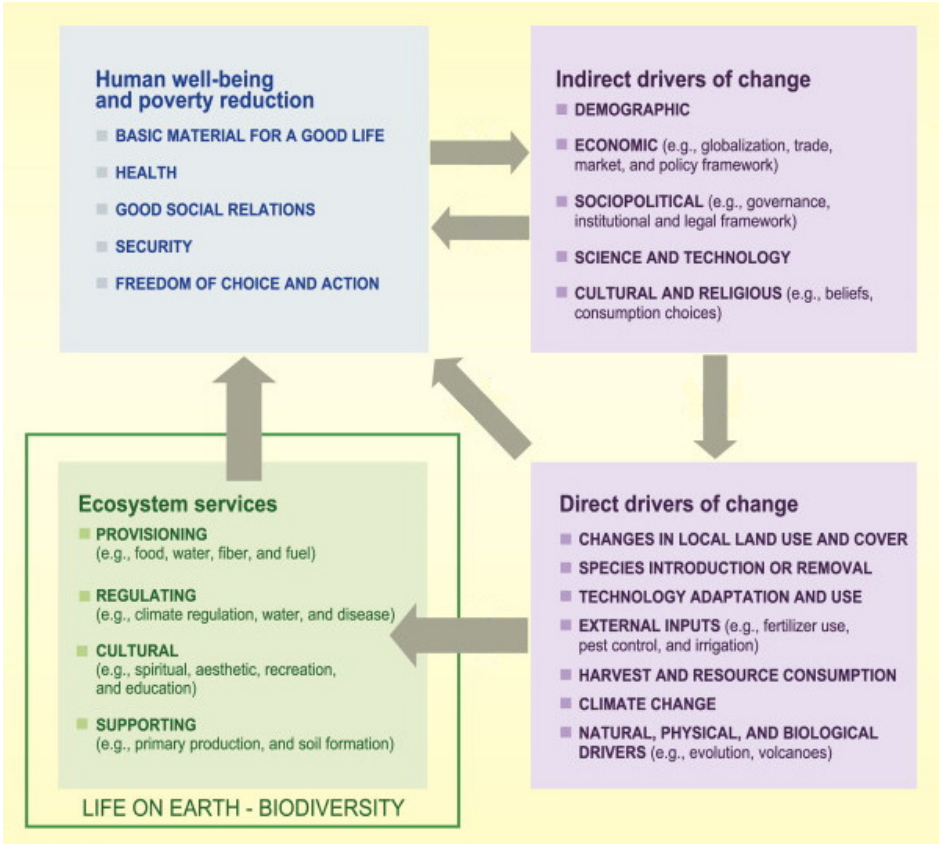


**Fig. 1.1:** Ecosystem services and their influence on human well-being which in turn are influenced by anthropogenic activities. Based on Assessment Millenium Ecosystem (2005).

However, these services are heavily affected by human activities like changes in land use, harvesting or anthropogenic-induced climatic changes, which are driven by demographic, economic, social, technological and cultural developments. Increasing population pressure and urbanization lead to loss in forest cover and fragmentation of forests for the benefit of other land use. The land-cover change is caused by resource extraction, agriculture, urban as well as suburban expansion and recreation (Dale et al. 2001). As a consequence, especially large scale ecosystem processes are disturbed. Further anthropogenic forest damages like acidification are caused by environmental pollution (Chen et al. 2000). Moreover, human-induced alterations of forests and their services are caused by introduction of non-native species, often in terms of large-scale monoculture. In addition, the ongoing climate change causes alterations in forest structure which in turn lead up to changes in phenology, biodiversity, stability, productivity as well as forest growth (IPCC 2014). Besides more frequently occurring damages caused by extreme weather events (e.g., droughts, storms, floods) and calamities, the changing climate induces challenging habitat conditions for the existent tree species. Consequently, the forests' complexity according to the spatial arrangement of tree size dimensions and species composition, which influences the fundamental boundary conditions for ecosystem processes, is changing (Harding et al. 1995). Natural disturbances interact with the human-induced changes and provoke dramatic alterations regarding global systems like the global carbon cycle.

To face these concerning trends and to preserve forest ecosystems and their essential services, sustainable forest management is inevitable. Especially in times of ongoing climate change, rising population pressure and increasing consumption of resources, sustainable forest management becomes more and more vital in order to preserve the forests' ecosystem services and to develop sufficient adaptation and mitigation strategies. In this context, targeted silvicultural activities are highly relevant, since the enhancement of structural diversity often positively affects biodiversity, productivity as well as growth of the forest (Pommerening 2006; Önal 1997). Therefore, it is important to encourage silvicultural activities that increase the structural diversity and thus the stability and resilience of the forests. It is indispensable to have a clear understanding of the condition of the world's forests and ongoing trends in order to manage forests' sustainably. On that account reliable and up-to-date information on the forests' state is a prerequisite to provide the basis for policy guidelines at global, national and local level (Gao et al. 2014; Kuuluvainen et al. 1996).

Especially information on stem volume is of great significance for decision-making in the context of sustainable forest management. Reliable estimations of stem volume per unit area have been the basis for sustainable forest management planning since the beginning of the 18th century (von Carlowitz 1713) as well as for monitoring of global changes in recent times (IPCC 2014). In association with climate change, felling budgets can be adapted to damages caused by increasing extreme weather events and calamities. Moreover, stem volume can be directly related to biomass, which is a crucial parameter to understand and quantify the global carbon cycle. Carbon is stored by building up of biomass and emitted to the atmosphere by destroying biomass due to fire, logging with subsequent energetic use, storms, decomposition, etc. (Houghton et al. 2009). These processes can be controlled by means of forest management strategies and thus, CO<sub>2</sub> emissions can be reduced (Schlamadinger & Marland 1996). Not only information on stem volume or biomass plays a key role for sustainable forest management, but also forest structure. High structural complexity characterized by spatial heterogeneity due to different tree size dimensions and diverse species compositions is often linked to high productivity and resilience of the forest (Pretzsch 2005; Carey & Wilson 2001). Moreover, high structural complexity is related to high

biodiversity (Bergen et al. 2009; McElhinny et al. 2005; Staudhammer & LeMay 2001). Accordingly, measures of horizontal and vertical stand structure (e.g., stand density, canopy closure, stand layering) serve as an indicator for the stability of the forest ecosystem as well as for prediction of growth and development (Pretzsch 2009: pp. 223-289). Monitoring of forest stand structure complexity promotes understanding the changes in habitat conditions due to climate change and thus enables the development of sufficient adaptation strategies. Furthermore, managing the forests' structural complexity provides the opportunity to positively influence their biodiversity, productivity, growth and resilience as protection, conservation and mitigation strategy.

In general, information on forest parameters is acquired in the scope of forest resources assessments at global level combining forest inventories at national, federal, and enterprise level. The first forest resources assessment at global level was published in 1948 by the FAO and has been regularly repeated at five to ten year intervals (MacDicken 2015). The Global Forest Resources Assessment (FRA) is based on country reports provided by national correspondents and remote sensing conducted by FAO in cooperation with national focal points and regional partners (FAO 2016). Thus, global information on the forests' condition (e.g., forest extent) and trends (e.g., deforestation) is acquired. The scope of the FRA has changed considerably since 1948, when only 101 countries and territories reported compared to 234 countries in 2015 (MacDicken 2015). This trend has benefited from the United Nations Collaborative Programme on Reducing Emissions from Deforestation and Forest Degradation in Developing Countries (UN-REDD) in recent years, which provides financing to support the development of national forest monitoring systems (Holloway & Giandomenico 2009). According to FAO (2016), 112 countries, representing about 83 % of the global forest area, reported that they had carried out or had an ongoing national forest assessment and 81 of these countries, representing 77 percent of global forest area, reported that they had either finalized or initiated their national forest resources assessment after 2010. At national, federal and enterprise level, information about the forests' condition is traditionally assessed by field surveys (in some cases supported by optical remote sensing). In Germany, forest inventories are usually conducted based on a sampling design which ensures representativity (Pretzsch 2009: pp. 112-120). Various essential and easy measurable forest parameters (e.g., tree height, diameter at breast height (dbh) and tree species) are repeatedly recorded at a usual interval of about ten years. However, the traditional terrestrial measurements are very cost- and labor-intensive. Another disadvantage of forest inventories is the sample-based survey design which does not provide wall-to-wall information and thus only enables statistics related to large areas or whole countries. An enhanced use of remote sensing offers a cost-efficient opportunity to overcome these problems by providing wall-to-wall data collection with different spatial and temporal resolutions.

Remote sensing has already been deployed for forest management since the early 1920s (Knoke et al. 2012) and has become a significant source of information regarding the assessment of forest resources. Remote sensing techniques are used for various fields of forestry applications. The derivation of inventory parameters like stand delineation, within-stand parameters (e.g., stem volume, dbh and height) and tree species composition by means of remote sensing facilitates field surveys and offers the opportunity to increase the temporal and spatial resolution of forest inventories (McRoberts & Tomppo 2007). Another important application of remote sensing in forestry is the detection and monitoring of forest health and natural disturbances like fires, insects and diseases (Wulder et al. 2005). The remotely sensed up-to-date information on the forests' condition also enables targeted silvicultural actions for mitigation purposes (e.g., containment of bark beetles). Finally, remote sensing becomes more and more important for the assessment of forest structure in order to support sustainable forest

management (Global Forest Observations Initiative (GFOI) 2016; Franklin 2001).

Passive optical remote sensing (i.e., aerial photography, satellite-based multi- and hyperspectral imagery) is by far most commonly used in forestry, whereas Light Detection and Ranging (LiDAR) and Radar Detection and Ranging (RaDAR) gained more and more importance (Sinha et al. 2015; Franklin 2001). Since RaDAR systems operate at longer wavelengths (cm to m) compared to LiDAR and passive optical systems (nm to  $\mu\text{m}$ ), these sensors benefit from all-weather-capability, independency of illumination and penetration ability. The ability to observe the Earth's surface independently from cloud cover is of high value, especially in the context of tropical forest areas. Furthermore, the data acquisition independent from illumination are advantageous regarding forested areas in higher latitudes, where the sunshine duration is shortened for large parts of the year. In the field of RaDAR systems, Synthetic Aperture RaDAR (SAR) provides global observations with sufficient spatial and temporal resolution and thus, such systems are beneficial for global forest assessment. Besides methods based on backscatter intensity (Santoro et al. 2011; Rauste 2005; Le Toan et al. 1992), interferometric SAR (InSAR) enables the detection of 3-d information corresponding to different scattering elements of the forest dependent on wavelength (i.e., leaves, branches and trunks), which allows the detection and investigation of vertical forest structure as well as its horizontal pattern (Varghese et al. 2016; Yang et al. 2014).

Numerous studies demonstrated the applicability of InSAR data at different wavelengths from different sensors on spaceborne as well as airborne platforms for biomass or stem volume estimation and forest structure assessment (De Grandi et al. 2016; Karila et al. 2015; Engelhart et al. 2011). At lower frequencies like P- (0.3-1 GHz) and L- (1-2 GHz) band, the radar signals penetrate deep into the forest canopy and are backscattered at big branches, tree trunks and the ground (Dobson et al. 1995; Le Toan et al. 1992). Due to the high penetration capability and thus high sensitivity to vertical forest structure, these longer wavelengths are in particular suitable for biomass and stem volume retrieval (Treuhaft et al. 2015; Antropov et al. 2013) as well as forest structure assessment (Kugler et al. 2014). In contrast, radar waves at higher frequencies (i.e., shorter wavelength) such as C- (4-8 GHz) and especially X- (8-12 GHz) band are mostly backscattered in the upper canopy, at small branches and leaves (Gama et al. 2010; Pulliainen et al. 2003). Consequently, these bands are less sensitive to the vertical forest structure. However, these frequencies tend to be better suited for stem volume estimation (e.g., Karila et al. 2015; Solberg et al. 2013; Wagner et al. 2003) by means of height information derived from InSAR data. Furthermore, large-scale applications using longer wavelengths in a global context by means of spaceborne InSAR systems, like ALOS-PalSAR (L-band) and RADARSAT (C-band), suffer limitations in accuracy due to temporal decorrelations and atmospheric disturbances caused by repeat-pass interferometry (Kugler et al. 2014). Thus, missions using shorter wavelengths must be considered to provide single-pass interferometry for global forest resources assessment.

The TanDEM-X mission is the first single-pass SAR interferometer in space and enables the acquisition of highly accurate across-track and along-track interferograms without the inherent accuracy limitations imposed by repeat-pass interferometry (Krieger et al. 2013). The mission is composed of the two almost identical satellites, TerraSAR-X (launched in 2007) and TanDEM-X (launched in 2010), flying in a close formation and provides high resolution, multi-polarized, single-pass interferometric X-band (9.65 GHz) data. The main objective of the mission is the generation of a worldwide, consistent, high-precision Digital Elevation Model (DEM), which is commercially referred to as WorldDEM (Rizzoli et al. 2017). Thus, the TanDEM-X mission provides a suitable data basis to investigate the potential of InSAR data for stem volume estimation and

assessment of forest structure diversity.

Several recent studies demonstrated the estimation of stem volume or biomass by means of information derived from X-band InSAR data. Karila et al. (2015) employed a nearest neighbor prediction model for stem volume estimation based on InSAR heights from TanDEM-X data in boreal forest stands in Southern Finland. In Treuhaft et al. (2015), coherence from TanDEM-X InSAR data was deployed for biomass estimation using linear regression in a tropical forest in Brazil. Schlund et al. (2015) estimated biomass by linear and non-linear regression models based on TanDEM-X coherence in a tropical forest test site in Indonesia. Rahlf et al. (2014) used InSAR heights from TanDEM-X together with a LiDAR-based Digital Terrain Model (DTM) for stem volume estimation in a boreal forest in Southern Norway. Solberg et al. (2013) compared linear and non-linear regression of interferometric height and biomass or stem volume based on TanDEM-X InSAR data in a boreal forest test site. In Solberg et al. (2010) a non-linear, mixed regression model based on InSAR height derived from TanDEM-X data was applied to estimate biomass in boreal forest stands, whereas Gama et al. (2010) used airborne X-band data for linear regression of interferometric height and stem volume in tropical forest.

Besides studies investigating the potential of InSAR for estimating forest attributes describing stand structure in boreal forests (e.g., Karila et al. 2015; Karjalainen et al. 2012; Solberg et al. 2010), only few studies discussed the classification of forest structure types based on InSAR data in tropical forests (e.g., De Grandi et al. 2015; De Grandi et al. 2016). Even less studies explored the potential of X-band InSAR data for forest structure assessment in temperate forest stands. For example, Pardini et al. (2016) investigated the relationship between TanDEM-X interferometric coherence and vertical forest structure of temperate forest stands in South Germany.

Besides, the effect of phenology on X-band InSAR data over forested areas was discussed in literature. Kugler et al. (2014) observed a clear seasonal dependence between summer and winter TanDEM-X single and dual-pol acquisitions in boreal forest stands dominated by Norway spruce and Scots pine in Sweden and mixed temperate forest stands dominated by Norway spruce, beech, and fir in Germany. A significantly lower scattering center location, indicating a larger penetration in winter compared to summer due to phenological differences especially in broadleaf and mixed forest stands (i.e., presence and absence of leaves) in combination with frozen vegetation conditions (i.e., decreased dielectric constant), was detected by Kugler et al. (2014). By comparison of X-band bistatic InSAR acquisitions over temperate broadleaf and mixed forest stands in Estonia, Olesk et al. (2015) also found a deeper penetration into the forest during leaf-off season compared to leaf-on season. In contrast, Solberg et al. (2015) and Sadeghi et al. (2017) did not detect a significant effect of phenology by analyzing X-band InSAR data of the TanDEM-X mission over boreal coniferous forest stands.

## **1.2 Objectives and Outline**

The objective of this thesis is to explore the potential of X-band InSAR data acquired by the TanDEM-X mission for detection and definition of important forest parameters. The thesis aims for three main topics: 1) estimation of stem volume (see Chapter 4.1), 2) detection of forest stand structure according to horizontal and vertical composition (see Chapter 4.2) and 3) investigation of the influence of phenology on forest structure assessment (see Chapter 4.3) in a mixed temperate forest.



In contrast to previous studies investigating stem volume estimation by means of X-band InSAR data, which were carried out in boreal and tropical forest stands, stem volume predictions within this thesis were conducted in mixed, more complex, temperate forest stands. The development of a regression model for stem volume prediction at plot and stand level based on the allometric relationship between stem volume and forest height was targeted under additional consideration of forest structure. In detail, the objectives were defined as (i) estimation of stem volume per unit area at plot and stand level based on height information derived from polarimetric interferometric TanDEM-X data and airborne LiDAR survey as well as terrestrial measurements for calibration and validation purposes and (ii) improvement of the predictions by integration texture parameters representing the horizontal stand structure.

Regarding forest structure assessment, the detection of the heterogeneity in height of the main forest layer was aimed to distinguish different forest structure classes. Compared to previous studies that sought for forest structure classification using predominantly longer wavelengths (i.e., P- and L-band), forest structure classification within this thesis was based on X-band InSAR data. Furthermore, these studies were carried out in tropical forests whereas the current investigations were realized in temperate forest stands. Hence, this thesis contributes to fill the research gap in the field of forest structure classification using short wavelengths (i.e., X-band) with regard to temperate forests. Furthermore, in order to ensure easy transferability, forest structure detection and classification should be implemented without any requirement of a-priori information on the present forest structure and its complexity. Therefore, the detailed objectives comprised i) extraction and ii) classification of forest structure by means of an unsupervised approach based on height information derived from X-band InSAR data. Based on the standardized TanDEM-X InSAR data, the classification approach of this thesis offers the opportunity to derive meaningful forest structure classes dependent on the users' definitions and requirements adapted to each test site, which enables easy transferability.

Based on several studies exploring the impact of phenology on X-band InSAR data (e.g., Sadeghi et al. 2017; Olesk et al. 2015; Kugler et al. 2014), this thesis aims to further investigate the seasonal dependency on forest structure assessment. An additional aim was to explore the influence of polarization mode using TanDEM-X acquisitions corresponding to leaf-on and leaf-off season as well as to VV- and HH-polarization. For this purpose, the detailed objectives were defined as i) assessment of phenology-based differences in height estimation dependent on polarization mode (i.e., VV-polarized and HH-polarized InSAR data) and ii) the consequent limitations in forest structure classification accuracy.

This thesis is organized as follows. Chapter 2 introduces the acquisition principles of RaDAR remote sensing and the theoretical background of forest growth in order to provide the basic knowledge on InSAR data and relations between different forest parameters for the subsequent chapters. Chapter 3 presents the study area and the utilized remote sensing data as well as in-situ measurements. Chapter 4 highlights the developed methods for stem volume retrieval, forest stand structure classification and assessment of phenological-induced impacts on X-band InSAR data. Moreover, Chapter 4 summarizes the obtained results of forest assessment of the cumulative thesis composed of three publications. Finally, Chapter 5 discusses the applied approaches as well as the achieved results, while Chapter 6 concludes the main findings of the thesis. The **Appendix** comprises the three publications approaching the main objectives of the thesis (i.e., stem volume estimation, forest structure classification and investigation of phenological effects) in detail.

## 2 Fundamentals of Radar Remote Sensing and Forest Growth

### 2.1 Synthetic Aperture RaDAR (SAR)

RaDAR (Radio Detection And Ranging) systems operate at the microwave range of the continuous electromagnetic spectrum and provide complementary information for Earth Observation to optical sensors, which acquire data in the visible and infrared region of the electromagnetic spectrum (Fig. 2.1).

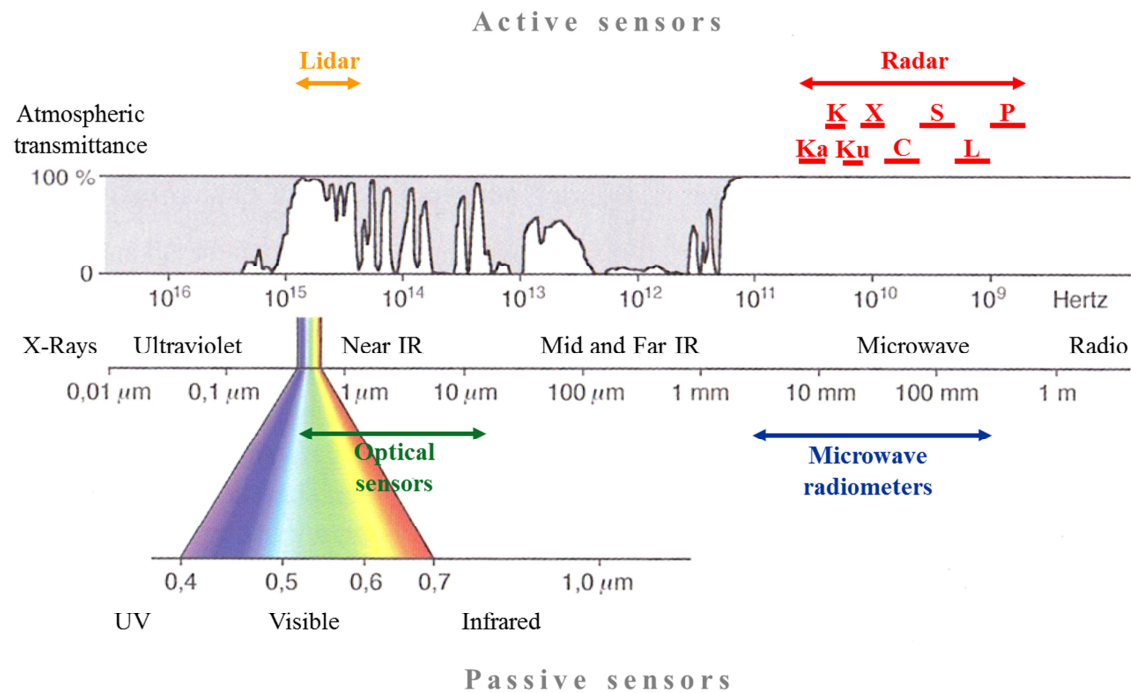


**Fig. 2.1:** The electromagnetic spectrum and the corresponding atmospheric transmittance as well as the ranges of different sensor types. Based on Albertz (2001: p. 11).

Since RaDAR systems transmit energy and record the backscattered signals, these systems are independent from solar illumination compared to optical systems imaging the energy emitted by the Earth's surface itself. Furthermore, RaDAR systems benefit from penetration ability through clouds and other media like vegetation canopies or dry soils due to the much longer wavelengths and atmospheric permeability in this region of the electromagnetic spectrum (Fig. 2.1). Therefore, these systems provide all-weather capability and volumetric as well as sub-surface information dependent on wavelength.

The range of the microwave part of the electromagnetic spectrum is divided into subsections, whereas Tab. 2.1 shows the commonly used frequency bands.

**Tab. 2.1:** Commonly used frequency bands for RaDAR systems with the corresponding frequency as well as wavelength range according to Moreira et al. (2013).

Frequency Band	Ka	Ku	X	C	S	L	P
Frequency [GHz]	40-25	17.6-12	12-7.5	7.5-3.75	3.75-2	2-1	0.5-0.25
Wavelength [cm]	0.75-1.2	1.7-2.5	2.5-4	4-8	8-15	15-30	60-120

The penetration ability of the transmitted signals increases with decreasing frequency and in turn increasing wavelength. Considering forests (Fig. 2.2), the RaDAR signal in shorter wavelengths like X-band is sensitive to scatterers like leaves and small branches, while the signal in longer wavelengths like L-band is backscattered at big branches, tree trunks and the ground (Le Toan et al. 1992; Pulliainen et al. 2003). Thus, the used wavelength determines the size of scatterers to which the sensor is sensitive.

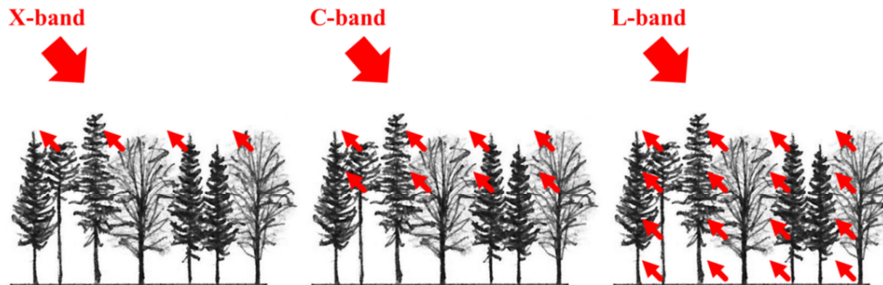


Fig. 2.2: Penetration ability into forest according to RaDAR frequency bands. Based on Albertz (2001: p. 64).

### 2.1.1 Imaging Principles

The RaDAR equipment is mounted on an airborne or spaceborne platform moving in a straight line in flight direction (azimuth /along-track) at altitude  $H$  above a  $x$ - $y$ -reference surface (Fig. 2.3a).

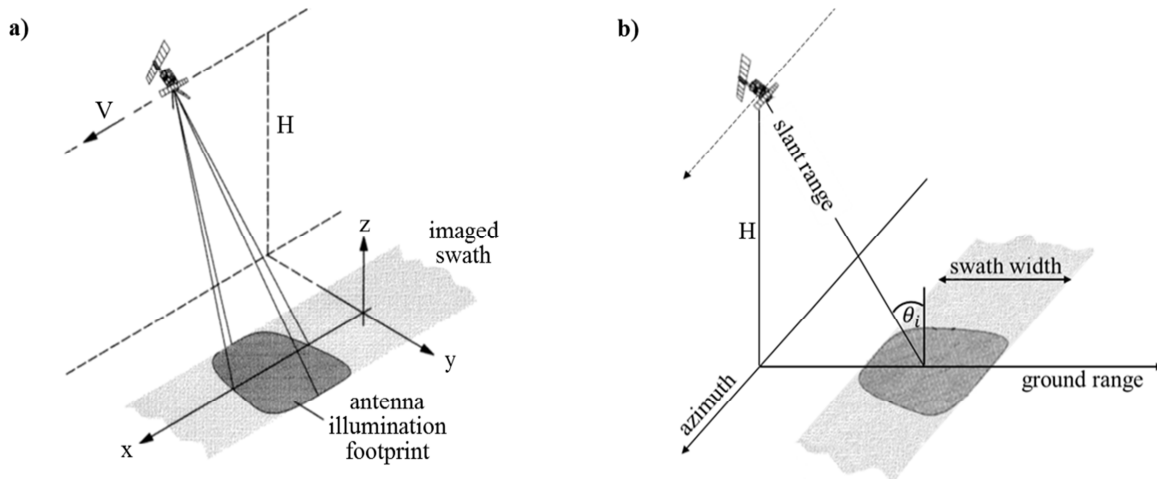
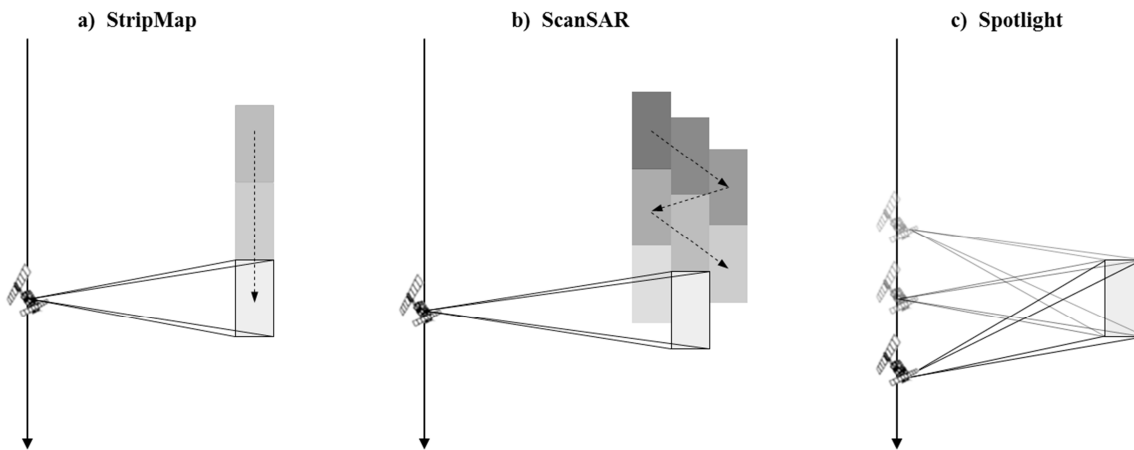


Fig. 2.3: Imaging geometry of a RaDAR system **a)** oblique view and **b)** cross-sectional view. Based on Bamler & Hartl (1998).

The sensor points laterally downwards perpendicular to the flight direction (range /across-track) and transmits energy in the form of short microwave pulses of the duration  $\tau$  travelling at almost speed of light  $c$  to a small part of the Earth's surface (referred as to illumination footprint) at the rate of the pulse repetition frequency ( $PRF$ ) (Woodhouse 2005: pp. 259-303). The  $PRF$  is synchronized with the forward velocity of the platform in such a way that a continuous stripe across the Earth's surface is built up in flight direction pulse by pulse (Richards 2009: pp. 53-74). The backscattered stream of echoes is detected by the receiver and separated into individual echoes (Bamler & Hartl 1998). For processing purposes, the echoes are stored as a 2-d matrix with

coordinates related to the distance of the scatterer to the sensor (i.e., slant range) and the position of the scatterer along the flight path (i.e., azimuth) (Fig. 2.3b). (Bamler & Hartl 1998). To allocate each echo to the corresponding pulse, all echoes must be received before the next pulse is transmitted. Accordingly, the *PRF* is constrained to the largest slant range (Richards 2009: pp. 53-74). Therefore, to avoid range ambiguities, the imaged swath is limited in the commonly used acquisition geometry referred to as StripMap mode (Fig. 2.4a). The ground swath is illuminated with a continuous sequence of pulses while the antenna beam is fixed in elevation and azimuth. In order to extend the swath regarding regional to global scale applications, the ScanSAR mode enables to image a wider swath, while the look angle of the antenna beam is changed during bunches of pulses periodically transmitted (Fig. 2.4b). Therefore, parallel swaths can be illuminated simultaneously. However, as a consequence, the spatial resolution in azimuth direction is reduced. In contrast, the Spotlight mode allows a higher azimuth resolution at the expense of the spatial coverage. The sensor steers continuously like a spotlight in the direction of a certain part of the Earth's surface in order to extend the illumination time and thus the spatial resolution (Fig. 2.4c). In the Spotlight mode, only selected and isolated patches of the Earth's surface can be imaged, whereas StripMap and ScanSAR mode facilitate stripes of theoretically unlimited length (Bamler & Hartl 1998).



**Fig. 2.4:** RaDAR imaging modes. **a)** StripMap mode, **b)** ScanSAR mode and **c)** Spotlight mode. Based on Richards (2009: p. 70).

## 2.1.2 Spatial Resolution

The accuracy of the measured information is a fundamental quality indicator of a RaDAR system. The spatial resolution in range direction depends on how two adjacent point targets  $T_1$  and  $T_2$  (Fig. 2.5) can be separated without any overlap of their echoes (Richards 2009: pp. 53-71). Therefore the slant range resolution  $\rho_r$  is equal to the length of the transmitted pulses in range direction which is defined by the velocity and the duration of the pulse (Fig. 2.5a):

$$\rho_r = \frac{c\tau}{2}, \quad (2.1)$$

where the factor 2 is due to the “there and back travelling” of the pulses (Woodhouse 2005: pp. 259-303). The ground range resolution  $\rho_g$ , which indicates how well targets can be resolved along the ground, can be determined including the incidence angle  $\Theta_i$ , which represents the angle of the beam incident to the ground (Fig. 2.5b):

$$\rho_g = \frac{c\tau}{2\sin\Theta_i}. \quad (2.2)$$

Since the ground range resolution depends on the incidence angle, it varies across the image swath in range direction. With increasing incidence angle, the ground range resolution increases. An incidence angle of  $\Theta_i = 0$  (i.e., directly under the platform) entails zero resolution which explains the requirement of a side-looking system (Richards 2009: pp. 53-71).

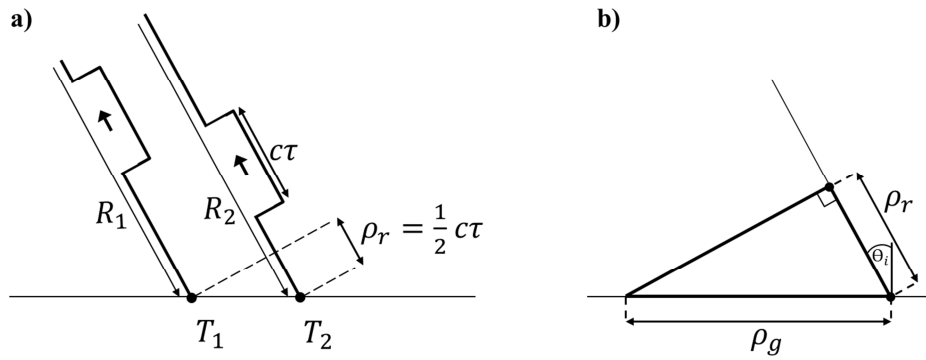


**Fig. 2.5:** Spatial Resolution of a RaDAR system. **a)** slant range direction and **b)** ground range direction. Based on Richards (2009: p. 85).

In order to improve the spatial resolution in range direction, the length of the transmitted pulses must be shortened. However by narrowing the pulse, the transmitted energy is reduced and thus the sensitivity of the RaDAR is weakened. To solve this problem, the frequency of the transmitted pulses is linearly modulated to a so called chirped pulse, so that overlapping echoes can be distinguished with accuracy much shorter than the length of the pluses (Woodhouse 2005: pp. 259-303).

The spatial resolution in azimuth direction  $\rho_a$  depends on the ability to separate two point targets at the same range (Woodhouse 2005: pp. 259-303). Since two targets can only be separated while they are not located in the same illumination footprint, the azimuth resolution is limited by the beamwidth in flight direction which is a function of the wavelength  $\lambda$ , the length of the antenna  $L$  and the range  $R$ :

$$\rho_a = \frac{\lambda}{L} R. \quad (2.3)$$

Assuming constant wavelength and length of the antenna, the distance of the target to the sensor and thus the flight altitude of the platform is determining the spatial resolution in azimuth direction. Thus, azimuth resolution decreases with increasing flight altitude. Accordingly, spaceborne platforms achieve much poorer spatial

resolutions compared to airborne platforms. In order to improve the azimuth resolution for spaceborne sensors, the length of the antenna must be extended tremendously. A practicable solution is realized in Synthetic Aperture RaDAR (SAR) systems by synthesizing a longer antenna by means of the linear forward motion of the platform (Richards 2009: pp. 53-71). While the platform moves forward along the flight path, the sensor transmits pulses and receives the corresponding echoes continuously which results in multiple irradiation of each part of the imaged swath due to overlapping illumination footprints (Fig. 2.6).

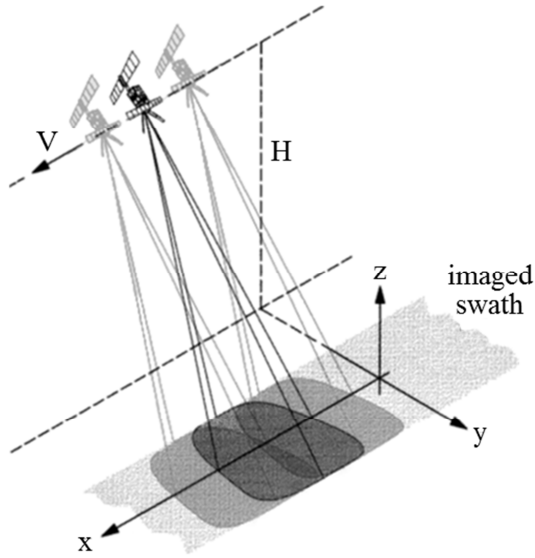


**Fig. 2.6:** Increase of the spatial resolution of a RaDAR system in azimuth direction by synthesizing a larger antenna. Based on Bamler & Hartl (1998).

Considering a single target on the Earth's surface, the sensor coherently receives the echoes corresponding to overlapping pulses transmitted from different positions in azimuth direction. Therefore, shortening of the antenna yields more high-frequency information about the scatterer caused by a broader beamwidth according to ( 2.3 ) (Bamler & Hartl 1998). The beamwidth of the synthesized antenna in azimuth direction is in the order of half of the real antenna length and determines the azimuth resolution:

$$\rho_a = \frac{L}{2}. \quad (2.4)$$

Neither range nor azimuth resolution are dependent on the distance between the platform and the target, and thus SAR systems, in general, can operate in any flight altitude without any decline in spatial resolution (Richards 2009: pp. 53-71).

The backscattered energy of a single point target is spread out in range and azimuth direction in the raw data. In range direction the backscattered signal is dispersed by the duration of the transmitted pulse, while in azimuth direction the backscattered signal is spread out by the duration the target is illuminated (i.e., length of the synthetic aperture). The signal compression in range direction is achieved by correlation of the received signal with a replica of the transmitted pulse. In azimuth direction the compression is performed by using the motion-induced Doppler Effect. The received echoes possess a frequency variation due to the motion of the platform

relative to the target (Richards 2009: pp. 53-71). This shift in frequency is known as the Doppler shift and leads to a shift of the backscattered signal towards higher frequencies in the front part of the beam and to lower frequencies in the rear part of the beam, respectively (Fig. 2.7). Based on the Doppler shift, the received signal is compressed in azimuth direction similar to range compression (Richards 2009: pp. 53-71).

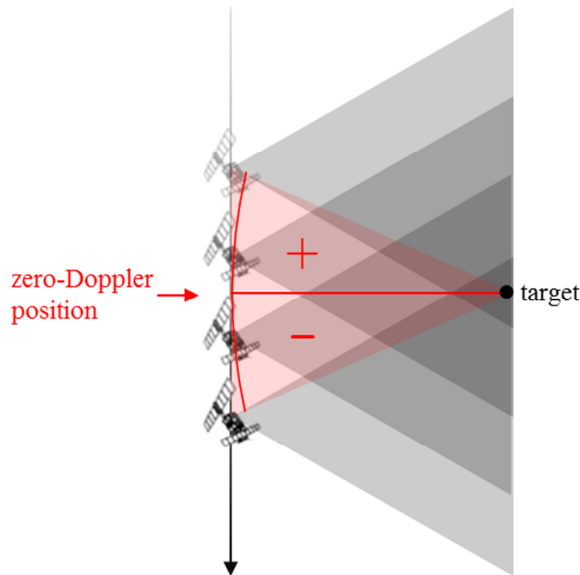


Fig. 2.7: Doppler Effect during a SAR acquisition. Based on Schmitt (2011: p. 24).

### 2.1.3 Characteristics of SAR Images

The focused 2-D SAR image is referred to as Single Look Complex (SLC) SAR image, where the received signals of each resolution cell are represented by a complex number associated to amplitude and phase information. The amplitude depends on acquisition geometry, wavelength and polarization of the transmitted pulse as well as on the properties of the scatterer. The phase information, however, is not related to the properties of the scatterer and will be applicable for height estimation of the scatterer (see Chapter 2.1.4).

#### 2.1.3.1 Radiometric Effects

The received magnitude of electromagnetic energy (i.e., backscatter coefficient) depends on the backscattered portion of the transmitted signal towards the sensor. In general, three characteristics of the target influence the scattering process dependent on wavelength: The dielectric constant, the surface roughness and the volumetric distribution of the scatterer. The dielectric constant is positively related to the reflectivity of the target and increases with increasing water content of the target. Furthermore, the surface roughness of the target is determinant for the magnitude of the backscattered energy. Targets with a smooth surface relative to the wavelength mostly reflect the transmitted signals as depicted in Fig. 2.8a. With increasing roughness of the surface relative to the wavelength, scattering in all directions (i.e., diffuse scattering) is increasing (Fig. 2.8b and Fig. 2.8c). Thus, the received magnitude of electromagnetic energy increases with increasing surface roughness.

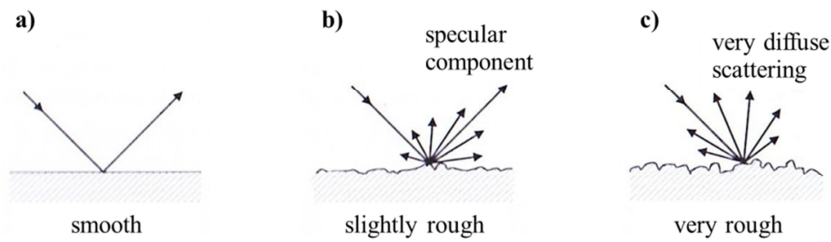


**Fig. 2.8:** Scattering of microwaves with respect to surface roughness: **a)** smooth surface, **b)** slightly rough and **c)** very rough surface relative to wavelength. From Richards (2009: p. 139).

Volume scattering occurs at targets (e.g., tree canopies) consisting of many individual scatterers. All scatterers contribute collectively to the backscattered energy as illustrated in Fig. 2.9 (Richards 2009: pp. 135-180). The extinction of the signal by the volume depends on distribution and size relative to the wavelength of the scatterers as well as the characteristics of the scatterers.

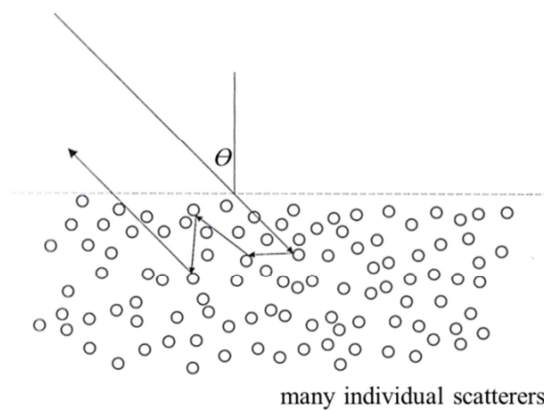


**Fig. 2.9:** Scattering from a volume consisting of many individual scatterers. From Richards (2009: p. 155).

The amplitude values of a SAR image are represented by greyscales. The brightness of the pixels increases with the magnitude of the received signal according to the mentioned scattering mechanisms. For example, waterbodies are represented very dark due to their smooth surface and thus high reflection of the signal.

However, the radiometric resolution of SAR images suffers from an inherent “salt and pepper” noise referred to as speckle (Woodhouse 2005: pp. 259-303). The speckle effect results from the interference of the coherent echoes corresponding to the individual scatterers within a resolution cell. The interference pattern depends on the characteristics of the individual scatterers and the relative position to the sensor, which in turn is determined by the imaging geometry and the topography. Admittedly, this effect is not predictable, but it is reproducible under exactly identical imaging conditions. Constructive superimposition of the backscattered echoes leads to a strengthening of the signal and a bright appearance in the SAR image, while destructive superimposition of the backscattered echoes yields a weak signal and a dark appearance in the SAR image (Lee & Pottier 2009, pp. 101-134). Thus, the speckle effect causes pixel-to-pixel variations in the backscattered intensity across homogeneous targets as shown in Fig. 2.10. In order to reduce speckle noise, several independent estimates of reflectivity are averaged (Lee & Pottier 2009: pp. 101-134). Either multi-temporal data is used to average reflectivity values for each resolution cell or neighboring reflectivity values of one image (i.e., mono-temporal) are combined (Richards 2009: pp. 109-134). In the case of mono-temporal speckle reduction, either a moving



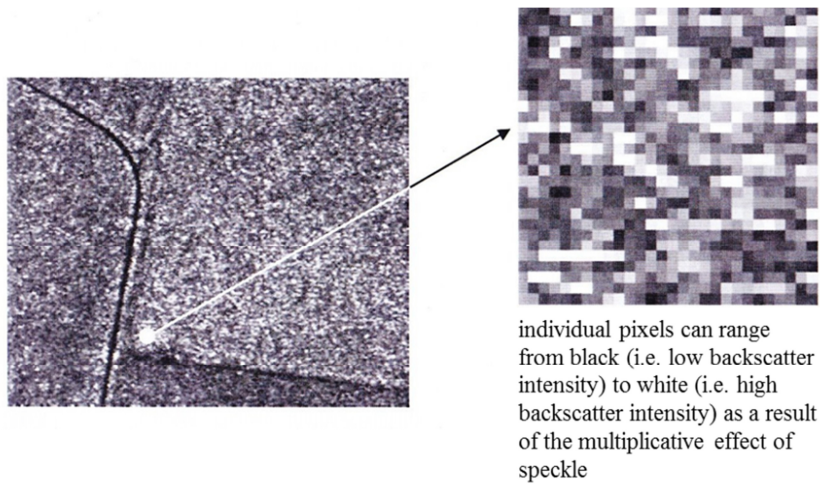


**Fig. 2.10:** Speckle effect in RaDAR images. From Richards (2009: p. 121).

window is used to derive a new value depending on the kernel function for the assigned center pixel or multiple neighboring pixels of the SLC SAR image are averaged in range and azimuth direction (i.e., multi-looking). The standard deviation of speckle is reduced by the square root of the number of averaged pixels (i.e., number of looks) (Richards 2009: pp. 109-134). In general, the number of looks is defined in order to achieve image pixels with squared pixel spacing (Lee & Pottier 2009: pp. 101-134).

### 2.1.3.2 Geometric Effects

Imaging of landscapes characterized by a distinct topography based on natural height variations (e.g., topography) and anthropogenic structures (e.g., buildings) is affected by geometric distortions due to the side-looking acquisition geometry of SAR systems. In general three effects occur: Layover, foreshortening and shadowing. As illustrated in Fig. 2.11, the objects A and B possess the same distance to the sensor which in consequence leads to layover of the echoes in the SAR image. The slope of the mountain is so steep that the

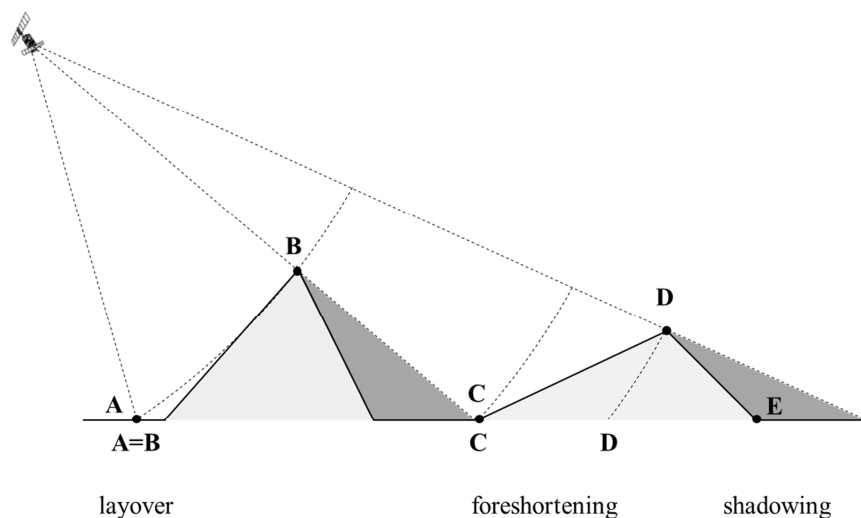


**Fig. 2.11:** Geometric effects in SAR imagery: layover, foreshortening and shadowing. Based on Albertz (2001: p. 80).

distance between B (i.e., top of the mountain) and the sensor is shorter than the distance between the foot of the mountain and the sensor. In case of the mountain, the slope between C and D is not as steep, however it yield a shortening of the distance between D (i.e., top of the mountain) and the sensor and thus a shortened distance between C and D in the SAR image. E is located next to the mountain which shadows the area behind and thus hampers the detection of E by the sensor. Layover can only be corrected if the signatures of the overlaid echoes are known. In case of foreshortening, the geometrical distortion can be compensated by means of a DEM (Huber et al. 2004). Lack of information caused by shadowing can only be filled by including supplementary acquisitions from different viewing points.

## 2.1.4 SAR Interferometry (InSAR)

### 2.1.4.1 Imaging Principles

The basic idea of SAR interferometry is to combine scattering signals acquired from a different position (i.e., across-track interferometry) or at a different time (i.e., along track interferometry) (Bamler & Hartl 1998). While conventional SAR images only provide 2-d coordinates (i.e., azimuth and range) of scatterers, an across-track interferometer facilitates their positioning in the 3-d space. SAR images acquired from different positions enable the reconstruction of the Earth's topography, whereas SAR images acquired at different times allow detecting movements of scatterers (e.g., glacier flows, land subsidence, ocean currents) (Moreira et al. 2013). Fig. 2.12 illustrates the concept of an across-track SAR interferometer.

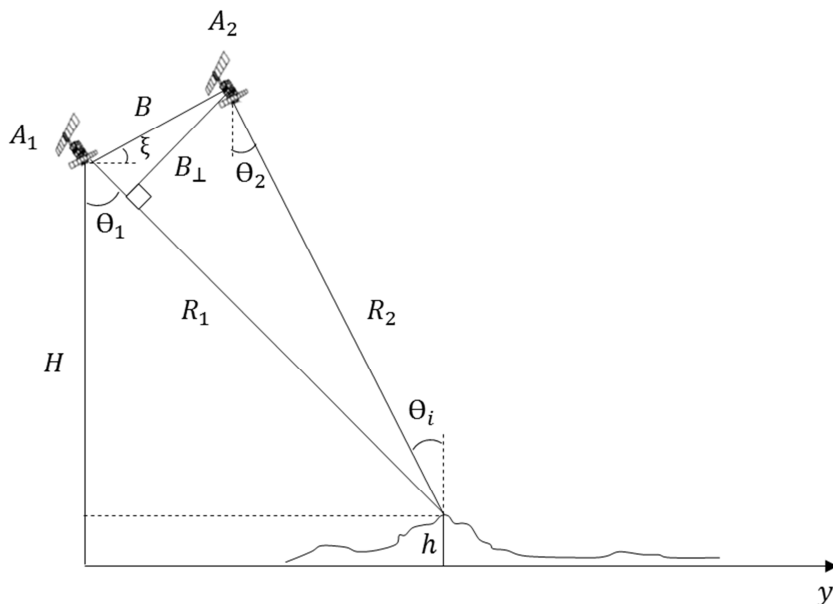


**Fig. 2.12:** Acquisition geometry of an across-track SAR interferometer. Based on Bamler & Hartl (1998).

Two antennas ( $A_1$ ,  $A_2$ ) fly on laterally displaced orbits and image the same part of the Earth's surface from slightly different positions. The distance between the antennas is referred to as the baseline  $B$  and its component perpendicular to the look direction as the effective baseline  $B_{\perp}$ . With given antenna positions and the two slant range distances ( $R_1$ ,  $R_2$ ), each point on the Earth's surface can be located in space by means of triangulation

(Bamler & Hartl 1998). The two antennas can either operate simultaneously (i.e., single-pass interferometry) or successively (i.e., repeat-pass interferometry).

In case of a coherent SAR, the difference in slant range direction is related to the phase difference between the two SAR images and given by

$$\Delta R = m(R_1 - R_2), \quad (2.5)$$

where the factor  $m$  takes into account whether only the “back” travelling path or the “there” as well as “back” travelling path of the signal contribute to the phase difference. Therefore, the factor  $m$  is 1 in case of single-pass interferometry (i.e., one antenna transmits and two antenna receive) and is 2 in case of repeat-pass interferometry (i.e., both antennas transmit and receive independently) (Moreira et al. 2013).

The phase difference  $\Delta\phi$  is then calculated by the wavelength fraction which fits into  $\Delta R$  according to

$$\Delta\phi = \frac{2\pi}{\lambda} \Delta R, \quad (2.6)$$

where  $\lambda$  is the wavelength.

Since  $B \ll R_1$  for a spaceborne interferometer, the slant range difference  $\Delta R$  induced by the different antenna positions can be determined according to the law of cosines

$$R_2^2 = R_1^2 + B^2 - 2R_1B\cos(180^\circ - \theta_1 + \xi), \quad (2.7)$$

leading to

$$\Delta R = -B\sin(\theta_1 - \xi), \quad (2.8)$$

and following that the corresponding phase difference can be expressed as

$$\Delta\phi = -\frac{2\pi}{\lambda} B\sin(\theta_1 - \xi). \quad (2.9)$$

With given baseline and angle  $\xi$ , the look angle  $\theta_1$  can be calculated from the phase difference according to (2.9) and the terrain height can be estimated by

$$h = H - R_1\cos\theta_1, \quad (2.10)$$

where  $H$  is the height of antenna  $A_1$  above ground.

#### 2.1.4.2 InSAR Processing

However, before the height of the terrain can be estimated, the phase differences must be derived from the SLC SAR images. First, precise co-registration of the complex SAR images is required to ensure that corresponding pixels represent the same part of the Earth's surface (Schreiber & Moreira 2000). Commonly, local shifts in range and azimuth direction are used to maximize the cross-correlation between the two images (Moreira et al. 2013). Based on the co-registered images, the complex interferogram was generated by multiplying one image with the complex conjugate of the other image. The interferometric phase can be extracted from the complex interferogram and represents the phase differences of the two SAR images and is characterized by a fringe pattern in range direction which is locally distorted by terrain height variations (Bamler & Hartl 1998). The systematically decreasing interferometric phase related to the flat Earth's surface is caused by an increase in range and thus an increase in look angle (Moreira et al. 2013). By subtracting the expected phase from an appropriate reference surface (i.e., flat Earth contribution), the interferometric phase related to the phase differences caused by topography is extracted (Woodhouse 2005: pp. 259-303). Since the interferometric phase can only be gathered as a  $2\pi$ -modulus, the phase estimation is ambiguous by multiples  $2\pi$ . The interferometric phase continuously wraps around to 0 when it reaches  $2\pi$ . The height of ambiguity ( $HoA$ ) corresponds to an elevation change in order of a phase change of  $2\pi$  and is defined as

$$HoA = \frac{\lambda m R_1 \sin(\theta_i)}{B_{\perp}}. \quad (2.11)$$

With decreasing  $HoA$  and thus increasing perpendicular baseline, the sensitivity of the interferometer to small elevation changes increases (Moreira et al. 2013). However, for rough terrain with steep slopes (e.g., tall forests, mountains, deep valleys) the  $HoA$  is limited for the purpose of correct phase-to-height conversion. Furthermore, the useful maximum length of the baseline is limited since the correlation between the two SAR images decreases with increasing baseline (Moreira et al. 2013). In order to infer the terrain heights for each pixel, the ambiguity must be resolved by phase unwrapping. The concept behind phase unwrapping is based on the assumption that the terrain is continuous without any abrupt height variations related to phase discontinuities up to  $\pm 2\pi$  (Woodhouse 2005: pp. 259-303; Bamler & Hartl 1998). An integer multiple of the  $2\pi$  cycle is assigned to each pixel to resolve the ambiguity. Starting from one location counting up the phase values, it is more likely that at  $2\pi$  the next little phase increment to the next pixel  $\Delta\phi$  corresponds to an absolute phase of  $2\pi + \Delta\phi$  than to an absolute phase of  $0 + \Delta\phi$ .  $2\pi$  has to be added to all subsequent phases until the next cycle is reached. Based on the unwrapped phase, the position of each image pixel is derived by means of trigonometry according to ( 2.9 ) and ( 2.10 ).

#### 2.1.4.3 Interferometric Coherence and Decorrelation

The complex coherence  $\gamma$  is defined as the normalized cross-correlation of the two SAR images (Woodhouse 2005: pp. 259-303). Its phase corresponds to the expected interferometric phase, while its magnitude is related to the quality of the interferogram (Bamler & Hartl 1998). The magnitude of the coherence indicates the degree of correlation and ranges from 0 (i.e., pure noise) to 1 (i.e., identical images without noise) (Moreira et al. 2013).

Coherence is usually estimated by a spatial average over a defined neighborhood around the pixel of interest using a moving window. The interferometric coherence is influenced by acquisition parameters and the characteristics of the scatterer. The correlation of the two SAR images suffers from several decorrelation sources. Decorrelation is mainly caused by receiver noise, temporal as well as geometric baseline and volume of the scatterer and can be defined as

$$\gamma = \gamma_{SNR} \cdot \gamma_{temp} \cdot \gamma_{geo} , \quad (2.12)$$

with

$\gamma_{SNR}$ , the noise decorrelation caused by the additive white noise contribution on the received signal which can be expressed related to the signal-to-noise ratio ( $SNR$ ),

$$\gamma_{SNR} = \frac{1}{1 + SNR^{-1}} , \quad (2.13)$$

$\gamma_{temp}$ , the decorrelation introduced by changes in scattering behavior of the scatterer (see Chapter 2.1.3) during the time interval between the two acquisitions, and

$\gamma_{geo}$ , the decorrelation caused by different projection of a 3-d scatterer into the two interferometric SAR images is due to the spatial baseline and thus different incidence angles.

To reduce the phase noise induced by the mentioned decorrelation sources, the complex interferogram is often locally averaged (i.e., multi-looking) before phase extraction. With increasing number of looks (i.e., averaged interferometric samples), the phase noise is reduced. However, with increasing number of looks, the spatial resolution decreases. Therefore, a trade-off between phase noise and spatial resolution is required (Moreira et al. 2013). In case of single-pass interferometry, temporal decorrelation is negligible due to the simultaneous acquisition of the two SAR images.

## 2.2 Principles of Forest Growth

### 2.2.1 Forest Growth Processes

Growth processes at individual tree level are mainly influenced by genetic factors and resource availability which is determined by environmental conditions such as temperature, humidity, and acidity. The combined effect of the environmental conditions affects the physical, biochemical and physiological processes (e.g., photosynthesis, evapotranspiration, and resource allocation) of each tree. These processes underlie a biological variability which makes it difficult to derive strict functional laws. Nevertheless, stochastic relationships enable the modelling of tree growth by simulating the complex interactions and processes biometrically (Pretzsch 2009: pp. 381-422). A well-established growth relationship is the allometric equation, which describes the growth development according to resource allocation within a single tree. However, the growth processes of individual

trees cannot be regarded independently of surrounding trees. Especially competition for resources (e.g., competition for growing space) has a high impact on the growth development of trees within a forest stand. Therefore, the growth processes at individual tree level as well as at stand level are considered below.

### 2.2.1.1 Allometry at Individual Tree Level

The phylo- and ontogenetic evolution towards a functional optimization affects the size and shape relations of trees and thus reflects the environmental conditions (Pretzsch 2009: pp. 381-422). In order to describe and understand the size-correlated variations, the theory of allometry can be used. Due to different growth velocities of the organs, the growth process is characterized by changes in the proportions of the organs to each other (Niklas 1994). An example for age-dependent changes in proportions for trees is the non-proportional shape development between tree height and crown size under solitary conditions as shown for the example of European beech in Fig. 2.13.

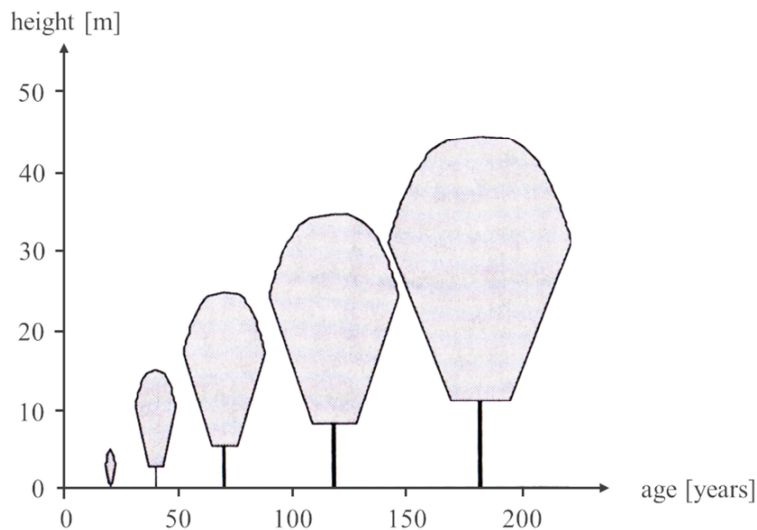


**Fig. 2.13:** Age-dependent non-proportional shape development of a European beech under solitary conditions. Based on Pretzsch (2009: p. 388).

According to Huxley (1932) and von Bertalanffy (1951), the relation of growth rate of a certain part  $y$  and the growth rate of another part or the whole body  $x$  is constant over time and can be expressed as

$$a = \frac{\frac{dy}{dt} \cdot \frac{1}{y}}{\frac{dx}{dt} \cdot \frac{1}{x}} \quad (2.14)$$

( 2.14 ) is known as the allometric equation and represents the distributing process of growth resources between the organs of the organism, where  $a$  indicates distributing factors for each organ (Pretzsch 2009: pp. 387-393).

By integration of ( 2.14 ) and logarithmic representation a linear relationship can be formed

$$y = b \cdot x^a, \quad (2.15)$$

leading to

$$\ln y = \ln b + a \cdot \ln x. \quad (2.16)$$

The linear function ( 2.16 ) is represented as a straight line with the constants  $b$  and  $a$  (Fig. 2.14).  $b$  is known as the integration constant specifying the value of  $y$  at  $x = 1$ .  $a$  is the constant allometric ratio of growth rates and defines the slope of the straight line. If  $a > 1$ ,  $y$  increases faster than  $x$  (positive allometry). If  $a = 1$ ,  $x$  and  $y$  increase proportionally (isometric growth). If  $a < 1$ ,  $x$  increases faster than  $y$  (negative allometry) (Huxley 1932; von Bertalanffy 1951).

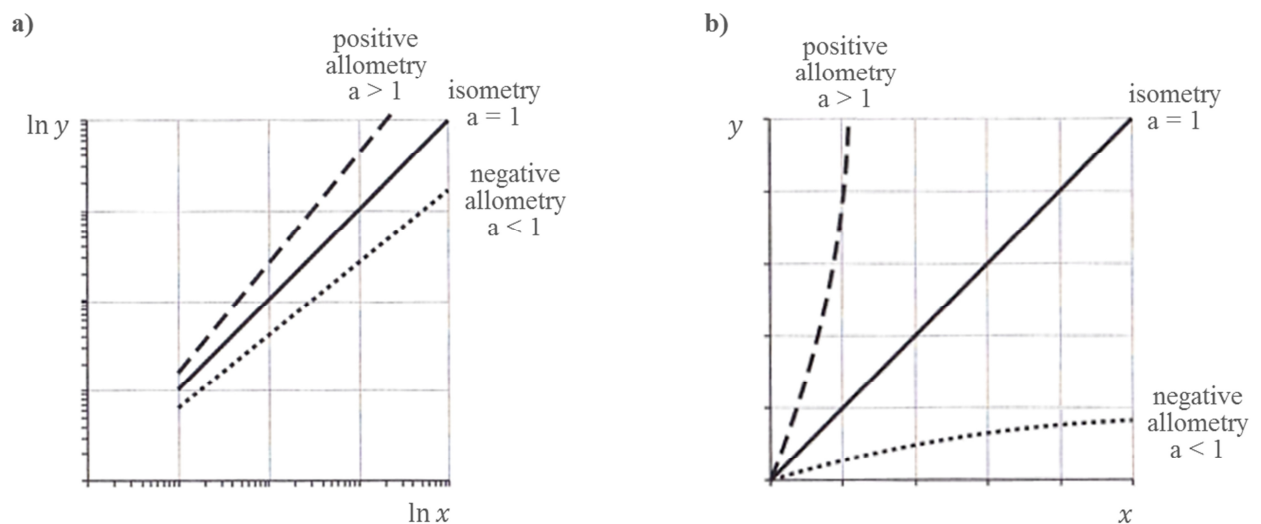


**Fig. 2.14:** Positive and negative allometry and isometry between  $x$  and  $y$  in **a)** double-logarithmic and **b)** Cartesian coordinate system. Based on Pretzsch (2009: p. 389).

Since the allometric behavior of trees underlies variations caused by different genetic factors and environmental conditions, allometry gives explanations about the adaptations of trees to their environment. Furthermore, it also enables the estimation of any desired size dimension (e.g., stem volume) based on available or easy measurable size dimension (e.g., tree height) according to the allometric relationships. For example, stem volume and height of a tree are interrelated by a positive allometric relationship, where stem volume increases exponentially with tree height. Accordingly, stem volume can be derived from tree height measurements using this allometric relationship.

### 2.2.1.2 Allometry at Stand Level

Forest growth is not only determined by the growth processes of the individual trees independent of their neighborhood within a stand, but also by the interaction of all individual trees within the stand. For example, strong competition within a forest stand (i.e., in case of high stand density) leads to an increase of the height

growth of a tree relative to its diameter growth in order to improve light availability (i.e., positive allometry of height growth). With improving conditions due to more growing space, the distribution of resources within the trees changes back towards a positive allometry of diameter growth (Pretzsch 2009: pp. 399-407).

### 2.2.1.2.1 Self-thinning

With ongoing growth, the demand for resources and growing space of each tree increases. As soon as the requirement of the entire forest stand exceeds the available resources, its maximum stand density is reached and self-thinning processes take place. The limit of stand density depends on tree species composition, development stage of the stand and environmental conditions. Applying the theory of allometry at stand level, size-density allometric relationships provide information about the species-specific critical demand for resources and growing space (Pretzsch 2009: pp. 399-407). The concept of size-density allometry under self-thinning relates the average tree size to the number of trees per stand. Fig. 2.15 depicts the logarithmic representation of the relationship between average tree size and stand density (Pretzsch & Biber 2005).

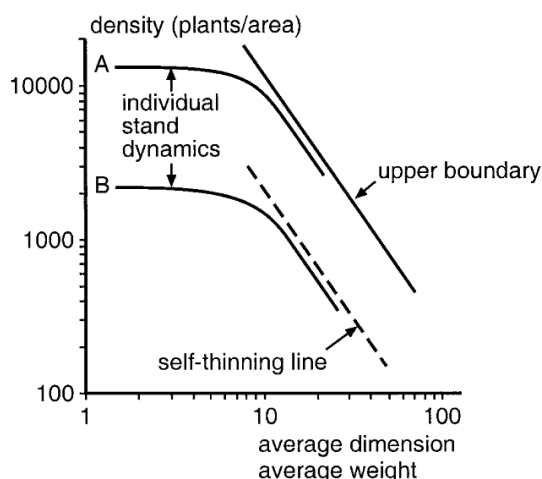


**Fig. 2.15:** Schematic illustration of self-thinning dependent on growth conditions, where A corresponds to a forest stand under optimal growing conditions and B represents a forest stands under suboptimal growing conditions. From Pretzsch & Biber (2005).

The upper boundary (i.e., solid line in Fig. 2.15) describes the possible maximum density for a species at given size in even-aged pure stands under optimal conditions, whereas the self-thinning line (i.e., dashed line in Fig. 2.15) represents the density-dimension relationship for any stand under suboptimal growing conditions. Stand A corresponds to a forest stand with optimal conditions, whereas B represents a forest stand with suboptimal conditions. The density-dimensions follow the corresponding self-thinning line in accordance with stand-specific conditions and stagnate at a certain absolute level. Thus, the self-thinning line is located below the upper boundary dependent on growing conditions.

A well-known size-density relationship is stated by the empirically derived stand density rule according to Reineke (1933). The stand density rule describes the relationship between mean tree diameter and number of trees per area in fully stocked, even-aged, untreated forest stands regardless of tree species and states that the



number of trees decreases with increasing mean tree diameter according to an allometric coefficient of -1.605 as expressed by

$$N = k \cdot dg^{-1.605}, \quad (2.17)$$

where  $N$  is the number of trees per area, constant  $k$  and  $dg$  is the mean tree diameter.

Using a logarithmic representation, the relationship can be linearized

$$\ln(N) = \ln(k) - 1.605 \cdot \ln(dg), \quad (2.18)$$

with intercept  $\ln(k)$  and slope  $-1.605$ .

The stand density index (SDI) was developed based on Reinecke's rule and describes the stand density dependent on the number of trees per hectare  $N$  and the mean diameter  $dg$  related to mean diameter of 25 cm for European forests:

$$SDI = N \cdot \left(\frac{25}{dg}\right)^{-1.605}. \quad (2.19)$$

The *SDI* enables quantification and control of stand density as well as prediction of stand development in pure and mixed forest stands (Pretzsch 2009: pp. 399-407). Independently from Reinecke's stand density rule, Kira et al. (1953) and Yoda et al. (1963) derived the so called -3/2-power rule of self-thinning for herbaceous plants, which describes the relationship between the mean weight and the number of plants per area in even-aged, fully-stocked, monospecific stands:

$$w = e^b \cdot N^{-\frac{3}{2}}, \quad (2.20)$$

where  $w$  is the mean weight and  $N$  is the number of trees per area.

Accordingly, stand density is an essential parameter regarding allometry at stand level which determinates the boundary conditions for within stand growing processes among other factors. Thus, stand density must be taken into account for the application of the allometric principle at stand level.

#### **2.2.1.2.2 Eichhorn's Rule**

Eichhorn's rule (1902), which is based on the three fundamental equations for stand development in forest science, defines the standing volume for a given mean height for untreated forest stands (see Fig. 2.16a) (Pretzsch 2009: pp. 432-444).

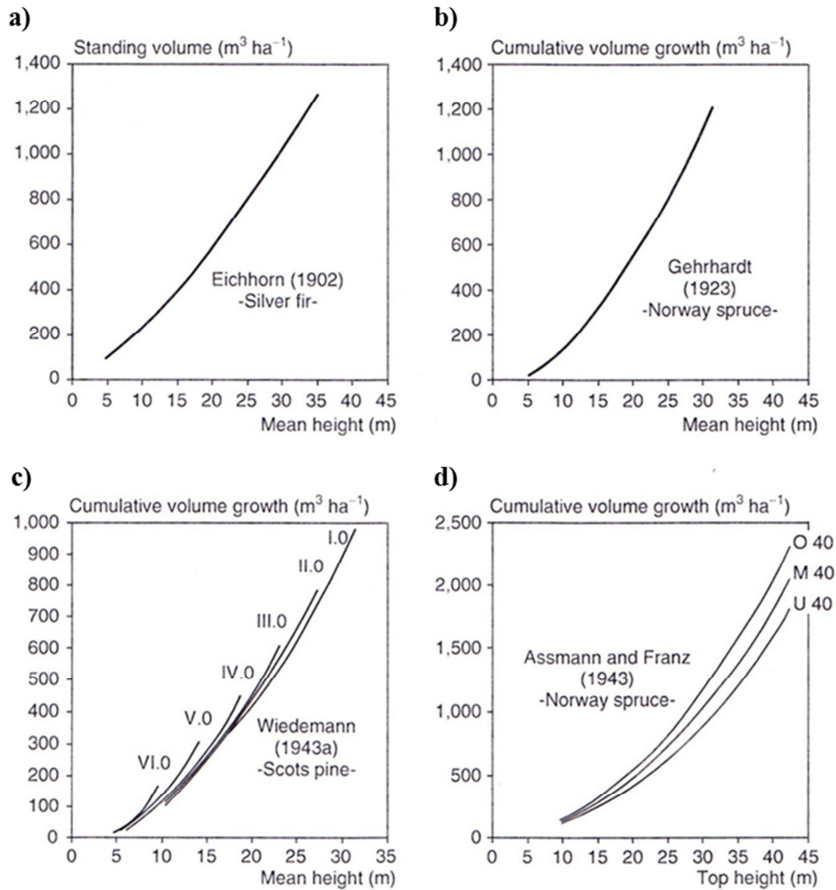


**Fig. 2.16:** From **a)** Eichhorn's rule (1902) Silver fir stands with moderate thinning to **b)** common yield levels from Norway spruce stands with medium strong thinning according to Gehrhardt (1923) to **c)** Special yield levels from Scots pine stands with moderate thinning from Wiedemann (1943) to **d)** Sub-divided special yield levels in Norway spruce stands with graduated thinning according to Assmann and Franz (1963). From Pretzsch (2009: p. 435).

The first relationship states that forest stands at a given site follow a particular height development with increasing age

$$height = f_1(age), \quad (2.21)$$

the second relationship describes that the total volume yield is a function of height

$$total\ volume\ yield = f_2(height), \quad (2.22)$$

and the third relationship as a result of ( 2.21 ) and ( 2.22 ) is

$$total\ volume\ yield = f_3(age). \quad (2.23)$$

Eichhorn defined the relationship between volume development and mean height ( 2.22 ) more precisely by means of a sufficient database from experimental plots. Using extended databases from experimental plots,

Gerhardt (1909; 1923; 1930) (Fig. 2.16b), Wiedemann (1943; 1948) (Fig. 2.16c) and Assmann & Franz (1963) (Fig. 2.16d) refined and further extended Eichhorn's rule to site-dependent height-volume relationship which defines the cumulative growth for a given mean height.

Accordingly, Eichhorn's rule and its extensions confirm the positive allometric relationship between stem volume and tree height at individual tree for stand level.

## 2.2.2 Forest Stand Structure

### 2.2.2.1 Description of Forest Stand Structure

Forest stand structure is generally characterized by size distribution and horizontal as well as vertical tree distribution patterns (del Río et al. 2016). It is a consequence of species selection, stand dynamics, human, biotic and abiotic disturbances (Pretzsch et al. 2015; Pommerening 2006; Kuuluvainen et al. 1996). The size and longevity of trees determine the stand-internal environmental conditions and flora as well as fauna habitats (Kuuluvainen et al. 1996). Stand structure and processes of forest growth are mutually dependent (Pukkala & von Gadow 2012). Any given stand structure causes corresponding growth processes by which these processes in turn generate particular stand structural characteristics. The feedback system between tree growth and stand structure is illustrated in Fig. 2.17. The feedback between growth conditions and tree growth reacts fast, whereas the feedback between growth conditions, tree growth and stand structure is slow (Pretzsch 2009: pp. 225-229).

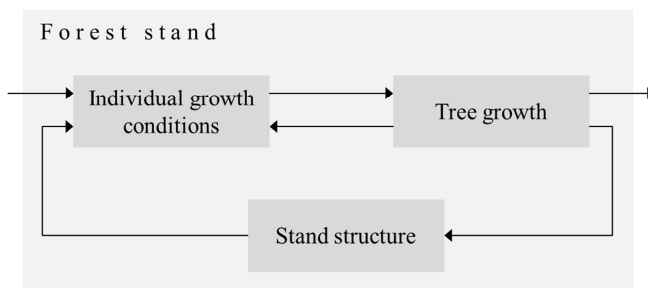


**Fig. 2.17:** Feedback system between tree growth and forest stand structure. Based on Pretzsch (2009, p. 226).

A variety of parameters (e.g., basal area, number of trees per hectare, tree height) as well as indices (e.g., SDI, leaf area index, index of patchiness) are usually measured and calculated to capture forest stand structure (del Río et al. 2016). Tree distribution and crown maps provide the basis for analyses of spatial occupancy patterns within the forest stand. Spatial occupancy patterns are further analyzed using tree distribution indices based on raster maps, sample quadrats (e.g., Aggregation Index according to Clark & Evans (1954)) and pair correlation functions (e.g., K- function according to Ripley (1977)). In order to quantify the density of spatial occupancy as well as the mean competition within the stand, stand density is derived based on parameters like mean basal area or indices like the SDI according to Reineke (1933) (see Chapter 2.2.1.2). To assess the species richness and composition, diversity indices (e.g., diversity index according to Shannon (1948)) are applied. Finally, model-based simulations of tree crowns enable three-dimensional reconstruction of the stand structure (e.g., Pretzsch, et

al. 2002), and thus facilitate the description and interpretation of forest structure by profile diagrams, front views and walk-throughs.

### 2.2.2.2 Gap Theory

According to the gap theory (or mosaic-cycle theory), which goes back to Aubréville (1938), large-scale ecosystems can be divided into a mosaic of individual patches in different successional stages. The assumed patch size varies from 100 m<sup>2</sup> to 1000 m<sup>2</sup>, where each patch passes through a cyclic succession process of establishment, growth and mortality of individual trees as shown in Fig. 2.18 (Bugmann 2001).

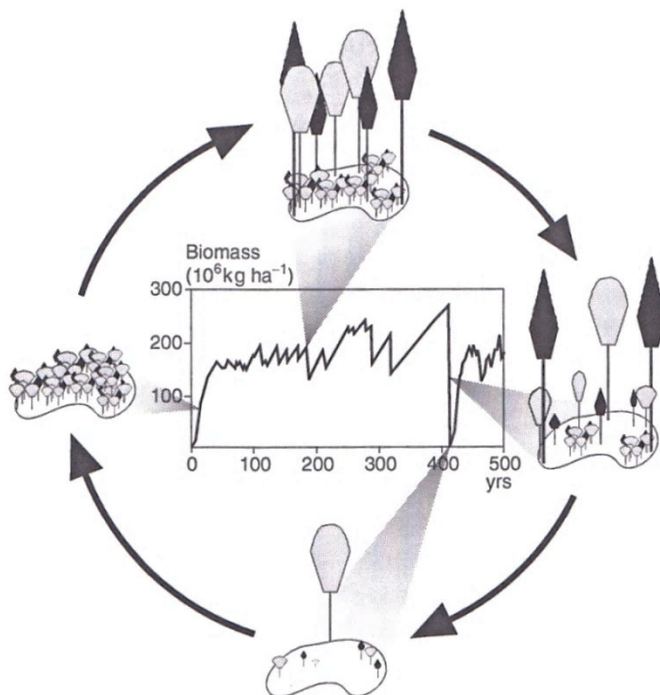


**Fig. 2.18:** Gap theory (or mosaic-cycle theory) assumes that large-scale ecosystems are composed of individual patches passing through a cyclic succession process of establishment, growth and mortality of individual trees. From Pretzsch (2009: p. 457).

According to the gap theory, the mortality or harvesting of a mature tree in the dominant stand layer creates a gap. Hence, the growing conditions regarding resource availability for underlying forest layers improve which leads to natural regeneration. The growing trees close the gap gradually and in accordance with the self-thinning process (see Chapter 2.2.1.2.1) new overstory is formed. Renewed losses in the dominant stand layer reinitiate the cycle (Pretzsch 2009: pp. 456-458). The cycles are desynchronized among different patches and the successional development stages possess varying durability (Begehold et al. 2016). Each development stage is characterized by a specific combination of various structural parameters like canopy cover, dbh, tree height, deadwood amount and regeneration cover (Begehold et al. 2016). Accordingly, the successional development at patch level is determinant for stand structure and spatial distribution of the development phases reflects forest structure patterns.

### 3 Materials

#### 3.1 Study Area

Traunstein forest is a highly structured, mixed, temperate municipal forest located close to the city of Traunstein, Germany (47°52' N, 12°38' E) (Fig. 3.1).

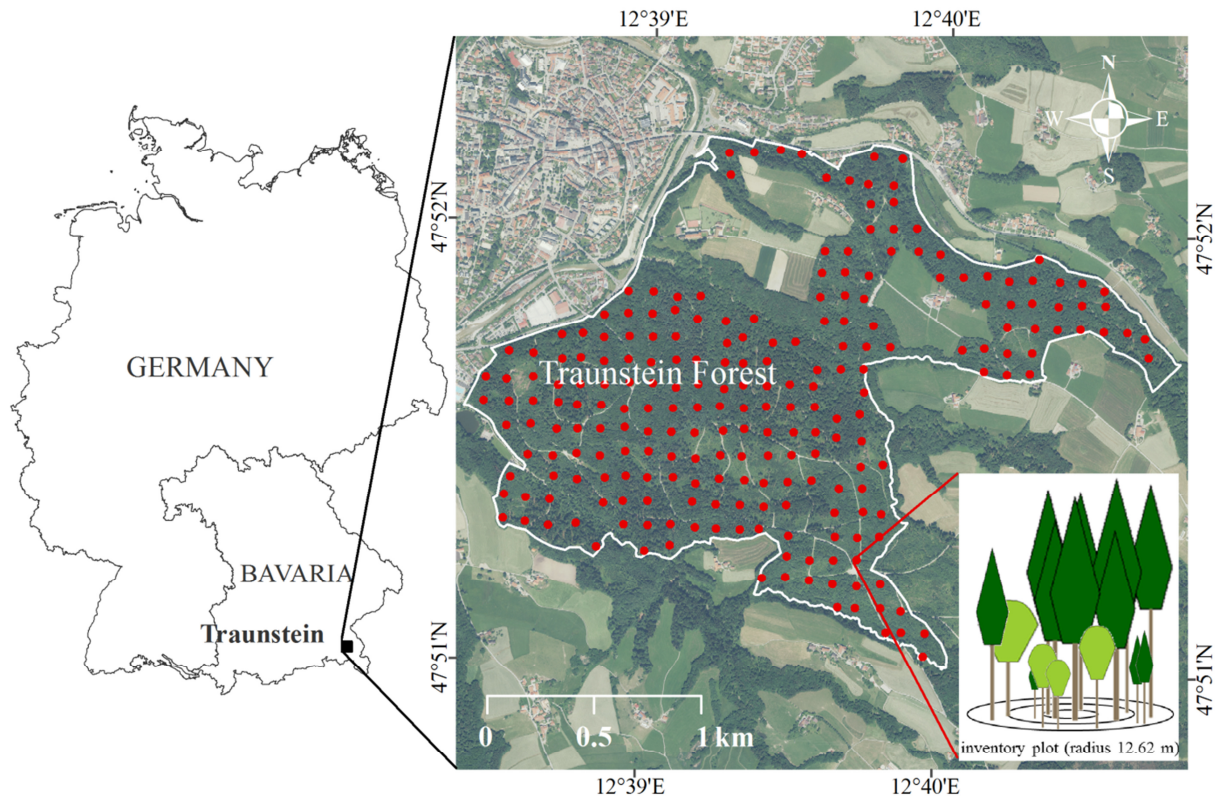


**Fig. 3.1:** The study area, a mixed, temperate and highly structured forest, is located east of the city of Traunstein in the South of Germany and covers an area of about 243 ha. Terrestrial measurements of the forest's condition are collected based on 228 permanent circular sampling plots and have been repeated regularly since 1988 on a common cycle of ten years.

Traunstein forest passes through an ongoing reconversion from a homogeneous one-age cohort forest to a structurally rich, heterogeneous forest due to “close-to-nature” silviculture (Pretzsch 1996). “Close-to-nature” forest management targets productivity, diversity, and especially continuity as well as stability of forest conditions at small scales (Bauhus et al. 2013) and thus leads to a very complex forest composed of forest stands with high tree species richness and heterogeneous vertical as well as horizontal structures. The high heterogeneity of Traunstein forest is reflected in a broad distribution of tree species and growth stages. Regarding the representativity with respect to the range of silviculture types in Central Europe, Traunstein forest is predestinated as study area to explore the potential of X-band InSAR data for the estimation of forest structure parameters in complex, temperate forest stands. The study area covers a forest area of 243 ha and is bounded by the districts Bürgerwald and Heiligengeistwald. The topography ranges from 630 to 720 m above sea level and includes small areas with steep slopes. The soils are composed of glacier sediments which belong to the pre-

alpine moraine landscape. The climatic conditions are characterized by a mean annual temperature of 7.3 °C and precipitation up to 1600 mm per year. The forest is predominantly composed of Norway spruce (*Picea abies*), European silver fir (*Abies alba*), European beech (*Fagus sylvatica*) and Sycamore maple (*Acer pseudoplatanus*).

## 3.2 Remote Sensing Data

Four dual-polarized interferometric TanDEM-X image pairs acquired on January 09, 2012, May 18, 2013, August 12, 2013 and March 09, 2014 were used. All images were acquired in bistatic StripMap mode with similar incidence angles of about 43-44°. The baselines between the two sensors vary from about 109 m to 143 m. A summary of the TanDEM-X acquisition parameters is given in Tab. 3.1.

**Tab. 3.1:** Acquisition parameters of the SAR data.

Acquisition date	Acquisition mode	Polarization mode	Orbit	Incidence angle	Baseline	Weather conditions
01/09/2012	Bistatic / StripMap	Dual-pol (HH, VV)	Ascending	43.1°	108.74 m	dry / snowfall
05/18/2013	Bistatic / StripMap	Dual-pol (HH, VV)	Ascending	43.2°	142.72 m	dry
08/12/2013	Bistatic / StripMap	Dual-pol (HH, VV)	Descending	44.9°	119.99 m	dry
03/09/2014	Bistatic / StripMap	Dual-pol (HH, VV)	Descending	44.9°	143.18 m	dry

In addition, an airborne LiDAR survey was conducted on November 18, 2012 with a flight height of about 500 m and a point density of about 25 dots per m<sup>2</sup> using the LMS-Q 680i Scanner from RIEGL GmbH. The associated DTM as well as Digital Surface Model (DSM) were provided by MILAN Geoservice GmbH.

### 3.2.1 Scattering Center Height

The interferometric concept uses phase differences between two complex SAR images to estimate the height corresponding to a resolution cell (Chapter 2.1.4.1). In this regard, the distributed scatterers within one resolution cell are treated like one single scatterer (Woodhouse 2005: pp. 259-303). The phase estimate of each pixel is related to an average value corresponding to all scatterers (i.e., scattering phase center). Considering resolution cells covered by forest, the scattering phase center is based on several vertically distributed scatterers (e.g., leaves, branches and tree trunks) and is located somewhere between the top of the canopy and the underlying ground surface dependent on canopy structure, incidence angle and wavelength. As depicted in Fig. 2.2, the penetration capability of the SAR signal increases with increasing wavelength, which in turn leads to a scattering phase center closer to the ground (Rosen et al. 2000). Therefore, even in X-band, the interferometrically retrieved DSM represents a surface below the top of the canopy. By subtracting the LiDAR-based DTM which corresponds to the ground surface, the DSM is normalized. The resulting normalized DSM (nDSM) is referred to as scattering center height (see Fig. 3.2) and underestimates the actual vegetation height.

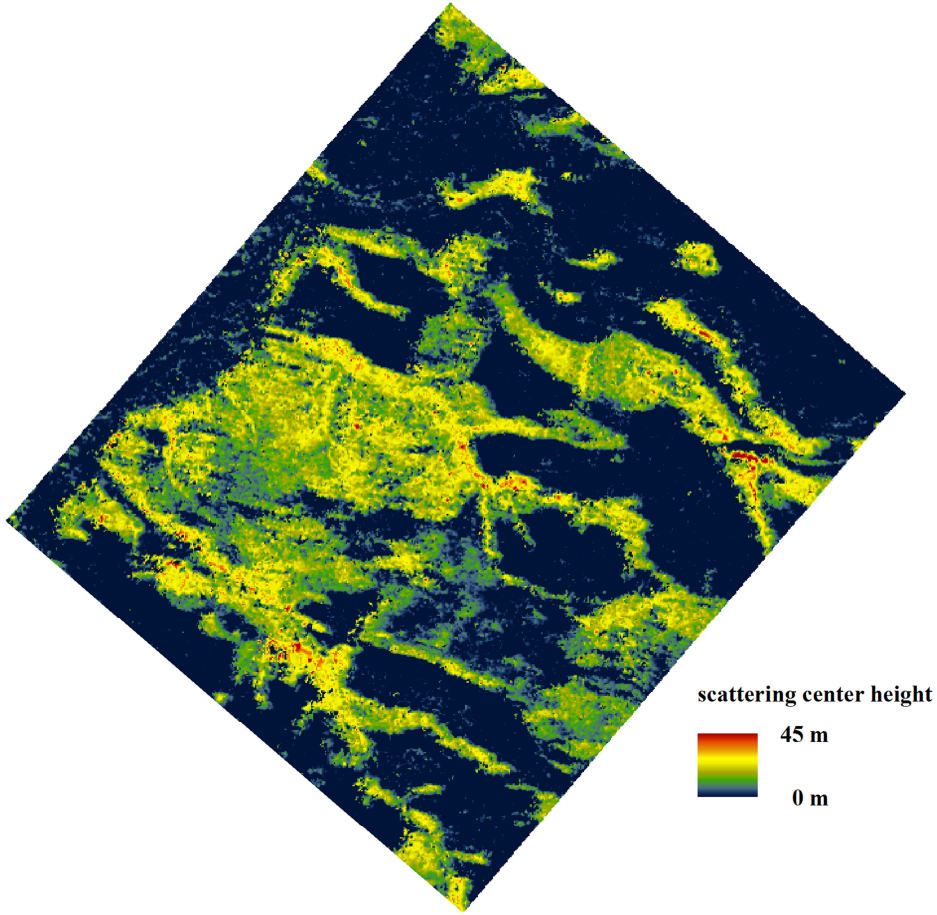


**Fig. 3.2:** Scattering center height based on HH-polarized TanDEM-X InSAR acquisitions from August 12, 2013.

### 3.2.2 Model-based Top Height

Decorrelation (Chapter 2.1.4.3) caused by different projection of 3-d scatterers into the two SAR images due to the spatial baseline  $\gamma_{geo}$  can be decomposed into range spectral decorrelation  $\gamma_{rg}$ , azimuth spectral decorrelation  $\gamma_{az}$  and volume decorrelation  $\gamma_{vol}$  (Moreira et al. 2013)

$$\gamma_{geo} = \gamma_{rg} \cdot \gamma_{az} \cdot \gamma_{vol}, \quad (3.1)$$

while range and azimuth spectral decorrelation are compensated by spectral band filtering, volume decorrelation is used to extract information about the vertical structure of the target. Volume decorrelation is related to the vertical distribution of scatterers  $F(z)$  through a (normalized) Fourier transformation relationship and can be expressed as

$$\gamma_{vol} = \exp(ik_z z_0) \frac{\int_0^{h_v} F(z') \exp(ik_z z') dz'}{\int_0^{h_v} F(z') dz'}, \quad (3.2)$$

with

$$k_z = \frac{2m\pi\Delta\theta}{\lambda\sin(\theta_i)} = \frac{2\pi}{HoA}, \quad (3.3)$$

where  $h_v$  is the height of the volume,  $k_z$  is the effective vertical wavenumber that depends on the imaging geometry,  $z_0$  is a reference height,  $z$  is the vertical position, and  $\Delta\theta$  is the incidence angle difference between the SAR images.

The estimation of  $F(z)$  from  $\gamma_{Vol}$  enables the derivation of the volume height within a resolution cell. For this purpose, multilayer statistical models which consider different scattering and propagation properties at different volume heights are applied for height estimation. A commonly used model for vegetation height estimation is a two-layered statistical model referred to as the Random Volume over Ground (RVoG) model (Treuhaft et al. 1996). The key idea of the RVoG model is to interpret the interferometric coherence dependent on the vertical distribution of scatterers along the volume height. The decrease of backscatter along the volume height caused by the attenuation of the signal (i.e., extinction) during its propagation through the volume is represented by the vertical backscatter function. The vegetation height can then be inverted with respect to extinction and ground influence. The vegetation layer is modeled as a volume layer with randomly oriented and distributed scatterers above a ground layer. Therefore,  $F(z)$  is composed of the volume scattering contribution and the ground scattering contribution and can be expressed as

$$F(z, \vec{w}) = f(z, \vec{w}) + m_G(\vec{w})\delta(z - z_0), \quad (3.4)$$

with the Dirac-like component

$$m_G(\vec{w})\delta(z - z_0), \quad (3.5)$$

as ground scattering amplitude, where  $\vec{w}$  indicates the different polarizations. Substituting ( 3.4 ) into ( 3.2 ) leads to

$$\gamma_{Vol}(k_z, \vec{w}) = \exp(i\phi_0) \frac{\tilde{\gamma}_{Vo} + m(\vec{w})}{1 + m(\vec{w})}, \quad (3.6)$$

with

$$\tilde{\gamma}_{Vo} = \frac{\int_0^{h_v} f_v(z') \exp(ik_z z') dz'}{\int_0^{h_v} f_v(z') dz'}, \quad (3.7)$$

as volume contribution of coherence in dependence of the vertical distribution of the scatterers in the vegetation layer  $f(z)$  and



$$m(\bar{w}) = \frac{m_G(\bar{w})}{\int_0^{h_v} f_v(z') dz'}, \quad (3.8)$$

as the effective ground-to-volume amplitude ratio accounting for the attenuation through the volume, where  $\phi_0$  denotes the phase related to the ground topography.

Due to the attenuation of the signal during its transition through the volume, as assumed for higher frequencies like X-band, the vertical distribution of the scatterers in the vegetation layer  $f(z)$  is modeled using an exponential function expressed as

$$f_v(z) = \exp\left(\frac{2\sigma z}{\cos(\theta_i)}\right), \quad (3.9)$$

where  $\sigma$  is the mean extinction for the vegetation layer indicating the attenuation of the signal (Papathanassiou & Cloude 2001). A schematic illustration of the RVoG model is given in Fig. 3.3.

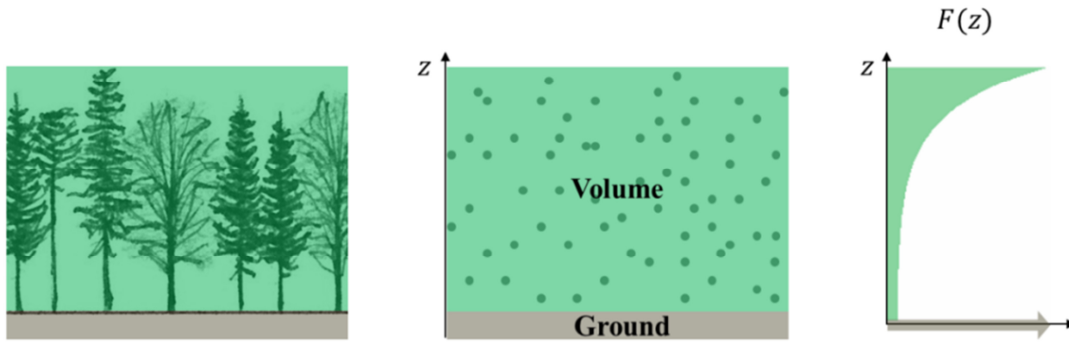


**Fig. 3.3:** Schematic illustration of the RVoG model with **a)** the two-layered representation of the forest, **b)** its simplified representation and the **c)** backscatter function along the height of the volume.

In terms of height estimation of the volume, ( 3.6 ) can be inverted. However, a single interferometric acquisition is not sufficient to solve the inversion problem. Therefore, several complex coherence measurements based on different baselines, frequencies or polarizations are required (Cloude & Papathanassiou 2003; Kugler et al. 2011; Kugler et al. 2014). In case of single-polarized data (i.e., HH or VV), the parameterization of the measured interferometric coherence in terms of ( 3.6 ) requires four parameters: vegetation height  $h_v$ , extinction  $\sigma$ , ground topography phase  $\phi_0$  and ground-to-volume amplitude ratio  $m(\bar{w})$  (Kugler et al. 2014). Since the assumption of no ground contribution is not sufficient to solve the inversion problem, additional assumptions or external information is required. In order to avoid restrictions on the performance of the RVoG model, the application of an external DTM (e.g., LiDAR-based DTM) for estimation of the ground topography phase  $\phi_0$  is suited. For this purpose, the DTM has to be converted to phase according to

$$\exp(i\phi_{DTM}) = \exp(ih_{DTM}k_z). \quad (3.10)$$

After calibrating the phase offset between the derived ground topography phase and the coherence by means of a corner reflector or a bare area with sufficient high coherence (i.e.,  $|\tilde{\gamma}(k_z, \bar{w}_i)| > 0.98$ ), vegetation height can be inverted by

$$\min_{h_v, \sigma} \|\tilde{\gamma}(k_z, \bar{w}_i) \exp(-i\phi_0) - \tilde{\gamma}_{V_0}(k_z, h_v, \sigma)\|. \quad (3.11)$$

Considering a forested area, the inverted height represents the top height (see Fig. 3.4) of the forest which is defined as the average of the hundred thickest trees (i.e., largest dbh) per hectare (Kugler et al. 2011).

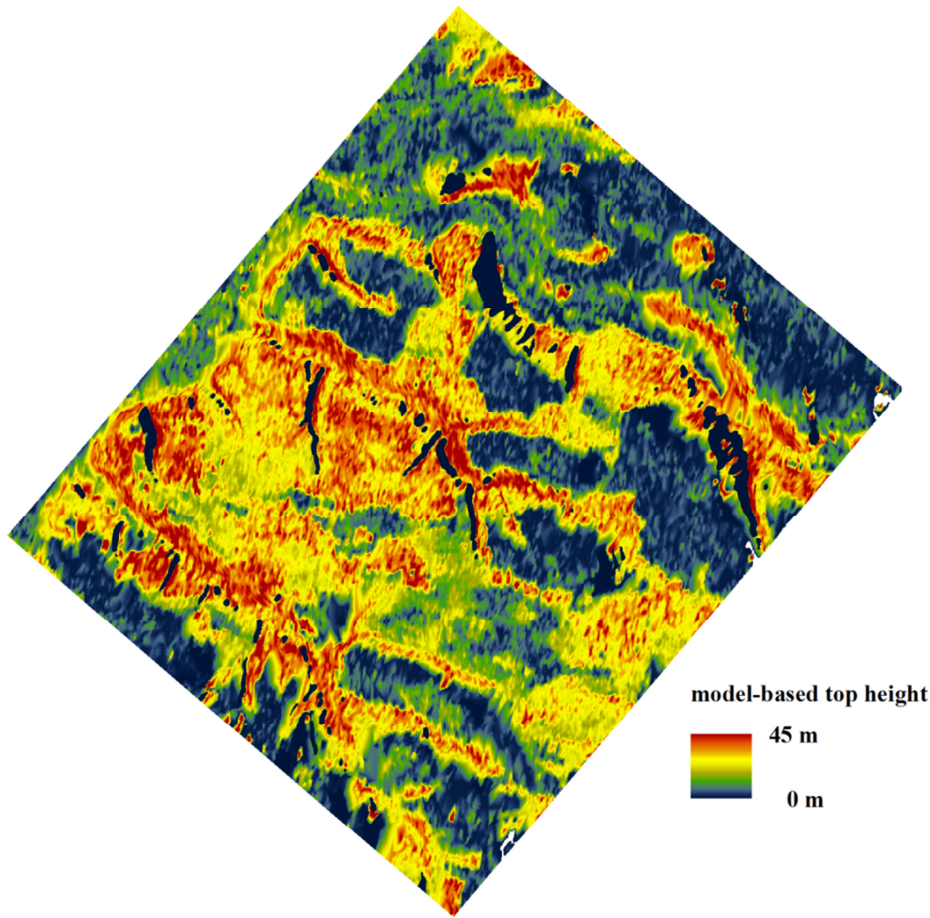


**Fig. 3.4:** Model-based top height based on HH-polarized TanDEM-X InSAR acquisitions from August 12, 2013, areas of NoData are marked black.

### 3.2.3 LiDAR-based Tree Height

A LiDAR-based nDSM was generated for verification of forest structure classification by subtracting the LiDAR-based DTM from the LiDAR-based DSM. The nDSM represents the vegetation height with a spatial resolution of 1 m and thus also reflects gaps between the plants as shown in Fig. 3.5. By using a threshold of 3 m, the nDSM was categorized into forest ( $\geq 3$  m) and non-forest ( $< 3$  m) (i.e., grassland and very small vegetation). The resulting LiDAR-based tree heights were applied for canopy cover estimation at units of

24 x 24 m<sup>2</sup> (corresponding to the spatial units of the forest classifications). Subsequently, the area percentage of height values  $\geq 3$  m per unit was calculated indicating canopy closure. Finally, the data was classified according to the degree of canopy closure into two classes: closed canopy ( $> 90\%$  of the considered area unit possess height values  $\geq 3$  m) and open canopy ( $\leq 90\%$  of the considered area unit possess height values  $\geq 3$  m).

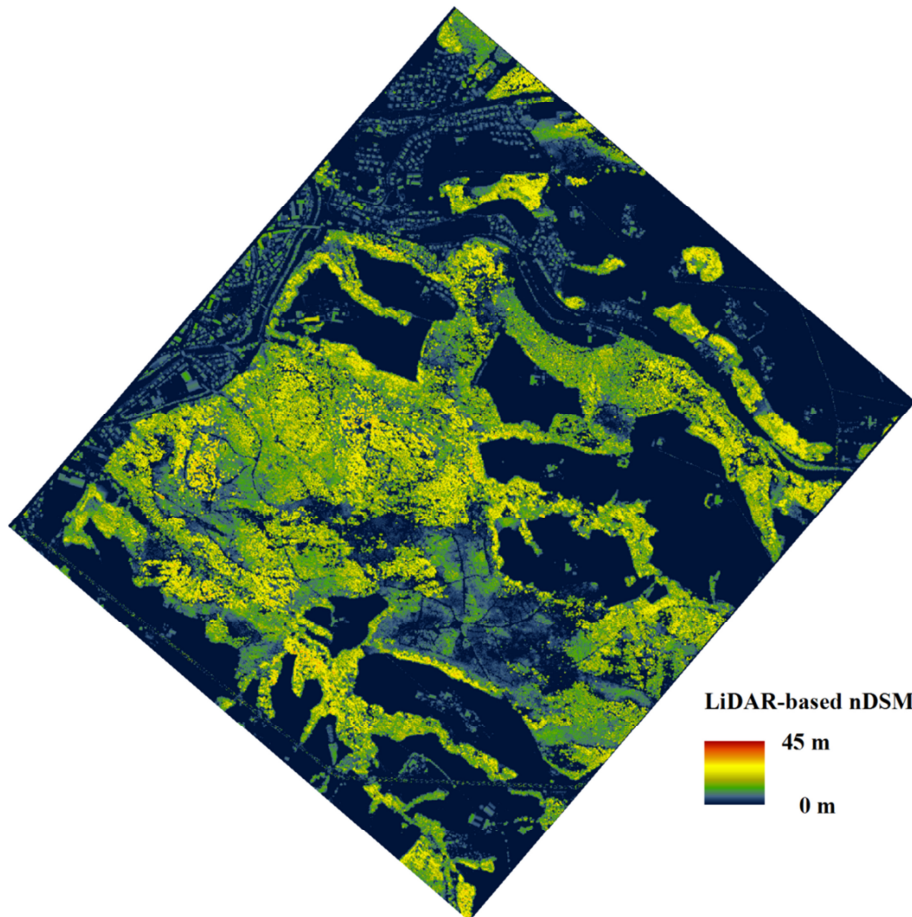


**Fig. 3.5:** LiDAR-based nDSM from November 18, 2012.

### 3.3 Forest Inventory Data

Terrestrial measurements of the forests' condition, which are usually acquired within the scope of forest inventories, were used for calibration and validation of stem volume retrieval and forest structure assessment. Parameters like stand density, basal area or height are collected to assess conservation and sustainability as well as temporal and spatial changes in forest structure and thus provide a basis of decision-making at local, national and global level (Gao et al. 2014; Kuuluvainen et al. 1996). Traditional forest inventories at national, federal and enterprise level are usually conducted based on sampling which is designed in a way to ensure representativity (Pretzsch 2009: pp. 112-120). In principle, a few practice-oriented basic forest parameters, such as tree height, dbh and tree species are repeatedly recorded typically on a common cycle of ten years in Germany.

The systematic inventory comprises 228 permanent circular sampling plots in the study area of Traunstein forest and has been repeated regularly since 1988 with the latest inventory in August 2013. The field data

of forest condition and the dynamics of stand parameters are collected according to the survey guidelines for forest inventory of the Bavarian State Forest Enterprise (Bayerische Staatsforsten 2011). All inventory plots are arranged on a regular 100 m by 100 m sampling grid (i.e., corresponding to a sampling density of one plot per hectare) (Fig. 3.6a). Each circular inventory plot covers an area of 500 m<sup>2</sup> and its center is permanently marked by a buried loadstone. Consequently, surveys can be easily repeated and the sampling error for alterations of the stand parameters can be reduced. Each inventory plot is partitioned into three concentric sub-circles with radii of 12.62 m, 6.31 m and 3.15 m, respectively. In order to measure on a sample basis, a specific dbh threshold is defined for each sub-circle as depicted in Fig. 3.6b.

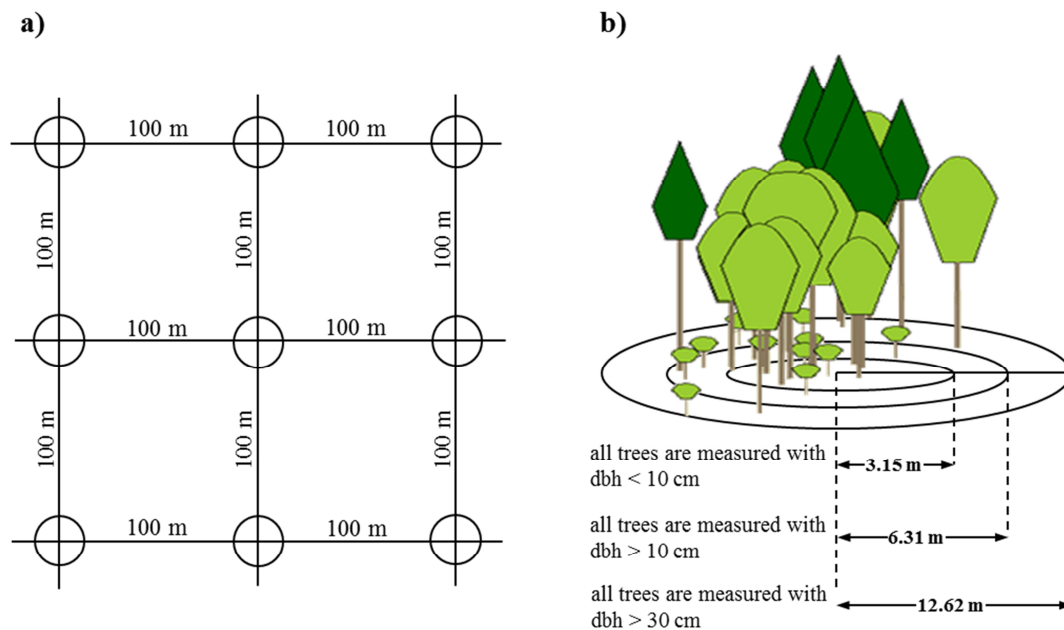


**Fig. 3.6:** a) Inventory sampling grid and b) thresholds in diameter measuring. Based on Abdullahi et al. (2016).

Accordingly, all trees with dbh > 30 cm within the largest circle (with radius 12.62 m), all trees with dbh > 10 cm within the middle circle (with radius 6.31 m) and all trees with dbh < 10 cm within the smallest circle (with radius 3.15 m) are recorded. The dbh and the polar coordinates (azimuth and range relative to the center of the plot) are gathered for any tree above the relevant threshold value of dbh. Tree height measurements are taken for a representative sample of each tree species per stand layer. In addition, other tree and forest stand attributes such as species, age, layering, damages, dead wood, and stem quality are recorded for each inventory plot.

### 3.3.1 Tree Height

Since tree height is not measured for all trees within the inventory plot, stand height curve systems are applied on the measured height sample to estimate the tree height for each recorded tree (Pretzsch 2009: pp. 186-197). Within a forest stand a non-linear statistical relationship between dbh and tree height exists. This relationship describes an increase of height with increasing dbh, as exemplary illustrated in Fig. 3.7. Such a height curve system can be derived graphically or by means of regression analysis based on in-situ

measurements of diameter and tree height for each forest stand. The deduced height-curve system enables height estimation for each tree with known (i.e., measured) diameter within the forest stand.

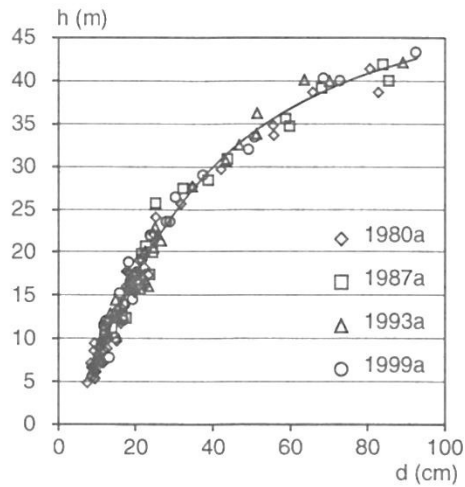


**Fig. 3.7:** Development of stand-height-curves (where  $h$  is height and  $d$  is diameter) in a Norway spruce-Silver fir-European beech selection forest based on inventory data from 1980, 1987, 1993, 1999 at a forest test site in Bavaria, Germany. From Pretzsch (2009: p. 189).

### 3.3.2 Stem Volume

For calibration and validation purposes, stem volume per hectare was derived from the in-situ measurements by means of tree height and dbh. Stem volume of each single tree was calculated according to a reference cylinder as depicted in Fig. 3.8. Accordingly, the height of the reference cylinder corresponds to the height of the considered tree and the area of circle is equivalent to the basal area at breast height (1.30 m) of the considered tree (i.e., diameter corresponding to dbh). Since the stem of a tree is tapered off with increasing height, the volume of the reference cylinder is reduced to the stem volume of the considered tree by multiplying the form factor according to ( 3.12 ) (Pretzsch 2009: pp. 196-199).

$$v = c \cdot f_{1.3}, \quad (3.12)$$

with

$$c = ba \cdot h, \quad (3.13)$$

where  $v$  is the stem volume of the tree,  $c$  is the volume of the cylinder,  $f_{1.3}$  is the form factor,  $ba$  is the basal area of the tree and  $h$  is the height of the tree.

The form factor is either related to merchantable wood, i.e., all above ground wood with a dbh > 7cm, or stem wood including the tree shaft of the considered tree only. In this case, the merchantable wood volume was estimated. The form factors for the most important tree species are derived according to Franz

et al. (1973). In a final step, the calculated stem volume of all trees within the considered inventory plot are summarized and extrapolated to the representation area of one hectare by means of a defined representation number per tree.

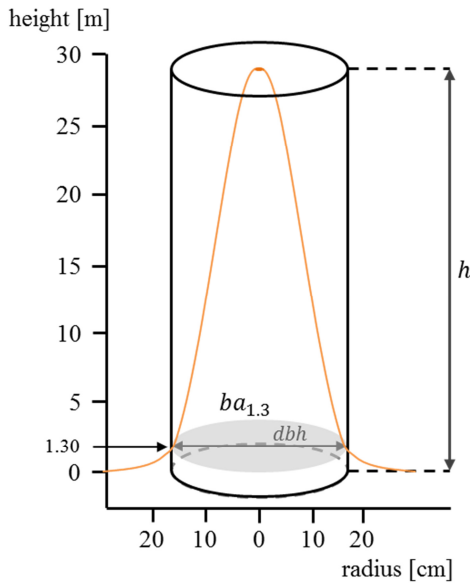


**Fig. 3.8:** Schematic representation of a reference cylinder for stem volume calculation. Based on Pretzsch et al. (2002).

Stem volume per hectare is calculated based on tree height, basal area (derived from dbh) and a form factor for all living trees according to ( 3.14 ).

$$V = \sum_{i=1}^N ba_i \cdot h_i \cdot f_{1.3i} \cdot r_i , \quad ( 3.14 )$$

where  $V$  is stem volume per hectare,  $N$  is the number of trees within the plot,  $ba_i$  is the basal area of tree  $i$ ,  $h_i$  is the height of tree  $i$ ,  $f_{1.3i}$  is the form factor of tree  $i$  and  $r_i$  is the number of representation per hectare of tree  $i$ .

According to Kramer & Akça (1987), the error for volume estimations based on field measurements can be commonly assumed as  $\pm 10 - 15 \%$ .

In the study area, stem volume per hectare ranges from  $0 \text{ m}^3\text{ha}^{-1}$  up to  $1049 \text{ m}^3\text{ha}^{-1}$  as shown in Tab. 3.1 containing the minimum, mean and maximum values of inventory parameters.

**Tab. 3.2:** Statistics of forest parameters per plot acquired during forest inventory 2013. Volume is specified as timber harvested ( $> 7 \text{ cm}$  at the smaller end) without bark. From Abdullahi et al. (2016).

	mean stem diameter [cm]	mean tree height [m]	stand basal area [ $\text{m}^2\text{ha}^{-1}$ ]	standing volume [ $\text{m}^3\text{ha}^{-1}$ ]
<b>min</b>	0.00	0.00	0.00	0.00
<b>mean</b>	32.44	23.24	28.80	312.82
<b>max</b>	67.53	40.20	83.50	1049.00

### 3.3.3 Forest Structure

In order to characterize the vertical stand structure by means of the in-situ measurements, the collected information on stand layering was used to classify each inventory plot according to the number of canopy layers. In the scope of the field survey, each recorded tree was assigned to a category dependent on development stage (e.g., overstory, understory and regeneration). Using this information, each inventory plot was classified into three classes comprising one-layered, two-layered and multi-layered forest stands. For example, an inventory plot containing trees solely assigned to “regeneration” was categorized as one-layered, while an inventory plot comprising trees assigned to “understory” as well as “overstory” was classified as two-layered. According to this principle, each inventory plot was classified.

Furthermore, a 3-d representation of each inventory plot was rendered based on the measurements of tree dimensions, species and tree positions according to Pretzsch et al. (2002) as illustrated in Fig. 3.9. These visualizations enable a better comprehension of the forest structure and its complexity and were additionally used for visual validation.

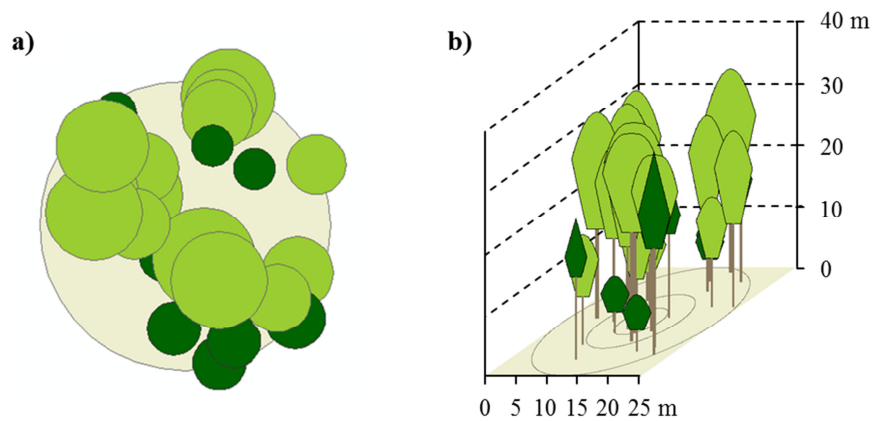


**Fig. 3.9:** a) Plan view of an inventory plot with b) the corresponding 3-d representation where light green represents broadleaf tree species and dark green represents coniferous tree species.

## 4 Methodology and Results

### 4.1 Stem Volume Estimation (Publication I)

Stem volume in  $\text{m}^3\text{ha}^{-1}$  was estimated at plot (circular plots of  $500 \text{ m}^2$ ) and stand (areas of 1.5 to 6.4 ha) level by means of X-band InSAR data using linear regression (Abdullahi et al. 2016) (see **Appendix A**). Forest height information was extracted from two interferometric dual-polarized TanDEM-X InSAR data sets corresponding to leaf-on (May 18, 2013) and leaf-off (January 01, 2012) season, respectively (see Chapter **3.2**). For each acquisition date, a DSM was calculated from the interferometric TanDEM-X data (see Chapter **2.1.4.2**). Using a LiDAR-based DTM as external terrain information, scattering center height was derived from the DSM (see Chapter **3.2.1**). Model-based top height was derived by applying the RVoG model (see Chapter **3.2.2**). Based on these input data sets, linear regression models based on scattering center height and model-based top height were developed using the allometric relationship between tree height and stem volume (see Chapter **2.2.1.1**). Field measurements of stem volume acquired in the course of the last inventory in Traunstein forest (see Chapter **3.3**) were used to fit the linear regression models for scattering center height and model-based top height from leaf-on and leaf-off season, respectively. These models were applied and evaluated at plot as well as stand level. However, besides forest height, horizontal forest structure is an essential factor regarding stem volume per hectare (see Chapter **2.2.1.2**). In order to improve the estimation results, the regression model was extended by integrating novel parameters derived from the Co-occurrence Matrix according to Haralick (1971) at plot level as surrogate for forest structure measures at stand level like SDI to include within-stand growth determinants (see Chapter **2.2.1.2.1**). The estimation of stem volume at plot level yielded better results for scattering center height compared to model-based top height. Scattering center height based on the acquisitions corresponding to leaf-on season yielded the best results with  $R^2$  of 60 % at plot level. The extension of this linear model by the Co-occurrence parameters improved the results and achieved predictions with  $R^2$  of 69.92 % and RMSE of about  $155.00 \text{ m}^3\text{ha}^{-1}$  (RMSE related to mean stem volume = 41.90 %). Therefore, stem volume estimations were improved in order of almost 10% with respect to the coefficient of determination. Quantifying the contribution of the Co-occurrence parameters according to the relative importance metric of Proportional Marginal Variance Decomposition (PMVD) (Grömping 2006), the Co-occurrence parameters possessed a contribution of 12.54 % of the explained variance of stem volume. Slight saturation effects occurred at about  $400 \text{ m}^3\text{ha}^{-1}$ . At stand level, stem volume predictions improved substantially compared to the results at plot level. In consistency to the results at plot level, stem volume estimations were more accurate based on scattering center height than based on model-based top height. The best results at stand level with  $R^2$  of 88 % and RMSE of about  $73 \text{ m}^3\text{ha}^{-1}$  were achieved using scattering center height corresponding to leaf-on season. The extension of this linear model yielded predictions with  $R^2$  of 0.94 and RMSE of  $44.25 \text{ m}^3\text{ha}^{-1}$ . At stand level no obvious saturation effects occurred. In general, scattering center height was found more suitable for stem volume estimation as well as application of the Co-occurrence parameters compared to model-based top height since it reflects the height variation in more detail. Furthermore, scattering center height corresponding to leaf-on season turned out preferable for stem volume estimation due to less penetration of the SAR signal and thus more accurate height estimation. Finally, the inclusion of parameters based on the Co-occurrence matrix describing forest structure improved stem volume predictions substantially.



## 4.2 Forest Structure Classification (Publication II)

An unsupervised two-stage clustering approach for forest structure classification based on X-band InSAR data was proposed and demonstrated in the complex temperate forest stands of Traunstein forest (Abdullahi et al. 2017) (see **Appendix B**). In particular, the classification process was composed of two partitional clustering methods, the Self-Organizing Map (SOM) according to Kohonen (1982) in the first stage and k-means (MacQueen 1967) in the second stage, which was introduced as an efficient unsupervised classification strategy by Vesanto & Alhoniemi (2000). The scattering center height was derived from an interferometric TanDEM-X acquisition acquired in May 2013 (see Chapters **2.1.4.2** and **3.2.1**). Based on this height data set, four first order statistics (i.e., minimum height, mean height, maximum height and standard deviation of height) were calculated for objects of 24 x 24 m<sup>2</sup> which were distributed gapless across the study area. The object size of 24 x 24 m<sup>2</sup> was chosen since forest successional processes take place at this spatial scale (see Chapter **2.2.2.2**). Besides, this spatial scale corresponds to the size of an inventory plot which facilitates the validation of the classification results. The normalized four-dimensional data set was non-linearly projected on the two-dimensional SOM and spatially ordered according to similarity based on the Euclidean distance in order to cluster the data and extract its fine structure. Subsequently, the derived clusters were summarized using k-means to achieve a reasonable and meaningful number of forest structure classes. A crucial parameter of the k-means algorithm is the number of clusters which was determined according to the “knee-point method” (Manning et al. 2008: pp. 360-367). In a final step, the resulting classes were labeled corresponding to their characteristics by means of height histograms for each cluster, an orthophoto and the LiDAR-based nDSM. In total, nine forest structure classes were distinguished according to spatial heterogeneity: Stand Initiation, Closed Canopy One-Stratum I-IV, Closed Canopy Multi-Strata, Open Canopy Two-Strata I-II and Open Canopy Multi-Strata. Stand Initiation contains all objects related to almost treeless areas where the sparsely represented vegetation is very low (< 3 m). Closed Canopy One-Stratum I-IV include objects which possess small height variation indicating forest stands with one closed canopy layer. The mean height increases from Closed Canopy One-Stratum I to Closed Canopy One-Stratum IV. Closed Canopy Multi-Strata exhibits much higher variation in height without very low values suggesting multi-layered forest stands with mainly closed canopy. Open Canopy Two-Strata I and Open Canopy Two-Strata II are characterized by high variations in height, but possess a considerable amount of very low height values, which implies forest gaps. Accordingly, both classes contain objects which are related to two-layered forest stands with an open canopy layer and gaps or low understory consisting of seedlings, shrubs and small trees. However, the main canopy layer of Open Canopy Two-Strata I is lower compared to the main canopy layer of Open Canopy Two-Strata II. Open Canopy Multi-Strata encompasses the highest variation in height. Very low height values indicate gaps or areas with very small vegetation while very high values are related to the tallest trees within the study area. Considering the height distribution, this cluster is related to multi-layered forest stands. Thus, this study demonstrated the capability of X-band InSAR data to capture the heterogeneity in height of the main forest layer and proposed an efficient unsupervised approach to classify forest structure in complex temperate forest stands. Visual validation using an orthophoto and a LiDAR-based nDSM confirmed the validity of the classification approach excluding limitations in accuracy due to X-band InSAR system. However, in order to provide more objective validation of the classification result, information based on forest inventory (see Chapter **3.3.3**) as well as LiDAR-based measurements (see Chapter **3.2.3**) were used additionally (see Chapter **4.3**).

### 4.3 Seasonal Effects on Forest Structure Classification (Publication III)

Forest structure classification was applied to multi-temporal X-band InSAR data corresponding to different polarization modes in order to assess the impact of phenology and polarization mode on forest structure assessment in complex temperate forests (Abdullahi et al. Submitted) (see **Appendix C**). In total, four TanDEM-X InSAR data sets from August 12, 2013 and March 09, 2014 acquired in HH-polarization and VV-polarization under very similar acquisition as well as weather conditions were used (see Chapter 3.2). The InSAR data sets of August 2013 recorded Traunstein forest under leaf-on conditions, while the InSAR data sets of March represented the forest in the leaf-off season. Especially the acquisition under very similar conditions (i.e., almost identical incidence angle, similar baseline and HoA) enabled the investigation of season-dependent changes in forest structure detection. Scattering center height was derived for all data sets (see Chapters 2.1.4.2 and 3.2.1) and the unsupervised classification approach according to Abdullahi et al. (2017) was applied (see **Appendix B**). For validation purposes, field measurements collected within the forest inventory in 2013 were categorized regarding the number of canopy layers (see Chapter 3.3.3) and the LiDAR-based nDSM was used to estimate canopy closure (see Chapter 3.2.3) related to the nine forest structure classes enumerated in Chapter 4.2. The classification results demonstrated that the phenological development stage of trees has a high impact on forest structure assessment in broadleaf-dominated forest stands, while coniferous forest stands were mainly unaffected. The differences between leaf-on and leaf-off season became clearly visible in HH polarization, whereas the differences were less distinct in VV polarization. The actual vegetation height was underestimated in the leaf-on as well as leaf-off season based on VV-polarized as well as HH-polarized data due to penetration of the SAR signal, whereas the most accurate height estimations could be achieved using VV-polarized InSAR data under leaf-on conditions. It was proven that the understory could not be detected below a dense canopy despite the penetration ability of the X-band SAR signal, which led to an overestimation of one-layered stands at simultaneous underestimation of two- and multi-layered stands. In general, the InSAR data set related to leaf-on season and HH polarization yielded the best classification result in coniferous forest stands while in case of broadleaf forest stands InSAR data corresponding to leaf-off season and HH polarization achieved the best result. Concerning canopy closure, the InSAR data related to winter (i.e., leaf-off) season and HH polarization led to the best results in coniferous forest stands, whereas the data based on summer (i.e., leaf-on) season and HH polarization achieved the best classification results in broadleaf forest stands. Summarizing, VV-polarized InSAR data related to leaf-on season is preferable to estimate height, whereas HH-polarized InSAR data corresponding to leaf-off season is more suitable to capture forest stand layering and canopy closure.

## 5 Discussion

This thesis investigates the potential of interferometric X-band InSAR data for detection and definition of forest structure in a complex temperate forest consisting of unevenly aged mixed forest stands with high range in stem volume and high species richness in different development stages. Stem volume retrieval based on InSAR height was demonstrated at plot level as well as stand level. The predictions were improved by including texture parameters describing the forest stand structure in the regression model. Moreover, an automated unsupervised classification approach was developed to distinguish different forest structure types and its applicability for mixed temperate forests was demonstrated. Furthermore, the influence of phenology on forest structure detection regarding the differences between leaf-on and leaf-off season dependent on polarization mode was explored.

Stem volume estimations (see Chapter 4.1) yielded similar or even superior results compared to previous studies using X-band InSAR data. At plot level (plot size of 500 m<sup>2</sup>), the best results were obtained by using the extended regression model employing InSAR height and derived texture parameters with R<sup>2</sup> of about 0.70 and RMSE of 155 m<sup>3</sup>ha<sup>-1</sup> (relative RMSE of 41.90 %). In comparison, Karila et al. (2015) estimated stem volume at plot level (plot size of about 300 m<sup>2</sup>) in the best case with RMSE of about 67.2 m<sup>3</sup>ha<sup>-1</sup> (relative RMSE = 32.2 %) and R<sup>2</sup> of about 0.65 in spruce and pine dominated boreal forest stands using a nearest neighbor prediction model based on TanDEM-X InSAR heights. Rahlf et al. (2014) estimated stem volume by means of a linear mixed model based on interferometric TanDEM-X data in spruce and pine dominated forest stands at plot level (plot size of 250 m<sup>2</sup>) with RMSE of 77.56 m<sup>3</sup>ha<sup>-1</sup> (relative RMSE of 41.60 %). In Solberg et al. (2013) stem volume predictions at plot level (plot size of 250 m<sup>2</sup>) with RMSE of about 94 m<sup>3</sup>ha<sup>-1</sup> (relative RMSE = 44 %) were achieved for spruce dominated boreal forest stands using linear regression based on height information derived from TanDEM-X data. Gama et al. (2010) demonstrated stem volume estimation by linear regression in tropical Eucalyptus plantations using interferometric airborne SAR data at plot level (plot size of about 400 m<sup>2</sup>) and achieved best results with RMSE of 33.56 m<sup>3</sup>ha<sup>-1</sup> (relative RMSE = 10.55 %) and R<sup>2</sup> of about 84 %. However, airborne data with considerable higher spatial resolution were used in this study. At stand level the extended regression model of this thesis yielded the best prediction results with R<sup>2</sup> of 94 % and RMSE of 44.25 m<sup>3</sup>ha<sup>-1</sup> (relative RMSE of 16.53 %). These results are comparable to stem volume estimations at stand level (stand size 1-3 ha) in less structured spruce and pine dominated boreal forest reported by Rahlf et al. (2014) with RMSE of about 33.74 m<sup>3</sup>ha<sup>-1</sup> (relative RMSE = 18.10 %) and Solberg et al. (2013) with R<sup>2</sup> of 81 % and RMSE of about 44 m<sup>3</sup>ha<sup>-1</sup> (relative RMSE = 20%). In the context of the previous studies, the results of the stem volume retrieval within this thesis are very promising in view of the fact that the estimations obtain similar or even better accuracies although the study area is composed of very complex, more structured and heterogeneous forest stands.

The development and application of the unsupervised two-stage clustering approach (see Chapter 4.2) demonstrated the discriminability of different forest structure types by means of X-band InSAR data. Several other studies investigated the potential of InSAR data for the detection of forest structure, but most of these studies estimated forest attributes describing stand structure in boreal forests without classification of forest structure types (e.g., Karila et al. 2015; Karjalainen et al. 2012; Solberg et al. 2010). Only few studies discussed the classification of forest structure types based on InSAR data (e.g., De Grandi et al. 2015; Liesenberg & Gloaguen 2013; Hoekman & Quiñones 2002). Moreover, these studies were mostly carried out in tropical

forests, whereas the current work investigated the utilization of X-band InSAR data for forest structure classification in temperate forests. Furthermore, the proposed classification approach enables handling of huge amounts of data automatically without any a priori information. The first-order statistics of InSAR height as a basis of the classification process are straightforward and easy to obtain. However, further investigations regarding the ability of the first-order statistics to fully capture the complexity of the forest structure are required. Huang et al. (2014) argued that first-order statistics are not sufficient to entirely detect the heterogeneity of forest stands, since they are not sensitive to the spatial arrangement of the trees. Nonetheless, the validation by means of in-situ measurements and LiDAR data showed promising results in case of horizontal forest structure. On the other hand, classification accuracies suffer from limitations caused by the relatively short wavelength of X-band. The vertical forest composition could not be completely detected due to the low penetration of the X-band SAR signal into the forest. The understory below dense canopies could not be captured which leads to overestimation of one-layered forest stands and underestimation of two- and multi-layered forest stands in the classification process. In general, a variety of parameters are used to describe and capture forest structure (see Chapter 2.2.2), however only a small fraction of these parameters can be detected by SAR-based technologies dependent on wavelength. Especially X-band InSAR enables the assessment of forest structure parameters related to height distribution and canopy closure of the main canopy layer (i.e., roughness of the canopy) only. Furthermore, the detection of these parameters strongly depends on the spatial resolution of the SAR data. Only high spatial resolution facilitates detailed capture of fine height variations and small gaps in the canopy. Therefore, the detection and definition of forest structure by means of X-band InSAR data is highly restricted and must be combined with additional data sources (e.g., field measurements, LiDAR surveys and optical remote sensing data) in order to capture forest structure comprehensively.

In this thesis, the influence of phenology on forest structure assessment by means of X-band InSAR data dependent on polarization mode was demonstrated comparing data acquired in leaf-on season and with data acquired in leaf-off season (see Chapter 4.3). Only few studies discussed the seasonal dependency on forest assessment by means of X-band InSAR data. Studies carried out in broadleaf and mixed forest stands (e.g., Olesk et al. 2015; Kugler et al. 2014) found less penetration into the forest in the leaf-on season compared to the leaf-off season. In contrast, investigations carried out in coniferous forest stands (e.g., Sadeghi et al. 2017; Solberg et al. 2015) reported no significant difference between leaf-on and leaf-off season. In accordance with these findings, the investigations within this thesis indicated no significant effect of phenology on forest assessment in coniferous forest stands by means of X-band InSAR, whereas over broadleaf forest stands an essential influence due to phenological differences between leaf-on and leaf-off season was detected. In general, higher penetration of the SAR signal was detected in the leaf-off season compared to the leaf-on season. The absence of leaves yields a decrease of relevant scatterers in the upper part of the canopy and thus leads to deeper penetration of the RaDAR signal. Regarding polarization mode, the effect of phenology was found to be more significant in case of HH polarization compared to VV polarization. The actual vegetation height was underestimated in all data sets (i.e., from leaf-on as well as leaf-off season based on VV- as well as HH-polarized InSAR data), where the most accurate height was derived using VV-polarized InSAR data corresponding to the leaf-on season. Admittedly, several studies explored the potential of InSAR data for forest structure assessment, but mostly disregarded the influence of phenology. Nevertheless, as demonstrated in this thesis, phenology considerably affects the assessment of forest structure. Especially regarding forest stands which are predominantly covered by broadleaf tree species, the classification results deviated significantly

between leaf-on and leaf-off season. While stem volume estimation as well as forest structure classification were mainly unaffected by seasonal variations in coniferous-dominated forest stands, the accuracies varied with season in broadleaf-dominated forest stands. Less accurate stem volume predictions were achieved using InSAR data from the leaf-off season caused by the underestimation of the actual vegetation height. The detection of stand layering was more accurate for coniferous-dominated compared to broadleaf-dominated forest stands. InSAR data acquired in leaf-on season demonstrated greater suitability for the detection of canopy closure within broadleaf-dominated forest stands. The comparison of the classification results corresponding to leaf-on and leaf-off season clarified the high impact of the phenological development stage on capturing forest structure based on a synoptic view. Therefore it is advisable to cautiously select the time of image acquisition with respect to the forest parameter under investigation. Moreover, to monitor the development of the forest structure within a certain time frame, it is of high importance to select data sets corresponding to the same phenological stage in order to mitigate the erroneous detection of changes caused by phenology. Beyond, the detected differences between leaf-on and leaf-off season present the prospect of monitoring and detecting seasonal changes in the course of the year. Well-chosen time series of X-band InSAR data facilitate detection of spatiotemporal phenology-related information about the forest. Especially in the context of ongoing climatic changes, time series provide the possibility to explore the shifting temporal cycle of phenological development stages. Moreover, the differences in penetration of the RaDAR signal between leaf-on and leaf-off season, which are mainly related to broadleaf-dominated forest stands, offer the opportunity to stratify forests according to coniferous and broadleaf tree species.

The polarization mode also showed an influence on forest structure assessment. In order to capture stand layering, HH-polarized data was found more suitable. In contrast, polarization mode had no significant influence on classification of canopy closure. Considering the best classification results in general, HH-polarized InSAR data from leaf-on season and HH-polarized data from leaf-off season should be preferred to estimate forest layering in coniferous and broadleaf forest stands, respectively. In addition, InSAR data from leaf-on season in HH polarization can be recommended to classify canopy closure.

All investigations within this thesis were conducted in the complex temperate forest of Traunstein comprising unevenly aged coniferous, broadleaf and mixed forest stands. This forest is characterized by high species richness and different development stages, which reflect a “close-to-nature” silviculture (Pretzsch et al. 2015). Tab. 5.1 summarizes and compares the general characteristics of global forest biomes according to Apps et al. (1993), Fischer (2003), Montagnini & Jordan (2005) and Thomas & Baltzer (2002). Boreal, temperate and tropical forests differentiate significantly regarding tree species diversity and structural complexity according to vertical and horizontal composition. While boreal forests are rather homogeneous, temperate and especially tropical forests possess higher tree species diversity and more complex stand structure. Regarding these differences in structural complexity, it is essential to investigate forest structure assessment in all forest biomes. Since the structural complexity influences biodiversity, productivity as well as growth of the forest, it is of high importance to take the variations of forests according to different forest biomes into account in order to monitor the world’s forests and to develop suitable forest management strategies. However up to now, studies exploring the potential of shortwave InSAR data for forest structure detection were mostly carried out in boreal (e.g., Karila et al. 2015; Rahlf et al. 2014; Solberg et al. 2013) and in tropical (e.g., De Grandi et al. 2015; Gama et al. 2010; Solberg et al. 2010) forest stands. Thus, further investigations are required to make use of InSAR data for

forest assessment. According to that, the current thesis contributes to exploit the potential of the globally available X-band InSAR data of the TanDEM-X mission regarding forest structure assessment in mixed, temperate forest stands.

**Tab. 5.1:** Generalized characteristics of the global forest biomes. From Abdullahi et al. (2016).

	<b>boreal forests</b>	<b>temperate forests</b>	<b>tropical forests</b>
<b>location</b>	circumpolar belt in high northern latitudes	between 25° and 50° on both hemispheres	between 25° and the equator
<b>climate</b>	short vegetation due to extreme weather conditions concerning temperature, precipitation and sunshine	oceanic, subcontinental and semi-aride and aride	wet and warm
<b>tree species</b>	limited number of tree species such as spruce, fir and pine	deciduous and evergreen species	dominated by evergreen or semi-deciduous species (typically 200-300 species per hectare)
<b>vertical structure</b>	closed canopy and low understorey	less dense canopy and more developed understorey	multi-layered

Furthermore, tree species composition should be considered in terms of forest assessment by means of InSAR data. The penetration capability of the SAR signal is affected by the canopy architecture and thus spatially differs mostly dependent on tree species. Therefore, InSAR height exhibits additional spatial variations as well as patterns which are independent from the actual vegetation height. Moreover, tree species composition is a crucial factor in the context of biodiversity. However, the proposed approach for forest structure detection and classification disregarded tree species composition. Therefore, further investigations are required to explore the influence of tree species composition on the backscattering process regarding InSAR data and thus on the detection of forest structure.

Besides, the obtained accuracies suffer from restrictions due to general limitations of the X-band InSAR data. First, the X-band SAR signal penetrates several meters into the forest canopy depending on forest structure, which yields an underestimation of the actual vegetation height and thus underestimation of stem volume. This effect is intensified using acquisitions corresponding to the leaf-off season in mixed and broadleaf forest stands. Regardless of the ability of the X-band SAR signal to penetrate into the upper part of the canopy, it is incapable to detect the understorey below a dense canopy. Therefore, the classification accuracies regarding layering are deteriorated in terms of an overestimation of one-layered forest stands. Consequently, the classification based on X-band InSAR data results in an underestimation of two- and multi-layered forest stands. To solve this problem, a combination of X-band with longer wavelengths (e.g., L-band) should be considered. The longer wavelengths would provide complementary information on forest layers below the main canopy due to the capability to penetrate deeper into the forest. In contrast to layering, the classification accuracies of canopy closure were found much better. Second, geometrical distortions (e.g., foreshortening, layover and shadowing) (see Chapter 2.1.3.2) lead to inaccurate height estimation and thus erroneous stem volume prediction and forest structure classification. Especially at small spatial units of about 500 m<sup>2</sup>, geometrical effects significantly influence the results. Regarding stem volume estimation at 500 m<sup>2</sup> units, only few measurements per inventory plot are involved in the predictions. Thus, geometrical effects have a higher impact and cause higher uncertainties and inaccuracies in stem volume estimation at plot level compared to stand level. However with respect to forest

structure, spatial units of about 500 m<sup>2</sup> are well-suited. Forest succession processes in “close-to-nature” forest stands take place on patches at this scale (see Chapter 2.2.2.2). These processes influence forest structure significantly, lead to changes in the canopy layer and thus, regulate the amount of available sunlight in the deeper forest layers by which the vertical architecture of the forest is affected. Accordingly, information about forest structure at this spatial scale is highly relevant in terms of sustainable forest management and biodiversity assessment. Thus, the classification results give evidence about the vertical structure of the forest stands as well as the complexity of the whole forest and thus serve as an indicator for biodiversity. Nevertheless, in order to increase classification accuracies, also larger spatial units should be considered for further investigations. Third, the processing and generation of the DEM itself include sources of error (see Chapter 2.1.4.3). Loss of accuracy can be caused by system noise, decorrelations due to temporal offset between acquisitions in case of repeat-pass interferometry or due to the slightly different sensor positions and thus slightly different incidence angles during image acquisition as well as terrain roughness (Marghany 2014; Moreira et al. 2013; Rosen et al. 2000). However, the TanDEM-X mission has the advantage of single-pass interferometry and thus enables acquisition of InSAR data without accuracy limitations due to temporal decorrelation (Krieger et al. 2013). Moreover, the TanDEM-X mission provides a global coverage of InSAR data.

Before the advantage of worldwide available consistent X-band InSAR data could be taken, the transferability of the proposed approaches for forest structure assessment must be validated. In case of stem volume retrieval, the use of an ancillary LiDAR-based DTM is the limiting factor since LiDAR surveys are not available worldwide. To overcome this problem, InSAR data based on longer wavelengths than X-band (like L- or P-band) can be applied additionally to derive information on ground elevation instead of a LiDAR-based DTM (Gama et al. 2010). Since the classification process for forest structure assessment is unsupervised without the requirement of any a-priori information about class numbers and definitions, this process is capable of global application. Nevertheless, the limitation that the labelling process is not fully automated and thus requires manual intervention must be considered. However, it can be assumed that the approach can be easily transferred to other forest stands by adaptation of the forest structure classes according to the users’ definitions and requirements. Accordingly, data from the TanDEM-X mission in combination with globally available data at L- or P- band (i.e., ALOS and the potential future mission TanDEM-L) could provide information about forest structure in a global context. Nevertheless, for this purpose further investigations based on forest stands of different structural complexity associated to different forest biomes (i.e., boreal, temperate and tropical forests) are needed.

## 6 Conclusion

This thesis investigates the use of X-band InSAR data for the detection and definition of forest structure. The applicability of height information derived from interferometric TanDEM-X acquisitions for stem volume estimation based on linear regression was developed. Forest structure classification at spatial units of 24 x 24 m<sup>2</sup> according to horizontal as well as vertical stand composition could be demonstrated, which returned nine meaningful classes according to canopy closure and stand layering. Moreover, the impact of phenology-induced changes on height estimation, stem volume estimation and forest structure classification was explored for coniferous, broadleaf and mixed temperate forest stands.

Although estimation and classification accuracies suffer general inherent restrictions of the X-band InSAR data (e.g., penetration of the signal, geometrical distortions and processing errors in general), it has a high potential for forest resources assessment. The use of remote sensing facilitates cost-efficient data collection and especially RaDAR systems offer the opportunity to acquire information on forests' condition without restrictions due to cloud cover over tropical forested areas and limited illumination over boreal forests in higher latitudes. This thesis shows the high value of X-band InSAR for reliable estimations of key parameters regarding sustainable forest management. Therefore, the consistent and globally available TanDEM-X data provides the ability to acquire up-to-date information about forests at global, national, federal and enterprise level in order to develop targeted silvicultural actions. Especially in the context of climate change, X-band InSAR data exhibits considerable capabilities to extract area-wide, wall-to-wall information on stem volume or biomass, forest structural diversity and thus aids to develop sufficient adaptation strategies. In general, VV-polarized InSAR data related to leaf-on season showed to be preferable to estimate forest height and stem volume, whereas HH-polarized TanDEM-X acquisitions were more suitable to capture forest structure.

Regarding global application of the proposed models and approaches for forest resources assessment, future work should investigate the transferability to other test sites related to different concepts of silvicultural land use and other forest biomes. In order to improve the assessment, further investigations should include information on tree species or tree species groups to consider underestimation of vegetation height dependent on varying crown architecture. For this purpose, a combination of optical remote sensing imagery and InSAR data should be considered. Additional consideration of longer wavelengths (i.e. P-band and L-band) should be contemplated to capture the vertical stand structure comprehensively.

Beyond, the analyses within this thesis present the prospect of monitoring and detecting seasonal changes in the course of the year. Well-chosen time series of X-band InSAR data could facilitate the detection of spatiotemporal phenology-related information about the forest. Especially in the context of ongoing climate change, time series could provide the possibility to explore the shifting temporal cycle of phenological development stages. Moreover, the differences in penetration of the RaDAR signal between leaf-on and leaf-off season, which were mainly related to broadleaf-dominated forest stands, offer the opportunity to stratify forests according to tree species groups by means of InSAR.



## 7 References

- Abdullahi, S., Kugler, F. & Pretzsch, H., 2016. Prediction of stem volume in complex temperate forest stands using TanDEM-X SAR data. *Remote Sensing of Environment*, Band 174, pp. 197-211.
- Abdullahi, S., Schardt, M. & Pretzsch, H., 2017. An unsupervised two-stage clustering approach for forest structure classification based on X-band InSAR data - A case study in complex temperate forest stands. *International Journal of Applied Earth Observation and Geoinformation*, Band 57, pp. 36-48.
- Abdullahi, S., Schneider, T., Schardt, M. & Pretzsch, H., Submitted. Seasonal Effects on Forest Structure Classification by means of X-band InSAR in complex temperate forests. *ISPRS International Journal of Photogrammetry and Remote Sensing*.
- Albertz, J., 2001. *Einführung in die Fernerkundung. Grundlagen der Interpretation von Luft- und Satellitenbildern*. 2. Überarbeitete und ergänzte Auflage Hrsg. Darmstadt: Wissenschaftliche Buchgesellschaft.
- Antropov, O., Rauste, Y., Ahola, H. & Häme, T., 2013. Stand-Level stem Volume of Boreal Forests from Spaceborne SAR Imagery at L-Band. *IEEE Journal of Selected Topics in Applied Earth Observation and Remote Sensing*, 6(1), pp. 35-44.
- Apps, M. J. et al., 1993. Boreal forests and tundra. In: *Water, Air, and Soil Pollution*. s.l.:Kluwer Academic Publishers, pp. 39-53.
- Assessment Millenium Ecosystem, 2005. *Ecosystems and Human Well-being Synthesis*, Washington, DC: Island Press.
- Assmann, E. & Franz, F., 1963. *Vorläufige Fichten-Ertragstafel für Bayern*. München: Institut für Ertragskunde der Forstlichen Forschungsanstalt.
- Aubréville, A., 1938. Regeneration patterns in closed forest of Ivory Coast. In: S. R. Eyre, Hrsg. *World Vegetation Types*. New York: Columbia University Press.
- Bamler, R. & Hartl, P., 1998. Synthetic aperture radar interferometry. *Inverse Problems*, Band 14, pp. R1-R54.
- Bauhus, J., Puettmann, K. J. & Kühne, C., 2013. Close-to-nature forest management in Europe: does it support complexity and adaptability of forest ecosystems?. In: C. Messier, K. J. Puettmann & K. D. Coates, eds. *Managing forests as complex adaptive systems: building resilience to the challenge of global change*. New York: Routledge, The Earthscan Forest Library, pp. 187-213.
- Bayerische Staatsforsten, 2011. *Richtlinie für die mittel- und langfristige Forstbetriebsplanung in den Bayrischen Staatsforsten (Forsteinrichtungsrichtlinie - FER 2011)*, Regensburg: s.n.
- Begehold, H., Rzanny, M. & Winter, S., 2016. Patch patterns of lowland beech forests in a gradient of management intensity. *Forest Ecology and Management*, Band 360, pp. 69-79.
- Bergen, K. M. et al., 2009. Remote sensing of vegetation 3-D structure for biodiversity and habitat: Review and implications for lidar and radar spaceborne missions. *Journal of Geophysical Research*, 114(G00E06).
- Bugmann, H., 2001. A Review of Forest Gap Models. *Climatic Change*, Volume 51, pp. 259-305.
- Carey, A. & Wilson, S., 2001. Induced Spatial Heterogeneity in Forest Canopies: Responses of Small Mammals. *Journal of Wildlife Management*, 65(4), pp. 1014-1027.

- Chen, G. X. et al., 2000. Effect of human activities on forest ecosystems: N cycle and soil fertility. *Nutrient Cycling in Agroecosystems*, Band 57, pp. 47-54.
- Clark, P. J. & Evans, F. C., 1954. Distance to nearest neighbour as a measure of spatial relationships in populations. *Ecology*, 35(4), pp. 445-453.
- Cloude, S. R. & Papathanassiou, K. P., 2003. Three stage inversion process for polarimetric SAR interferometry. *IEE Proceedings-Radar Sonar Navigation*, 150(3), pp. 125-134.
- Dale, V. H. et al., 2001. Climate Change and Forest Disturbances: Climate change can affect forests by altering the frequency, intensity, duration, and timing of fire, drought, introduced species, insect and pathogen outbreaks, hurricanes, windstorms, ice storms, or landslides. *BioScience*, 51(9), pp. 723-734.
- De Grandi, E. C., Mitchard, E. & Hoekman, D., 2016. Wavelet Based Analysis of TanDEM-X and LiDAR DEMs across a Tropical Vegetation Heterogeneity Gradient Driven by Fire Disturbance in Indonesia. *Remote Sensing*, 8(641).
- De Grandi, E. C., Mitchard, E. T. A., Woodhouse, I. H. & Verhegghen, A., 2015. IEEE International Geoscience and Remote Sensing Symposium (IGARSS). July, pp. 1805-1808.
- del Río, M. et al., 2016. Characterization of the structure, dynamics, and productivity of mixed-species stands: review and perspectives. *European Journal of Forest Research*, 135(1), pp. 23-49.
- Dobson, M. C. et al., 1995. Dependence of Radar Backscatter on Coniferous Forest Biomass. *IEEE Transactions on Geoscience and Remote Sensing*, Band 2, pp. 412-415.
- Engelhart, S., Keuck, V. & Siegert, F., 2011. Aboveground biomass retrieval in tropical forests - The potential of combined X- and L-band SAR data use. *Remote Sensing of Environment*, pp. 1260-1271.
- FAO, 2006. *The new generation of watershed management programmes and projects*. Rome, Italy: s.n.
- FAO, 2013. *Forests and Water - International Momentum and Action*. Rome. Italy: s.n.
- FAO, 2016. *Global Forest Resources Assessment 2015*. Rome: Food and Agriculture Organization of the United Nations.
- Fischer, A., 2003. Forstliche Vegetationskunde. Eine Einführung in die Geobotanik. In: 3. Auflage ed. Stuttgart (Hohenheim): Verlag Eugen Ulmer GmbH & Co., pp. 85-129.
- Franklin, S. E., 2001. *Remote Sensing for Sustainable Forest Management*. s.l.:CRC Press LLC.
- Franz, F. et al., 1973. *Bayerische Waldinventur 1970/71: Inventurabschnitt I: Großrauminventur, Aufnahme- und Auswertungsverfahren*. Kennel, E Hrsg. München: Univ.-Buchhandlung Frank.
- Gama, F. F., Santos, J. R. & Mura, C. J., 2010. Eucalyptus Biomass and Volume Estimation Using Interferometric and Polarimetric SAR Data. *Remote Sensing*, 2(4), pp. 939-956.
- Gao, T., Hedblom, M., Emilsson, T. & Nielsen, A. B., 2014. The role of forest stand structure as biodiversity indicator. *Forest Ecology and Management*, Volume 330, pp. 82-93.
- Gerhardt, E., 1909. Ueber BEstandes-Wachstumsgesetze und ihre Anwendung zur Aufstellung von Ertragstafeln. *Allgemeine Forst- und Jagdzeitung*, Band 85, pp. 117-128.
- Gerhardt, E., 1923. *Ertragstafeln für Eiche, Buche, Tanne, Fichte und Kiefer*. Berlin: Julius Springer.

- Gerhardt, E., 1930. *Ertragstafeln für reine und gleichaltrige Hochwaldbestände von Eiche, Buche, Tanne, Fichte, Kiefer, Grüner Douglasie und Lärche*. Berlin: Julius Springer.
- GFOI, 2016. *Integration of remote-sensing and ground-based observations for estimation of emissions and removals of greenhouse gases in forests: Methods and Guidance from the Global Forest Observations Initiative*. Rome: s.n.
- Grömping, U., 2006. Relative Importance for Linear Regression in R: The Package relaimpo. *Journal of Statistical Software*, Band 1.
- Hamilton, L. S., 2008. *Forests and water - a thematic study prepared in the framework of the Global Resources Assessment 2005*. Rome, Italy: s.n.
- Haralick, R. M., 1971. *On a texture-context feature extraction algorithm for remotely sensed imagery*. Gainesville, FL, USA. 15-17 December 1971, s.n., pp. 650-657.
- Harding, D. J., Blair, J. B., Rodriguez, E. & Michel, T., 1995. Airborne laser altimetry and interferometric SAR measurements of canopy structure and sub-canopy topography in the Pacific Northwest. *Second Topical Symposium on Combined Optical-Microwave Earth and Atmosphere Sensing*, 3-6 April, Band Conference Proceedings, pp. 22-24.
- Hoekman, D. H. & Quiñones, M. J., 2002. Biophysical Forest Type Characterization in the Colombian Amazon by Airborne Polarimetric SAR. *IEEE Transactions on Geoscience and Remote Sensing*, 40(6), pp. 1288-1300.
- Holloway, V. & Giandomenico, E., 2009. *Carbon Planet White Paper: The History of REDD Policy*, Adelaide: Carbon Planet Limited.
- Houghton, R., Hall, F. & Goetz, S., 2009. Importance of biomass in the global carbon cycle. *Journal of Geophysical Research*, 114(G2), pp. 1-13.
- Huang, Q., Swatantran, A., Dubayah, R. & Goetz, S. J., 2014. The Influence of Vegetation Height Heterogeneity on Forest and Woodland Bird Species Richness across the United States. *PLoS ONE*, 9(8).
- Huber, M. et al., 2004. Technical aspects of Envisat-ASAR geocoding capability at DLR. *Proceedings of 2004 Envisat & ERS Symposium*, Band Envisat and ERS Symposium.
- Huxley, J. S., 1932. Problems of relative growth. In: 36 Essex Street W.C. London: Methuen & Co. Ltd., pp. 1-38.
- IPCC, 2014. *Climate Change 2014: Mitigation of Climate Change. Working Group III Contribution to the IPCC 5th Assessment Report*. [Online] Available at: [http://report.mitigation2014.org/drafts/final-draft-postplenary/ipcc\\_wg3\\_ar5\\_final-draft\\_postplenary\\_chapter11.pdf](http://report.mitigation2014.org/drafts/final-draft-postplenary/ipcc_wg3_ar5_final-draft_postplenary_chapter11.pdf) [Accessed 27 June 2014].
- IPCC, 2014. *Climate Change 2014: Impacts, Adaptation, and Vulnerability. Contribution of Working Group II to the Fifth Assessment Report of the Intergovernmental Panel on Climate Change*, Cambridge, United Kingdom and New York, NY, USA: Cambridge University Press.
- Karila, K., Vastaranta, M., Karjalainen, M. & Kaasalainen, S., 2015. Tandem-X interferometry in the prediction of forest inventory attributes in managed boreal forests. *Remote Sensing of Environment*, Volume 159, pp. 259-268.
- Karjalainen, M. et al., 2012. Prediction of plot-level forest variables using TerraSAR-X stereo SAR data. *Remote Sensing of Environment*, Volume 117, pp. 338-347.

- Kira, T., Ogawa, H. & Sakazaki, N., 1953. Intraspecific competition among higher plant. Competition-yield-density interrelationship in regularly dispersed populations. *Journal of the Institute of Polytechnics*, Band Osaka City Univ Series D, pp. 1-16.
- Knoke, T. et al., 2012. *Forstbetriebsplanung als Entscheidungshilfe*. Stuttgart: Eugen Ulmer KG.
- Kohonen, T., 1982. Self-organized formation of topologically correct feature maps. *Biological Cybernetics*, 43(1), pp. 59-69.
- Kramer, H. & Akca, A., 1987. Leitfaden für Dentrometrie und Bestandesinventur. In: Frankfurt am Main: J. D. Sauerländer's Verlag, pp. 162-189.
- Krieger, G. et al., 2013. TanDEM-X: A radar interferometer with two formation-flying satellites. *Acta Astronautica*, Volume 89, pp. 83-98.
- Kugler, F., Hajnsek, I. & Papathanassiou, K., 2011. Forest Characterisation by means of TerraSAR-X and TanDEM-X (Polarimetric and ) Interferometric Data. *Proceedings PolInSAR*, 24-29 January, pp. 2578-2581.
- Kugler, F. et al., 2014. TanDEM-X Pol-InSAR Performance for Forest Height Estimation. *IEEE Transactions on Geoscience and Remote Sensing*, 52(10), pp. 6404-6422 .
- Kuuluvainen, T., Penttinen, A., Leinonen, K. & Nygren, M., 1996. Statistical Opportunities for Comparing Stand Structural Heterogeneity in Managed and Primeval Forests: An Example from Boreal Spruce Forest in Southern Finland. *Silva Fennica*, 30(2-3), pp. 315-328.
- Le Toan, T., Beaudoin, A., Riou, J. & Guyon, D., 1992. Relating Forest Biomass to SAR Data. *IEEE Transactions on Geoscience and Remote Sensing*, Band 2, pp. 403-411.
- Lee, J.-S. & Pottier, E., 2009. *Polarimetric Radar Imaging. From Basics to Applications*. Boca Raton(Florida): CRC Press. Taylor & Francis Group.
- Liesenberg, V. & Gloaguen, R., 2013. Evaluating SAR polarization modes at L-band for forest classification purposes in Eastern Amazon, Brazil. *International Journal of Applied Earth Observation and Geoinformation*, Volume 21, pp. 122-135.
- MacDicken, K. G., 2015. Global Forest Resources Assessment 2015: What, why, how?. *Forest Ecology and Management*, Band 352, pp. 3-8.
- MacQueen, J., 1967. Some methods for classification and analysis of multivariate observations. *Proceedings of the Fifth Berkeley Symposium on Mathematical Statistics and Probability*, Volume 1: Statistics, pp. 281-297.
- Manning, C. D., Raghavan, P. & Schütze, H., 2008. *Introduction to Information Retrieval*. Cambridge: University Press.
- Marghany, M., 2014. A Three-dimensional of Coastline Deformation using the Sorting RELiability Algorithm of ENVISAT Interferometric Synthetic Aperture Radar. In: *Advanced Geoscience Remote Sensing*. s.l.:InTech, pp. 105-121.
- McElhinny, C., Gibbons, P., Brack, C. & Bauhus, J., 2005. Forest and woodland stand structural complexity: Its definition and measurement. *Forest Ecology and Management*, Volume 218, pp. 1-24.
- McRoberts, R. E. & Tomppo, E. O., 2007. Remote sensing support for national forest inventories. *Remote Sensing of Environment*, Band 110, pp. 412-419.

- Miura, S. et al., 2015. Protective functions and ecosystem services of global forests in the past quarter-century. *Forest Ecology and Management*, Band 352, pp. 35-46.
- Montagnini, F. & Jordan, C., 2005. Characteristics of Tropical Forests. In: *Tropical Forest Ecology. The Basis for Conservation and Management*. Berlin. Heidelberg: Springer, pp. 19-73.
- Moreira, A. et al., 2013. A Tutorial on Synthetic Aperture Radar. *IEEE Geoscience and Remote Sensing Magazine*, March, 1(1), pp. 6-43.
- Niklas, K. J., 1994. Plant Allometry. The scaling of Form and Process. In: Chicago and London: The University of Chicago Press, pp. 1-41.
- Olesk, A. V. K., Vain, A., Noorma, M. & Parks, J., 2015. Seasonal Differences in Forest Height Estimation From Interferometric TanDEM-X Coherence Data. *IEEE Journal of Selected Topics in Applied Earth Observation and Remote Sensing*, 12(8), pp. 5565-5572.
- Önal, H., 1997. Trade-off between Structural Diversity and Economic Objectives in Forest Management. *American Journal of Agricultural Economics*, 79(3), pp. 1001-1012.
- Papathanassiou, K. P. & Cloude, S. R., 2001. Single-Baseline Polarimetric SAR Interferometry. *IEEE Transactions on Geoscience and Remote Sensing*, 39(11), pp. 2352-2363.
- Pardini, M., Qi, W., Dubayah, R. & Papathanassiou, K. P., 2016. Exploiting TanDEM-X Pol-InSAR Data for Forest Structure Observation and Potential Synergies with NASA's Global Ecosystem Dynamics Investigation LiDAR. *Proceedings of EUSAR 2016: 11th European Conference on Synthetic Aperture Radar*, 6-9 June.
- Pommerening, A., 2006. Evaluation structural indices by reversing forest structural analysis. *Forest Ecology and Management*, Volume 224, pp. 266-277.
- Pretzsch, H., 1996. Structural diversity as a result of silvicultural treatment. *Allgemeine Forst- und Jagdzeitung*, Band 11, pp. 213-221.
- Pretzsch, H., 2005. Diversity and Productivity in Forests: Evidence from Long-Term Experimental Plots. In: M. Scherer-Lorenzen, C. Körner & E. Schulze, eds. *Forest diversity and function. Temperate and Boreal Systems*. Ecological Studies 176 ed. Heidelberg Berlin: Springer Verlag, pp. 41-64.
- Pretzsch, H., 2009. *Forest Dynamics, Growth and Yield*. Berlin Heidelberg: Springer-Verlag.
- Pretzsch, H. & Biber, P., 2005. A Re-Evaluation of Reineke's Rule and Stand Density Index. *Forest Science*, 51(4), pp. 304-320.
- Pretzsch, H., Biber, P. & Ďurský, J., 2002. The single tree-based stand simulator SILVA: construction, application and evaluation. *Forest Ecology and Management*, Band 162, pp. 3-21.
- Pretzsch, H., Biber, P., Uhl, E. & Dauber, E., 2015. Long-term stand dynamics of managed spruce-fir-beech mountain forests in Central Europe: structure, productivity and regeneration success. *Forestry*, 88(4), pp. 407-428.
- Pukkala, T. & von Gadow, K. Hrsg., 2012. Forest Structure and Diversity. In: *Continuous Cover Forestry*. s.l.:Springer Science+Business Media B. V., pp. 29-83.
- Pulliaainen, J., Engdahl, M. & Hallikainen, M., 2003. Feasibility of multi-temporal interferometric SAR data for stand-level estimation of boreal forest stem volume. *Remote Sensing of Environment*, 85(4), pp. 397-409.

- Rahlf, J. et al., 2014. Comparison of four types of 3D data for timber volume estimation. *Remote Sensing of Environment*, pp. 325-333.
- Rauste, Y., 2005. Multi-temporal JERS SAR data in boreal forest biomass mapping. *Remote Sensing of Environment*, Band 97, pp. 263-275.
- Reineke, L. H., 1933. Perfecting a stand-density index for even-aged forests. *Journal of Agricultural Research*, Band 46, pp. 627-638.
- Richards, J. A., 2009. *Remote Sensing with Imaging Radar*. Berlin Heidelberg: Springer-Verlag.
- Ripley, B. D., 1977. Modelling spatial patterns (with discussion). *Journal of Royal Statistical Society*, 39(2), pp. 172-212.
- Rizzoli, P. et al., 2017. Generation and performance assessment of the global TanDEM-X digital elevation model. *ISPRS Journal of Photogrammetry and Remote Sensing*, Band 132, pp. 119-139.
- Rosen, P. A. et al., 2000. Synthetic Aperture Radar Interferometry. *Proceedings of the IEEE*, 88(3), pp. 333-382.
- Sadeghi, Y., St-Onge, B., Leblon, B. & Simard, M., 2017. Effects of TanDEM-X Acquisition Parameters on the Accuracy of Digital Surface Models of a Boreal Forest Canopy. *Canadian Journal of Remote Sensing*, 43(2), pp. 1-14.
- Santoro, M. et al., 2011. Retrieval of growing stock volume in boreal forest using hyper-temporal series of Envisat ASAR ScanSAR backscatter measurements. *Remote Sensing of Environment*, Band 115, pp. 490-507.
- Schlamadinger, B. & Marland, G., 1996. The role of forest and bioenergy strategies in the global carbon cycle. *Biomass and Bioenergy*, 10(5-6), pp. 275-300.
- Schlund, M. et al., 2015. TanDEM-X data for aboveground biomass retrieval in a tropical peat swamp forest. *Remote Sensing of Environment*, pp. 255-266.
- Schmitt, A., 2011. *Änderungserkennung in multitemporalen und multipolarisierten Radaraufnahmen*. Dissertation Hrsg. Karlsruhe: s.n.
- Schreiber, R. & Moreira, A., 2000. Coregistration of Interferometric SAR Images Using Spectral Diversity. *IEEE Transactions on Geoscience and Remote Sensing*, 38(5), pp. 2179-2191.
- Shannon, C. E., 1948. A mathematical theory of communication. *The Bell System Technical Journal*, Band 27, pp. 379-423.
- Sinha, S., Jeganathan, C., Sharma, L. K. & Nathawat, M. S., 2015. A review of radar remote sensing for biomass estimation. *International Journal of Environmental Science and Technology*, Band 12, pp. 1779-1792.
- Solberg, S. et al., 2010. Deriving forest monitoring variables from X-band InSAR SRTM height. *Canadian Journal of Remote Sensing*, 36(1), pp. 68-79.
- Solberg, S. et al., 2013. Monitoring spruce volume and biomass with InSAR data from TanDEM-X. *Remote sensing of Environment*, Volume 139, pp. 60-67.
- Solberg, S. et al., 2010. Estimating spruce and pine biomass with interferometric X-band SAR. *Remote Sensing of Environment*, pp. 2353-2360.

- Solberg, S., Weydahl, D. J. & Astrup, R., 2015. Temporal Stability of X-Band Single-Pass InSAR Heights in a Spruce Forest: Effects of Acquisition Properties and Season. *IEEE Transactions on Geoscience and Remote Sensing*, 53(3), pp. 1607-1614.
- Staudhammer, C. L. & LeMay, V. M., 2001. Introduction and evaluation of possible indices of stand structural diversity. *Canadian Journal of Forest Research*, Volume 31, pp. 1105-1115.
- Thomas, S. & Baltzer, J., 2002. Tropical Forests. *Encyclopedia of Life Sciences*.
- Treuhaft, R. et al., 2015. Tropical-Forest Biomass Estimation at X-Band From the Spaceborne TanDEM-X Interferometer. *IEEE Geoscience and Remote Sensing Letters*, Band 2, pp. 239-243.
- Treuhaft, R. N., Madsen, S. N., Moghaddam, M. & van Zyl, J. J., 1996. Vegetation characteristics and underlying topography from interferometric radar. *Radio Science*, 31(6), pp. 1449-1485.
- Varghese, A. O., Suryavanshi, A. & Joshi, A. K., 2016. Analysis of different polarimetric target decomposition methods in forest density classification using C band SAR data. *International Journal of Remote Sensing*, 37(3), pp. 694-709.
- Vesanto, J. & Alhoniemi, E., 2000. Clustering of the Self-Organizing Map. *IEEE Transactions on Neural Networks*, 11(3), pp. 586-600.
- von Bertalanffy, L., 1951. Theoretische Biologie. Zweiter Band: Stoffwechsel, Wachstum. In: Bern: A. Francke AG Verlag, pp. 311-331.
- von Carlowitz, H. C., 1713. *Sylvicultura Oeconomica oder haußwirthliche Nachricht und Naturgemäße Anweisung zur Wilden Baum-Zucht*. Leipzig: Johanna Friedrich Braun.
- Wagner, W. et al., 2003. Large-scale mapping of boreal forest in SIBERIA using ERS tandem coherence and JERS backscatter data. *Remote Sensing of Environment*, pp. 125-144.
- Wiedemann, 1948. *Die Kiefer 1984. Waldbauliche und ertragskundliche Untersuchungen*. Hannover: M. & H. Schaper.
- Wiedemann, E., 1943. Kiefern-Ertragstafel für mäßige Durchforstung, starke Durchforstung und Lichtung. In: *Die Kiefer 1984*. Hannover: M. & H. Schaper.
- Woodhouse, H. I., 2005. Imaging radar. In: *Introduction to microwave remote sensing*. Boca Raton, Florida, USA: CRC Press, Taylor & Francis Group, pp. 259-304.
- Wulder, M. A., Hall, R. J. & Franklin, S. E., 2005. Remote Sensing and GIS in forestry. In: S. Aronoff, Hrsg. *Remote Sensing for GIS managers*. Redlands: ESRI Press, pp. 351-362.
- Yang, H. et al., 2014. Simulation of Interferometric SAR Response for Characterizing Forest Successional Dynamics. *IEEE Geoscience and Remote Sensing Letters*, 11(9), pp. 1529-1533.
- Yoda, K. T. K. T., Ogawa, H. & Hozumi, K., 1963. Self-thinning in overcrowded pure stands under cultivated and natural conditions. *Journal of Institute of Polytechnic*, Band Osaka Uni D 14, pp. 107-129.

## Appendix

### A Publication I

**Title:** Prediction of stem volume in complex temperate forest stands using TanDEM-X SAR data

**Authors:** Sahra Abdullahi, Florian Kugler, Hans Pretzsch

**Journal:** *Published* in Remote Sensing of Environment (RSE)

**Impact Factor:** 6.265 (2016)

**Contribution:** TanDEM-X InSAR data was processed and provided by the Microwave and Radar Institute of the German Aerospace Center (DLR). The collection of field measurements in the scope of a forest inventory was conducted by staff of the Chair of Forest Growth and Yield Science of the Technical University of Munich. All data analyses including data preparation, development and implementation of the models, validation of the results as well as writing and composing the manuscript were performed by the first author Sahra Abdullahi. All co-authors contributed to the design and content of the paper by scientific advice, discussion and language editing.

© Remote Sensing of Environment, Elsevier <https://doi.org/10.1016/j.rse.2015.12.012>, Reprinted with permission.





# Prediction of stem volume in complex temperate forest stands using TanDEM-X SAR data



Sahra Abdullahi <sup>a,\*</sup>, Florian Kugler <sup>b</sup>, Hans Pretzsch <sup>a</sup>

<sup>a</sup> Technische Universität München (TUM), Chair for Forest Growth and Yield Science, Hans-Carl-von-Carlowitz-Platz 2, 85354 Freising, Germany

<sup>b</sup> German Aerospace Center (DLR), Microwave and Radar Institute, Münchner Str. 20, 82234 Wessling, Oberpfaffenhofen, Germany

## ARTICLE INFO

### Article history:

Received 27 April 2015

Received in revised form 30 November 2015

Accepted 10 December 2015

Available online xxxx

### Keywords:

TanDEM-X

Temperate forest

Forest inventory

Stem volume

Linear regression

## ABSTRACT

Reliable estimations of stem volume are important for sustainable forest management planning as well as for monitoring of global changes. However, the derivation of stem volume in cubic meters per hectare based on traditional sampling-based forest inventories (usually with a repetition rate of ten years) is very expensive, labor-intensive and only available for the minority of the forest areas worldwide. Thus, spaceborne synthetic aperture radar (SAR) data can provide estimations of forest parameters with sufficient spatial and temporal resolution for large areas. Height information extracted from two interferometric dual-polarized TanDEM-X data sets were used to investigate the potential of polarimetric interferometric X-band SAR data for stem volume estimation in the complex forest stands of the Traunstein forest in Southeast Bavaria, Germany. In contrast to other studies of forest parameter estimation from X-band SAR data carried out in boreal or tropical forest stands, the current study investigated stem volume estimation based on X-band SAR data in complex temperate forest stands. A linear regression model based on the allometric relationship of forest height (estimated from SAR data combined with an airborne LiDAR-based Digital Terrain Model) and stem volume per unit area (deduced from traditional forest inventory) was derived. Moreover, the model was extended and thus improved by integrating novel parameters derived from the co-occurrence matrix as surrogates for horizontal forest structure. This linear regression model predicted stem volume at plot (circular plots of 500 m<sup>2</sup>) level with a coefficient of determination of  $R^2 = 69\%$  and a root mean square error of  $RMSE = 155 \text{ m}^3 \text{ ha}^{-1}$  and stand (areas of 1.5 to 6.4 ha) level with  $R^2 = 94\%$  and  $RMSE = 44 \text{ m}^3 \text{ ha}^{-1}$  respectively.

© 2015 Elsevier Inc. All rights reserved.

## 1. Introduction

Stem volume is one of the key parameters in forest inventory. Reliable estimations of stem volume per unit area have been the basis for sustainable forest management planning since the beginning of the 18th century (von Carlowitz, 1713) as well as for monitoring of global changes in recent times (IPCC, 2014). Especially in the context of climate change, felling budget can be adapted to damages caused by increasing extreme weather events and calamities. Moreover, stem volume can be directly related to stem biomass as a function of the tree species-specific wood density. For generalization and simplification, a first-order approximation with a density of  $500 \text{ kg m}^{-3}$  (corresponding to a density factor of  $0.5 \text{ t m}^{-3}$ ) is assumed (Pretzsch, 2009), while the Food and Agriculture Organization of the United Nations (FAO) suggests generalized region-specific density factors of about  $0.6 \text{ t m}^{-3}$  (FAO, 2001). The total above ground biomass can be estimated by the additional use of the biomass expansion factor, which expands stem biomass to account for non-merchantable biomass components such as branches, foliage, and non-commercial trees (Brown, 1997). Stem volume estimations

provide the required basis for sustainable management, and by means of conversion into biomass a crucial parameter to understand and quantify the global carbon cycle. Carbon is stored by building up biomass and emitted to the atmosphere by destroying biomass due to fire, logging with subsequent energetic use, storms, decomposition, etc. (Houghton, Hall, & Goetz, 2009). By means of forest management strategies this process can be controlled and the CO<sub>2</sub> emissions can be reduced (Schlamadinger & Marland, 1996).

Stem volume per unit area is expressed in cubic meters per hectare. For the purpose of this study we use its definition as harvested timber volume under bark which is most widespread among practitioners. It can be derived from terrestrial forest inventory based on diameter at breast height (dbh) and tree height measurements (Pretzsch, 2009). Traditional forest inventories, like National Forest Inventory in Germany, Sweden or Great Britain (usually with a repetition rate of ten years) are very expensive, labor-intensive and only available for the minority of the forest areas worldwide. A unique example at global scale is the Forest Resources Assessment (FRA) conducted by the FAO every five to ten years in order to assess the areal extent and changes of forests worldwide (FAO & JRC, 2012). This information can be used as the basis for global sustainable forest management but is still lacking more detailed information on forest volume, associated biomass and its

\* Corresponding author.

E-mail address: [Sahra.Abdullahi@lrz.tum.de](mailto:Sahra.Abdullahi@lrz.tum.de) (S. Abdullahi).

changes. For this purpose, remote sensing offers area-wide information with high spatial and temporal resolution and thus can enable sustainable forest management planning and detailed monitoring of changes in a global context.

Radar systems are all-weather systems, which is an advantage over optical systems. The penetration depth of microwaves into the forest canopy depends on the wavelength. The TanDEM-X mission is composed of the two almost identical satellites TerraSAR-X (launched in 2007) and TanDEM-X (launched in 2010) flying in a closely controlled formation. The TanDEM-X mission provides high resolution, multi-polarized, single-pass interferometric X-band (9.65 GHz) data. Especially single-pass interferometry is very suitable for forest applications due to the simultaneous acquisition of the two interferometric images (Kugler, Schulze, Hajnsek, Pretzsch, & Papathanassiou, 2014). The simultaneous acquisition avoids possible errors due to temporal decorrelation and atmospheric disturbances, which is one of the significant benefits of the TanDEM-X mission (Krieger et al., 2007).

Numerous studies investigate the potential of SAR data at different wavelengths from different sensors on satellite and airborne platforms for biomass and stem volume estimation over boreal, temperate and tropical forests. At lower frequencies like P- (0.3–1 GHz) and L- (1–2 GHz) band, the radar signals penetrate deep into the forest canopy and are backscattered at big branches, tree trunks and the ground (Dobson et al., 1992; Le Toan, Beaudoin, Riou, & Guyon, 1992). Due to the high penetration capability and thus high sensitivity to vertical forest structure, the intensity of radar backscatter at longer wavelengths are in particular suitable for biomass retrieval (e.g. Engelhart, Keuck, & Siegert, 2011; Luckman, Baker, Honzák, & Lucas, 1998; Rauste, 2005) but can also be used for stem volume estimations (e.g. Antropov, Rauste, Ahola, & Häme, 2013; Askne, Smith, & Santoro, 2004; Gonçalves, Santos, & Treuhaft, 2011). In contrast, microwaves with higher frequencies (i.e. shorter wavelength) such as C- (4–8 GHz) and especially X- (8–12 GHz) band are just as well able to penetrate down to the ground but are mostly backscattered in the upper part of the crowns (Gama, Santos, & Mura, 2010; Pulliainen, Engdahl, & Hallikainen, 2003). Consequently, the radar backscatter intensity at these bands is less sensitive to the vertical forest structure but hence is well suited to derive height information of the canopy by use of ancillary information on ground elevation (e.g. LiDAR-based DTM). Thus, C- and X- band microwaves tend to be more appropriate for both biomass (e.g. Gama et al., 2010; Solberg, Riegler, & Nonin, 2015; Treuhaft et al., 2015) and stem volume (e.g. Karila, Vastaranta, Karjalainen, & Kaasalainen, 2015; Solberg, Astrup, Breidenbach, Nilsen, & Weydahl, 2013; Wagner et al., 2003) estimation by means of height information derived from SAR data. Biomass and stem volume estimations by means of height information derived from shortwave radar data are based on either SAR radargrammetry (e.g. Karjalainen, Kankare, Vastranata, Holopainen, & Hyyppä, 2012; Solberg et al., 2015; Vastaranta, Holopainen, Karjalainen, Kankare, & Hyyppä, 2014) or SAR interferometry (e.g. Gama et al., 2010; Solberg et al., 2013; Treuhaft et al., 2015).

Several recent studies demonstrated the estimation of biomass and stem volume by means of interferometric information derived from X-band SAR data. Karila et al. (2015) employed a nearest neighbor prediction model for stem volume estimation based on InSAR heights from TanDEM-X data in boreal forest stands in Southern Finland. In Treuhaft et al. (2015), coherence from TanDEM-X InSAR data was deployed for biomass estimation using linear regression in a tropical forest in Brazil. Schlund, von Poncet, Kuntz, Schmillius, and Hoekman (2015) estimated biomass by linear and non-linear regression models based on TanDEM-X coherence in a tropical forest test site in Indonesia. Rahlf, Breidenbach, Solberg, Naesset, and Astrup (2014) used InSAR heights from TanDEM-X in combination with a LiDAR-based DTM (Digital Terrain Model) for stem volume estimation in a boreal forest in Southern Norway. Solberg et al. (2013) compared linear and non-linear regression of interferometric height and biomass or stem volume

based on TanDEM-X SAR data in a boreal forest test site. In Solberg, Astrup, Gobakken, Naesset, and Weydahl (2010) a non-linear, mixed regression model based on InSAR height derived from TanDEM-X data was applied to estimate biomass in boreal forest stands, whereas Gama et al. (2010) used airborne X-band data for linear regression of interferometric height and stem volume in tropical forest.

In contrast to previous studies which were carried out in boreal or tropical forest stands using X-band radar data, the current study investigates stem volume estimation based on height information derived from polarimetric interferometric SAR (PolInSAR) data from TanDEM-X in temperate complex forest stands. Nevertheless, few studies based on non-X-band interferometric SAR data already exist in temperate forests. Li, Chen, Li, Ke, and Zhan (2015) estimated biomass from vertical reflectivity profiles based on airborne L-band data in temperate forest stands in Traunstein, Southeast Germany. Neumann, Ferro-Famil, and Reigber (2010) derived forest height information based on polarimetric interferometric airborne L-band SAR data in temperate forest stands in Traunstein. In Lavalle, Solimini, Pottier, and Desnos (2010) the potential of compact-polarimetric airborne InSAR data of multiple frequencies was investigated for estimation of forest parameters in temperate forest stands of Traunstein forest.

The objective of this study is to explore the potential of height information derived from X-band PolInSAR data for stem volume estimation based on a statistically fitted regression model in temperate forest stands. Thereby, this study is linked to previous studies which investigate the potential of X-band PolInSAR data to derive height information over complex temperate and tropical forest stands (e.g. Hajnsek, Kugler, Lee, & Papathanassiou, 2009; Kugler et al., 2014) while applying the derived height information for stem volume estimation. In detail, the aims of this study were defined as (i) estimation of stem volume per unit area at plot (circular plots of 500 m<sup>2</sup>) and stand level (areas of 1.5 to 6.4 ha) based on height information derived from polarimetric interferometric TanDEM-X data in combination with airborne LiDAR data and terrestrial measurements and (ii) improvement of the predictions by integration of texture parameters representing the horizontal stand structure.

## 2. Materials

### 2.1. Study area

The study area (Fig. 1) is located in a highly structured, mixed, temperate municipality owned forest close to the city of Traunstein, Germany (47°52' N, 12°38' E). Traunstein forest covers an area of about 580 ha and is supervised and used as teaching and research forest by the Chair for Forest Growth and Yield Science of the Technische Universität München (TUM). The study area is limited to a forest area of 243 ha bounded by the districts Bürgerwald and Heiligengeistwald. The topography ranges from 630 to 720 m a.s.l. and includes small areas with steep slopes. The soils are composed of glacier sediments which belong to the pre-alpine moraine landscape. The climatic conditions are characterized by a mean annual temperature of 7.3 °C and precipitation of up to 1600 mm/year. The main tree species are Norway spruce (*Picea abies*), European silver fir (*Abies alba*), European beech (*Fagus sylvatica*) and Sycamore maple (*Acer pseudoplatanus*). The forest stands are very complex concerning tree species richness and heterogeneous stand structures due to close-to-nature silviculture (Pretzsch, 1996) which is reflected by the distribution of tree species (Table 1) and percentage of development stages (Table 2) within the study area.

### 2.2. Remote sensing data

Two dual-polarized interferometric TanDEM-X image pairs acquired on January 09, 2012 and May 18, 2013 were used. The images were acquired in bistatic StripMap mode in ascending orbit and almost identical incidence angles of roughly 43°. The baseline between the two sensors was 108.74 m and 142.72 m, respectively. A summary of

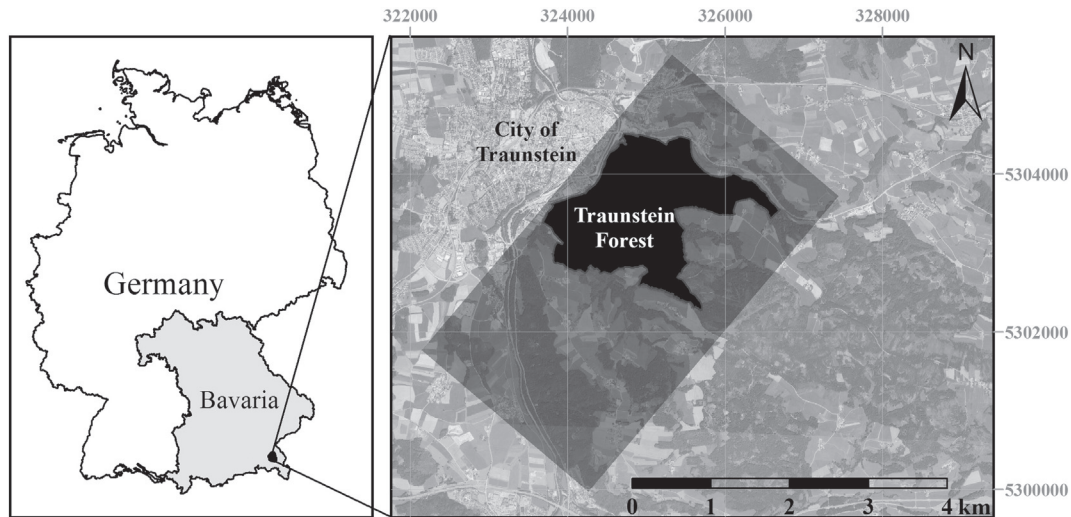


Fig. 1. Map of the study area: Municipal Forest Traunstein located in Southeast Bavaria, Germany.

the TanDEM-X acquisition parameters is given in Table 3. In addition, an airborne LiDAR survey was conducted on November 18, 2012 with a flight height of about 500 m and a point density of about 25 dots/m<sup>2</sup> using the LMS-Q 680i Scanner from RIEGL. The associated Digital Terrain Model (DTM) as well as Digital Surface Model (DSM) was provided by MILAN Geoservice GmbH.

### 2.3. Reference data

A forest inventory comprising 228 permanent circular sampling plots was carried out in summer 2013. Forest condition and the dynamics of stand parameters are detected based on the survey guidelines of the Bavarian State Forest Enterprise (Bayerische Staatsforsten, 2011). In Traunstein forest, inventory has been carried out according to this concept since 1988. For permanent systematic inventory sampling according to these guidelines, the center of the concentric inventory plots is permanently marked with buried lodestones. For each inventory plot the polar coordinates (azimuth and range relative to the center of the plot) are recorded for all measured trees with a diameter at breast height (dbh) of at least 10 cm. Thus, repeated surveys can be easily conducted and the sampling error for alterations of the stand parameters can be reduced. The plots are arranged on a regular 100 m by 100 m sampling grid (Fig. 2a) with a resulting sampling density of 1 plot/ha. The spatial distribution of the inventory plots within the study area is depicted in Fig. 3. Each circular inventory plot covers an area of 500 m<sup>2</sup> and consists of three concentric sub-circles with radii of 12.62 m, 6.31 m and 3.15 m respectively. For each sub-circle, a specific threshold dbh for a tree in order to be recorded is defined (as shown in Fig. 2b). The dbh is measured for any tree above the relevant

threshold value. Tree height measurements are taken for a representative sample of each tree species per stand layer. Additionally, other tree and forest stand attributes such as species, age, layering, damages, dead wood, and stem quality are recorded. Standard height curve systems are used for estimating tree height based on the measured height sample. Subsequently, stem volume per unit area is calculated for all living trees based on tree height, basal area (derived from dbh) and a form factor according to Eq. (1).

$$V = \sum_{i=1}^N ba_i \cdot h_i \cdot f_{1,3i} \cdot r_i \quad (1)$$

where  $V$  is stem volume per hectare,  $N$  is the number of trees within the plot,  $ba_i$  is the basal area of tree  $i$ ,  $h_i$  is the height of tree  $i$ ,  $f_{1,3i}$  is the form factor of tree  $i$  and  $r_i$  is the number of representation per hectare of tree  $i$ . Stem volume per unit area ranges from 0 m<sup>3</sup> ha<sup>-1</sup> up to 1049 m<sup>3</sup> ha<sup>-1</sup> in the study area as shown in Table 4 containing the minimum, mean and maximum values of inventory parameters. In general, the error for volume estimations can be assumed as  $\pm 10$ –15% (Kramer & Akça, 1987).

In Traunstein, inventory plots are attributed to different stages of development. The following development stages are distinguished, describing the condition and structure of the stands:

- Youth stage: slow growing up until a closed canopy has established.
- Growth stage: rapid growth, increase of growing stock until culmination of increment of volume.
- Maturity stage: subsiding growth of growing stock and growth; typically, trees are concentrated in one stand layer, and regeneration is missing due to absence of light at the forest floor.
- Regeneration stage: upcoming regeneration under the cover of the old trees.
- Plenter stage: forest structure is at least three-layered (including understorey and regeneration).

Table 1

Area percentages of tree species within the study area.

Area percentages of tree species [%]	
Spruce	41
Fir	14
Pine	1
Larch	2
Douglas fir	1
Beech	23
Oak	1
Real deciduous woods	12
Other deciduous woods	5

Table 2

Area percentages of development stages within the study area.

Area percentages of development stages [%]	
Youth stage	21
Growth stage	15
Maturity stage	12
Regeneration stage	31
Plenter stage	21

**Table 3**  
Acquisition parameters of the SAR data.

Acquisition date	Acquisition mode	Polarization mode	Orbit	Incidence angle	Baseline	Weather conditions
09.01.2012	Bistatic/StripMap	Dualpol (HH, VV)	Ascending	43.1°	108.74 m	Snowfall
18.05.2013	Bistatic/StripMap	Dualpol (HH,VV)	Ascending	43.2°	142.72 m	Dry

These development stages were used for the selection of stands for stem volume estimation at stand level, while only those stands containing at least three inventory plots were chosen. Characteristic values for each stand can be found in Table 5. In total 20 stands with sizes ranging from about 1.5 ha to about 6.4 ha were used. The development stages represent areas of similar structure. Therefore, the range of stand areas of about 4 ha is negligible concerning the accuracy of stem volume estimations at stand level. The spatial distribution of the 20 stands is given in Fig. 3. Plot-wise stem volume derived from the inventory data as well as the height information deduced from the SAR data over the inventory plots were averaged per stand for linear regression.

Stem volume estimations are based on both scales, plot- and stand level. Since the terrestrial measurements are carried out on spatial units of 500 m<sup>2</sup>, this scale is convenient to avoid uncertainties due to aggregation or extrapolation of in-situ measurements. However, stem volume predictions at stand level are more suitable to provide area-wide information. By using stands which are based on repeated forest inventories and defined concerning structure and growth stage, the terrestrial measurements can be aggregated to reliable and meaningful stem volume values per stand and thus enables area-wide stem volume estimations.

### 3. Methods

#### 3.1. Generation of height information from PolInSAR data

Two different height information data sets were derived from the polarimetric interferometric SAR data. A DSM calculated from the interferometric TanDEM-X data, which represents the height of the earth surface including all elevated objects (i.e. buildings and vegetation), was normalized by subtracting the LiDAR-based DTM, which represents the height of the earth surface without elevated objects. The normalized DSM (nDSM) corresponds to the phase height (*scattering center height*), which reflects the average of tree height dependent on penetration depth and spatial resolution. Tree height is clearly defined in forestry as the height difference between tree top and tree base. Furthermore, the top height (*modeled top height*) is derived from the TanDEM-X data by a PolInSAR modeling technique and is related to the silvicultural relevant parameter top height H100 which corresponds to the hundred

largest trees per hectare (Kugler et al., 2014). Both data sets are correlated with stem volume and used for stem volume estimation by comparison.

For estimation of the *scattering center height*, a DSM was calculated from the interferometric data (Bamler & Hartl, 1998). From the available dual-polarized TanDEM-X data the VV polarization was chosen for height estimation. Previous studies in Traunstein showed that the VV polarization is probably more suitable since it has less ground scattering contribution compared with HH (Kugler, Hajnsek, & Papathanassiou, 2011). Nevertheless, it has to be noted that in general VV and HH polarizations lead to similar results (Kugler et al., 2014). The scattering signals, acquired simultaneously from slightly different positions by the TanDEM-X sensors, were coherently combined in an interferogram for digital elevation model generation (Krieger et al., 2013; Rosen et al., 2000). The interferometric phase describes the phase differences of the two acquisitions mainly affected by the differences in range (Bamler & Hartl, 1998). After resolving the ambiguity of the interferometric phase by phase unwrapping, the phase differences can be converted into height based on the interferometer geometry for terrain reconstruction (Rosen et al., 2000). The derived DSM was normalized by subtracting the LiDAR-based DTM and thus, a vegetation height model corresponding to the height of scattering center was generated. The scattering center height underdetermines the actual vegetation height due to the penetration of the radar wave.

The *modeled top height* was derived by applying the Random Volume over Ground (RVoG) model, a PolInSAR technique (Cloude & Papathanassiou, 2003; Kugler et al., 2014; Papathanassiou & Cloude, 2001; Treuhaf, Madsen, Moghaddam, & van Zyl, 1996). The RVoG model represents the scattering from volume and ground by means of a two-layer vegetation model. It is based on volume decorrelation which is observed in interferometric radar acquisitions over forested areas (Papathanassiou & Cloude, 2001). Volume decorrelation is interpreted as a function of the vertical distribution of scatterers along the height of a volume. A decrease of backscattering along volume height can be interpreted as signal extinction. In case of no extinction and uniform backscattering along height, the volume layer has the form of a rectangle (Fig. 4a). If the electromagnetic wave is attenuated during its transition through the volume – as assumed for higher frequencies like X-band – the volume layer has an exponential form

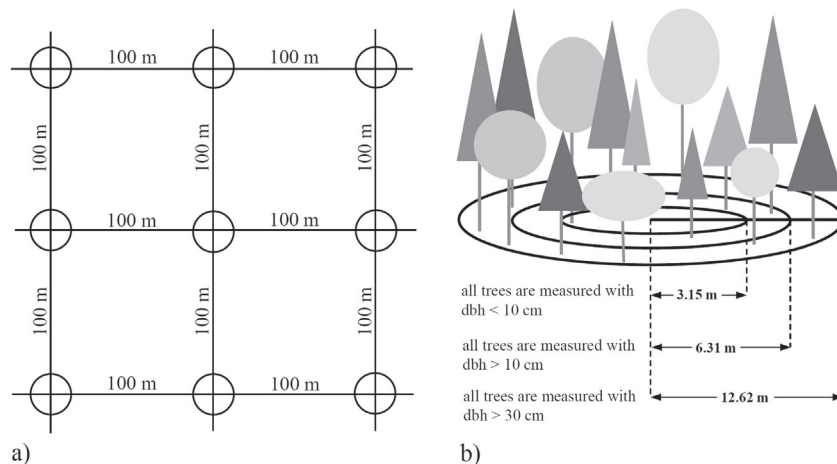


**Fig. 2.** a) Inventory sampling grid and b) thresholds in diameter measuring.

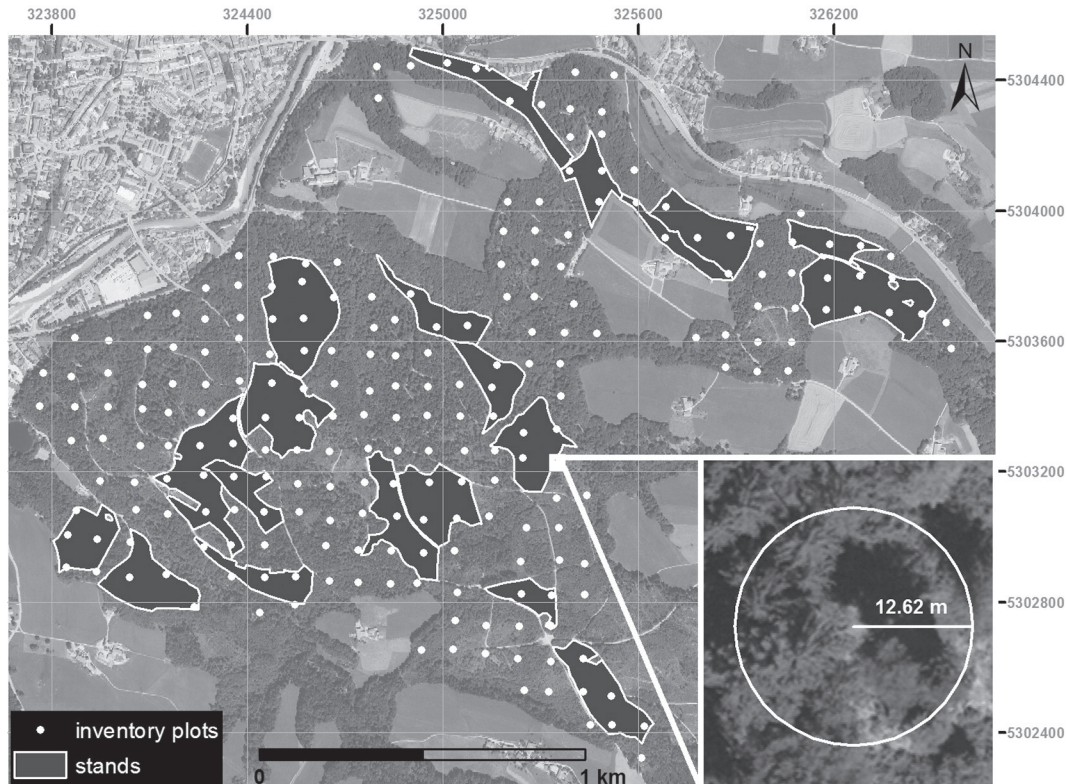


Fig. 3. Spatial distribution of inventory plots and stands within the study area.

(Fig. 4b). In general, magnitude of the ground scattering depends on frequency, polarization and extent of extinction. For TanDEM-X data of Traunstein forest ground scattering is assumed to be extremely low and was therefore neglected in the height estimation (Kugler et al., 2014). The implementation of the RVoG model for TanDEM-X data is detailed as described in Kugler et al. (2014) and Cloude and Papathanassiou (2003). In this study TanDEM-X single-polarization data in VV was used since it yields the best results for Traunstein forest (Kugler et al., 2014). However, in the case of single-polarization data the inversion problem is underdetermined and requires external information on the ground elevation under the modeled forest layer. Information on the elevation of the ground was taken from a LiDAR-based DTM (Kugler et al., 2011, 2014).

Fig. 5 depicts the comparison of the modeled top height (Fig. 5a), the scattering center height (Fig. 5b) and the LiDAR-based nDSM (Fig. 5c) along a transect of about 250 m. The LiDAR-based nDSM is only used for comparison and not included in the stem volume estimations. Additionally, two ground measured values of top height H100 are inserted at the position 5 m and 140 m of the transect (Fig. 5d). Modeled top height is related to the top height H100, i.e. average height of the hundred largest trees per hectare. The top height H100 is a silvicultural relevant parameter and can be calculated for reference units of at least 100 m<sup>2</sup> by considering the height of the dominating tree. Dependent on the reference unit of commonly 1 ha, top height H100 does not

reflect small-scale forest structure due to considering solely the dominating trees. Modeled top height is based on reference units of about 15 × 15 m<sup>2</sup>. Therefore, the forest structure concerning areas smaller than units of about 15 × 15 m<sup>2</sup> is not reflected. The scattering center height underestimates the vegetation height due to the penetration of the microwaves into the forest. In general, the LiDAR-based nDSM also underestimates vegetation height because of penetration into the forest (Nilsson & Holgren, 2003; van Laar & Akça, 2007), which is increased due to acquisition in the off-leaf season. As the modeled top height considers only the dominating trees and the scattering center height as well as the LiDAR-based nDSM underestimates vegetation height obvious height differences between the data sets occur. Comparing the top height H100 values based on in-situ measurements from the forest inventory, the modeled top height yields reasonable values. On closer consideration of the area along the transect in combination with the height profiles of Fig. 5d, the differences between modeled top height and LiDAR-based nDSM become reasonable. Between 0 m and 50 m as well as between 150 m and 200 m the forest stand has very low parts and gaps, i.e. it is less dense. For this reason the LiDAR-based nDSM as well as the scattering center height is variable. In contrast, the modeled top height has higher height values due to the larger reference unit of about 15 × 15 m<sup>2</sup> which also contains higher trees. As opposed to this, between 50 m and 100 m the forest stand is much denser. Therefore, the height differences between LiDAR-based nDSM, scattering center height and modeled top height are less. Moreover, additional effects such as spatial resolution of the data sets, spatial offset and side-looking acquisition of the SAR sensor influence the differences between the height data sets (modeled top height, scattering center height and LiDAR-based nDSM). A comparison between scattering center height and the LiDAR-based nDSM, the scattering center height shows less variation in height mainly as a consequence of worse spatial resolution of the SAR data.

The scattering center height and the modeled top height were generated for the two polarimetric interferometric TanDEM-X acquisitions. All

Table 4

Statistics of forest parameters per plot acquired during forest inventory 2013. Volume is specified as timber harvested (>7 cm at the smaller end) without bark.

	Mean stem diameter [cm]	Mean tree height [m]	Stand basal area [m <sup>2</sup> ha <sup>-1</sup> ]	Standing volume [m <sup>3</sup> ha <sup>-1</sup> ]
Min	0.00	0.00	0.00	0.00
Mean	32.44	23.24	28.80	312.82
Max	67.53	40.20	83.50	1049.00

**Table 5**  
Statistics of forest parameters acquired per plot during forest inventory 2013 aggregated per stand. Stem volume is specified as timber harvested (>7 cm at the smaller end) without bark.

Stand	Growth stage	Number of plots	Area [ha]	Mean tree height [m]	Stem volume [m <sup>3</sup> ha <sup>-1</sup> ]
1	Youth	4	4.00	10.61	16.03
2	Youth	5	3.79	6.72	23.40
3	Youth	3	2.06	14.76	91.73
4	Growth coniferous	7	5.85	10.32	104.36
5	Youth	3	3.57	20.77	105.10
6	Youth	3	2.00	19.93	107.70
7	Youth	3	1.46	10.18	122.50
8	Regeneration coniferous	3	2.24	27.75	281.43
9	Youth	4	2.73	18.03	300.58
10	Regeneration deciduous	3	3.29	29.40	311.60
11	Maturity deciduous	3	3.90	28.83	329.60
12	Maturity coniferous	5	4.81	24.41	332.76
13	Plenter	3	2.50	27.33	342.13
14	Regeneration coniferous	3	3.74	22.77	347.10
15	Regeneration deciduous	3	1.54	25.31	358.33
16	Regeneration coniferous	3	1.74	29.14	376.50
17	Regeneration deciduous	7	6.42	31.76	380.06
18	Maturity coniferous	6	5.96	29.75	439.13
19	Regeneration coniferous	3	2.48	31.49	468.20
20	Regeneration coniferous	3	3.55	32.32	514.33

data sets were processed to a pixel spacing of 6 m. In total, four height data sets were used for stem volume estimation in this study, the scattering center height as well as the modeled top height, both for the winter (January 2012) and the summer (May 2013) acquisition, respectively. A summary of the derived height information is given in Table 6.

### 3.2. Linear regression model based on allometric equation

Allometry is the science of size-correlated variations in organic form and process (Niklas, 1994). Allometry describes the unproportional growth of two dimensions to each other compared with isometry which denotes a proportional growth of two dimensions to each other. According to Huxley (1932) and von Bertalanffy (1951), the relation of growth rate of a certain part  $y$  and the growth rate of another part or the whole body  $x$  is constant over time:

$$a = \frac{\frac{dy}{dt} \cdot \frac{1}{y}}{\frac{dx}{dt} \cdot \frac{1}{x}} \quad (2)$$

The ratio  $a$  describes the relationship of the different growth rates during time  $t$ . In terms of tree growth, an allometric relation between

stem volume and tree height exists, where  $y$  is the stem volume and  $x$  is the tree height:

$$a = \frac{\frac{dV}{dt} \cdot \frac{1}{V}}{\frac{dH}{dt} \cdot \frac{1}{H}} \quad (3)$$

where  $V$  is volume in cubic meters per hectare,  $H$  is scattering center height or modeled top height in meters per inventory plot.

Stem volume and tree height grow unequally however constant to each other according to the constant allometric ratio of growth rates  $a$ . By integration and logarithmic representation of Eq. (2) a linear relationship is formed which expresses that the stem volume grows proportional to a power of the tree height:

$$y = b \cdot x^a \quad (4)$$

$$\ln y = \ln b + a \cdot \ln x. \quad (5)$$

The linear model (5) is represented as a straight line with the constants  $b$  and  $a$ .  $b$  is known as the integration constant specifying the value of  $y$  at  $x = 1$ .  $a$  is the constant allometric ratio of growth rates and defines the slope of the straight line. If  $a > 1$ ,  $y$  increases faster than  $x$  (positive allometry). If  $a = 1$ ,  $x$  and  $y$  increase proportionally (isometric growth). If  $a < 1$ ,  $x$  increases faster than  $y$  (negative allometry) (Huxley, 1932; von Bertalanffy, 1951). In general as well as in the present case of the inventory conducted in 2013, stem volume per unit area  $V$  and averaged tree height  $H$  per inventory plot possess a positive allometric relationship as depicted in Fig. 6a. The logarithmic representation of this relationship is shown in Fig. 6b.

In order to determine the relationship between the two forest variables, stem volume per unit area and averaged scattering center height or modeled top height, a linear model based on the log-transformed allometric Eq. (5) was fitted:

$$\ln V = \ln a_0 + a_1 \cdot \ln H \quad (6)$$

where  $V$  is volume in cubic meters per hectare,  $H$  is scattering center height or modeled top height in meters per inventory plot,  $\ln a_0$  is the intercept with the  $y$ -axis and  $a_1$  is the slope. Stem volume per unit area is predicted by the calculated regression line of model (6), deriving the expected mean value of  $\ln V$  for specific values of  $\ln H$ . The regression line describes the best line of fit between stem volume and scattering center height or modeled top height (Niklas, 1994). To fit model (6), total stem

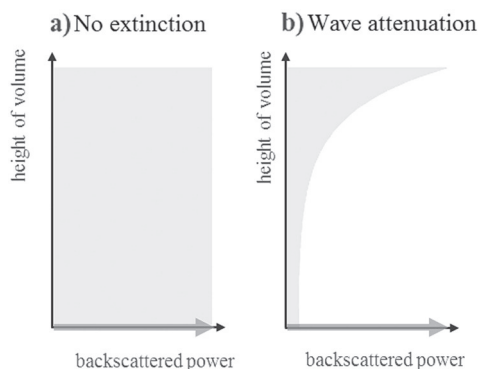


**Fig. 4.** Functions of backscattering along volume height according to the RVoG model: a) in case of no extinction and b) in case of extinction for higher frequencies like X-band.

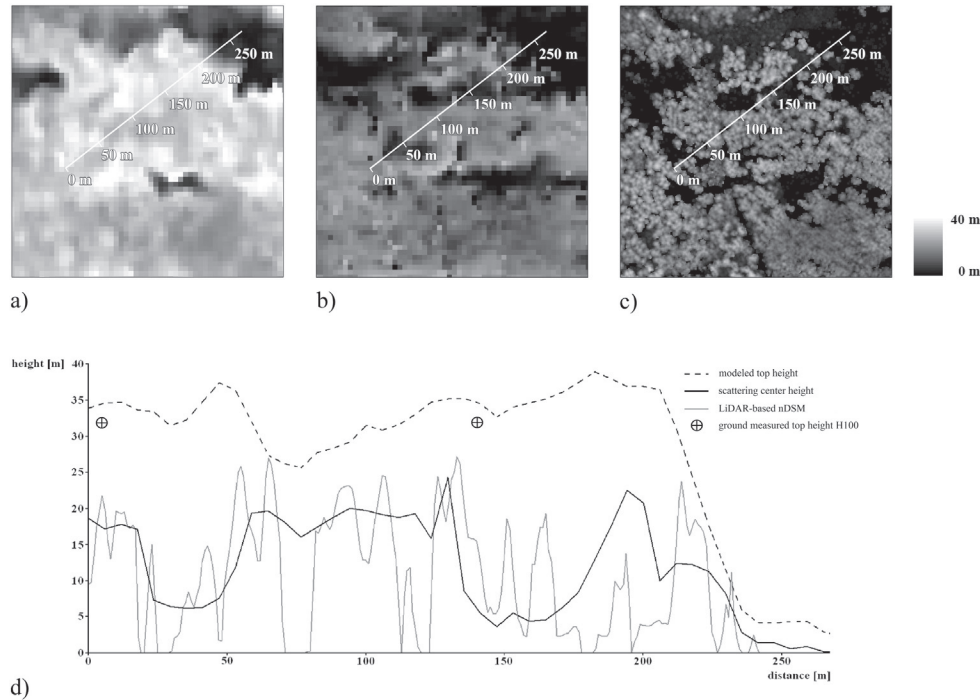


**Fig. 5.** Comparison of different height information data sets based on the TanDEM-X acquisition in May 2013 along a transect of about 250 m. a) Modeled top height. b) Scattering center height. c) LiDAR-based normalized DSM. d) Height profile of modeled top height (dashed black), scattering center height (solid black), LiDAR-based normalized DSM (solid grey) and two ground measurements of top height H100 (black crosses).

volume per hectare and mean scattering center height or modeled top height for each inventory plot, were used. For plot level estimations, stem volume was calculated according to Eq. (1) from the in-situ measurements for each inventory plot and scattering center height and modeled top height were averaged per inventory plot. For stand level estimations, stem volume and averaged scattering center height or modeled top height per inventory plot were averaged per stand.

### 3.3. Extension of the linear regression model

Stem volume per unit area depends mainly on tree height and stand density. In terms of volume prediction using the linear model (6), height information was derived from the TanDEM-X data. However, stand basal area representing stand density as used in (1) was not considered in the model. To improve the prediction results, the linear model has to be extended by additional parameters that describe stand density, or, more generally, horizontal forest structure. For this purpose, novel texture parameters were derived from the TanDEM-X height information using the Co-occurrence Matrix according to Haralick (1971). The co-occurrence matrix is a second-order statistical analysis for the extraction of texture within an image. This method determines how often a pair of pixels of certain values and a certain spatial relationship occurs within the image (Haralick, 1979). With respect to the inventory plots used in this study, the neighborhood relation of tree height values within each inventory plot is identified by means of the amount of pairs of pixels with certain height values and a certain spatial relationship. The

spatial relationship is defined by the distance  $d$  and the direction  $\alpha$  of the pixels to each other which fixed at the beginning of the analysis. In general, the analysis can be performed for each distance and direction. The directions according to  $\alpha=0^\circ$ ,  $\alpha=45^\circ$ ,  $\alpha=90^\circ$ ,  $\alpha=135^\circ$ ,  $\alpha=180^\circ$ ,  $\alpha=225^\circ$ ,  $\alpha=270^\circ$  and  $\alpha=315^\circ$  can be used for texture extraction. In this study, the co-occurrence approach was applied to the scattering center height of each inventory plot with a distance of  $d=1$  and all non-redundant directions with the angles  $\alpha=0^\circ$ ,  $\alpha=45^\circ$ ,  $\alpha=90^\circ$  and  $\alpha=135^\circ$ . The scattering center height was used since it reflects the horizontal forest structure better compared with the modeled top height (Fig. 5). Fig. 7 shows an example of the derivation of the Co-occurrence Matrix for angle  $\alpha=0^\circ$ . The height data had to be classified, because otherwise all height values were slightly different to each other and accordingly the Co-occurrence Matrix entailed no meaningful results. For this purpose, the Jenks natural breaks classification algorithm was applied to define ten height classes in relation to the maximum height value of the height data set in the whole study area to make all plots comparable. This method seeks to group the data into classes based on the histogram in order to minimize within-class variance and maximize between-class variance while iteratively optimizing the class allocation according to the minimum sum of squared deviations from the class mean values (Jenks & Caspall, 1971).

Subsequently, the resulting Co-occurrence Matrices were interpreted according to the diagonal deriving the following four parameters for each Co-occurrence Matrix:

- 1) The weighted center of gravity of the Co-occurrence Matrix along the diagonal, called center diagonal  $c_d$ .

$$c_d = \frac{\sum \left( \frac{(i+j)}{2} \cdot M(i,j) \right)}{\sum M(i,j)} \quad (7)$$

where  $i$  and  $j$  are the indices of columns and rows and  $M(i,j)$  are the values of the Co-occurrence Matrix elements at position  $(i,j)$ .

**Table 6**

Derived height information based on TanDEM-X data.

Data set	Height information	Acquisition date	Pixel spacing
1	Scattering center height	09.01.2012	6 m
2	Model based height	09.01.2012	6 m
3	Scattering center height	18.05.2013	6 m
4	Model based height	18.05.2013	6 m

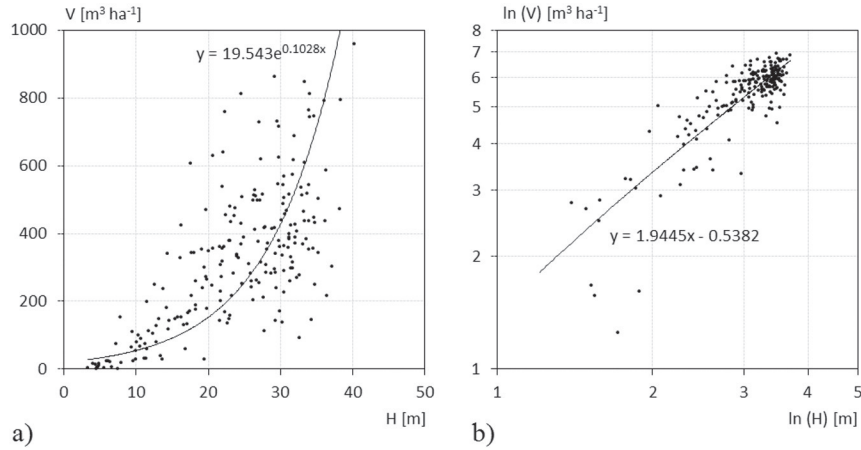


**Fig. 6.** a) The positive allometric relationship between mean tree height  $H$  on the x-axis and stem volume per hectare  $V$  on the y-axis per inventory plot based on in-situ measurements from 2013 which shows that stem volume growth proportional to a power of tree height. b) The logarithmic representation of the positive allometric relationship between mean tree height on the x-axis and stem volume per hectare on the y-axis per inventory plot based on in-situ measurements from 2013 which depicts a linear relation.

The center diagonal describes the weighted mean of occurring height classes within each inventory plot. Thus, the center diagonal is a measure in direct relation to stand height.

- 2) The weighted center of gravity of the Co-occurrence Matrix perpendicular to the diagonal, called center perpendicular  $c_p$ .

$$c_p = \frac{\sum((i-j) + 1) \cdot M(i,j)}{\sum M(i,j)} \tag{8}$$

where  $i$  and  $j$  are the indices of columns and rows and  $M(i,j)$  are the values of the Co-occurrence Matrix elements at position  $(i,j)$ .

The center perpendicular describes the variation of height as a function of occurring differences of neighboring height classes. Thus, the center perpendicular is a measure of homogeneity.

- 3) The standard deviation along the diagonal of the Co-occurrence Matrix, called standard deviation diagonal  $s_d$ .

$$s_d = \frac{\sum (M(i,j) - \mu_d)^2}{\sum M(i,j)} \tag{9}$$

where  $i$  and  $j$  are the indices of columns and rows,  $M(i,j)$  are the values of the Co-occurrence Matrix elements at position  $(i,j)$  and  $\mu_d$  is the mean of the values projected onto the diagonal.

The standard deviation diagonal is derived by projecting all values onto the diagonal and calculating the standard deviation as

shown in Fig. 8. Thus, the standard deviation diagonal is a measure of homogeneity.

- 4) The standard deviation perpendicular to the diagonal of the Co-occurrence Matrix, called standard deviation perpendicular  $s_p$ .

$$s_p = \frac{\sum (M(i,j) - \mu_p)^2}{\sum M(i,j)} \tag{10}$$

where  $i$  and  $j$  are the indices of columns and rows,  $M(i,j)$  are the values of the Co-occurrence Matrix elements at position  $(i,j)$  and  $\mu_p$  is the mean of the values projected perpendicular to the diagonal.

The standard deviation perpendicular is derived by projecting all values onto the perpendicular of the diagonal and calculating the standard deviation (Fig. 8). Thus, the standard deviation perpendicular is a measure of homogeneity.

It can be assumed that stem volume increases with increasing center diagonal, since this parameter is directly related to stand height and thus the stands become higher (Fig. 9a). In contrast, it is assumed that stem volume decreases with increasing center perpendicular at constant center diagonal, because the differences in height become larger within the considered area and consequently the stand becomes less dense (Fig. 9b). For the same reason, stand density decreases with increasing standard deviation of the Co-occurrence Matrix along the diagonal (Fig. 9c) as well as perpendicular to the diagonal (Fig. 9d) at constant center diagonal.

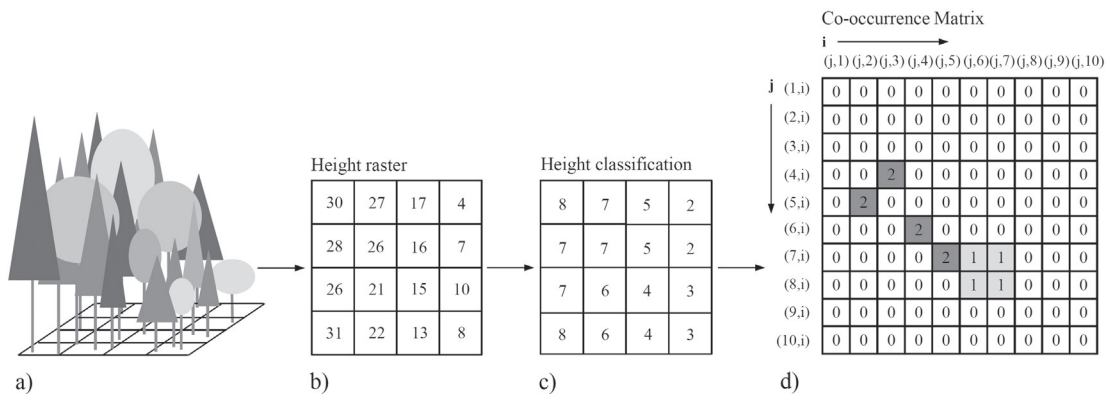


**Fig. 7.** Schematic representation of the processing steps for derivation of the Co-occurrence Matrix from height data. a) Height information is derived from the polarimetric interferometric TanDEM-X data set. b) The derived height is represented in a regular raster grid and c) classified according to Jenks natural breaks classification algorithm into ten height classes. d) The Co-occurrence Matrix is derived based on this height classification which represents the probability of occurrence of two neighboring pixels separated by distance  $d = 1$  and angle  $\alpha = 0^\circ$ .



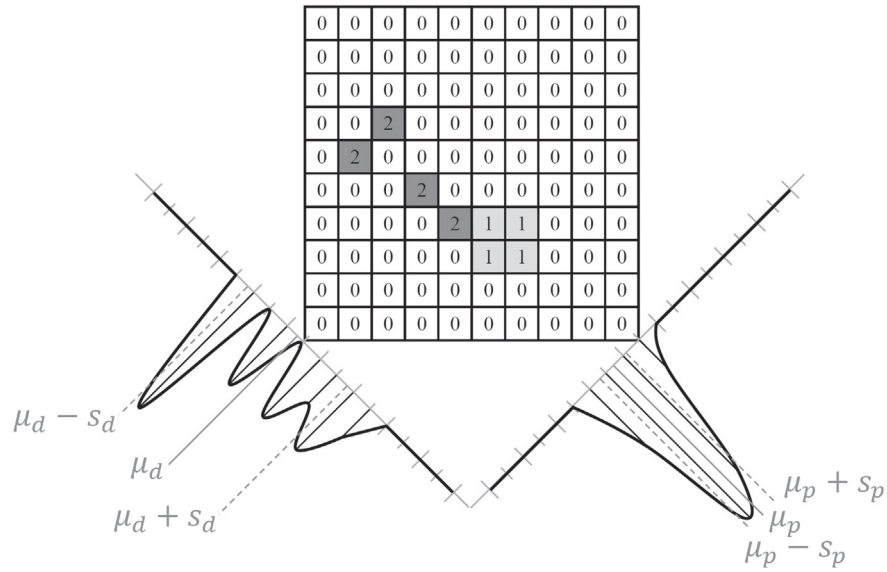


**Fig. 8.** Illustration of the derivation process of standard deviation diagonal and standard deviation perpendicular, where  $\mu_d$  and  $s_d$  are mean and standard deviation along the diagonal and  $\mu_p$  and  $s_p$  are mean and standard deviation along the perpendicular to the diagonal.

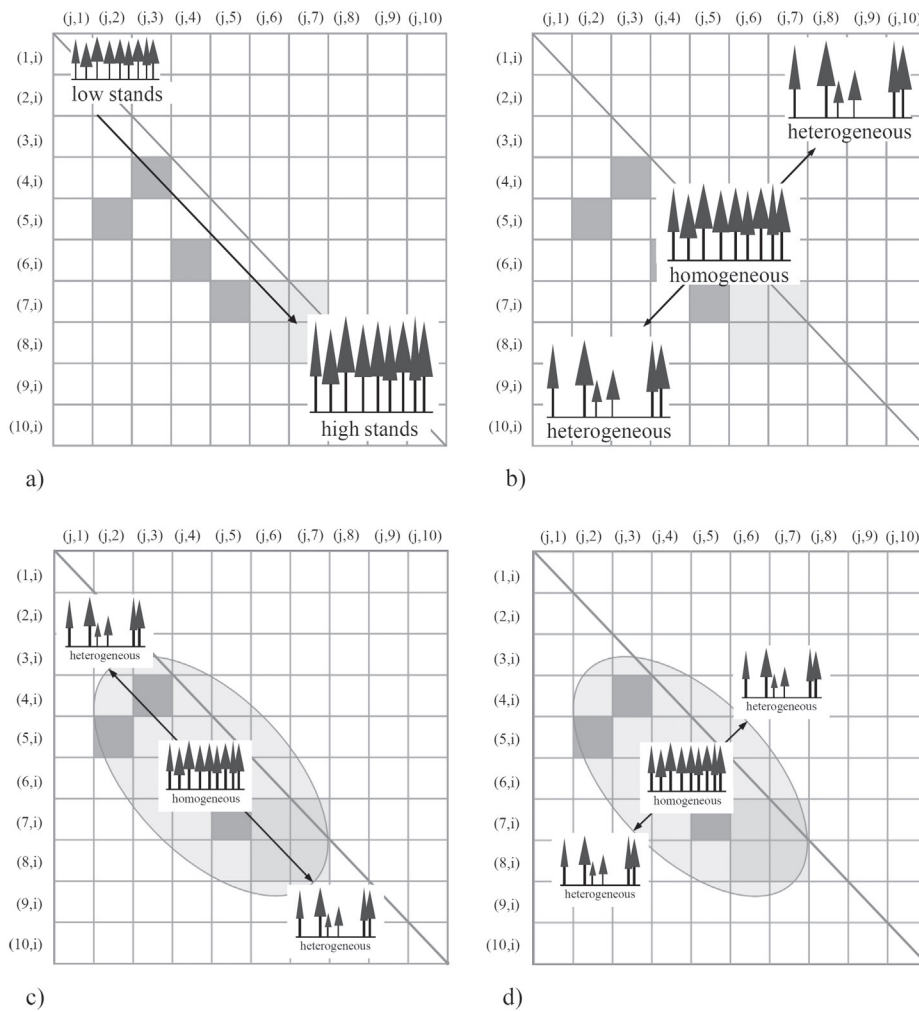


**Fig. 9.** Interpretation of the Co-occurrence Matrix based on forest height information. a) Stem volume increases with increasing center along the diagonal. b) Stem volume decreases with increasing center perpendicular to the diagonal. c) Stand density decreases with increasing standard deviation of the Co-occurrence Matrix along the diagonal. d) Stand density decreases with increasing standard deviation of the Co-occurrence Matrix perpendicular to the diagonal.

Consequently, the three co-occurrence parameters center perpendicular, standard deviation diagonal and standard deviation perpendicular are related to center diagonal since they represent a different kind of information. It is assumed that the three ratios  $\frac{C_p}{C_d}$ ,  $\frac{S_d}{C_d}$  and  $\frac{S_p}{C_d}$  in combination based on all directions can capture forest structure.

In order to improve the regression of stem volume per unit area, the linear model (6) was expanded by these ratios:

$$\ln V = \ln a_0 + a_1 \cdot \ln H + a_2 \cdot \ln \frac{C_{p0}}{C_{d0}} + a_3 \cdot \ln \frac{S_{d0}}{C_{d0}} + a_4 \cdot \ln \frac{S_{p0}}{C_{d0}} + \dots + a_{13} \cdot \ln \frac{S_{p135}}{C_{d135}} \quad (11)$$

where  $V$  is volume in cubic meters per hectare,  $H$  is averaged scattering center height or modeled top height in meters per inventory plot,  $\frac{C_p}{C_d}$ ,  $\frac{S_d}{C_d}$  and  $\frac{S_p}{C_d}$  are the ratios based on the Co-occurrence Matrix with the subscripts according to the angle  $\alpha$  (0, 45, 90, 135),  $\ln a_0$  is the intercept with the y-axis and  $a_{1-13}$  are the regression coefficients.

The expanded linear regression model for stem volume estimation was applied at plot as well as at stand level. To fit the model, total stem volume and averaged scattering center height or modeled top height for each inventory plot were used and averaged per stand. The co-occurrence parameters were calculated per inventory plot

according to (7)–(10) at plot level and averaged per stand at stand level.

Metrics describing the relative importance of each predictor were used to quantify the contribution of the co-occurrence parameters to the coefficient of determination  $R^2$  of the multiple regression model (11). Relative importance indices give information about the contribution of each explanatory variable to the prediction by itself and in combination with other variables (Tonidandel & LeBreton, 2011). Traditional measures include the comparison of zero-order correlations of an explanatory variable with the criterion, the increase in  $R^2$  by adding each explanatory variable to all others and standardized regression coefficients (Johnson & LeBreton, 2004). However, these measures are only valid for uncorrelated explanatory variables (Johnson & LeBreton, 2004). Since the co-occurrence parameters are correlated, these traditional measures are not suitable. Moreover, different orderings of the explanatory variables lead to different decompositions of the explained sum of squares for the same multiple regression model (Grömping, 2006). This disregard of the ordering of the explanatory variables entails that the relative importance of explanatory variables is dependent on the ordering. Alternative measures overcome these problems by averaging the contribution of each explanatory variable across all possible orderings of variables (Johnson & LeBreton, 2004).

According to Grömping (2006) the Proportional Marginal Variance Decomposition (PMVD) metric is a suitable solution to address

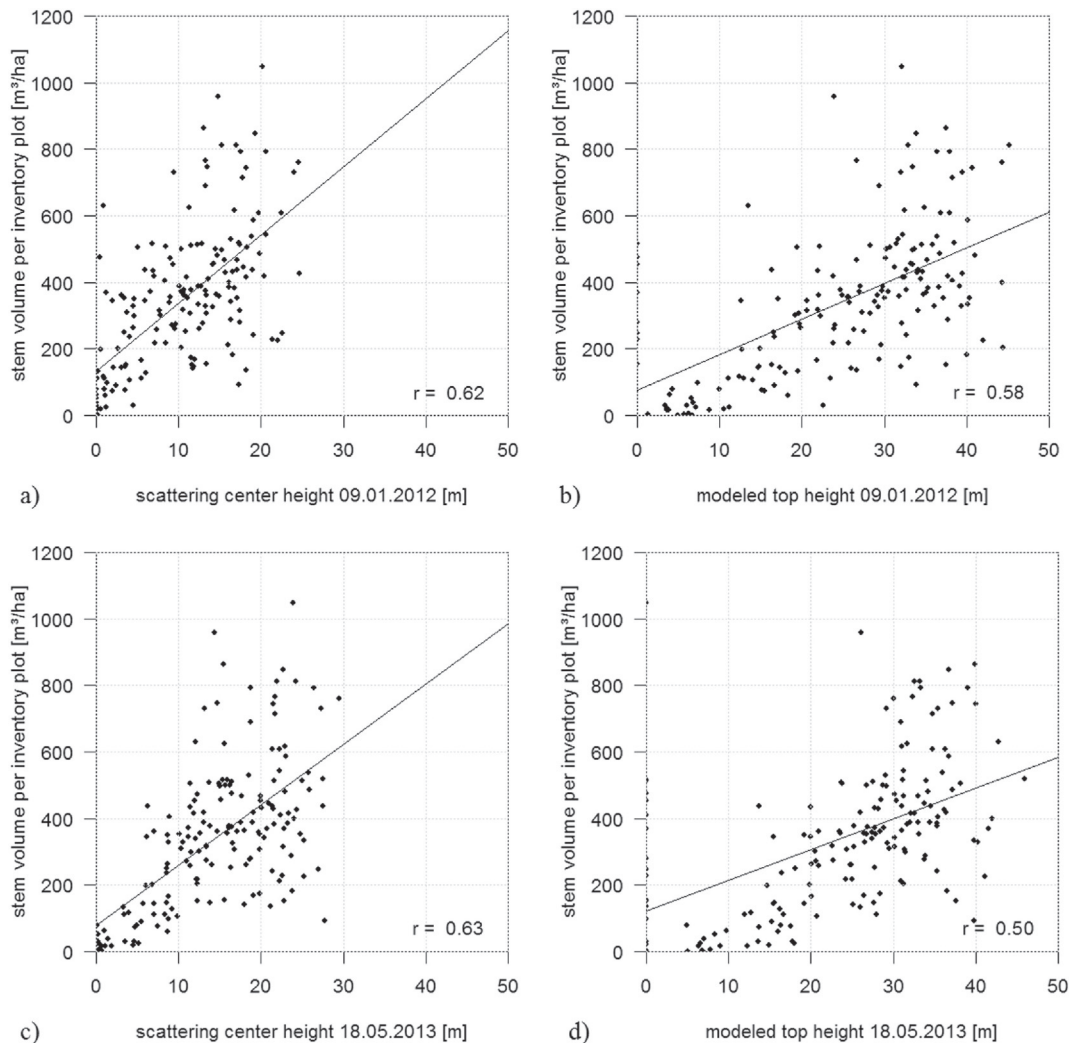


**Fig. 10.** Scatterplots of stem volume per hectare at plot level derived from the inventory data 2013 on the y-axis and height information derived from the TanDEM-X data on the x-axis with regression lines a) scattering center height from January 2012, b) modeled top height from January 2012, c) scattering center height from May 2013 and d) modeled top height from May 2013.

**Table 7**

Results from the linear regression model relating scattering center height or modeled top height from winter (09.01.2012) or summer (18.05.2013) acquisitions to stem volume at plot level described by the standard error SE of the parameters, root means square error RMSE of the predictions, RMSE related to the mean stem volume and the coefficient of determination  $R^2$ . Significance levels:  $p < 0.001$  \*\*\*\*  $p < 0.01$  \*\*\*  $p < 0.05$  \*\*  $p < 0.1$ .

Parameter	Intercept ( $\ln a_0$ )	$SEa_0$	$a_1$	$SEa_1$	RMSE [ $m^3 ha^{-1}$ ]	RMSE [%]	$R^2$
Scattering center height (winter)***	4.50***	0.09	0.57	0.04	164.30	44.40	0.56
Modeled top height (winter)***	0.45*	0.40	1.59	0.12	180.00	48.64	0.54
Scattering center height (summer)***	2.86***	0.19	1.09	0.07	179.81	48.59	0.60
Modeled top height (summer)***	0.76*	0.49	1.96	0.15	181.22	48.97	0.54

relative importance to the explanatory variables based on averaging the contributions across all possible orderings. The PMVD approach uses data-dependent weights for the averaging process to avoid that variables benefit from each other due to their correlation. This method was applied to the expanded linear model (11) in order to quantify the contribution of the co-occurrence parameters to stem volume estimation.

## 4. Results

### 4.1. Correlation of stem volume and TanDEM-X height information

Fig. 10 shows the scatterplot of stem volume in cubic meters per hectare estimated from terrestrial inventory against height information (scattering center height and modeled top height) in meters derived from TanDEM-X data of the winter and the summer acquisition for each inventory plot with the corresponding correlation coefficients ( $r$ ). Stem volume per hectare exhibits a positive linear correlation with scattering center height as well as modeled top height. The scattering center height has a stronger correlation with stem volume compared with the modeled top height. For scattering center height the correlation coefficient is slightly higher for the summer acquisition than for the winter acquisition as opposed to the modeled top height. The best correlation was achieved with the scattering center height derived from the summer acquisition.

### 4.2. Stem volume estimation at plot level

Table 7 shows the results of stem volume prediction based on the linear model (6) for the winter as well as for the summer acquisition for scattering center height and modeled top height respectively. Predictions of stem volume per unit area at plot level (circular plots of  $500 m^2$ ) were more accurate based on scattering center height compared with the results based on modeled top height. The regression model including scattering center height from the summer acquisition explains 60% of the variance of stem volume and thus led to the highest coefficient of determination.

The extension of the linear model by the three ratios of the co-occurrence parameters for each direction according to Eq. (11) led to predictions in the best case with  $R^2$  of 69.92% and RMSE of about  $155.00 m^3 ha^{-1}$  (RMSE related to mean stem volume = 41.90%) based on the scattering center height from the summer acquisition (Table 8). This can be related to the original estimation of stem volume (Table 7) in terms of improvement of coefficient of determination of

almost 10%. Concerning deviation of absolute values, RMSE is reduced by about  $25 m^3 ha^{-1}$ . Quantifying the contribution of the co-occurrence parameters according to the relative importance metric of PMVD, the co-occurrence parameters possess a contribution of 12.54% of the explained variance of stem volume. This contribution is equally distributed across all co-occurrence parameters and thus, all ratios and directions are important.

Fig. 11 illustrates the correlation between the predicted stem volume values at plot level based on the model employing the scattering center height and the co-occurrence parameters from the summer acquisition and the measured values. Slight saturation effects occur at about  $400 m^3 ha^{-1}$ .

### 4.3. Stem volume estimation at stand level

At stand level (areas of 1.5 to 6.4 ha), the predictions of stem volume using the linear model (6) improved substantially compared with the results at plot level (Table 7). As shown in Table 9 the estimations of stem volume were more accurate based on the scattering center height compared with the modeled top height. The best results at stand level with  $R^2$  of 88% and RMSE of about  $73 m^3 ha^{-1}$  were achieved using the scattering center height from the summer acquisition. This is consistent with the results at plot level.

Fig. 12 illustrates the differences between stem volume estimation at the plot and stand level using the linear model (6). In the case of stand level estimations, no obvious saturation effects occur. Altogether, stem volume predictions at stand level from the summer acquisition were better in direct comparison with plot level.

At stand level, the best results ( $R^2 = 0.94$ , RMSE =  $44.25 m^3 ha^{-1}$ /16.53%) were achieved using the extended linear regression model (11) based on the summer acquisition of scattering center height (Table 10).

As shown in Fig. 13, the prediction of stem volume per unit area at stand level based on the extended model (11) has a high correlation with the measured values without obvious saturation effects.

A positive linear correlation between the derived height information (scattering center height and modeled top height) and stem volume per unit area which is described by the integrated log-transformed allometric equation was found. The linear regression model based on scattering center height or modeled top height achieved prediction results with accuracies ranging from  $R^2$  of 0.54 to 0.60 at plot level and accuracies between  $R^2$  of 0.68 and 0.88 at stand level. The predictions based on the summer acquisition were better compared with the predictions on the basis of the winter acquisition. Moreover, stem volume estimations based on scattering center height possess higher

**Table 8**

Comparison of the results from the simple linear regression model and the extended linear regression model at plot level described by the standard error SE of the parameters, root mean square error RMSE of the predictions, RMSE related to the mean stem volume and the coefficient of determination  $R^2$ . The models are based on scattering center height or modeled top height from winter (09.01.2012) or summer (18.05.2013) acquisitions.

Parameter	Linear model			Extended linear model		
	RMSE [ $m^3 ha^{-1}$ ]	RMSE [%]	$R^2$	RMSE [ $m^3 ha^{-1}$ ]	RMSE [%]	$R^2$
Scattering center height (winter)	164.30	44.40	0.56	163.65	44.22	0.63
Modeled top height (winter)	180.00	48.64	0.54	175.01	47.29	0.62
Scattering center height (summer)	179.81	48.59	0.60	155.00	41.90	0.69
Modeled top height (summer)	181.22	48.97	0.54	148.05	40.01	0.66

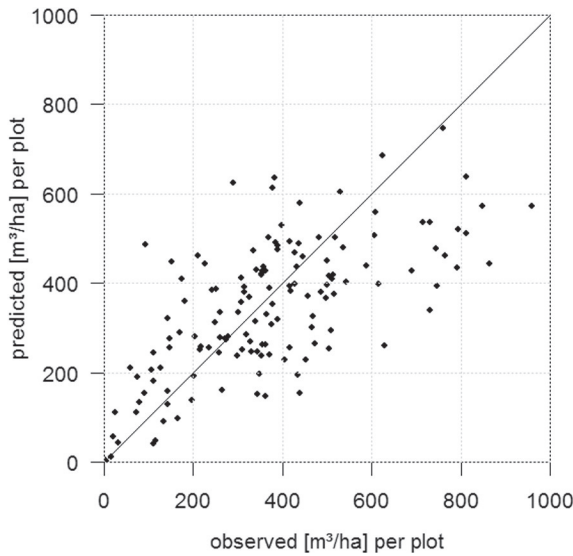


**Fig. 11.** Scatterplot comparing measured stem volume (on the x-axis) and predicted stem volume based on the extended model employing scattering center height and ratios of the co-occurrence parameters based on the summer acquisition (on the y-axis) per inventory plot.

accuracies compared with the estimations based on modeled top height. The results could be improved substantially by extending the linear regression model with the co-occurrence parameters representing forest structure.

## 5. Discussion

The current study presented the potential of stem volume estimation in a complex temperate forest consisting of unevenly aged mixed forest stands with high range in stem volume (Table 4) and high species richness (Table 1) in different development stages (Table 2) based on X-band SAR data. In contrast, other studies which investigate biomass or stem volume retrieval based on interferometric X-band SAR data are mostly carried out in boreal (e.g. Karila et al., 2015; Rahlf et al., 2014; Solberg et al., 2013) and tropical (e.g. Gama et al., 2010; Schlund et al., 2015; Treuhaft et al., 2015) forest stands. Table 11 shows the generalized characteristics of global forest biomes according to Apps et al. (1993); Fischer (2003); Montagnini and Jordan (2005) and Thomas and Baltzer (2002). Boreal forests are rather homogeneous concerning species diversity and vertical structure (Malhi, Baldocchi, & Jarvis, 1999). Temperate forests are characterized by a higher tree species diversity and productivity compared with boreal forests (Fischer, 2003; Pretzsch, 2003). Due to the favorable climatic conditions in tropical forests, the diversity of tree species is very high and the stands are multi-layered (Malhi et al., 1999; Montagnini & Jordan, 2005). Taking account of these differences in complexity of forest stands, the abovementioned studies are not completely comparable with the current study. Stem volume per unit area and thus its estimation is strongly influenced by the complexity of the forest stands. Consequently, stand diversity defined by stand density, vertical structure or

tree species composition, among others, is not as crucial for stem volume retrieval performed in boreal forest test sites as for heterogeneous temperate and tropical forests. In the case of the temperate forest of Traunstein, the targeted reconversion from homogeneous even-aged pure forests to close-to-nature, structurally rich, heterogeneous forests is far advanced. Hence, the stands are rich in tree species composition and highly structured and thus essentially more heterogeneous compared with forest areas investigated in most other studies performing stem volume estimation based on interferometric X-band SAR data.

However, the obtained estimations of stem volume yield similar results at plot level and at stand level compared with the other studies using interferometric X-band SAR data for biomass or stem volume estimation. At plot level (plot size 500 m<sup>2</sup>) simple linear regression based on height information achieved stem volume predictions with R<sup>2</sup> ranging from 56% to 60% and RMSE between 164.30 m<sup>3</sup> ha<sup>-1</sup> and 181.22 m<sup>3</sup> ha<sup>-1</sup> (relative RMSE between 44.40% and 48.97%). The multiple linear regression model employing the height information and the co-occurrence parameters led to the best results with R<sup>2</sup> of about 70% and RMSE of 155 m<sup>3</sup> ha<sup>-1</sup> (relative RMSE of 41.90%). In comparison Karila et al. (2015) obtained stem volume estimations at plot level (plot size about 300 m<sup>2</sup>) in the best case with RMSE of about 67.2 m<sup>3</sup> ha<sup>-1</sup> (relative RMSE = 32.2%) and R<sup>2</sup> of about 0.65 in spruce and pine dominated boreal forest stands using a nearest neighbor prediction model for stem volume estimation based on InSAR heights from TanDEM-X data. Rahlf et al. (2014) also predicted stem volume in spruce and pine dominated forest stands based on 250 m<sup>2</sup> plots by means of a linear mixed model based on interferometric TanDEM-X data with RMSE of 77.56 m<sup>3</sup> ha<sup>-1</sup> (relative RMSE of 41.60%). Solberg et al. (2013) obtained stem volume estimations at plot level (plot size 250 m<sup>2</sup>) with RMSE of about 94 m<sup>3</sup> ha<sup>-1</sup> (relative RMSE = 44%) in spruce dominated boreal forest stands using linear regression based on height information derived from TanDEM-X data. Gama et al. (2010) estimated stem volume by linear regression in tropical Eucalyptus plantations using interferometric airborne SAR data at plot level (size of about 400 m<sup>2</sup>) and achieved best results with RMSE of 33.56 m<sup>3</sup> ha<sup>-1</sup> (relative RMSE = 10.55%) and R<sup>2</sup> of about 84%. However, airborne data with considerable higher spatial resolution were used in this study.

At stand level (areas of 1.5 to 6.4 ha) stem volume estimation could be improved with R<sup>2</sup> between 68% and 88% and RMSE ranging from 72.35 m<sup>3</sup> ha<sup>-1</sup> to 91.20 m<sup>3</sup> ha<sup>-1</sup> (relative RMSE 27.03%–34.08%) using the linear regression model based on height information. The extension of the model with the co-occurrence parameters led to the best results at stand level with R<sup>2</sup> of 94% and RMSE of 44.25 m<sup>3</sup> ha<sup>-1</sup> (relative RMSE of 16.53%). These results are similar or even better compared with the stem volume estimations at stand level (stand size 1–3 ha) in spruce and pine dominated boreal forest reported by Rahlf et al. (2014) with RMSE of about 33.74 m<sup>3</sup> ha<sup>-1</sup> (relative RMSE = 18.10%) and Solberg et al. (2013) with R<sup>2</sup> of 81% and RMSE of about 44 m<sup>3</sup> ha<sup>-1</sup> (relative RMSE = 20%). Schlund et al. (2015) and Treuhaft et al. (2015) achieved biomass estimations based on interferometric TanDEM-X data in tropical forest stands (stand size <1 ha) with RMSE of 53 t ha<sup>-1</sup> (relative RMSE of about 20%) and 52–62 m<sup>3</sup> ha<sup>-1</sup> (relative RMSE of about 29%–35%) respectively. In Solberg et al. (2010) biomass retrievals with R<sup>2</sup> ranging from 0.45 to 0.81 and RMSE

**Table 9**  
Results from the linear regression model relating scattering center height or modeled top height from winter (09.01.2012) or summer (18.05.2013) acquisitions to stem volume per unit area at stand level described by the standard error SE of the parameters, root means square error RMSE of the predictions, RMSE related to the mean stem volume and the coefficient of determination R<sup>2</sup>.

Significance levels: p < 0.001 \*\*\*\* p < 0.01 \*\*\* p < 0.05 \*\* p < 0.1.

Parameter	Intercept( $\ln a_0$ )	SE $a_0$	$a_1$	SE $a_1$	RMSE [m <sup>3</sup> ha <sup>-1</sup> ]	RMSE [%]	R <sup>2</sup>
Scattering center height (winter)***	4.25***	0.21	0.58	0.09	77.02	28.78	0.68
Modeled top height (winter)***	0.27	0.78	1.74	0.24	73.35	27.41	0.73
Scattering center height (summer)***	2.64***	0.23	1.11	0.09	72.35	27.03	0.88
Modeled top height (summer)***	1.79	0.94	2.21	0.29	91.20	34.08	0.75

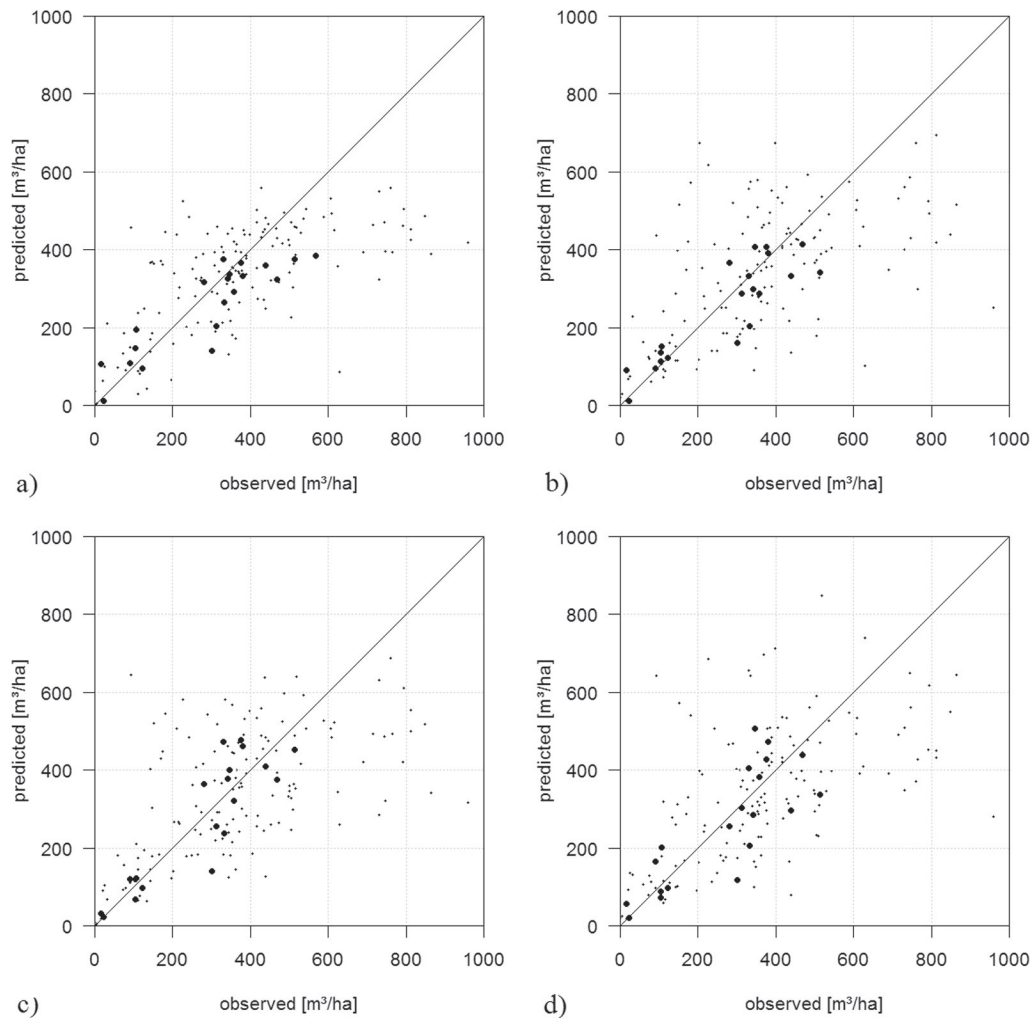


**Fig. 12.** Scatterplots comparing measured stem volume (on the x-axis) and predicted stem volume based on model (6) (on the y-axis) at plot (small dots) and stand level (large dots). Comparison of plot and stand level stem volume estimation based on a) scattering center height (09.01.2012), b) modeled top height (09.01.2012), c) scattering center height (18.05.2013), and d) modeled top height (18.05.2013).

of about  $17 \text{ t ha}^{-1}$  to  $36 \text{ t ha}^{-1}$  (relative RMSE of 21% to 36%) in boreal forest stands (stand size  $>2 \text{ ha}$ ) dominated by spruce and pine were achieved using a linear regression model based on interferometric height information from SRTM.

Compared with these studies carried out in boreal and tropical forests, the results of the current study are very viable in view of the fact that the volume estimations obtain similar or even better accuracies in the complex temperate forest stands of Traunstein. Also compared with stand-wise biomass prediction with  $R^2$  of 0.883 and RMSE of  $39.98 \text{ t ha}^{-1}$  (relative RMSE of 13.15%) based on L-band airborne data in Traunstein reported by Li et al. (2015), the results are similar. Nevertheless, the results show seasonal differences between the predictions based on the winter and the summer acquisitions. Especially the

estimates based on scattering center height are much better for the summer data. In areas dominated by deciduous tree species the scattering center height is situated rather far below the canopy due to lack of foliage in winter. In contrast, the modeled top height is less affected by the off-leaf effect. Therefore, the scattering center height from the summer acquisition is more appropriate for stem volume estimation. The modeled top height is related to the silvicultural parameter top height H100 (Kugler et al., 2011). In contrast, the scattering center height captures the spatial variations in height much better despite the penetration of the signal resulting underestimation of the actual tree height. For this reason, integration of the co-occurrence parameters is performed based on the summer acquisition of scattering center height. It was shown that the co-occurrence parameters improve stem

**Table 10**

Comparison of the results from the simple linear regression model and the extended linear regression model at stand level described by the standard error SE of the parameters, root mean square error RMSE of the predictions, RMSE related to the mean stem volume and the coefficient of determination  $R^2$ . The models are based on scattering center height or modeled top height from winter (09.01.2012) or summer (18.05.2013) acquisitions.

Parameter	Linear model			Extended linear model		
	RMSE [ $\text{m}^3 \text{ ha}^{-1}$ ]	RMSE [%]	$R^2$	RMSE [ $\text{m}^3 \text{ ha}^{-1}$ ]	RMSE [%]	$R^2$
Scattering center height (winter)	77.02	28.78	0.68	37.58	14.04	0.93
Modeled top height (winter)	73.35	27.41	0.73	35.87	13.40	0.93
Scattering center height (summer)	72.35	27.03	0.88	44.25	16.53	0.94
Modeled top height (summer)	91.20	34.08	0.75	54.74	20.45	0.91

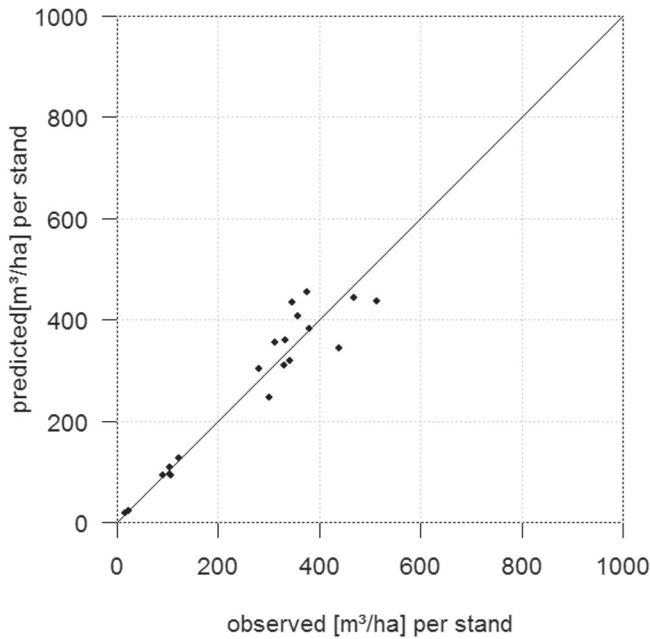


Fig. 13. Scatterplot comparing measured stem volume (on the x-axis) predicted stem volume based on model (11) (on the y-axis) per stand.

volume estimation substantially, i.e. the coefficient of determination was enhanced by 10% to 14% at plot level and 6% to 26% at stand level, respectively. The results at stand level are generally much better compared with the estimations at plot level. At plot level the limiting factor is the spatial resolution of scattering center height and modeled top height. With respect to inventory plots of 500 m<sup>2</sup>, each plot contains only 3 to 13 real height measurements at maximum. Consequently, stem volume estimations at plot level entails uncertainties and inaccuracies due to the limited detection of small-scale spatial variations. Furthermore, slight saturation effects occur at about 400 m<sup>3</sup> ha<sup>-1</sup> at plot level due to the insufficient spatial resolution of height information and thus missing sensitivity for high stand densities.

## 6. Conclusions

The aims of this study were defined as (i) estimation of stem volume per unit area at plot (circular plots of 500 m<sup>2</sup>) and stand level (areas of 1.5 to 6.4 ha) based on height information derived from TanDEM-X data and (ii) improvement of the predictions by integration of novel texture parameters representing horizontal stand structure.

A positive linear correlation between stem volume deduced from inventory data and height information derived from polarimetric interferometric TanDEM-X acquisitions was obvious. Stem volume per unit area was estimated by a linear regression model at plot and stand level based on scattering center height and modeled top height respectively. The prediction results showed that the scattering center height based on the summer acquisition was most suitable to predict stem volume per unit area. The results could be improved substantially by

extending the linear regression model by parameters derived from the Co-occurrence Matrix. The prediction results are very viable considering that the study area consists of very complex, heterogeneous, temperate forest stands using X-band satellite radar data.

The study shows the high potential of polarimetric interferometric X-band SAR data for the derivation of reliable stem volume estimations. To make a contribution to global sustainable forest management planning, the approach should be applied to other test sites regarding different concepts of silvicultural land use and forest biomes. By detecting and defining the homogeneous stands concerning forest structure by means of remote sensing, this approach could be extended and potentially deployed worldwide.

## Acknowledgments

This study was supported by the Federal Ministry for Economic Affairs and Energy under Project 50EE1261 and by the 'Helmholtz Alliance Remote Sensing and Earth System Dynamics' funded by the Initiative and Networking Fund of the Helmholtz Association under Project HA-3010. The authors would like to thank the German Aerospace Agency (DLR) for providing the TanDEM-X data and the Municipal Forest of Traunstein for supplying the inventory data. We also thank the anonymous reviewers for many constructive comments on the manuscript.

## References

- Antropov, O., Rauste, Y., Ahola, H., & Häme, T. (2013). Stand-level stem volume of boreal forests from spaceborne SAR imagery at L-band. *IEEE Journal of Selected Topics in Applied Earth Observations and Remote Sensing*, 6(1), 35–44.
- Apps, M.J., Kurz, W.A., Luxmoore, R.L., Nilsson, L.O., Sedjo, R.A., Schmidt, R., et al. (1993). Boreal forests and tundra. *Water, air, and soil pollution*, Vol. 70. (pp. 39–53). Kluwer Academic Publishers.
- Askne, J., Smith, G., & Santoro, M. (2004). L-band observations of boreal forest stem volume. *Remote Sensing in Transition*, 35(1), 159–165.
- Bamler, R., & Hartl, P. (1998). Synthetic aperture radar interferometry. *Inverse Problems*, 14, R1–R54.
- Bayerische Staatsforsten (2011). *Richtlinie für die mittel- und langfristige Forstbetriebsplanung in den Bayerischen Staatsforsten (Forsteinrichtungsrichtlinie – FER 2011)*. (Regensburg).
- Brown, S. (1997). Estimating biomass and biomass change of tropical forests: A primer. *FAO Forestry Paper*, 134.
- Cloude, S.R., & Papathanassiou, K.P. (2003). Three stage inversion process for polarimetric SAR interferometry. *IEEE Proceedings, Radar, Sonar and Navigation*, 150(3), 125–134.
- Dobson, M.C., Ulaby, F.T., Le Toan, T., Beaudoin, A., Kasischke, E.S., & Christensen, N. (1992). Dependence of radar backscatter on coniferous forest biomass. *IEEE Transactions on Geoscience and Remote Sensing*, 30(2), 412–415.
- Engelhart, S., Keuck, V., & Siegert, F. (2011). Aboveground biomass retrieval in tropical forests – the potential of combined X- and L-band SAR data use. *Remote Sensing of Environment*, 115, 1260–1271.
- FAO (2001). *Global forest resources assessment 2000*. Rome, Italy: FAO.
- FAO, & JRC (2012). *Global forest land-use change 1990–2005*. In E.J. Lindquist, R. D'Annunzio, A. Gerrand, K. MacDicken, F. Achard, & R. Beuchle (Eds.), *FAO forestry paper no. 169. Food and Agriculture Organization of the United Nations and European Commission Joint Research Centre*. Rome: FAO.
- Fischer, A. (2003). *Forstliche Vegetationskunde. Eine Einführung in die Geobotanik*. Stuttgart (Hohenheim): Verlag Eugen Ulmer GmbH & Co.
- Gama, F.F., Santos, J.R., & Mura, C.J. (2010). Eucalyptus biomass and volume estimation using interferometric and polarimetric SAR data. *Remote Sensing*, 2(4), 939–956.
- Gonçalves, F.G., Santos, J.R., & Treuhart, R.N. (2011). Stem volume of tropical forests from polarimetric radar. *International Journal of Remote Sensing*, 32(2), 503–522.
- Grömping, U. (2006). Relative importance for linear regression in R: The package relaimpo. *Journal of Statistical Software*, 17(1), 1–27.

Table 11  
Generalized characteristics of the global forest biomes.

	Boreal forests	Temperate forests	Tropical forests
Location	Circumpolar belt in high northern latitudes	Between 25° and 50° on both hemispheres	Between 25° and the equator
Climate	Short vegetation due to extreme weather conditions concerning temperature, precipitation and sunshine duration	Oceanic, sub-continental and semi-arid and arid	Wet and warm
Tree species	Limited number of tree species such as spruce, fir and pine	Deciduous and evergreen species	Dominated by evergreen or semi-deciduous species (typically 200–300 species/ha)
Vertical structure	Closed canopy and low understorey	Less dense canopy and more developed understorey	Multi-layered

- Hajnsek, I., Kugler, F., Lee, S.-K., & Papathanassiou, K.P. (2009). Tropical-forest-parameter estimation by means of Pol-InsAR: The INDREX-II campaign. *IEEE Transactions on Geoscience and Remote Sensing*, 47(2), 481–493.
- Haralick, R.M. (1971). On a texture-context feature extraction algorithm for remotely sensed imagery. *Proceedings IEEE Decision and Control Conference* (pp. 650–657).
- Haralick, R.M. (1979). Statistical and structural approaches to texture. *Proceedings of the IEEE*, 67(5), 786–804.
- Houghton, R., Hall, F., & Goetz, S. (2009). Importance of biomass in the global carbon cycle. *Journal of Geophysical Research*, 114, 1–13.
- Huxley, J.S. (1932). *Problems of relative growth*. 36 Essex Street W.C., London: Methuen & Co. Ltd.
- IPCC (2014). Climate change 2014: Mitigation of climate change. *Working group III contribution to the IPCC 5th assessment report* (Retrieved June 27, 2014, from [http://report.mitigation2014.org/drafts/final-draft-postplenary/ipcc\\_wg3\\_ar5\\_final-draft\\_postplenary\\_chapter11.pdf](http://report.mitigation2014.org/drafts/final-draft-postplenary/ipcc_wg3_ar5_final-draft_postplenary_chapter11.pdf)).
- Jenks, G.F., & Caspall, F.C. (1971). Error on choroplethic maps: Definition, measurement, reduction. *Annals of the Association of American Geographers*, 61(2), 217–244.
- Johnson, J.W., & LeBreton, J.M. (2004). History and use of relative importance indices in organizational research. *Organizational Research Methods*, 7(3), 238–257.
- Karila, K., Vastaranta, M., Karjalainen, M., & Kaasalainen, S. (2015). Tandem-X interferometry in the prediction of forest inventory attributes in managed boreal forests. *Remote Sensing of Environment*, 159, 259–268.
- Karjalainen, M., Kankare, V., Vastranata, M., Holopainen, M., & Hyypää, J. (2012). Prediction of plot-level forest variables using TerraSAR-X stereo SAR data. *Remote Sensing of Environment*, 117, 338–347.
- Kramer, H., & Akça, A. (1987). *Leitfaden für Dentrometrie und Bestandesinventur*. Frankfurt am Main: J. D. Sauerländer's Verlag.
- Krieger, G., Moreira, A., Fiedler, H., Hajnsek, I., Werner, M., Younis, M., et al. (2007). TanDEM-X: A satellite formation for high-resolution SAR interferometry. *IEEE Transactions on Geoscience and Remote Sensing*, 45(11), 3317–3337.
- Krieger, G.Z., Bachmann, M., Bräutigam, B., Schulze, D., Martone, M., Rizzoli, P., et al. (2013). TanDEM-X: A radar interferometer with two formation-flying satellites. *Acta Astronautica*, 89, 83–98.
- Kugler, F., Hajnsek, I., & Papathanassiou, K. (2011). Forest characterisation by means of TerraSAR-X and TanDEM-X (polarimetric and) interferometric data. *Proceedings PolInSAR* (pp. 2578–2581).
- Kugler, F., Schulze, D., Hajnsek, I., Pretzsch, H., & Papathanassiou, K.P. (2014). TanDEM-X Pol-InsAR performance for forest height estimation. *IEEE Transactions on Geoscience and Remote Sensing*, 52(10), 6404–6422.
- Lavalle, M., Solimini, D., Pottier, E., & Desnos, Y. -L. (2010). Compact polarimetric SAR interferometry. *IEEE Radar, Sonar and Navigation*, 4(3), 449–456.
- Le Toan, T., Beaudoin, A., Riou, J., & Guyon, D. (1992). Relating forest biomass to SAR data. *IEEE Transactions on Geoscience and Remote Sensing*, 30(2), 403–411.
- Li, W., Chen, E., Li, Z., Ke, Y., & Zhan, W. (2015). Forest aboveground biomass estimation using polarization coherence tomography and PolSAR segmentation. *International Journal of Remote Sensing*, 36(2), 530–550.
- Luckman, A., Baker, J., Honzák, M., & Lucas, R. (1998). Tropical forest biomass density estimation using JERS-1 SAR: Seasonal variation, confidence limits, and application to image mosaics. *Remote Sensing of Environment*, 63, 126–139.
- Malhi, Y., Baldocchi, D.D., & Jarvis, P.G. (1999). The carbon balance of tropical, temperate and boreal forests. *Plant, Cell and Environment*, 22(6), 715–740.
- Montagnini, F., & Jordan, C. (2005). Characteristics of tropical forests. *Tropical forest ecology. The basis for conservation and management* (pp. 19–73). Berlin, Heidelberg: Springer.
- Neumann, M., Ferro-Famil, L., & Reigber, A. (2010). Estimation of forest structure, ground, and canopy layer characteristics from multibaseline polarimetric interferometric SAR data. *IEEE Transactions on Geoscience and Remote Sensing*, 48(3), 1086–1104.
- Niklas, K.J. (1994). *Plant allometry. The scaling of form and process*. Chicago and London: The University of Chicago Press.
- Nilsson, M., & Holgren, J. (2003). Prediction of forest variables using LiDAR measurements with different footprint sizes and measurement densities. *Proceedings of the ScandLaser scientific workshop on airborne laser scanning of forests* (pp. 125–133).
- Papathanassiou, K.P., & Cloude, S.R. (2001). Single-baseline polarimetric SAR interferometry. *IEEE Transactions on Geoscience and Remote Sensing*, 39(11), 2352–2363.
- Pretzsch, H. (1996). Structural diversity as a result of silvicultural treatment. *Allgemeine Forst- und Jagdzeitung*, 11, 213–221.
- Pretzsch, H. (2003). Diversity and productivity of forests. *Allgemeine Forst- und Jagdzeitung*, 5/6, 88–98.
- Pretzsch, H. (2009). *Forest dynamics, growth and yield*. Berlin, Heidelberg: Springer-Verlag.
- Pulliaainen, J., Engdahl, M., & Hallikainen, M. (2003). Feasibility of multi-temporal interferometric SAR data for stand-level estimation of boreal forest stem volume. *Remote Sensing of Environment*, 85(4), 397–409.
- Rahlf, J., Breidenbach, J., Solberg, S., Naesset, E., & Astrup, R. (2014). Comparison of four types of 3D data for timber volume estimation. *Remote Sensing of Environment*, 325–333.
- Rauste, Y. (2005). Multi-temporal JERS SAR data in boreal forest biomass mapping. *Remote Sensing of Environment*, 97, 263–275.
- Rosen, P.A., Hensley, S., Joughin, I.R., Li, F.K., Madsen, S.N., Rodriguez, E., et al. (2000). Synthetic aperture radar interferometry. *Proceedings of the IEEE*, 88(3), 333–382.
- Schlamadinger, B., & Marland, G. (1996). The role of forest and bioenergy strategies in the global carbon cycle. *Biomass and Bioenergy*, 10(5–6), 275–300.
- Schlund, M., von Poncet, F., Kuntz, S., Schmillius, C., & Hoekman, D.H. (2015). TanDEM-X data for aboveground biomass retrieval in a tropical peat swamp forest. *Remote Sensing of Environment*, 158, 255–266.
- Solberg, S., Astrup, R., Gobakken, T., Naesset, E., & Weydahl, D.J. (2010). Estimating spruce and pine biomass with interferometric X-band SAR. *Remote Sensing of Environment*, 114, 2353–2360.
- Solberg, S., Astrup, R., Breidenbach, J., Nilsen, B., & Weydahl, D. (2013). Monitoring spruce volume and biomass with InSAR data from TanDEM-X. *Remote Sensing of Environment*, 139, 60–67.
- Solberg, S., Riegler, G., & Nonin, P. (2015). Estimating forest biomass from TerraSAR-X stripmap radargrammetry. *IEEE Transactions on Geoscience and Remote Sensing*, 53(1), 154–161.
- Thomas, S., & Baltzer, J. (2002). Tropical forests. *Encyclopedia of life sciences*.
- Tonidandel, S., & LeBreton, J.M. (2011). Relative importance analysis: A useful supplement to regression analysis. *Journal of Business and Psychology*, 26(1), 1–9.
- Treuhaft, R.N., Madsen, S.N., Moghaddam, M., & van Zyl, J.J. (1996). Vegetation characteristics and underlying topography from interferometric data. *Radio Science*, 31(6), 1449–1495.
- Treuhaft, R., Gonçalves, F., dos Santos, J.R., Keller, M., Palace, M., Madsen, S.N., et al. (2015). Tropical-forest biomass estimation at X-band from the spaceborne TanDEM-X interferometer. *IEEE Geoscience and Remote Sensing Letters*, 12(2), 239–243.
- Van Laar, A., & Akça, A. (2007). *Forest mensuration (managing forest ecosystems)*. Dordrecht, The Netherlands: Springer-Verlag, 118–121.
- Vastaranta, M., Holopainen, M., Karjalainen, M., Kankare, V., & Hyypää, J.K. (2014). TerraSAR-X stereo radargrammetry and airborne scanning LiDAR height metrics in imputation of forest aboveground biomass and stem volume. *IEEE Transactions on Geoscience and Remote Sensing*, 52(2), 1197–1204.
- von Bertalanffy, L. (1951). *Theoretische Biologie. Zweiter Band: Stoffwechsel, Wachstum*. Bern: A. Francke AG Verlag.
- von Carlowitz, H.C. (1713). *Sylvicultura Oeconomica oder haußwirthliche Nachricht und naturgemäße Anweisung zur wilden Baum-Zucht*. Leipzig: Johanna Friedrich Braun.
- Wagner, W., Luckman, A., Vietmeier, J., Tansey, K., Baltzer, H., Schmillius, C., et al. (2003). Large-scale mapping of boreal forest in Siberia using ERS tandem coherence and JERS backscatter data. *Remote Sensing of Environment*, 85, 125–144.

## **B Publication II**

**Title:** An unsupervised two-stage clustering approach for forest structure classification based on X-band InSAR data – A case study in complex temperate forest stands

**Authors:** Sahra Abdullahi, Mathias Schardt, Hans Pretzsch

**Journal:** *Published* in International Journal of Applied Earth Observation and Geoinformation (JAG)

**Impact Factor:** 3.930 (2016)

**Contribution:** TanDEM-X InSAR data was processed and provided by the Microwave and Radar Institute of the German Aerospace Center (DLR). Data analyses including data preparation, development and implementation of the classification approach, validation of the results as well as writing and composing the manuscript were performed by the first author Sahra Abdullahi. All co-authors contributed to the design and content of the paper by scientific advice, discussion and language editing.

© International Journal of Applied Earth Observation and Geoinformation, Elsevier  
<https://doi.org/10.1016/j.jag.2016.12.010>, Reprinted with permission.





Contents lists available at ScienceDirect

# International Journal of Applied Earth Observation and Geoinformation

journal homepage: [www.elsevier.com/locate/jag](http://www.elsevier.com/locate/jag)

## An unsupervised two-stage clustering approach for forest structure classification based on X-band InSAR data – A case study in complex temperate forest stands

Sahra Abdullahi<sup>a,\*</sup>, Mathias Schardt<sup>b,c</sup>, Hans Pretzsch<sup>a</sup><sup>a</sup> Technical University of Munich (TUM), Chair for Forest Growth and Yield Science, Hans-Carl-von-Carlowitz-Platz 2, 85354, Freising, Germany<sup>b</sup> Remote Sensing and Geoinformation, Institute for Information and Communication Technologies, Joanneum Research, Steyrergasse 17, 8010 Graz, Austria<sup>c</sup> Graz University of Technology, Institute of Remote Sensing and Photogrammetry, Steyrergasse 30, 8010 Graz, Austria

### ARTICLE INFO

#### Article history:

Received 8 August 2016

Received in revised form

12 December 2016

Accepted 14 December 2016

#### Keywords:

Forest structure

Unsupervised classification

TanDEM-X

InSAR

Self-Organizing Map (SOM)

k-means

Temperate forest

### ABSTRACT

Forest structure at stand level plays a key role for sustainable forest management, since the biodiversity, productivity, growth and stability of the forest can be positively influenced by managing its structural diversity. In contrast to field-based measurements, remote sensing techniques offer a cost-efficient opportunity to collect area-wide information about forest stand structure with high spatial and temporal resolution. Especially Interferometric Synthetic Aperture Radar (InSAR), which facilitates worldwide acquisition of 3d information independent from weather conditions and illumination, is convenient to capture forest stand structure. This study purposes an unsupervised two-stage clustering approach for forest structure classification based on height information derived from interferometric X-band SAR data which was performed in complex temperate forest stands of Traunstein forest (South Germany). In particular, a four dimensional input data set composed of first-order height statistics was non-linearly projected on a two-dimensional Self-Organizing Map, spatially ordered according to similarity (based on the Euclidean distance) in the first stage and classified using the k-means algorithm in the second stage. The study demonstrated that X-band InSAR data exhibits considerable capabilities for forest structure classification. Moreover, the unsupervised classification approach achieved meaningful and reasonable results by means of comparison to aerial imagery and LiDAR data.

© 2016 Elsevier B.V. All rights reserved.

### 1. Introduction

Forest structure can be treated at different spatial scales. However, patch or stand level is the most important spatial unit for most forest plants and animals. By their size and longevity, trees determine the structure, stand-internal environmental conditions and flora and fauna habitats (Kuuluvainen et al., 1996). In general, stand density, size distribution and horizontal as well as vertical tree distribution patterns are used for the description of stand structure (del Río et al., 2015). Stand structure is a consequence of species selection, stand dynamics, human, biotic and abiotic disturbances (Pretzsch et al., 2015b; Pommerening, 2006; Kuuluvainen et al., 1996). Managed forest stands are often limited in structure due to homogeneous one-age-cohort forests and thus restricted in diversity and complexity (Perry, 1994). As opposed to this, unmanaged

or “close-to-nature” forest stands often exhibit a heterogeneous and much more complex structure with uneven-aged trees and diverse species composition (Pretzsch et al., 2015a; Bauhus et al., 2013). On the basis of such a complexity, characterized by spatial heterogeneity due to different tree size dimensions and diverse species compositions, the productivity and resilience of the forest is often positively influenced (Pretzsch, 2005; Carey and Wilson, 2001). Consequently, measures of stand structure diversity serve as an indicator for the stability of the forest ecosystem as well as a predictor for growth and development (Pretzsch, 2009). Moreover, stand structure is a surrogate for stand biodiversity, since high biodiversity is related to stands comprising multiple tree species and sizes (Bergen et al., 2009; McElhinny et al., 2005; Staudhammer and LeMay, 2001). Accordingly, stand structure plays a key role for sustainable forest management, since the biodiversity, productivity, growth and stability of the forest can be positively influenced by managing its structural diversity (Pommerening, 2006; Önal, 1997).

Terrestrial measurements as part of forest inventories of structure attributes, such as stand density, basal area or height, can be

\* Corresponding author.

E-mail address: [Sahra.Abdullahi@lrz.tum.de](mailto:Sahra.Abdullahi@lrz.tum.de) (S. Abdullahi).

conducted to assess conservation and sustainability as well as temporal and spatial changes in forest structure and thus provide a basis of decision-making at local, national and global level (Gao et al., 2014; Kuuluvainen et al., 1996). However, the major disadvantage of traditional forest inventories (like National Forest Inventory in Germany, Sweden or Great Britain with an usual repetition rate of ten years) in terms of forest stand structure is its sample-based survey design. The spatial patterns cannot be captured properly without area-wide information. Furthermore, these inventories are very expensive, labor-intensive and only available for the minority of the forest areas worldwide.

In contrast, remote sensing techniques offer a good and cost-efficient opportunity to overcome these problems, since they provide area-wide data collection with high spatial and temporal resolution. Numerous studies investigate the potential of remote sensing data for the estimation of forest structure. On the one hand, forest attributes, such as height, basal area, canopy cover, stand density or biomass, are derived to describe the forest stand structure (e.g. Pfeifer et al., 2016; Naidoo et al., 2015; Gómez et al., 2012). On the other hand, forests are categorized or classified into different structure types according to parameters, such as height, species, biomass, canopy cover as well as heterogeneity (e.g. Huesca et al., 2016; Varghese et al., 2016; Falkowski et al., 2009).

Studies in this field are based on different remote sensing techniques, i.e. multispectral, hyperspectral, LiDAR (Light Detection And Ranging) or RaDAR (Radio Detection And Ranging) sensors. In case of multi- and hyperspectral data, spectral information in terms of reflectance (e.g. Gómez et al., 2012; Castillo-Santiago et al., 2010; Liu et al., 2008), spectral indices (e.g. Pfeifer et al., 2016; Chen et al., 2015; Peña et al., 2012) and texture features (e.g. Beguet et al., 2013; Kayitakire et al., 2006; Coburn and Roberts, 2004) are commonly used to detect forest structure. LiDAR acquisitions based on airborne platforms are widely used to derive height information to capture forest structure (e.g. Hollaus et al., 2011; Falkowski et al., 2009; Hyyppä et al., 2008). In the case of RaDAR, either backscatter intensity (e.g. Varghese et al., 2016; Naidoo et al., 2015; Chand and Badarinath, 2007) or derived height information (e.g. Karila et al., 2015; Karjalainen et al., 2012; Solberg et al., 2010) are frequently employed to estimate forest stand structure.

Among these remote sensing systems, active RaDAR sensors are convenient compared to passive optical (i.e. multi- and hyperspectral) sensors since they are operating in the microwave instead of the visible and infrared range of the electromagnetic spectrum. The longer wavelengths enable observations of the Earth's surface independently from cloud cover and illumination. Especially over tropical forest areas, the all-weather capability of radar systems is its biggest advantage over optical systems. Synthetic Aperture Radar (SAR) systems offer worldwide observations with high spatial and temporal resolution. Interferometric SAR (InSAR) systems facilitate the acquisition of 3d information and thus are an appropriate basis for the detection and investigation of forest structure in a global context. Depending on the wavelength and thus the penetration ability of the signal, such systems are sensitive to 3d distribution of different scattering elements of the forest (i.e. leaves, branches and trunks) and provide additional information on different vertical forest layers (Varghese et al., 2016; Yang et al., 2014). Compared to LiDAR data, InSAR data is preferable due to its worldwide availability and more cost-efficient acquisition.

However, only few studies explore the potential of InSAR data for forest type and/or forest structure classification. For example, Hoekman and Quiñones (2002) distinguished several forest classes based on polarimetric coherence from AirSAR C-, L- and P-band data of tropical forest in Central Colombia. Liesenberg and Gloaguen (2013) classified interferometric L-band ALOS PALSAR data into different forest types in the tropical forest of Eastern Amazon in Brazil and De Grandi et al. (2015) used interferometric TanDEM-X data to

map forest spatial structure in tropical forest of the Republic of Congo.

In contrast to previous studies that aim for forest structure classification using predominantly longer wavelengths (i.e. P- and L-band), the current study investigates forest structure classification based on X-band InSAR data. Furthermore, compared to other studies concerning forest structure classification which were carried out in tropical forests this work was carried out in complex temperate forest stands. Hence, this study contributes to fill the research gap in the field of forest structure classification using short wavelengths (i.e. X-band) with regard to temperate forests. The heterogeneity in height of the main forest layer is captured by means of interferometric height information derived from TanDEM-X data to distinguish different forest structure classes. In order to ensure easy transferability to any given forest, an approach without any requirement of a-priori information about the present forest structure and its complexity or the number of classes and class definitions is developed. For this purpose, an unsupervised two-stage clustering approach is proposed. In particular, a four dimensional input data set composed of first-order height statistics was non-linearly projected on a two-dimensional Self-Organizing Map, spatially ordered according to similarity (based on the Euclidean distance) in the first stage and classified using the k-means algorithm in the second stage. As case study, the temperate forest of Traunstein in Southeast of Bavaria (Germany) was chosen due to its structural richness and heterogeneous forest stands. Therefore, the objectives of this work encompass i) extraction and ii) classification of forest structure by means of an unsupervised approach based on height information derived from X-band InSAR data.

## 2. Materials

### 2.1. Study area

The highly structured, mixed, temperate municipal forest close to the city of Traunstein, Germany (47°52' N, 12°38' E) serves as study area (Fig. 1). Traunstein forest is supervised and used for teaching and research purposes by the Chair for Forest Growth and Yield Science of the Technical University of Munich (TUM). The study area is limited by the coverage of the TanDEM-X acquisition to a forest area of 243 ha bounded by the districts Bürgerwald and Heiligengeistwald. The topography ranges from 630 to 720 m above sea level and includes small areas with steep slopes. The soils are composed of glacier sediments which belong to the pre-alpine moraine landscape. The climatic conditions are characterized by a mean annual temperature of 7.3 °C and precipitation up to 1600 mm per year. The forest is predominantly composed of Norway spruce (*Picea abies*), European silver fir (*Abies alba*), European beech (*Fagus sylvatica*) and Sycamore maple (*Acer pseudoplatanus*). Traunstein forest passes through an ongoing reconversion from a homogeneous one-age cohort forest to a structurally rich, heterogeneous forest. The forest stands are very complex concerning tree species richness and heterogeneous stand structures due to “close-to-nature” silviculture (Pretzsch, 1996), which is reflected in a broad distribution of tree species (Fig. 2a) and growth stages (Fig. 2b). Therefore, Traunstein forest is a perfect example for the whole spectrum of silviculture types in Central Europe. Furthermore, as a result of new concepts of silviculture due to climate change and policy guidelines, more and more forests will undergo a change from homogeneous one-age-cohort forests to structurally rich heterogeneous forests. Consequently, forest Traunstein is predestinated as case study for forest structure classification in temperate forests.

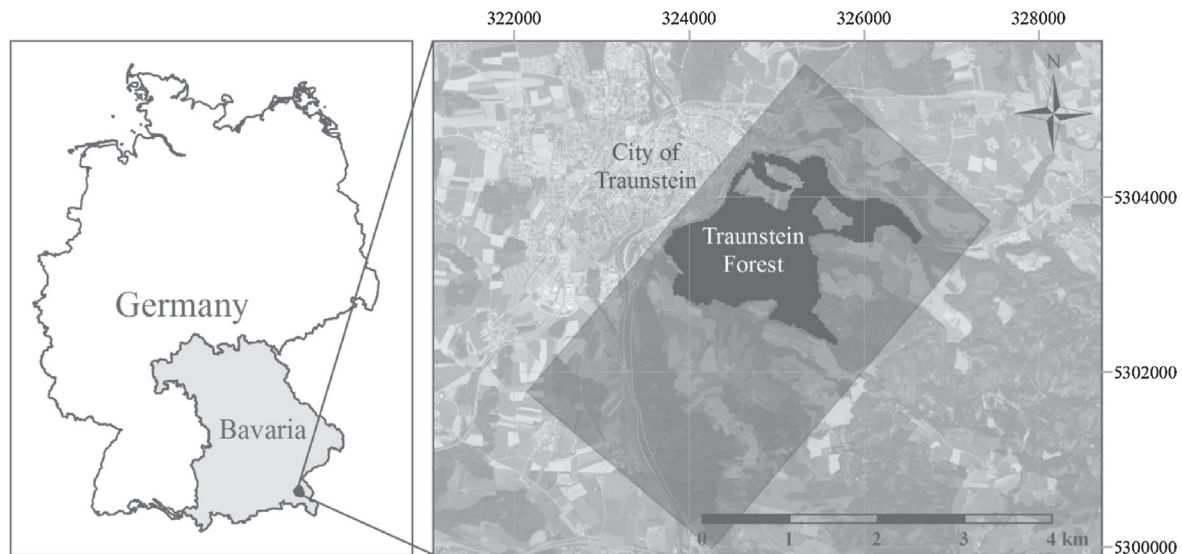


**Fig. 1.** The study area is located next to the city of Traunstein in the South of Germany and covers an area of about 243 ha. The mixed, temperate forest is highly structured due to “close-to-nature” silviculture.

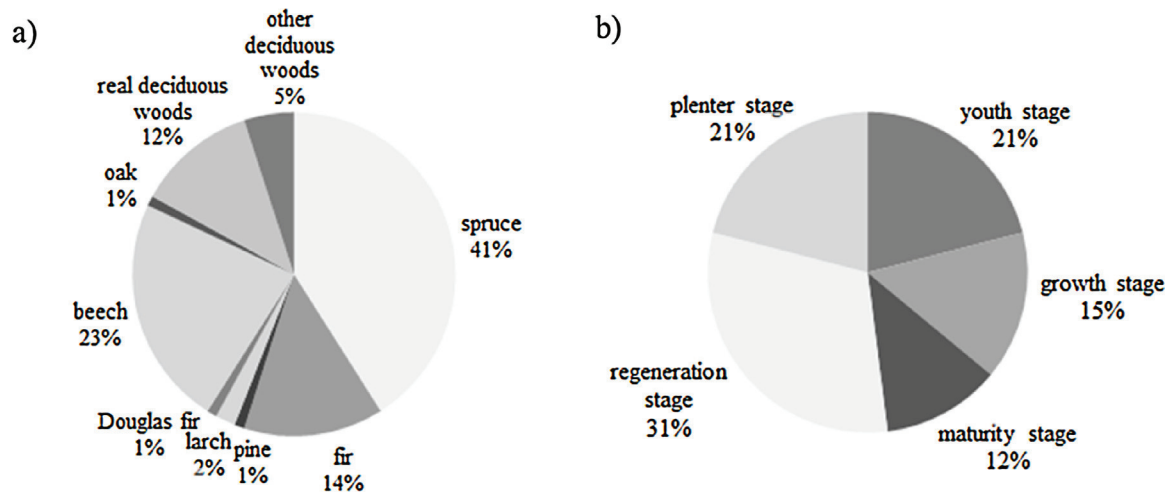


**Fig. 2.** a) Area percentages of tree species and b) area percentages of development stages within the study area.

## 2.2. Remote sensing data

Two dual-polarized interferometric images acquired on May 18, 2013 during the TanDEM-X mission were used. The mission is composed of the two almost identical radar satellites TerraSAR-X (launched in 2007) and TanDEM-X (launched in 2010) which are operating in X- (8–12 GHz) band. The images were acquired in bistatic StripMap mode in ascending orbit with an incidence angle of 43.2° under dry weather conditions. The baseline between the two sensors was 142.72 m. In addition, an airborne LiDAR survey was conducted on November 18, 2012 with a flight height of about 500 m and a point density of about 25 dots per m<sup>2</sup> using the LMS-Q 680i Scanner from RIEGL. The associated Digital Terrain Model (DTM) as well as Digital Surface Model (DSM) was provided by MILAN Geoservice GmbH.

First a DSM, which represents the height of all elevated objects on the Earth's surface, was calculated with a pixel-spacing of 6 m from the interferometric TanDEM-X acquisitions (Abdullahi et al., 2016). In a second step, the derived DSM was normalized by subtracting the LiDAR-based DTM. The DSM was calculated from the VV-polarized InSAR data, since previous studies in Traunstein forest indicate that the VV polarization is more suitable for height

estimation due to less ground scattering contribution compared to HH (Kugler et al., 2011). For the generation of the DSM, the scattering signals, which were simultaneously acquired from slightly different positions, were coherently combined in an interferogram (Krieger et al., 2013; Rosen et al., 2000). The phase differences of the two acquisitions are represented by the resulting interferometric phase, which is mainly affected by the differences in range (Bamler and Hartl, 1998). For terrain reconstruction, phase unwrapping was employed to resolve the ambiguity of the interferometric phase by conversion of the phase differences into height based on the interferometer geometry (Rosen et al., 2000). The derived DSM was normalized by subtracting the LiDAR-based DTM. The normalized DSM (nDSM), referred to as scattering center height, corresponds to a vegetation height model. Due to the penetration of the radar signal, the scattering center height underdetermines the actual vegetation height.

## 3. Methods

An unsupervised clustering approach was utilized to classify forest structure without any requirement of a-priori information about class definitions. Cluster analysis, which partitions input data

into groups (or clusters) taking account of the similarity (or dissimilarity) between each data object (Webb and Copsey, 2011; Hastie et al., 2009), was applied to extract the structure behind the derived height data. In general, clustering methods can be divided into two basic approaches: hierarchical and partitional clustering (Kaski, 1997). Thereby, either smaller clusters are merged successively into larger ones (agglomerative approaches), or larger clusters are split successively into smaller ones (divisive methods) (Kaski, 1997). In contrast, partitional clustering methods directly assign data objects to a predefined number of clusters by minimizing a criterion (Xu and Wunsch, 2005; Kaski, 1997). Regarding forest structure classification based on a huge amount of input data (due to the small spatial units of  $24 \times 24 \text{ m}^2$  in this case), partitional clustering methods are more suitable compared to hierarchical methods, which have high computational costs and thus are inappropriate. Indeed, partitional techniques possess the disadvantage in terms of unsupervised classification that a-priori definition of the number of clusters is required. However, as a solution, the optimal number of clusters can be determined based on the criterion which has to be minimized.

Vesanto and Alhoniemi (2000) demonstrated that a two-stage partitional clustering approach consisting of the Self-Organizing Map (SOM) according to Kohonen (1982) and followed by the k-means algorithm based on MacQueen (1967) performs well when compared with direct clustering of the data. Prototype vectors corresponding to groups of similar data samples were produced by means of the SOM in the first stage and clustered using the k-means algorithm in the second stage. Furthermore, the two-stage clustering approach is appropriate to classify forest structure due to its low computational load and its low sensitivity to random variations (Vesanto and Alhoniemi, 2000).

Therefore, an unsupervised two-stage clustering approach composed of the partitional clustering methods SOM and k-means was applied to the calculated object-based features of  $24 \times 24 \text{ m}^2$  units to extract and classify forest structure. Fig. 3 depicts the workflow of the classification process. The processing of the object-based features contains a chessboard segmentation of the whole study area as a basis for the subsequent feature calculation and feature normalization. The forest structure classification was performed according to two steps: 1) capturing of the data structure by means of the SOM and 2) classification of the pre-structured data set using the k-means algorithm. Subsequently, the resulting clusters were labeled according to their characteristics by means of height histograms for each cluster, an orthophoto and the LiDAR-based nDSM.

### 3.1. Processing of object-based features

#### 3.1.1. Chessboard segmentation

Chessboard segmentation was applied to the whole study area by means of the Definiens Developer Software (Definiens, 2009) to split the test site into squared objects with a size of  $24 \times 24 \text{ m}^2$ . The object area was defined in order to cover approximately a circular inventory plot with a radius of 12.62 m as commonly used for traditional forest inventory in Germany. Another reason is that, forest successional processes, which substantially affect forest structure in near natural forest stands, take place on patches at this spatial scale (Pretzsch, 2009; Bugmann, 2001).

#### 3.1.2. Feature calculation

For each derived object, four first order statistics of the scattering center height were extracted: minimum height, mean height, maximum height and standard deviation of height according to (1)–(4)

$$\text{minimum}_i = \min(H(a, b)_i) \quad (1)$$

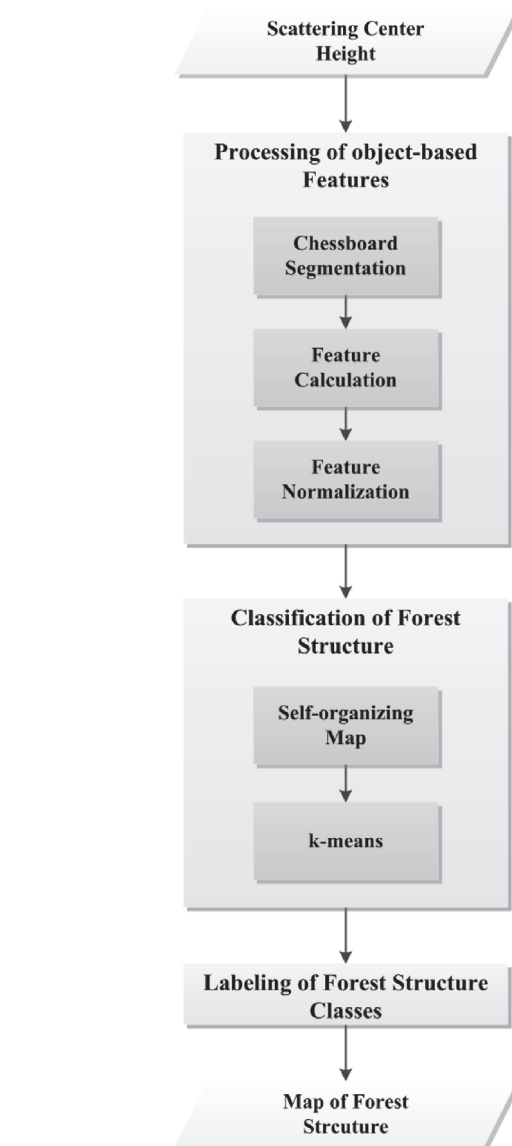


Fig. 3. Workflow of the forest structure classification.

$$\text{mean}_i = \frac{\sum H(a, b)_i}{N} \quad (2)$$

$$\text{maximum}_i = \max H(a, b)_i \quad (3)$$

$$\text{standard deviation}_i = \frac{\sum (H(a, b)_i - \text{mean}_i)^2}{\sum H(a, b)_i} \quad (4)$$

where  $i$  is the index of the objects,  $a$  and  $b$  are the indices of columns and rows,  $H(a, b)$  is the value of the scattering center height raster of object  $i$  at the position  $(a, b)$ .

The applicability of first-order statistics in the context of forest structure has already been demonstrated in several studies (e.g. Huang et al., 2014; Hyde et al., 2006).

Since it is assumed that the clustering approach will be less sensitive to the forest structure if open spaces are included, all areas, which are related to almost treeless areas with predominantly seedlings and shrubs, were excluded by applying a threshold. Thereby, all objects, which possess zero value as the majority and a mean value less than 3 m were left out of the following analyses.

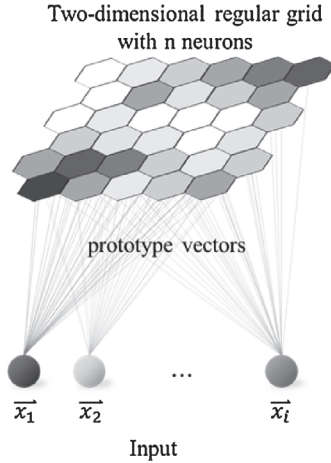


**Fig. 4.** Self-Organizing Map (SOM) architecture consisting of  $n$  neurons which are organized on a regular grid and represented by  $d$ -dimensional (equal to the dimension of the input vectors  $\mathbf{x}$ ) prototype vectors. Each prototype vector is connected to all input vectors.

### 3.1.3. Feature normalization

The four dimensional input data set consisting of the summary height statistics was normalized by a linear transformation which scales the variables to mean value of 0 and standard deviation of 1 according to (5), while preserving the relation of the variables to each other (Vesanto et al., 2000).

$$x_{norm} = \frac{x - \mu}{\sigma} \quad (5)$$

where  $x_{norm}$  is the normalized variable,  $x$  is the input variable,  $\mu$  is the mean value of  $x$  and  $\sigma$  is the standard deviation of  $x$ .

Normalization of the variables is of particular importance, since clustering algorithms are based on distance measures, commonly the Euclidean distance. To achieve good results, it is crucial to normalize the variables in order to balance the influence of the input features (Kantardzic, 2011). Assuming the variables possess different range of values, their impact would be varying and hence, few variables dominate the clustering process.

## 3.2. Classification of forest structure

### 3.2.1. Self-Organizing Map

The Self-Organizing Map (SOM) is a low-dimensional artificial neural network which was introduced by Kohonen (1982). It partitions data into groups according to similarity which are optimally represented by prototype vectors and ordered spatially (Kohonen, 2013). The SOM consists of  $n$  neurons which are organized on a regular (commonly two-dimensional) grid and represented by  $d$ -dimensional (equal to the dimension of the input vectors  $\mathbf{x}$ ) prototype vectors  $m_i = [m_{i_1} m_{i_2} \dots m_{i_d}]$ . Each prototype vector is connected to all input vectors (see Fig. 4). During the iterative learning process, each input vector is assigned to one prototype vector by minimizing a distance measure (commonly the Euclidean distance). Subsequently, the prototype vector and its topological neighbors are adjusted and ordered spatially until the map is stabilized (Kohonen, 2013; Ritter and Kohonen, 1989). As a consequence, a non-linear projection of the input data, which represents the neighborhood relationships between the input vectors and thus, a spatial representation of the data structure, is generated (Kohonen, 1990; Ritter and Kohonen, 1989).

The SOM algorithm was applied to the extracted object-based feature set of statistical height information by using the SOM Toolbox implemented in Matlab according to Vesanto et al. (2000).

First, the appropriate total number of neurons was estimated based on a heuristic formula, where the number of neuron is defined as the square root of the number of input data samples multiplied by five (Vesanto et al., 2000). Subsequently, the ratio of the horizontal and vertical dimension of the network was determined according to the ratio of the two largest eigenvalues of the input data (Kohonen, 2013). The actual network dimensions were set in order that their product is as close as possible to the predefined number of neurons by preserving the defined ratio (Kohonen, 2014). Furthermore, the neurons were arranged on a hexagonal lattice, since it is much more accurate compared to other grid structures (Kohonen, 2013).

Second, the prototype vectors were linearly initialized based on a two-dimensional sequence along a hyperplane spanned by the two largest eigenvalues of the input data, since it is significantly faster compared to random initialization (Kohonen, 2013; Vesanto et al., 2000).

Third, batch-type training was applied to the network to adjust and spatially order the prototype vectors. The batch-type training, which applies all input vectors at once (i.e. as one batch) instead of sequentially as in the case of stepwise-recursive to the algorithm until a stable state is reached, is advantageous regarding computation time and accuracy (Kohonen, 2013).

The training process is composed of competition and adjustment and was performed according to the following steps:

1) Each input vector  $\mathbf{x}$  was compared with all prototype vectors  $m$

2) For each input vector, the best matching unit (BMU) with the smallest Euclidean distance (i.e. with the highest similarity) to the input vector was determined. The BMU is defined according to (6) (Vesanto et al., 2000):

$$\|\mathbf{x} - m_c\| = \min_i \{\|\mathbf{x} - m_i\|\} \quad (6)$$

, where  $c$  is the BMU and  $m_c$  the prototype vector associated to the BMU.

3) The neighborhood for each BMU was determined according to the neighborhood function, which is maximal at the BMUs, decreases monotonically with increasing distance to the BMUs and is independent of the BMUs location. The Gaussian neighborhood function  $h_{c_i}$  is defined as (Vesanto et al., 2000):

$$h_{c_i} = e^{-\frac{r_c - r_i}{2\sigma(t)^2}} \quad (7)$$

, where  $r_c - r_i$  is the distance between BMU  $c$  and map unit  $i$  and  $\sigma(t)$  is the neighborhood radius at time  $t$ .

4) The BMUs and their neighbors were adjusted by the replacement of the old prototype vectors with the averages of the assigned input vectors and their projection into the neighborhood weighted by the neighborhood function according to (8) (Vesanto et al., 2000):

$$m_i(t+1) = \frac{\sum_{j=1}^n h_{c_{i(j)}}(t) x_j}{\sum_{j=1}^n h_{c_{i(j)}}(t)} \quad (8)$$

, where  $m_i(t+1)$  is the prototype vector of map unit  $i$  at time  $t+1$ ,  $c(j)$  is the BMU of the input vector  $x_j$ ,  $h_{c_{i(j)}}$  the corresponding neighborhood function and  $n$  the number of input vectors.

The training steps were reiterated until adequate accuracy and a stable map were achieved.

Based on the SOM the input feature set was grouped into many clusters and thus extracts the fine underlying structure of the height information. However, in terms of meaningfulness as well as practicability the number of forest structure classes had to be reduced while grouping similar map units.

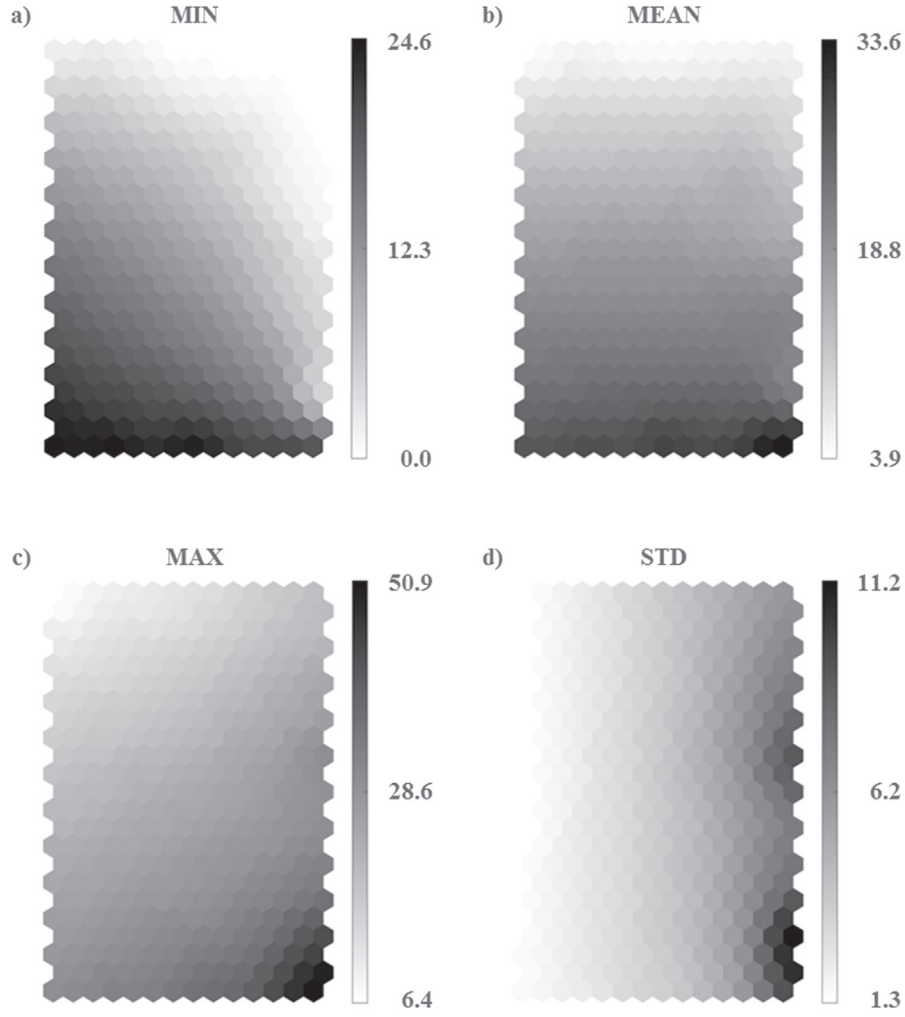


Fig. 5. SOM split into its four denormalized components: a) minimum, b) mean, c) maximum and d) standard deviation of height.

### 3.2.2. *k*-means

The *k*-means algorithm according to MacQueen (1967) is one of the simplest unsupervised clustering techniques; nevertheless it yields to satisfying results and is still widely used (Jain, 2010). A given data set  $x$  is grouped into  $k$  a-priori fixed clusters by minimizing the total within cluster variance (i.e. the sum of squared errors) (Jain, 2010; Hastie et al., 2009).

The clustering process is also composed of competition and adjustment and was implemented according to the following steps:

- 1) The centroids  $\mu$  of the  $K$  desired clusters  $C = \{c_k, k = 1, \dots, K\}$  were initialized randomly
- 2) Each data sample  $x_i$  was assigned to the closest cluster centroid  $\mu_k$ , i.e. with the smallest Euclidean distance. Accordingly, the sum of the squared error (i.e. within cluster variance) over all clusters is minimized (Jain, 2010; Xu and Wnsch, 2010):

$$J(C) = \min \left\{ \sum_{k=1}^K \sum_{x_i \in C_k} \|x_i - \mu_k\|^2 \right\} \quad (9)$$

, where  $J(t)$  is the sum of the squared error and  $\mu_k$  is the cluster centroid of cluster  $c_k$ .

- 3) The cluster centroids were adjusted by the replacement with the mean values of all associated data samples according to (10) (Jain, 2010; Xu and Wnsch, 2010):

$$\mu_k(t+1) = \frac{1}{N_k} \sum_{x_i \in C_k} x_i \quad (10)$$

, where  $\mu_n(t+1)$  is the cluster centroid of cluster  $j$  at time  $t+1$  and  $N_k$  is the number of data samples in cluster  $c_k$ .

The processing steps 2) and 3) were reiterated until a stabilized state (i.e. cluster membership does not change anymore) is reached. To avoid the convergence to a local minimum, the algorithm was replicated 1000 times and the most frequent result was used. However, without any a-priori information about the expected number of forest structure types and class definitions, the a-priori determination of  $k$  was not feasible. To solve this problem, the optimal number of clusters was determined by means of the within cluster variance (i.e. within-cluster sum of distances from the data points to the cluster centroids). For different values of  $k$  (i.e. different number of clusters) the within-cluster sum of distances was calculated in the replicative clustering process and plotted against  $k$ . The within-cluster sum of distances decreases with increasing values of  $k$ , since the size of clusters become smaller and thus the variance around the cluster centroids decreases. The point of the curve where the successive decrease in the within-cluster sum of distances become significantly smaller (i.e. significant flattening of the curve) iden-

tifies the optimal  $k$  to describe the data structure (Manning et al., 2008).

#### 4. Results

As a result of the forest structure classification based on  $24 \times 24 \text{ m}^2$  spatial units by means of an unsupervised two-stage clustering approach, nine classes were distinguished concerning vertical layering and canopy coverage of the forest stands.

##### 4.1. Forest structure classification – first stage

In the first stage of the classification process, a SOM composed of 322 map units was generated based on 4093 four-dimensional input data vectors. The appropriate network size of  $23 \times 14$  was determined by means of the two largest eigenvalues of the input data set. The four dimensional input data set composed of first-order height statistics (i.e. minimum height, mean height, maximum height and standard deviation of scattering center height) was non-linearly projected on the two-dimensional map and spatially ordered according to similarity. Thus, each input vector was assigned to a map unit according to its characteristics. Fig. 5 depicts the SOM for each of the four components. Each hexagon corresponds to one map unit and represents the mean characteristic of minimum height, mean height, maximum height or standard deviation of height of the associated input vectors, respectively. For illustration purposes, the components are denormalized to show their original value range. The minimum height rises from the upper right corner of the map to the lower left corner (Fig. 5a). In contrast, mean height increases from top to bottom (Fig. 5b) and maximum height from upper left to lower right (Fig. 5c). The standard deviation of height raises from left to right, however there are two spatially separated areas of very high standard deviation (Fig. 5d). Accordingly, data samples which were assigned to the upper left area of the map describe rather homogeneous, low forest stands, since minimum, mean, maximum height have similar values and standard deviation of height is low. As opposed to that, data samples corresponding to the lower right part of the map were derived from heterogeneous multi-layer forest stands with very high and very small trees. In principle, all data samples referred to the left part of the SOM originate from rather homogeneous forest stands due to the low standard deviation whereas all data samples assigned to the right part of the map belong to rather heterogeneous forest stands with higher standard deviation in height.

Fig. 6 shows the distribution of the 4093 input vectors on the map units of the SOM (i.e. hits per map unit) or, in other words, the distribution of BMUs. The more the hexagons are filled, the more often the corresponding map unit was determined as BMU for an input vector. In general all map units are occupied, however in some parts of the SOM a concentration of BMUs can be observed. Especially parts of the map with low standard deviation of height (Fig. 5d), thus map units corresponding to rather homogeneous forest stands, are more densely populated compared to map units with high standard deviation of height (Fig. 5d) which correspond to heterogeneous areas of the forest.

Fig. 7 illustrates the similarity in height characteristic (i.e. minimum, mean, maximum and standard deviation of scattering center height) of the map units to each other by related color shades. The difference in color clarifies the separation (i.e. the distance) between the map units. Consequently, similar map units have similar colors and dissimilar map units have different colors. For instance, the map units on the left part (with shades of green to yellow) can be easily distinguished from the map units on the right part (with shades of blue to pink) of the map. Compared to Fig. 5d, the coloring divided homogeneous forest stands (represented by

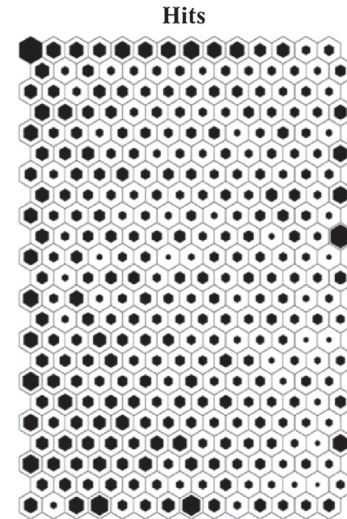


Fig. 6. Hits per map unit. The bigger the black hexagons, the more often the corresponding map units were determined as BMU.

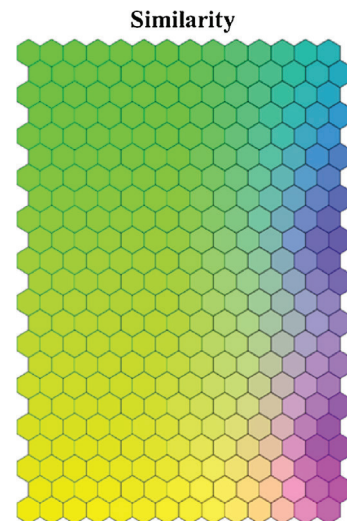


Fig. 7. Similarity of the map units.

the map units belonging to the left part) and heterogeneous forest stands (represented by the map units belonging to the right part) according to low and high standard deviation of height. Furthermore, the difference in height from top to bottom of the SOM corresponding to low and high mean height (Fig. 5b) is well illustrated by the color transition from shades of green and blue to shades of yellow and pink.

Concluding, the SOM reflects the spatial patterns of similarity and dissimilarity in the four height characteristics of the input data vectors and thus extracts the fine structure of the data set. Fig. 5 illustrated that the input data vectors were not only clustered according to their characteristics, but also the clusters (i.e. map units) were spatially ordered. Fig. 7 showed that homogeneous and heterogeneous as well as low and high forest stands were well separated. However, a total of 322 map units (i.e. forest structure classes) are not reasonable for practical applications and therefore a meaningful forest structure classification was investigated by further clustering the SOM using the k-means algorithm.

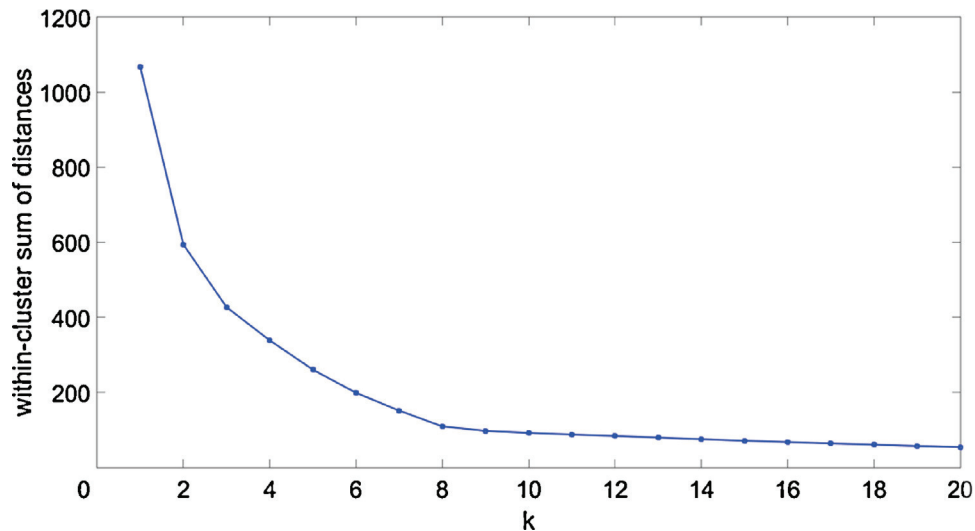


Fig. 8. Within-cluster sum of point-to-centroid distances against number of clusters  $k$ .

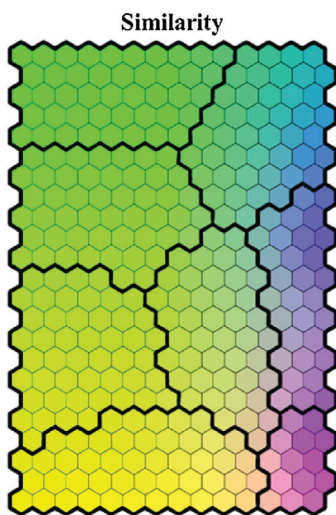


Fig. 9. Similarity of map units related to color shades with cluster boundaries according to k-means.

#### 4.2. Forest structure classification – second stage

In order to apply the k-means algorithm to cluster the map units of the SOM, the number of desired clusters has to be defined. For this purpose, the within-cluster variance (i.e. within-cluster sum of point-to-centroid distances) was used to determine the optimal number of clusters. Fig. 8 shows the plot of the within-cluster sum of point-to-centroid distances plotted against the number of clusters  $k$ . As shown in Fig. 8, the within-cluster sum of distances decreases significantly until  $k = 8$ , flattens at this point and approaches the minimum. Therefore, the optimal number of clusters was eight in case of the SOM based on the TanDEM-X InSAR data of Traunstein forest.

Accordingly, the k-means clustering was applied to the SOM with the predefined number of classes  $k = 8$ . Fig. 9 shows the similarity of the map units according to color shades (Fig. 7) and the boundaries of the consequent clusters. Obviously, similar map units were grouped.

The additional consideration of Fig. 10, which depicts the SOM for each component (Fig. 5) together with the cluster boundaries according to k-means, exemplifies the composition of the eight clusters. Clusters 1–4 include map units related to homogeneous

forest stands related to low standard deviation (Fig. 10d) with increasing absolute height from cluster 1 via cluster 2 and cluster 3 through cluster 4 (Fig. 10b). Cluster 5 is composed of map units which reflect more heterogeneous forest stands. Clusters 6 and 7 represent heterogeneous forest stands whereas cluster 6 comprises map units related to forest stands with very small trees (Fig. 10a) and thus, comparably lower stands on average (Fig. 10b). Finally, cluster 8 encompasses data samples based on very heterogeneous forest stands related to high standard deviation (Fig. 10d) and consisting of different height layers from small to very high trees.

#### 4.3. Forest structure classification – labeling

As a final step in the classification of forest structure, the resulting clusters had to be labeled in a meaningful way. For this purpose, the height histograms for each cluster of map units were additionally considered in addition to a visual comparison by means of an orthophoto and a LiDAR-based nDSM (Fig. 11). The spatial locations of the detailed views from the orthophoto and the LiDAR-based nDSM are shown in Fig. 12. The numbering matches the number of the clusters.

In addition to the eight clusters, which result from the clustering analysis, another cluster (cluster 0) was formed by the initially excluded objects. Cluster 0 contains all objects related to almost treeless areas where the sparsely represented vegetation is very low (<3 m) and consists of seedlings, shrubs and a few small trees (Fig. 11a). Accordingly, cluster 0 was labeled as “Stand Initiation”. Clusters 1–4 include objects which possess small height variation and differ mainly in average height. This indicates forest stands with one closed canopy layer (Fig. 11b–e). Thus, clusters 1–4 were labeled as “Closed Canopy One-Stratum I” to “Closed Canopy One-Stratum IV”. Cluster 5 exhibits much higher variation in height compared to clusters 1–4 (Fig. 11f). The height values vary from 5 m to 35 m with a mean value of about 20 m. Thus, a multi-layered forest with a mostly closed canopy is assumed. According to its characteristics, Cluster 5 was termed as “Closed Canopy Multi-Strata”. Clusters 6 and 7 are also characterized by higher variations in height (Fig. 11g–h). Cluster 6 exhibits a height range of about 30 m with average height of 10 m whereas cluster 7 has a height range of almost 40 m and an average height of about 18 m. Both clusters possess a considerable amount of very low height values, which implies forest gaps. Accordingly, clusters 6 and 7 contain objects which are related to two-layered forest stands with an open canopy layer and gaps or low understory consisting of seedlings,



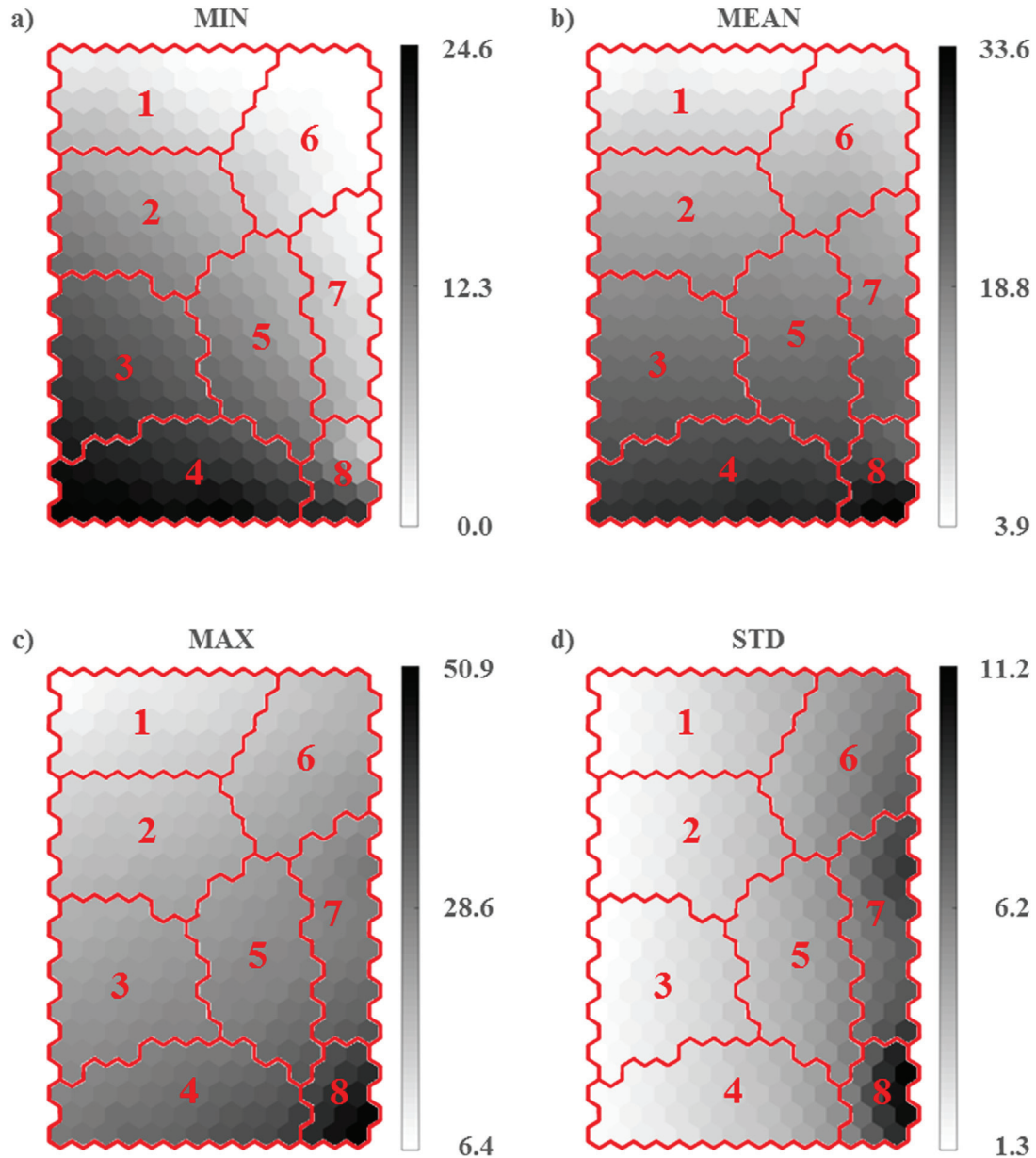


Fig. 10. SOM variables grouped by k-means into eight clusters.

shrubs and small trees. However, the canopy layer of cluster 6 is lower compared to the canopy layer of cluster 7. Therefore, clusters 6 and 7 are referred to as “Open Canopy Two-Strata I” and “Open Canopy Two-Strata II”. Finally, cluster 8 encompasses the highest range in height with almost 60 m and an average height of about 28 m (Fig. 11i). The very low height values indicate gaps or areas with very small vegetation. As opposed to this, cluster 8 also contains the highest values of the whole study area related to very high trees. Considering the height distribution, cluster 8 is related to multi-layered forest stands and was labeled as “Open Canopy Multi-Strata”.

Fig. 12 shows the resulting forest structure map of Traunstein forest. In conjunction with Fig. 11, which shows the description of each forest structure class of the map (Fig. 12), the complexity of the whole forest can be assessed. It becomes apparent, that some parts of the forest are very homogeneous (see central parts of the forest) while other parts are very heterogeneous (see western and northern parts of the forest). Especially in the central parts of the forest closed canopy stands with one stratum dominate. In this

area, the forest height increases from south-west to north-east. The open spaces in the southern parts of the forest, which were caused by storm events, are also clearly visible. The targeted reconversion from homogeneous even-aged pure forest to “close-to-nature”, structurally rich, heterogeneous forest is far advanced in Traunstein forest. The derived forest structure classification reflects the high complexity of Traunstein forest with its patchy spatial pattern of different structure types next to homogeneous areas at different height levels.

Summarizing, the classification approach comprising the SOM as the first stage and the k-means algorithm as the second stage yield eight forest structure classes concerning canopy closure and vertical layering. In addition a ninth class, composed almost tree-less areas dominated by seedlings and shrubs, was extracted. The visual validation by means of an orthophoto and a LiDAR-based nDSM showed high accordance and thus good accuracy of the classification.

### 5. Discussion

This study proposed an unsupervised two-stage clustering approach for forest structure classification based on interferometric X-band SAR data. As case study, a complex temperate forest consisting of unevenly aged mixed forest stands with high range in biomass and high species richness in different development

stages (Pretzsch et al., 2015b) was chosen in order to demonstrate the practical applicability of the approach. Several other studies investigated the potential of interferometric SAR data for the detection of forest structure. However, most of these studies estimated forest attributes describing stand structure in boreal forests without classification of forest structure types (e.g. Karila et al., 2015; Karjalainen et al., 2012; Solberg et al., 2010). Only few studies

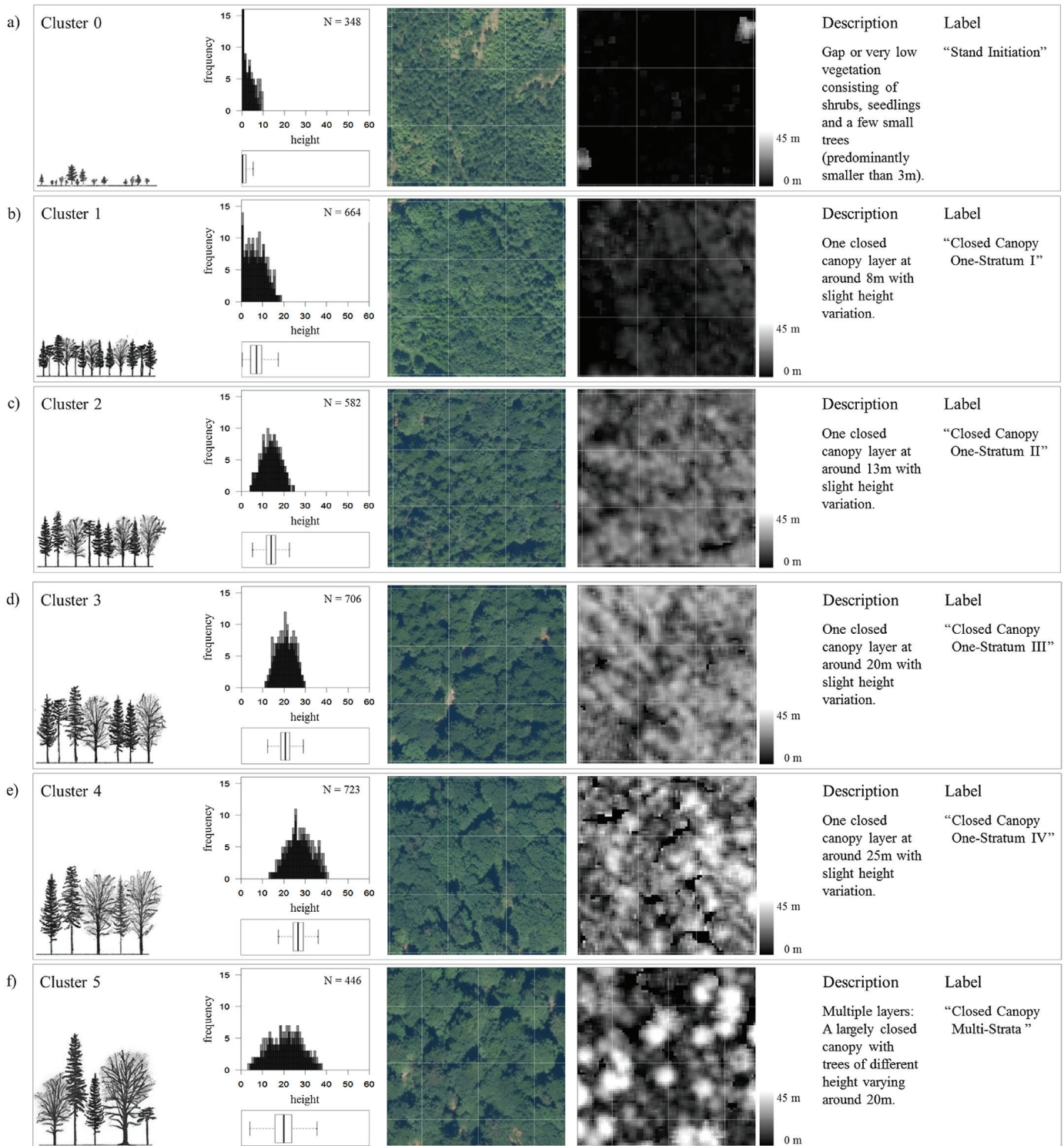


**Fig. 11.** Forest structure cluster description composed of (from left to right) schematic representation, height histogram based on the scattering center height (where N denotes the number of corresponding input data samples), exemplary excerpts of an orthophoto and LiDAR-based nDSM, description and label for the nine resulting classes **a)** cluster 0, **b)** cluster 1, **c)** cluster 2, **d)** cluster 3, **e)** cluster 4, **f)** cluster 5, **g)** cluster 6, **h)** cluster 7 and **i)** cluster 8.

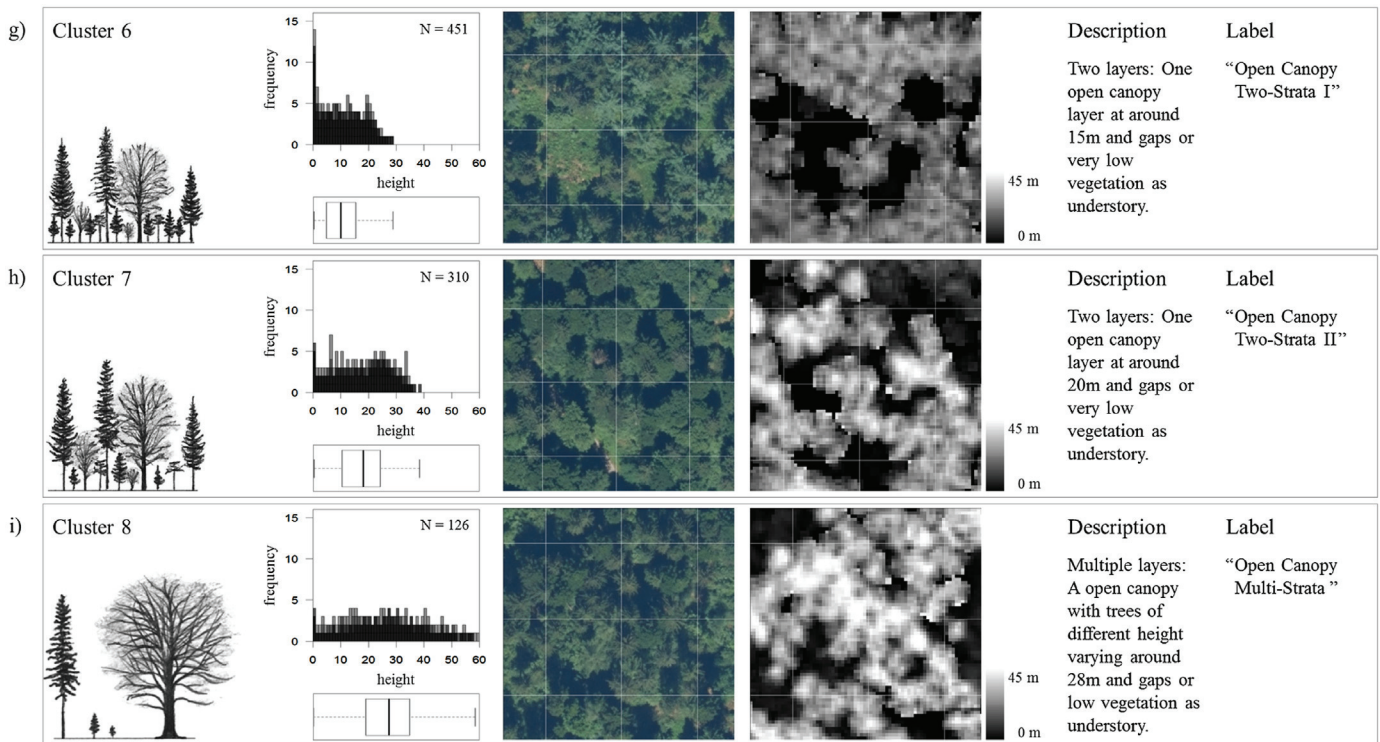


Fig. 11. (Continued)

discussed the classification of forest structure types based on interferometric SAR data (e.g. De Grandi et al., 2015; Liesenberg and Gloaguen, 2013; Hoekman and Quiñones, 2002). Moreover, these studies were mostly carried out in tropical forests. Consequently, the current work gives a contribution to fill the gap concerning the utilization of interferometric X-band SAR data in the context of forest structure classification in complex temperate forest stands. Furthermore, the proposed approach affords the opportunity to handle huge amounts of information about the forest and extract the inherent structure without any a-priori information in an unsupervised and computationally time-efficient way.

Before the advantage of worldwide available consistent interferometric X-band SAR data could be taken, the transferability of the approach must be validated. Since the whole classification process is unsupervised without the requirement of any a-priori information about class number and definitions, it can be assumed that the approach can be easily transferred to other forest stands. Nevertheless, for this purpose further investigations based on forest stands of different structural complexity associated to different forest biomes (i.e. boreal, temperate and tropical forests) are needed. Furthermore, it must be considered that the labelling process is not fully automated and thus requires manual intervention.

Concerning transferability, the use of an ancillary LiDAR DTM is a crucial aspect. LiDAR data are not available worldwide and thus are a limiting factor. To overcome this problem, SAR data based on much longer wavelength than X-band (like L- or P-band) can additionally be applied to derive information on ground elevation instead of a LiDAR-based DTM (Gama et al., 2010). Accordingly, data from the TanDEM-X mission in combination with globally available data at L- or P- band (i.e. ALOS and the potential future mission TanDEM-L) could provide information about forest structure.

Besides, some restrictions due to limitations of X-band InSAR have to be taken into account. First, geometrical effects like displacements predominately at transitions from forest to open spaces lead to inaccurate estimations of height, which becomes crucial at small spatial units of about 500 m<sup>2</sup>. Second, the X-band signal is

able to penetrate into the upper part of the forest canopy, but the understory below a closed canopy cannot be detected. Third, the penetration of the signal is affected by the canopy architecture and thus, it spatially differs mostly dependent on tree species. Thus, the derived height information exhibits additional spatial variations as well as patterns that are independent from the actual forest height. In addition, the processing and generation of the DEM itself include sources of error. Loss of accuracy can be caused by system noise, decorrelations due to temporal offset between acquisitions (in case of repeat-pass interferometry) or due to the slightly different sensor positions and thus slightly different incidence angles during image acquisition as well as terrain roughness (Marghany, 2014; Moreira et al., 2013; Rosen et al., 2000). However, the TanDEM-X mission has the advantage of single-pass interferometry, which enables the acquisition of InSAR data without accuracy limitations due to temporal decorrelations (Krieger et al., 2013).

The first-order statistics based on the forest stand height information as a basis for the classification process are straightforward and easy to obtain. However, it must be investigated in future research if these simple statistics adequate to fully capture the complexity of forest structure. Huang et al. (2014) argue that first-order statistics are not sufficient to entirely detect the heterogeneity of forest stands, since they are not sensitive to the spatial arrangement of the trees. Nonetheless, the visual validation by means of an orthophoto and a LiDAR-based nDSM showed that the presented classification based on these metrics yield meaningful and reasonable results. However, further work on validation is required.

The spatial units of about 500 m<sup>2</sup> to extract the first-order statistics are suitable to detect forest structure, since forest succession processes in near natural forest stands take place on patches at this scale (Pretzsch, 2009; Bugmann, 2001). Forest succession processes influence the forest structure significantly and lead to changes in the canopy layer. Consequently, these processes also regulate the amount of available sunlight in the deeper forest layers and thus affect the vertical architecture of the forest. Consequently, information about forest structure at this spatial scale is highly rel-

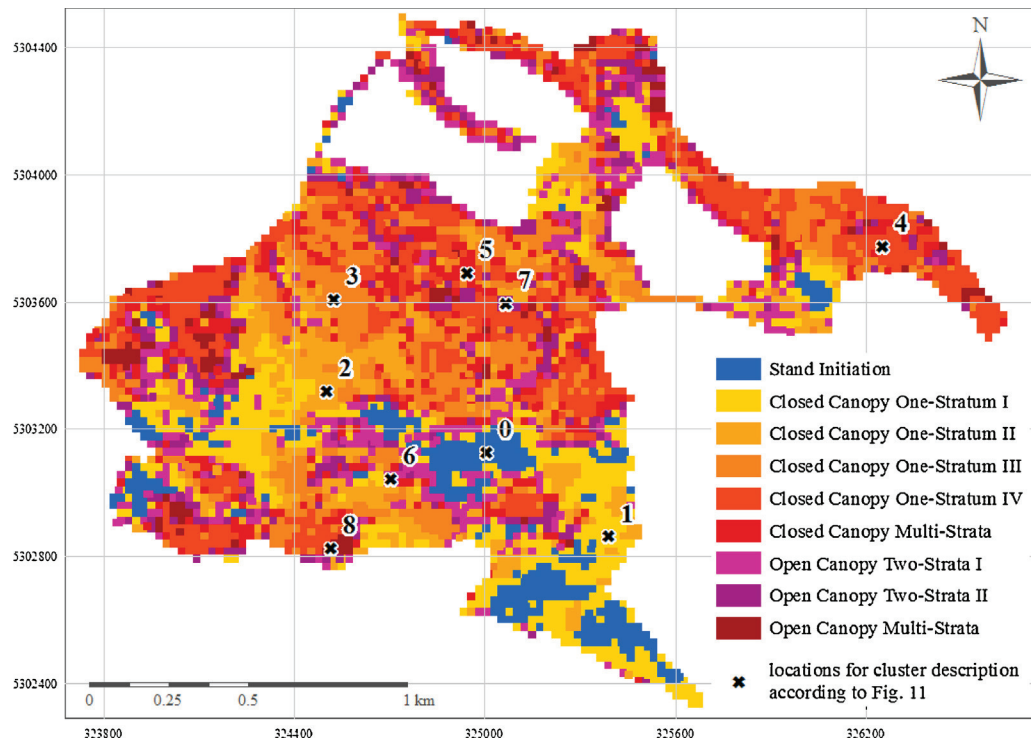


**Fig. 12.** Forest structure classification of Traunstein forest comprising nine different classes concerning vertical layering and canopy coverage of the forest stands. The black crosses are associated to the locations of the details from the orthophoto and the LiDAR-based nDSM corresponding to Fig. 11. The numbering is related to the number of the clusters.

evant in terms of sustainable forest management and biodiversity assessment. Thus, the classification results give evidence about the vertical structure of the forest stands as well as the complexity of the whole forest and thus serve as an indicator for biodiversity. However, it must be considered that tree species composition is a crucial factor in the context of biodiversity, which cannot be detected by applying the proposed approach. As a solution, optical data could be included for tree species classification. In this context, future work should also investigate the influence of tree species composition on the backscattering process regarding the InSAR data and thus on the detection of forest structure.

## 6. Conclusion

An unsupervised two-stage clustering approach for forest structure classification based on height information derived from interferometric X-band SAR data was proposed and conducted in complex temperate forest stands of Traunstein forest. The initially defined objectives comprising i) extraction and ii) classification of forest structure by means of an unsupervised approach based on height information derived from X-band InSAR data were realized. The study has demonstrated that X-band InSAR data exhibits considerable capabilities for forest structure classification taking account for some limitations determined by the acquisition system. In an unsupervised method, the four dimensional input data set composed of first-order height statistics was non-linearly projected on a two-dimensional SOM, spatially ordered according to similarity in the first stage and classified by means of the k-means algorithm in the second stage. The unsupervised classification approach achieved meaningful and reasonable results by means of comparison to aerial imagery and LiDAR data.

The globally available TanDEM-X DEM, which was used in the current study, offers the opportunity to assess forest structure types according to the proposed approach worldwide. The use of first-order statistics to capture forest structure has proven to return

reasonable results. However, first of all further work on validation and transferability to other forests comprising different levels of structural complexity and different forest biomes is required. Future work could investigate the application of additional variables for more detailed information about the forest structure.

## Acknowledgements

This research work was supported by the German Federal Ministry for Economic Affairs and Energy under Project 50EE1261 and the Bavarian State Ministry for Education, Science and the Arts through the Laura Bassi-Award. The authors would like to thank the German Aerospace Agency (DLR) for providing the TanDEM-X data. We also thank the anonymous reviewers for the valuable and helpful comments on the manuscript.

## References

- Önal, H., 1997. Trade-off between structural diversity and economic objectives in forest management. *Am. J. Agric. Econ.* 79 (3), 1001–1012.
- Abdullahi, S., Kugler, F., Pretzsch, H., 2016. Prediction of stem volume in complex temperate forest stands using TanDEM-X SAR data. *Remote Sens. Environ.* 174, 197–211.
- Bamler, R., Hartl, P., 1998. Synthetic aperture radar interferometry. *Inverse Prob.* 14, R1–R54.
- Bauhus, J., Puettmann, K.J., Kühne, C., 2013. Is close-to-Nature forest management in Europe compatible with managing forests as complex adaptive forest ecosystems? In: Messier, C., Puettmann, K.J., Coates, K.D. (Eds.), *Managing Forests as Complex Adaptive Systems. Building Resilience to the Challenge of Global Change*. Routledge, New York, pp. 187–213.
- Beguét, B., Boukir, S., Guyon, D., Chehata, N., 2013. Modelling-based feature selection for classification of forest structure using very high resolution multispectral imagery. *IEEE International Conference on Systems, Man, and Cybernetics*, 4294–4299.
- Bergen, K.M., Goetz, S.J., Dubayah, R.O., Henebry, G.M., Hunsaker, C.T., Imhoff, M.L., et al., 2009. Remote sensing of vegetation 3-D structure for biodiversity and habitat: review and implications for lidar and radar spaceborne missions. *J. Geophys. Res.* 114 (G00E06).
- Bugmann, H., 2001. A review of forest gap models. *Clim. Change* 51, 259–305.

- Carey, A., Wilson, S., 2001. Induced spatial heterogeneity in forest canopies: responses of small mammals. *J. Wildl. Manage.* 65 (4), 1014–1027.
- Castillo-Santiago, M.A., Ricker, M., de Jong, B.H., 2010. Estimation of tropical forest structure from SPOT-5 satellite images. *Int. J. Remote Sens.* 31 (10), 2767–2782.
- Chand, T.R., Badarinarath, K.V., 2007. Analysis of ENVISAT ASAR data for forest parameter retrieval and forest type classification – a case study over deciduous forests of central India. *Int. J. Remote Sens.* 28 (22), 4985–4999.
- Chen, C., Bian, Z., Li, S., Tang, P., Wu, H., 2015. Improving forest type classification using the vegetation local difference index. *Int. J. Remote Sens.* 36 (14), 3701–3713.
- Coburn, C.A., Roberts, A.C., 2004. A multiscale texture analysis procedure for improved forest stand classification. *Int. J. Remote Sens.* 25 (20), 4287–4308.
- De Grandi, E.C., Mitchard, E.T., Woodhouse, I.H., Verhegghen, A., 2015. IEEE International Geoscience and Remote Sensing Symposium (IGARSS) (2015, July), pp. 1805–1808.
- Definiens, 2009. *Definiens eCognition Developer 8 Reference Book*. Definiens AG, Munich.
- Falkowski, M.J., Evans, J.S., Martinuzzi, S., Gessler, P.E., Hudak, A. t., 2009. Characterizing forest succession with lidar data: an evaluation for the Inland Northwest, USA. *Remote Sens. Environ.* 113, 946–956.
- Gómez, C., Wulder, M.A., Montes, F., Delgado, J.A., 2012. Modeling forest structural parameters in the Mediterranean pines of central Spain using quickBird-2 imagery and classification and regression tree analysis (CART). *Remote Sens.* 4, 135–159.
- Gama, F.F., dos Santos, J.R., Mura, J.C., 2010. Eucalyptus biomass and volume estimation using interferometric and polarimetric SAR data. *Remote Sens.* 2, 939–956.
- Gao, T., Hedblom, M., Emilsson, T., Nielsen, A.B., 2014. The role of forest stand structure as biodiversity indicator. *For. Ecol. Manage.* 330, 82–93.
- Hastie, T., Tibshirani, R., Friedman, J., 2009. *The Elements of Statistical Learning. Data Mining, Inference, and Prediction*. Springer Science + Business Media, New York, USA.
- Hoekman, D.H., Quiñones, M.J., 2002. Biophysical forest type characterization in the colombian amazon by airborne polarimetric SAR. *IEEE Trans. Geosci. Remote Sens.* 40 (6), 1288–1300.
- Hollaus, M., Aubrecht, C., Höfle, B., Steinnocher, K., Wagner, W., 2011. Roughness mapping on various vertical scales based on full-waveform airborne laser scanning data. *Remote Sens.* 3, 503–523.
- Huang, Q., Swatantran, A., Dubayah, R., Goetz, S.J., 2014. The influence of vegetation height heterogeneity on forest and woodland bird species richness across the United States. *PLoS One* 9 (8).
- Huesca, M., García, M., Roth, K.L., Casas, A., Ustin, S.L., 2016. Canopy structural attributes derived from AVIRIS imaging spectroscopy data in mixed broadleaf/conifer forest. *Remote Sens. Environ.* 182, 208–226.
- Hyde, P., Dubayah, R., Walker, W., Blair, J.B., Hofton, M., Hunsaker, C., 2006. Mapping forest structure for wildlife habitat analysis using multi-sensor (LiDAR, SAR/InSAR, ETM+, Quickbird) synergy. *Remote Sens. Environ.* 102, 63–73.
- Hyypä, J., Hyypä, H., Leckie, D., Gougeon, F., Yu, X., Maltamo, M., 2008. Review of methods of small-footprint airborne laser scanning for extracting forest inventory data in boreal forests. *Int. J. Remote Sens.* 29 (5), 1339–1366.
- Jain, K.A., 2010. Data clustering: 50 years beyond K-Means. *Pattern Recognit. Lett.* 31 (8), 651–666.
- Kantardzic, M., 2011. *Data Mining: Concepts, Models, Methods, and Algorithms*, 2nd ed. John Wiley & Sons, Hoboken, New Jersey.
- Karila, K., Vastaranta, M., Karjalainen, M., Kaasalainen, S., 2015. Tandem-X interferometry in the prediction of forest inventory attributes in managed boreal forests. *Remote Sens. Environ.* 159, 259–268.
- Karjalainen, M., Kankare, V., Vastaranta, M., Holopainen, M., Hyypä, J., 2012. Prediction of plot-level forest variables using TerraSAR-X stereo SAR data. *Remote Sens. Environ.* 117, 338–347.
- Kaski, S., 1997. *Data exploration using self-organizing maps*. Dissertation.
- Kayitakire, F., Hamel, C., Defourny, P., 2006. Retrieving forest structure variables based on image texture analysis and IKONOS-2 imagery. *Remote Sens. Environ.* 102, 390–401.
- Kohonen, T., 1982. Self-organized formation of topologically correct feature maps. *Biol. Cybern.* 43 (1), 59–69.
- Kohonen, T., 1990. The self-organizing map. *Proc. IEEE* 78 (9), 1465–1480.
- Kohonen, T., 2013. *Essentials of the self-organizing map*. *Neural Netw.* 37, 52–65.
- Kohonen, T., 2014. *MATLAB Implementations and Applications of the Self-Organizing Map*. Unigrafia Oy, Helsinki, Finland.
- Krieger, G., Zink, M., Bachmann, M., Bräutigam, B., Schulze, D., Martone, M., et al., 2013. TanDEM-X: A radar interferometer with two formation-flying satellites. *Acta Astronaut.* 89, 83–98.
- Kugler, F., Hajnsek, I., Papathanassiou, K., 2011. Forest characterisation by means of TerraSAR-X and TanDEM-X (Polarimetric and) interferometric data. In: *Proceedings PolInSAR*, (2011, January 24–29), pp. 2578–2581.
- Kuuluvainen, T., Penttinen, A., Leinonen, K., Nygren, M., 1996. Statistical opportunities for comparing stand structural heterogeneity in managed and primeval forests: an example from boreal spruce forest in southern Finland. *Silva Fennica* 30 (2-3), 315–328.
- Liesenberg, V., Gloaguen, R., 2013. Evaluating SAR polarization modes at L-band for forest classification purposes in Eastern Amazon, Brazil. *Int. J. Appl. Earth Obs. Geoinf.* 21, 122–135.
- Liu, W., Song, C., Schroeder, T.A., Cohen, W.B., 2008. Predicting forest successional stages using multitemporal Landsat imagery with forest inventory and analysis data. *Int. J. Remote Sens.* 29 (13), 3855–3872.
- MacQueen, J., 1967. Some methods for classification and analysis of multivariate observations. *Proceedings of the Fifth Berkeley Symposium on Mathematical Statistics and Probability*, 1: Statistics, 281–297.
- Manning, C.D., Raghavan, P., Schütze, H., 2008. *Introduction to Information Retrieval*. Cambridge, University Press.
- Marghany, M., 2014. A three-dimensional of coastline deformation using the sorting reliability algorithm of ENVISAT interferometric synthetic aperture radar. In: Marghany, M. (Ed.), *Advanced Geoscience Remote Sensing*. pp. 105–121 (InTech).
- McElhinny, C., Gibbons, P., Brack, C., Bauhus, J., 2005. Forest and woodland stand structural complexity: its definition and measurement. *For. Ecol. Manage.* 218, 1–24.
- Moreira, A., Prats-Iraola, P., Younis, M.K., Hajnsek, I., Papathanassiou, K.P., 2013. A tutorial on synthetic aperture radar. *IEEE Geosci. Remote Sens. Mag.* 1 (1), 6–43.
- Naidoo, L., ybhans, W., Wessels, K., Asner, G., Leblon, B.R., Main, R., et al., 2015. Savannah woody structure modelling and mapping using multi-frequency (X-C- and L-band) Synthetic Aperture Radar data. *ISPRS J. Photogramm. Remote Sens.* 105, 234–250.
- Peña, M.A., Brenning, A., Sagredo, A., 2012. Constructing satellite-derived hyperspectral indices sensitive to canopy structure variables of a Cordilleran Cypress (*Austrocedrus chilensis*) forest. *ISPRS J. Photogramm. Remote Sens.* 74, 1–10.
- Perry, D.A., 1994. *Forest Ecosystems*. The John Hopkins University Press, Baltimore, Maryland.
- Pfeifer, M., Kor, L., Nilus, R., Turner, E., Cusack, J., Lysenko, I., et al., 2016. Mapping the structure of Borneo's tropical forests across a degradation gradient. *Remote Sens. Environ.* 176, 84–97.
- Pommerening, A., 2006. Evaluation structural indices by reversing forest structural analysis. *For. Ecol. Manage.* 224, 266–277.
- Pretzsch, H., del Río, M., Ammer, C., Avdagic, A., Barbeito, I., Bielak, K., et al., 2015a. Growth and yield of mixed versus pure stands of Scots pine (*Pinus sylvestris* L.) and European beech (*Fagus sylvatica* L.) analysed along a productivity gradient through Europe. *Eur. J. For. Res.* 134 (5), 927–947.
- Pretzsch, H., Biber, P., Uhl, E., Dauber, E., 2015b. Long-term stand dynamics of managed spruce-fir-beech mountain forests in Central Europe: structure, productivity and regeneration success. *Forestry* 88 (4), 407–428.
- Pretzsch, H., 1996. Structural diversity as a result of silvicultural treatment. *Allgemeine Forst- und Jagdzeitung* 11, 213–221.
- Pretzsch, H., 2005. Diversity and productivity in forests: evidence from long-term experimental plots. In: Scherer-Lorenzen, M., Körner, C., Schulze, E.-D. (Eds.), *Forest Diversity and Function. Temperate and Boreal Systems*. , 176 ed. Springer Verlag, Heidelberg Berlin, pp. 41–64 (Ecological Studies).
- Pretzsch, H., 2009. *Forest Dynamics, Growth and Yield*. Springer-Verlag, Berlin Heidelberg.
- Ritter, H., Kohonen, T., 1989. Self-Organizing semantic maps. *Biol. Cybern.* 61, 241–254.
- Rosen, P.A., Hensley, S., Joughin, I.R., Li, F.K., Madsen, S.N., Rodriguez, E., et al., 2000. Synthetic aperture radar interferometry. *Proc. IEEE* 88 (3), 333–382.
- Solberg, S., Astrup, R., Bollandsås, O.M., Næsset, E., Weydahl, D.J., 2010. Deriving forest monitoring variables from X-band InSAR SRTM height. *Can. J. Remote Sens.* 36 (1), 68–79.
- Staudhammer, C.L., LeMay, V.M., 2001. Introduction and evaluation of possible indices of stand structural diversity. *Can. J. For. Res.* 31, 1105–1115.
- Varghese, A.O., Suryavanshi, A., Joshi, A.K., 2016. Analysis of different polarimetric target decomposition methods in forest density classification using C band SAR data. *Int. J. Remote Sens.* 37 (3), 694–709.
- Vesanto, J., Alhoniemi, E., 2000. Clustering of the self-organizing map. *IEEE Trans. Neural Netw.* 11 (3), 586–600.
- Vesanto, J., Himberg, J., Alhoniemi, E., Parhankangas, J., 2000. *SOM toolbox for matlab 5*. Helsinki University of Technology, Finland.
- Webb, A.R., Copsey, K.D., 2011. *Statistical Pattern Recognition*, third edition. Jhon Wiley & Sons Ltd., Chichester, West Sussex, United Kingdom.
- Xu, R., Wunsch, D.C., 2010. Clustering algorithms in biomedical research: a review. *IEEE Rev. Biomed. Eng.* 3, 120–154 (S).
- Xu, R., Wunsch, D., 2005. Survey of clustering algorithms. *IEEE Trans. Neural Netw.* 16 (3), 645–678.
- Yang, H., Liu, D., Sun, G., Guo, Z., Zhang, Z., 2014. Simulation of interferometric SAR response for characterizing forest successional dynamics. *IEEE Geosci. Remote Sens. Lett.* 11 (9), 1529–1533.
- del Río, M., Pretzsch, H., Alberdi, I., Bielak, K., Bravo, F., Brunner, A., et al., 2015. Characterization of the structure, dynamics, and productivity of mixed-species stands: review and perspectives. *Eur. J. For. Res.*

## **C Publication III**

**Title:** Seasonal effects on forest structure classification by means of X-band InSAR in complex temperate forests

**Authors:** Sahra Abdullahi, Thomas Schneider, Mathias Schardt, Hans Pretzsch

**Journal:** *Submitted* to ISPRS International Journal of Photogrammetry and Remote Sensing (Under Review)

**Impact Factor:** 6.387 (2016)

**Contribution:** TanDEM-X InSAR data was processed and provided by the Microwave and Radar Institute of the German Aerospace Center (DLR). The collection of field measurements in the scope of a forest inventory was conducted by staff of the Chair of Forest Growth and Yield Science of the Technical University of Munich. All data analyses including data preparation, application of developed approaches, validation of the results as well as writing and composing the manuscript were performed by the first author Sahra Abdullahi. All co-authors contributed to the design and content of the paper by scientific advice, discussion and language editing.

**Copyright in case of final acceptance retains with ISPRS Journal of Photogrammetry and Remote Sensing, Elsevier, Reprinted preliminary manuscript.**

# Seasonal Effects on Forest Structure Classification by means of X-band InSAR in complex temperate forests

Sahra Abdullahi<sup>1</sup>, Thomas Schneider<sup>2</sup>, Mathias Schardt<sup>3, 4</sup>, Hans Pretzsch<sup>1</sup>

- 1 Technical University of Munich (TUM), Chair for Forest Growth and Yield Science, Hans-Carl-von-Carlowitz-Platz 2; 85354 Freising; Germany, [sahra.abdullahi@tum.de](mailto:sahra.abdullahi@tum.de)
- 2 Technical University of Munich (TUM), Institute of Forest Management (IFM), Hans-Carl-von-Carlowitz-Platz 2; 85354 Freising; Germany
- 3 Remote Sensing and Geoinformation, Institute for Information and Communication Technologies, Joanneum Research, Steyrergasse 17, 8010 Graz, Austria
- 4 Graz University of Technology, Institute of Remote Sensing and Photogrammetry, Steyrergasse 30, 8010 Graz, Austria

**Keywords:** TanDEM-X, InSAR, phenology, forest structure, temperate forest

## Abstract

Recent and projected climatic changes cause alterations in forest structure, which further entail changes in biodiversity, stability, productivity as well as phenology. Besides more frequently occurring damages caused by extreme weather events (e.g., droughts and storms) and calamities, the changing climate induces challenging habitat conditions for existent tree species. For this reason, detection and monitoring of forest structure is inevitable in order to face these trends and to develop sufficient adaptation and mitigation strategies for forests worldwide. Remote sensing techniques offer a cost-efficient opportunity to collect area-wide information about forest stand structure with high spatial and temporal resolution. Especially Interferometric Synthetic Aperture Radar (InSAR), which facilitates worldwide acquisition of 3-d information independent from weather conditions and illumination, is convenient to capture forest stand structure. This study investigates the effect of phenological development stage on forest height estimation and forest structure classification in mixed, coniferous and broadleaf temperate forest stands. In addition, the influence of polarization mode (i.e. VV-polarized and HH-polarized InSAR data) is explored. In accordance with previous studies, the current work indicates that X-band InSAR over coniferous forest stands is not significantly affected by phenology, whereas height estimation over broadleaf forest stands is essentially influenced by the phenological differences between leaf-on and leaf-off season. Furthermore, it could be demonstrated that phenology considerably affects the assessment of forest structure. Especially regarding forest stands which are predominantly covered by broadleaf tree species, the classification results differentiate significantly between leaf-on and leaf-off season.

## 1. Introduction

Ongoing climate change causes alterations in forest structure, which in turn lead up to changes in biodiversity, stability, productivity as well as phenology (IPPC, 2014). Besides more frequently occurring damages caused by extreme weather events (e.g.,

droughts and storms) and calamities, the changing climate induces challenging habitat conditions for existent tree species. As a result of adaptation, disappearance of existent tree species and appearance of new tree species, forest's complexity according to the spatial arrangement of tree size dimensions and species composition is changing. Consequently, the

fundamental boundary conditions for ecosystem processes are influenced (Bonan, 2008; Harding et al., 1995). To face these concerning trends and to develop sufficient adaptation and mitigation strategies, detection and monitoring of forest structure is inevitable. In this context, targeted silvicultural and forest management activities are highly relevant, since the enhancement of structural diversity often positively affects biodiversity, productivity as well as growth of the forest (Pommerening, 2006; Carey & Wilson, 2001; Önal, 1997). Therefore, it is important to encourage silvicultural and forest management activities that increase the structural diversity and thus the stability and resilience of the forest. On that account reliable information on forest structure is a prerequisite to provide the basis for policy guidelines at local, national and global level (Gao et al., 2014; Kuuluvainen et al., 1996).

In general, forest structure is described at stand level (i.e., tens of meters) by size distribution and horizontal as well as vertical tree distribution patterns (del Río et al., 2015), whereas its complexity is defined according to spatial heterogeneity comprising tree size dimensions and species compositions (Pretzsch, 2005). A variety of parameters (e.g., basal area, number of trees per hectare, tree height) as well as indices (e.g., stand density index, leaf area index, index of patchiness) are usually measured and calculated to capture forest stand structure (del Río et al., 2015).

However, acquisition of such traditional terrestrial measurements as part of forest inventories is very cost-intensive. In addition, these measurements are conducted on a sample-based survey design with a usual repetition rate of ten years and more. Moreover, in-situ measurements of canopy vertical structure are inherently laborious and time consuming, and thus are usually very limited in scope (Harding et al., 1995). Another disadvantage of traditional in-situ measurements is its poor availability for most forested areas worldwide due to property situation and inaccessibility. In contrast, remote sensing techniques are more cost-effective and suitable for area-wide, wall-to-wall and comprehensive detection as well as monitoring of forest stand structure with high spatial and temporal resolution. These techniques enable the collection and automatic interpretation of large amounts of data for detailed forest monitoring (Moran et al., 2017).

Radio Detection And Ranging (RaDAR) systems have the advantage of all-weather-capability, independency of illumination and penetration ability over other remote

sensing systems, e.g., multispectral, hyperspectral and Light Detection And Ranging (LiDAR). Especially Synthetic Aperture Radar (SAR) systems provide global observations with high spatial and temporal resolution. Regarding forest structure monitoring, SAR systems are beneficial since the backscatter is responsive to multiple structural elements of forest canopies depending on frequency, polarization, and viewing angle (Townsend, 2002). Interferometric SAR (InSAR) systems enable the detection of 3-d information corresponding to different scattering elements (i.e., leaves, branches and trunks) of the forest canopy dependent on wavelength (Varghese et al., 2016; Yang et al., 2014) and thus facilitates detection and investigation of horizontal as well as vertical forest structure.

Several studies demonstrated the applicability of InSAR at different wavelengths from different sensors on airborne or spaceborne platforms for forest structure assessment (De Grandi et al., 2016; (Liesenberg & Gloaguen, 2013; Hoekman & Quiñones, 2002). At lower frequencies like P- (0.3-1 GHz) and L- (1-2 GHz) band, the RaDAR signal penetrates deep into the forest canopy and is backscattered at big branches, tree trunks and the ground (Dobson et al., 1995; Le Toan et al., 1992). Due to the high penetration capability and thus high sensitivity to vertical forest structure, these longer wavelengths are in particular suitable for forest structure assessment (Kugler et al., 2014). In contrast, RaDAR waves with higher frequencies (i.e., shorter wavelengths) such as C- (4-8 GHz) and especially X- (8-12 GHz) band are mostly backscattered in the upper part of the canopy, at small branches and leaves (Gama et al., 2010; Pulliainen et al., 2003). Consequently, these bands are less sensitive to the vertical forest structure. However, large-scale applications based on longer wavelengths in a global context by means of spaceborne SAR systems, like ALOS-PaLSAR, suffer limitations in accuracy due to temporal decorrelations and atmospheric disturbances caused by repeat-pass interferometry (Kugler et al. 2014). In contrast, the TanDEM-X mission, which is the first single-pass SAR interferometer in space, enables the acquisition of highly accurate across-track and along-track interferograms without the inherent accuracy limitations imposed by repeat-pass interferometry (Krieger et al., 2013). The mission is composed of the two almost identical satellites TerraSAR-X (launched in 2007) and TanDEM-X (launched in 2010) flying in a close formation and provides high-resolution, multi-polarized, single-pass interferometric X-band (9.65 GHz) data.



Besides weather conditions and technical properties (e.g., wavelength, acquisition mode, incidence angle), phenology is determinant for the accuracy of forest structure estimation (Sadeghi et al., 2017). The different phenological development stages eventuate in interannual variations in the appearance of the forest canopy and thus in deviating detection by the SAR sensor. Especially the canopy of broadleaf trees is affected by phenology during the course of the year. In spring the process of leaf unfolding modifies the appearance of the canopy in a highly dynamic manner and thus affects the SAR backscatter. In autumn, leaf fall changes the canopy appearance again and consequently its appearance in the SAR image. Therefore, it is essential to take account of the phenological development stage at the time of acquisition for detection of forest structure.

Kugler et al. (2014) observed a clear seasonal dependence between summer and winter TanDEM-X single and dual-pol acquisitions in boreal forest stands dominated by Norway spruce and Scots pine in Sweden as well as in mixed temperate forest stands dominated by Norway spruce, beech and fir in Germany. In this study, a significantly lower phase center location, indicating a deeper penetration in winter compared to summer due to frozen vegetation conditions (i.e., decreased dielectric constant) in combination with absence of leaves, was detected (Kugler et al., 2014). By comparison of X-band bistatic InSAR acquisitions over temperate coniferous and deciduous forest stands in Estonia, Olesk et al. (2015) also found a deeper penetration into the forest during leaf-off season compared to leaf-on season. In contrast, Solberg et al. (2015) and Sadeghi et al. (2017) did not detect a highly significant effect of phenology by analyzing X-band InSAR data of the TanDEM-X mission over boreal coniferous forest stands.

Although several studies demonstrated the potential of InSAR data for the detection of forest structure, these studies disregarded the influence of phenology. For this reason, the current study investigates the influence of phenology on forest structure assessment by means of X-band InSAR data. Phenology-based differences in height estimation as well as in forest structure classification are explored over complex temperate forest stands by means of TanDEM-X acquisitions corresponding to leaf-on and leaf-off season. In addition, the dependency on polarization mode (i.e. VV-polarized and HH-polarized InSAR data) is investigated. The study is directly linked to previous

work on forest structure classification based on height information derived from X-band InSAR data (Abdullahi et al., 2017) and extends this approach by further analyses regarding differences in forest structure detection due to phenological changes. For this purpose, the objectives of the current study are defined as i) assessment of phenology-based differences in height estimation, under additional consideration of polarization mode (i.e. VV-polarized and HH-polarized InSAR data) and ii) presentation of the consequent limitations in forest structure classification and its accuracy. As study area, the temperate Traunstein forest, which is located in the Southeast of Germany and composed of structurally rich coniferous, broadleaf and mixed forest stands, was chosen.

## 2. Materials

### 2.1. Study Area

Coniferous, broadleaf as well as mixed forest stands of the highly structured, temperate forest close to the city of Traunstein, Germany (47°52′ N, 12°38′ E) serve as study area (**Fig. 1**). The study area covers an area of 243 ha. Since Traunstein forest is used for teaching as well as research purposes by the Chair of Forest Growth and Yield Science of the Technical University of Munich (TUM), it provides a huge and consistent data set of historical and recent measurements on the forest's condition. The topography of Traunstein forest ranges from 630 to 720 m above sea level and includes small areas with steep slopes. The soils are composed of glacier sediments which belong to the pre-alpine moraine landscape. A mean annual temperature of 7.3 °C and precipitation up to 1600 mm per year characterize the climatic conditions. The forest is predominantly composed of Norway spruce (*Picea abies*), European silver fir (*Abies alba*), European beech (*Fagus sylvatica*) and Sycamore maple (*Acer pseudoplatanus*). Due to an ongoing reconversion from a homogeneous one-age cohort forest to a structurally rich, heterogeneous forest, the forest stands are very complex concerning tree species richness and heterogeneous stand structures (Pretzsch, 1996). The applied "close-to-nature" silviculture yields a broad distribution of tree species (**Fig. 2a**) and growth stages (**Fig. 2b**). Consequently, Traunstein forest is an ideal example for the whole spectrum of silviculture types in Central Europe and thus is predestinated as study area for forest structure assessment in temperate forests.

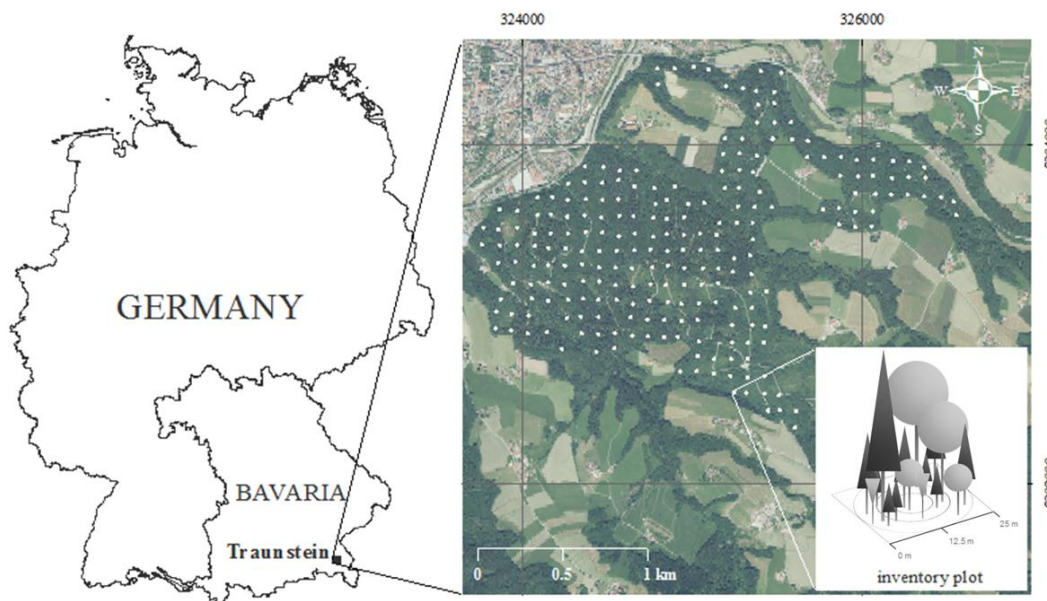


**Fig. 1:** The study area is located in a highly structured, mixed, temperate forest next to the city of Traunstein in the Southeast of Germany and covers an area of about 243 ha. The study area is covered permanent inventory grid with a sampling density of one plot per hectare. Each circular inventory plot covers an area of 500 m<sup>2</sup>.

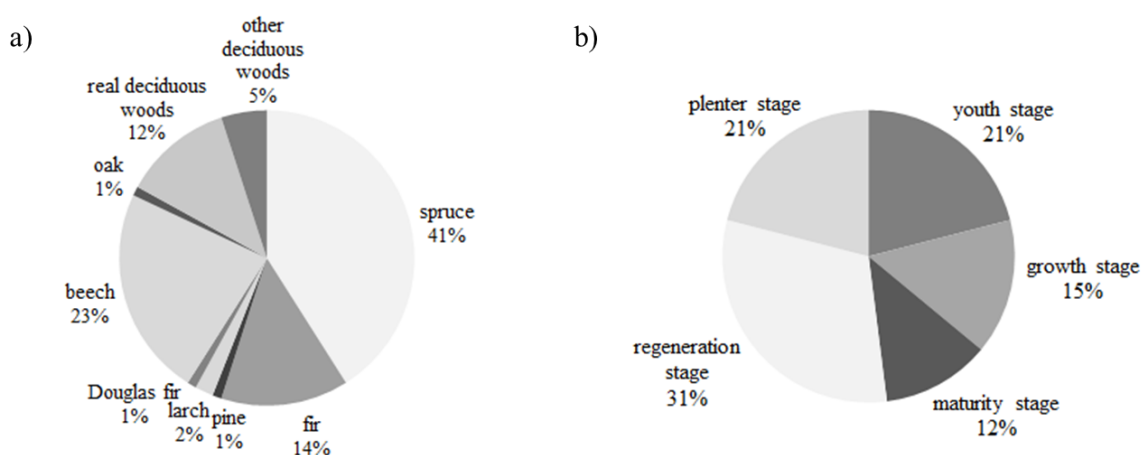


**Fig. 2:** a) Area percentages of tree species and b) area percentages of development stages within the study area.

## 2.2. Field Data

In summer 2013, field data on forest condition and the dynamics of stand parameters were collected within a forest inventory according to the survey guidelines of the Bavarian State Forest Enterprise (Bayerische Staatsforsten, 2011). In the study area, the systematic inventory comprises 228 permanent circular sampling plots and has been repeated regularly since 1988. All inventory plots are arranged on a regular 100 m by 100 m sampling grid (i.e. a sampling density of one plot per hectare) (**Fig. 3a**). Each circular inventory plot covers an area of

500 m<sup>2</sup> and its center is permanently marked by a buried lodestone. Consequently, surveys can be easily repeated and the sampling error for alterations of the stand parameters can be reduced. Each inventory plot is partitioned into three concentric sub-circles with radii of 12.62 m, 6.31 m and 3.15 m, respectively. In order to measure on a sample basis, a specific diameter of breast height (dbh) threshold is defined for each sub-circle (**Fig. 3b**). Accordingly, all trees with dbh > 30 cm within the largest circle (with radius 12.62 m), all trees with dbh > 10 cm within the medium circle (with radius 6.31 m) and all trees with dbh < 10 cm within the

smallest circle (with radius 3.15 m) are recorded, respectively. The dbh and the polar coordinates (azimuth and range relative to the center of the inventory plot) are gathered for any tree above the relevant dbh threshold value. Tree height measurements are taken for a representative sample of each tree species per stand layer. Standard height curve systems are applied on the measured height sample to estimate the tree height for each recorded tree (Pretzsch, 2009). Additionally, other tree and forest stand attributes such as species, age, layering, damages, dead wood, and stem quality are recorded for each inventory plot.

### 2.3. Remote Sensing Data

Two dual-polarized interferometric X-band image pairs acquired by the TanDEM-X mission on August 12, 2013 in summer (leaf-on season) and March 09, 2014 in spring (leaf-off season) were used. The image pairs

were acquired under very similar technical and weather conditions (**Tab. 1**). All images were recorded in the bistatic StripMap mode with descending orbit with identical incidence angle of about  $44.9^\circ$ . The effective baselines between the two sensors were about 120.0 m and 143.2 m, respectively. However, the image pairs were acquired under different phenological stages. The acquisition of August 2013 reflects the study area during the leaf-on season while the acquisition of March 2014 represents the forest in the leaf-off season.

In addition, airborne LiDAR (Light Detection and Ranging) data acquired on November 18, 2012 (i.e. leaf-off season) is available for normalization of the TanDEM-X InSAR heights as well as validation purposes. LiDAR data was collected using the LMS-Q 680i Scanner from RIEGL with a flight altitude of about 500 m and a point density of about 25 dots per  $m^2$ . MILAN Geoservice GmbH provided the associated Digital Terrain Model (DTM) and Digital Surface Model (DSM).

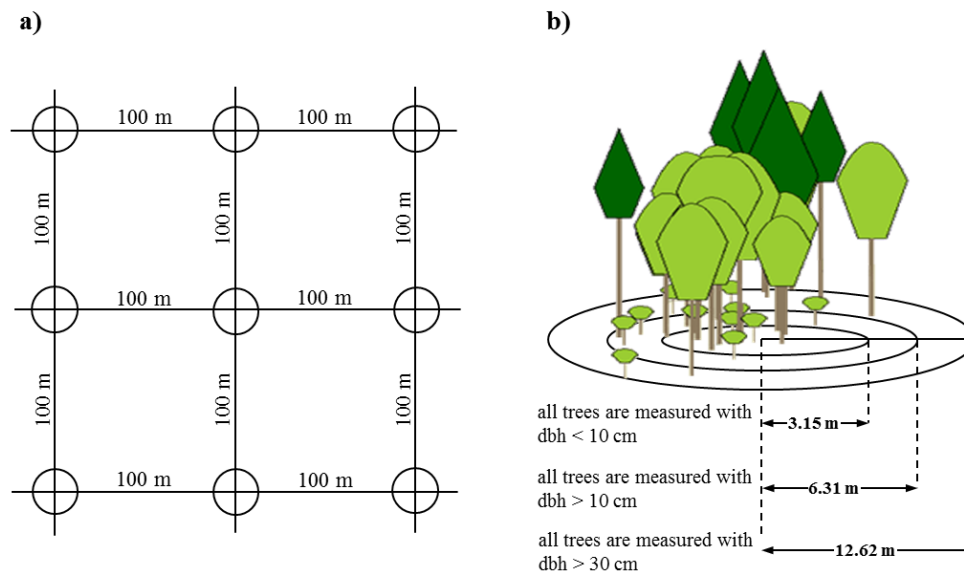


**Fig. 3:** a) Inventory sampling grid and b) thresholds in diameter measuring.

**Tab. 1:** Acquisition parameters of the interferometric image pairs.

<b>Acquisition Date</b>	12.08.2013	09.03.2014
<b>Acquisition Mode</b>	Bistatic / StripMap	Bistatic / StripMap
<b>Polarization Mode</b>	Dualpol (HH, VV)	Dualpol (HH, VV)
<b>Orbit</b>	Descending	Descending
<b>Incidence Angle</b>	$44.93^\circ$	$44.94^\circ$
<b>Effective Baseline</b>	119.99 m	143.18 m
<b>HoA</b>	65.05 m	54.25 m
<b>Weather Conditions</b>	dry / unfrozen	dry / unfrozen

According to **Fig. 2a**, about 40% of the study area is covered by deciduous tree species, whereby beech is the most commonly occurring species. As an example, **Fig. 4** schematically illustrates the size relations of the different stages of leaf unfolding for beech. The completely unfolded leaves can reach a length up to 10 cm and a width up to 5 cm and thus are highly relevant with respect to scattering of radar signals at a wavelength of about 3 cm (i.e., X-band). In early spring, the buds (with a length of about 2 cm) shoot and the old leaves are shed. The subsequent development of leaves can take up to several weeks dependent on environmental and genetic conditions (Schüler et al., 2012; Cornelius et al., 2013). In Traunstein forest, the leaves of beeches were completely developed in August at the time of the first InSAR acquisition (**Fig. 4e**), while the buds were still closed in March at the time of the second InSAR acquisition (**Fig. 4a**). According to phenological observations conducted by the German Weather Service DWD (DWD, 2016), the leaves of other main broadleaf tree species in the study area were also still undeveloped at the time of acquisition in March.

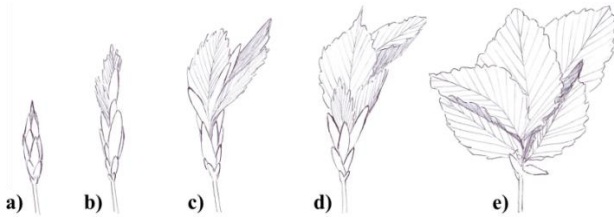


**Fig. 4:** Schematic illustration of flushing taking the example of beech: from a) the bud via b), c), d) until the completely unfolded leaves.

### 3. Methods

#### 3.1. Generation of scattering center height

Based on the interferometric TanDEM-X image pairs, a Digital Surface Model (DSM) was generated for each acquisition date (i.e., leaf-on and leaf-off season) using both polarization modes available (i.e., VV and HH polarization). In total four DSMs, which reflect the height of all elevated objects on the Earth's surface,

were calculated corresponding to leaf-on season and VV polarization, leaf-on season and HH polarization, leaf-off season and VV polarization as well as leaf-off season and HH polarization (Abdullahi et al., 2016).

The scattering signals of each image pair were simultaneously acquired from slightly different positions and coherently combined in an interferogram (Rosen et al., 2000; Krieger et al., 2013). The resulting interferometric phase of each image pair describes the phase differences of the two acquisitions and is mainly affected by the differences in range (Bamler & Hartl, 1998). Subsequently, the ambiguity of the interferometric phase was resolved by phase unwrapping and finally, the phase differences were converted into height based on the interferometer geometry for terrain reconstruction (Rosen et al., 2000). To estimate the vegetation height within the forest, the derived DSMs were normalized by subtracting the LiDAR-based DTM. However, the resulting height data sets underestimate the actual vegetation height dependent on the canopy architecture due to the penetration of the RaDAR signals in to the upper part of the canopy. The nDSMs (normalized DSM), referred to as scattering center height, were generated with a pixel spacing of 6 m. A summary of the derived height information is given in **Tab. 2**.

#### 3.2. Forest Structure Classification

An unsupervised two-stage clustering approach according to Abdullahi et al. (2017) was applied to the scattering center heights to classify forest structure on spatial units of 24 x 24 m<sup>2</sup> concerning vertical layering and closure of the canopy. The classification procedure is composed of two partitioning clustering methods, the Self-Organizing Map and the k-means algorithm. As depicted in **Fig. 5**, the process comprises the derivation of object-based features as a pre-processing step, a two-stage clustering for classification of forest structure and final labelling of the resulting classes which can be considered as a post-processing step.

**Tab. 2:** Derived height information based on TanDEM-X data.

Data Set	Height Information	Acquisition Date	Season	Pixel Spacing	Polarization
1	scattering center height	12.08.2013	leaf-on	6 m	HH
2	scattering center height	12.08.2013	leaf-on	6 m	VV
3	scattering center height	09.03.2014	leaf-off	6 m	HH
4	scattering center height	09.03.2014	leaf-off	6 m	VV

Pre-processing included the following three steps: First, chessboard segmentation was applied to the complete study area by means of the Definiens Developer Software (Definiens, 2009) in order generate squared objects with a size of 24 x 24 m<sup>2</sup>. The object size was defined according to the size of an inventory plot, which also matches the spatial scale on which forest successional processes take place (Pretzsch 2009; Bugmann, 2001). Second, four first order statistics of the scattering height (i.e., minimum height, mean height, maximum height and standard deviation of height) were extracted for each object. Since higher sensitivity to the vertical forest structure can be expected when open spaces are excluded, almost treeless areas with predominantly seedlings and shrubs (i.e., majority of values within an object is zero and the mean value is less than three meters) were left out of the clustering and added in post-processing as a separate class (Abdullahi et al., 2017). Third, the four-dimensional data set consisting of the first order height statistics was normalized in order to balance the influence of the features comprising different ranges of value (Kantardzic, 2011). For this purpose, a linear transformation was used to scale the variables to a mean value of zero and a standard deviation of one while preserving the relation of variables to each other (Vesanto et al., 2000).

The classification process was composed of two steps: In a first stage, the Self-Organizing Map (SOM) according to Kohonen (1982), a low-dimensional artificial neural network, was applied to partition the four-dimensional input feature set into groups according to similarity. Each neuron arranged on a regular hexagonal grid was represented by a prototype vector, which possess the same dimension as the input data samples. All prototype vectors were linearly initialized and a batch-type training algorithm was deployed to the network in order to adjust and spatially order the prototype vectors. At batch-type training, each input data sample was compared with all prototype vectors

and the best matching unit (BMU) (i.e., the prototype vector with the smallest Euclidean distance to the input sample) was determined. Following this, the neighborhood for each BMU was set according to a neighborhood function, which decreases monotonically with increasing distance to the BMU and is independent of the BMUs location. Finally, the BMUs and their neighbors were adjusted by the replacement of the old prototype vectors with the averages of the assigned input vectors and their projection into the neighborhood weighted by the neighborhood function. All training steps were reiterated until a stable state of the network was reached. Consequently, the input data was grouped into clusters according to similarity (each network unit represents one cluster) and thus the fine underlying structure of the height information was extracted. In terms of meaningfulness as well as practicability the number of forest structure classes was reduced in a second stage while grouping similar network units using the k-means algorithm according to MacQueen (1967). First, a number of predefined cluster centroids were initialized randomly and each network unit was assigned to its closest (i.e. with the smallest Euclidean distance to the network unit) centroid. The optimal number of centroids was determined corresponding to the minimum within cluster variance (Manning et al., 2008). The cluster centroids were adjusted by the replacement with the mean values of all associated data samples. The processing steps were reiterated until the cluster membership was stable. To avoid the convergence to only a local minimum, the algorithm was replicated 1000 times and the most frequent result was used.

As post-processing, the resulting clusters were labelled considering height histograms of each object per cluster as shown in Abdullahi et al. (2017). The height distributions per cluster allow conclusions about the stand layering as well as canopy closure. As an example, **Fig. 6** illustrates the labelling process for an exemplary inventory plot. The height histogram based

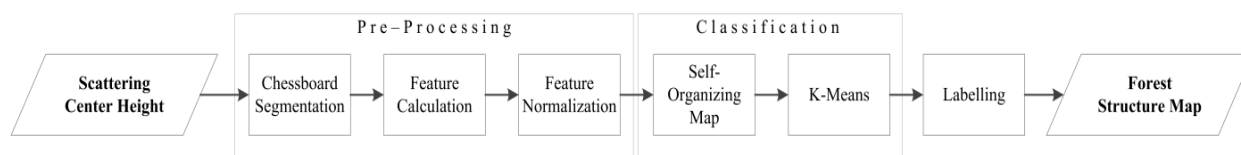


**Fig. 5:** Workflow of the forest structure classification.

on the scattering center height (**Fig. 6a**) indicates a one-layered forest stand with a closed canopy (as illustrated in **Fig. 6b**) due to the small height variation. In order to validate the labelling, an orthophoto with spatial resolution of 20 cm from 2012 (Bayerische Vermessungsverwaltung, 2017), the LiDAR-based nDSM (normalized DSM) as well as 3d-representations based on the in-situ measurements (as depicted in **Fig. 6c**) were considered.

**Fig. 7** depicts the classification scheme of the nine structure classes comprising a schematic representation as well as exemplary excerpts of the orthophoto and the LiDAR-based nDSM: a) Stand Initiation (**Fig. 7a**), b) Closed Canopy One-Stratum I (**Fig. 7b**), c) Closed Canopy One-Stratum II (**Fig. 7c**), d) Closed Canopy One-Stratum III (**Fig. 7d**), e) Closed Canopy One-Stratum IV (**Fig. 7e**), f) Closed Canopy Multi-Strata (**Fig. 7f**), g) Open Canopy Two-Strata I (**Fig. 7g**), h) Open Canopy Two-Strata II (**Fig. 7h**) and i) Open Canopy Multi-Strata (**Fig. 7i**). *Stand Initiation* contains all objects related to almost treeless areas where the sparsely represented vegetation is very low (< 3 m) and consists of seedlings, shrubs and a few small trees. *Closed Canopy One-Stratum I-IV* include objects which possess small height variation and differ mainly in average height. This indicates forest stands with one closed canopy layer. The mean height increases from Closed Canopy One-Stratum I to Closed Canopy One-Stratum IV. *Closed Canopy Multi-Strata* exhibits much higher variation in height compared to Closed Canopy One-Stratum I-IV without very low values which indicates a multi-layered forest with a mostly closed canopy. *Open Canopy Two-Strata I* and *Open Canopy Two-Strata II* are also characterized by higher variations in height. Both classes possess a considerable amount of very low height values, which implies forest gaps. Accordingly, both classes contain objects which are related to two-layered forest stands with an open canopy

layer and gaps or low understory consisting of seedlings, shrubs and small trees. However, the canopy layer of Open Canopy Two-Strata I is lower compared to the canopy layer of Open Canopy Two-Strata II. *Open Canopy Multi-Strata* encompasses the highest range in height. Very low height values indicate gaps or areas with very small vegetation. As opposed to this, this cluster also contains the highest values of the whole study area related to very high trees. Considering the height distribution, this cluster is related to multi-layered forest stands.

### 3.3. Accuracy Assessment

In terms of accuracy assessment of the forest structure classification dependent on different phenological development stages and polarization modes, the field measurements were used to validate the categorization of layering while the LiDAR data were employed to evaluate the assignment according to canopy closure (i.e., closed and open canopy). For consistency, validation was only performed at the location of inventory plots.

Information on stand layering was collected for each inventory plot during forest inventory. Each measured tree was categorized dependent on stand layering (e.g., regeneration, understory, overstory). By means of these field measurements, each inventory plot was classified regarding the number of canopy layers into three classes comprising one-layered, two-layered and multi-layered forest stands. Furthermore, based on the measurements of tree dimensions, species and tree positions, a 3-d representation of each inventory plot was rendered according to Pretzsch et al. (2002). These visualizations enable a better comprehension of the forest structure and its complexity and were additionally used for visual validation.

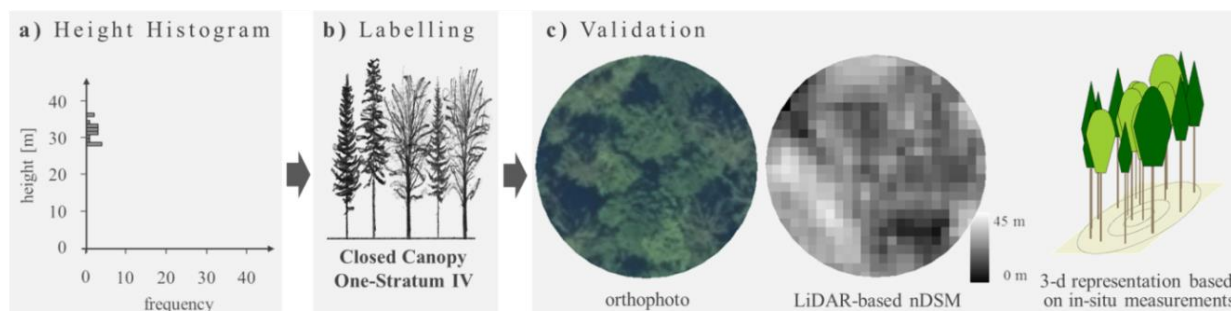


**Fig. 6:** Illustration of labelling process by means of an exemplary inventory plot. **a)** Height histogram of the inventory plot. **b)** The assigned label according the height distribution. **c)** Detail of the orthophoto, Lidar-based nDSM and 3-d representation based on the in-situ measurements for validation purposes.

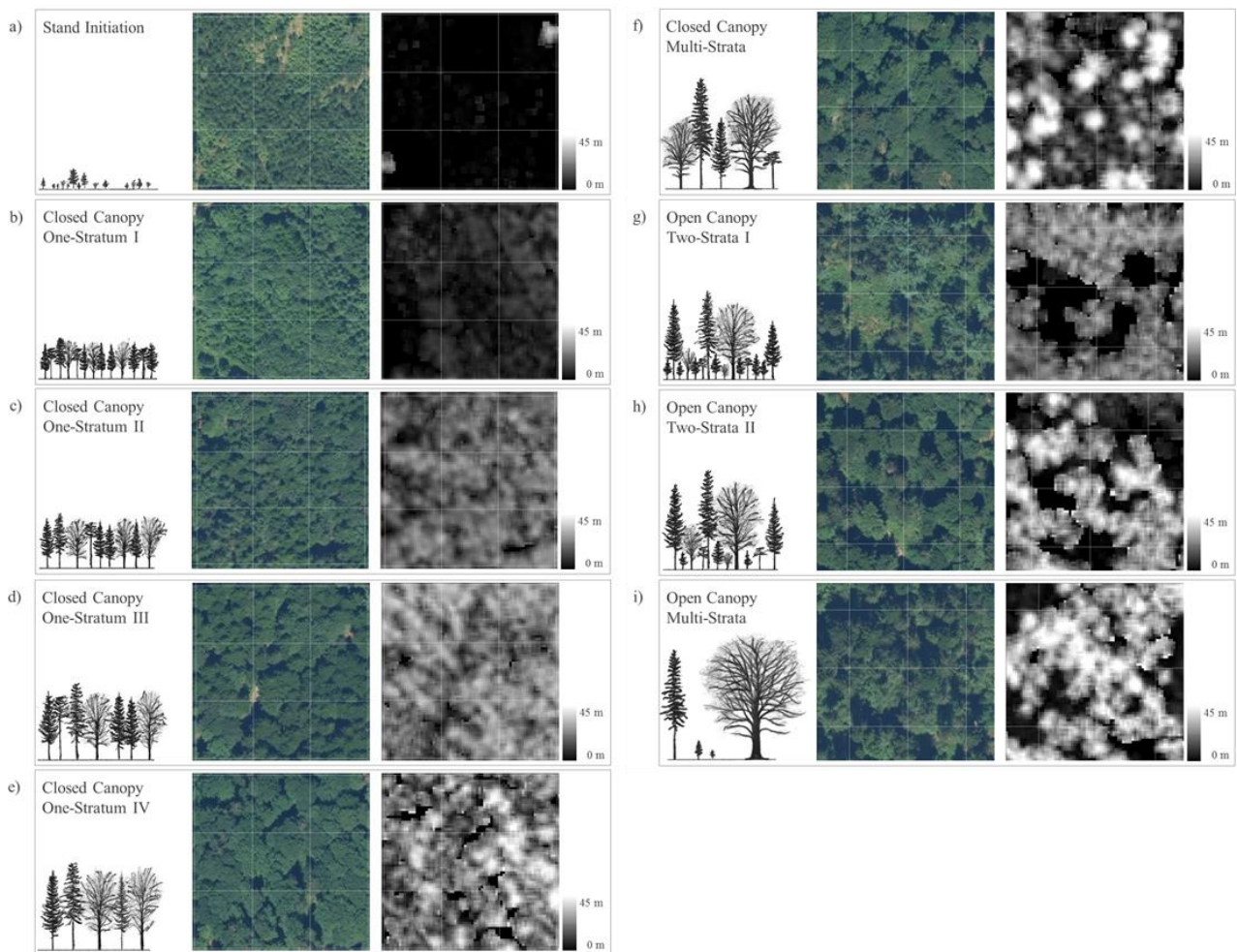


**Fig. 7:** Forest structure class description composed of (from left to right) schematic representation, exemplary excerpts of an orthophoto (spatial resolution of 20 cm) and LiDAR-based nDSM for the nine resulting classes **a)** Stand Initiation, **b)** Closed Canopy One-Stratum I, **c)** Closed Canopy One-Stratum II, **d)** Closed Canopy One-Stratum III, **e)** Closed Canopy One-Stratum IV, **f)** Closed Canopy Multi-Strata, **g)** Open Canopy Two-Strata I, **h)** Open Canopy Two-Strata II and **i)** Open Canopy Multi-Strata.

Since the field measurements do not provide area-wide information about crown cover, the LiDAR data at the location of the inventory plots were used for validation purposes regarding canopy closure. The LiDAR-based DSM was normalized by subtracting the LiDAR-based DTM and the resulting nDSM was applied to canopy cover estimation at units of  $24 \times 24 \text{ m}^2$  (corresponding to the spatial units of the forest classifications). Using a threshold of 3 m, the nDSM was categorized into forest ( $\geq 3\text{ m}$ ) and no forest ( $< 3\text{ m}$ ). Subsequently, the area percentage of height values per unit was calculated indicating canopy closure. Finally, the data was classified according to the degree of canopy closure into two classes: closed canopy ( $> 90\%$  of the considered area unit possess height values  $\geq 3\text{ m}$ ) and open canopy ( $\leq 90\%$  of the considered area unit possess height values  $\geq 3\text{ m}$ ).

Based on these data sets, the confusion matrices for each forest structure classification according to layering and closure of the canopy, respectively, were calculated. To assess the accuracy, the metrics of overall accuracy, producer's accuracy and user's accuracy were derived (Congalton, 1991).

With regard to phenological differences between the data sets (i.e., leaf-on and leaf-off season) each inventory plot was stratified according to the dominated tree species group (i.e., coniferous and broadleaf tree species). The sample-based field measurements were statistically completed according to the representativity of each inventory plot and the growing space of each tree was calculated. Inventory plots exceeding 80 % coverage of coniferous tree species of the summarized growing space were assigned to coniferous forest while

inventory plots with more than 80 % coverage of broadleaf tree species were referred to as broadleaf forest. Accordingly, the accuracy matrices and metrics were derived for coniferous and broadleaf forest, respectively. In total, 65 inventory plots were classified as coniferous while 51 plots were identified as broadleaf forest, respectively.

## 4. Results

### 4.1. Scattering Center Height

**Fig. 8** shows the scattering center heights based on the interferometric TanDEM-X acquisitions in case of leaf-on season (**Fig. 8a** and **Fig. 8b**) and leaf-off season (**Fig. 8c** and **Fig. 8d**) corresponding to VV polarization (**Fig. 8a** and **Fig. 8c**) and HH polarization (**Fig. 8b** and **Fig. 8d**), respectively. In addition, the LiDAR-based nDSM from November 2012 is depicted for comparison (**Fig. 8e**). In general, all height data sets represent the same general structure of the forest. The open spaces in-between the forest stands are clearly visible and the height distributions are very similar. However, the detailed local forest structure including small forest

gaps and paths are only visible in the LiDAR-based nDSM due to its better spatial resolution. In general, the scattering center heights underestimate the actual vegetation height due to penetration of the RaDAR signal into the upper part of the canopy. However, the scattering center heights overestimate the vegetation height in less dense areas, since openings and small forest gaps were not captured by the RaDAR-based DSM due to reduced spatial resolution compared to LiDAR-based DSM (Sadeghi et al., 2017). Furthermore, the scattering center heights corresponding to the leaf-on season are higher in mixed and broadleaf forest stands than the LiDAR-based nDSM acquired in the leaf-off season due to the increased penetration of the LiDAR pulses caused by the absence of leaves (Nilsson & Holgren, 2003; Van Laar & Akça, 2007). For both acquisitions dates, the scattering center height corresponding to VV-polarized data is higher compared to HH-polarized data. Averaged over the study area, the differences are 0.5 m and 1.2 m for the leaf-on and leaf-off season, respectively. In addition, the scattering center heights corresponding to leaf-on season are higher compared to leaf-off season. The difference for the VV data set is 0.7 m on average, while for the HH data set the difference is 1.5 m on average.

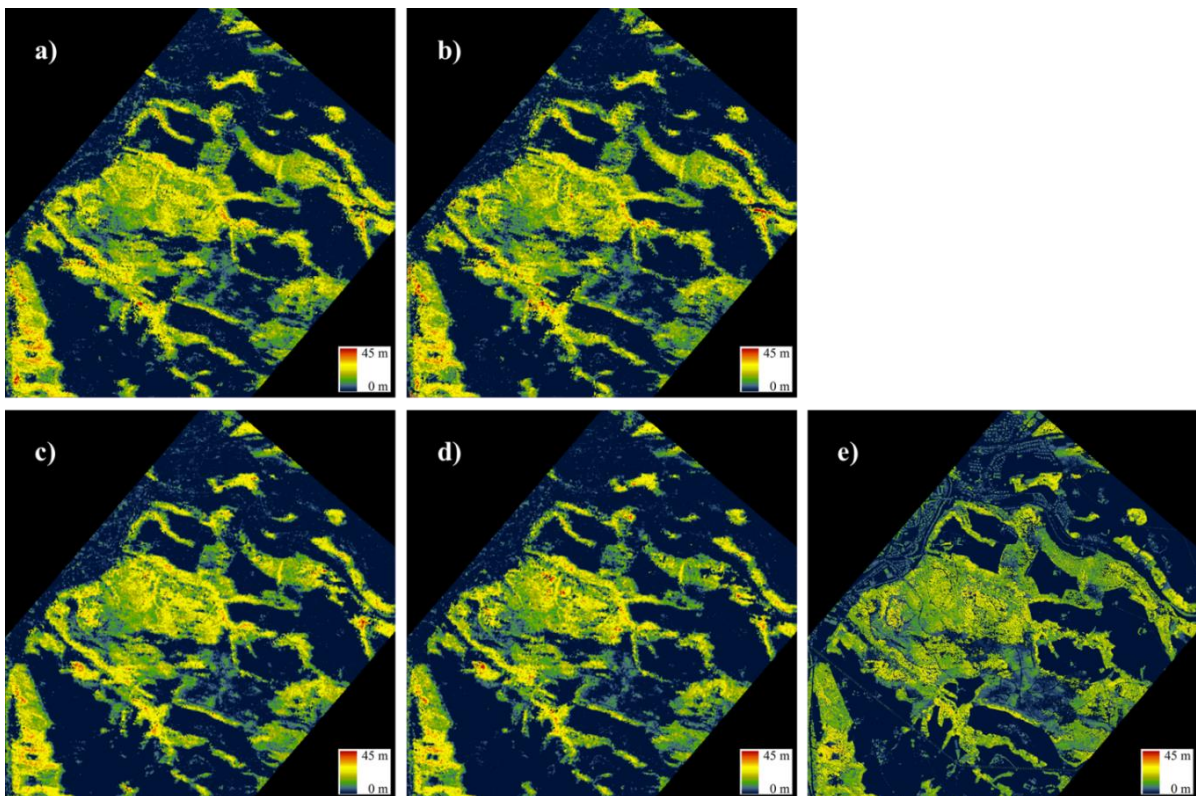


**Fig. 8:** Scattering center height derived from the interferometric TanDEM-X acquisitions of **a)** leaf-on season and VV polarization, **b)** leaf-on season and HH polarization, **c)** leaf-off season and VV polarization, **d)** leaf-off season and HH polarization, and **e)** the LiDAR-based nDSM.



The comparison of the averaged measured tree height per inventory plot (horizontal axis) with scattering center heights (vertical axis) illustrates the underestimation of the actual vegetation height (**Fig. 9**). In general, the scattering center heights based on the leaf-on season (**Fig. 9a** and **Fig. 9b**) correspond better to the measured height values than the scattering center heights from the leaf-off season due to less penetration into the forest canopy. By comparison of the height information based on VV and HH polarization for each season (**Fig. 9a**, **Fig. 9c**, **Fig. 9b** and **Fig. 9d**, respectively), the VV data sets better reflect the measured forest heights.

**Fig. 10** shows the comparison of leaf-off (horizontal axis) and leaf-on (vertical axis) season at plot level for VV and HH polarization, respectively. Data samples corresponding to coniferous forest stands (i.e.,  $\geq 80\%$  of the growing space corresponds to coniferous tree species) and broadleaf forest stands (i.e.,  $\geq 80\%$  of the growing space corresponds to broadleaf tree species) are colored dark green and yellow, respectively. By

comparison of leaf-on and leaf-off season for VV polarization (**Fig. 10a**), the broadleaf data samples are slightly higher in leaf-on season than in leaf-off season, while the scattering center heights corresponding to coniferous forest stands do not change between the seasons. Regarding HH polarization (**Fig. 10b**), the difference of broadleaf forest stands between leaf-on and leaf-off season is more significant. However, in both cases (i.e., VV as well as HH polarization), the scattering center heights are stable concerning coniferous forest stands excluding some outliers and higher in leaf-on season concerning broadleaf forest stands.

To demonstrate the impact of phenology on scattering center height, **Fig. 11** and **Fig. 12** show two 600 m transects, where the transect of **Fig. 11** is located in predominately coniferous forest stands and the transect of **Fig. 12** in broadleaf forest stands within the study area. The transects were placed in order to intersect as many inventory plots as possible to provide in-situ measurements in addition to the LiDAR-based nDSM.

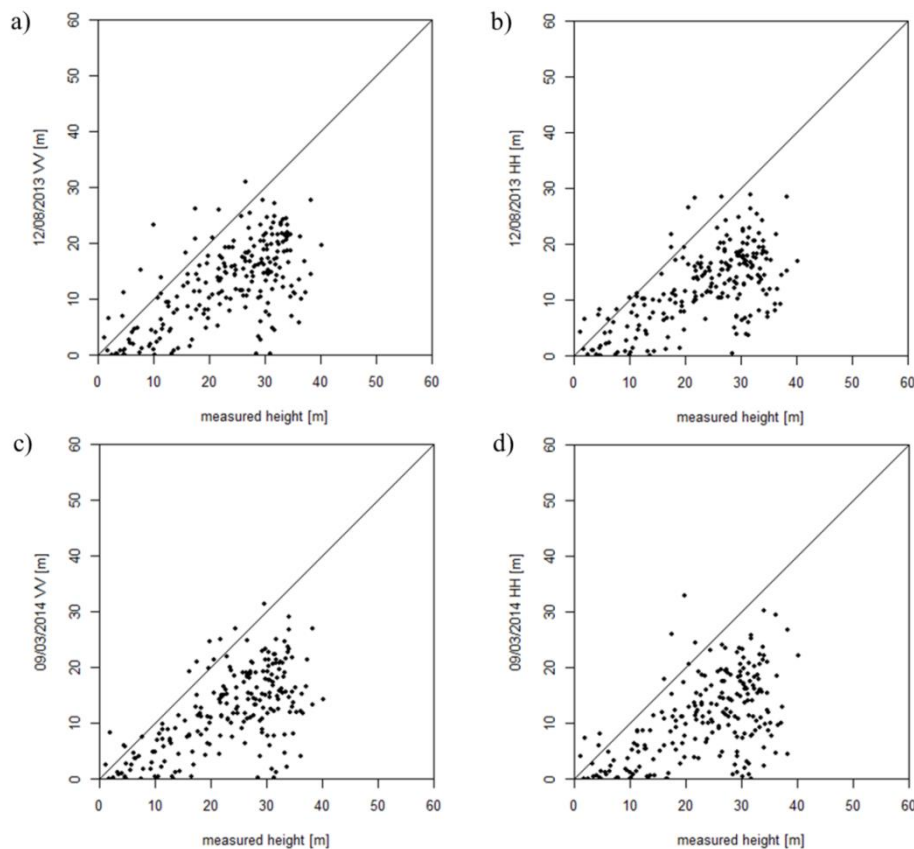


**Fig. 9:** Comparison of the averaged measured tree height per inventory plot (horizontal axis) with scattering center heights (vertical axis) for a) leaf-on season and VV polarization, b) leaf-on season and HH polarization, c) leaf-off season and VV polarization and d) leaf-off season and HH polarization.

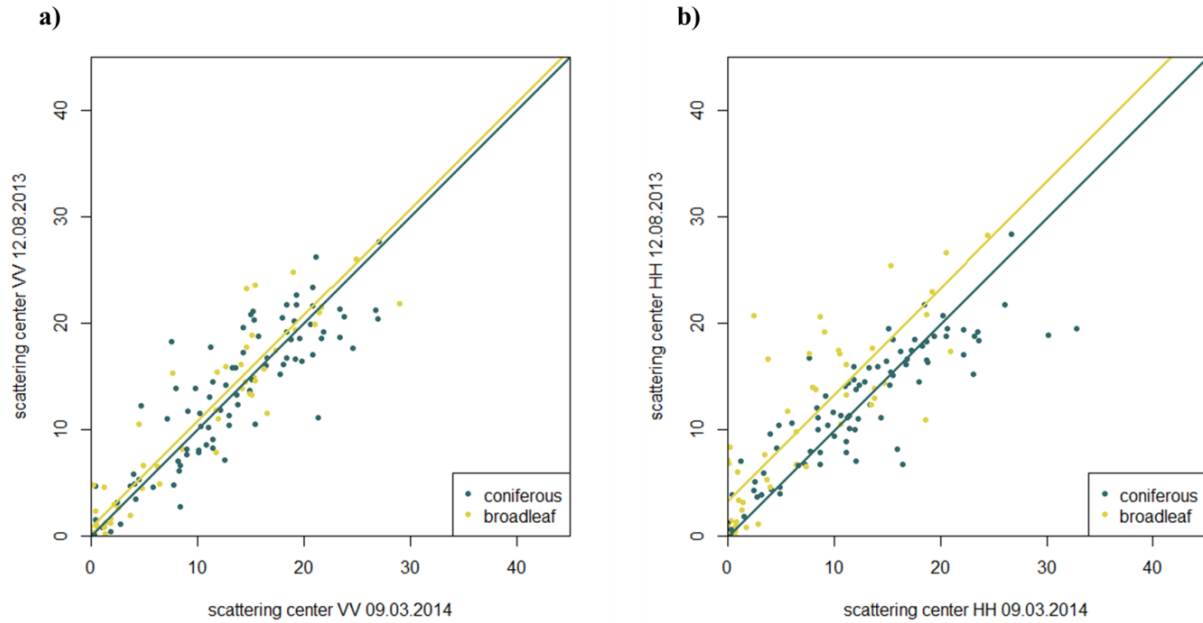


**Fig. 10:** Comparison of leaf-off (horizontal axis) and leaf-on (vertical axis) season at plot level for **a)** VV and **b)** HH polarization, where data samples corresponding to coniferous forest stands (i.e.,  $\geq 80\%$  of the growing space corresponds to coniferous tree species) and broadleaf forest stands (i.e.,  $\geq 80\%$  of the growing space corresponds to broadleaf tree species) are colored dark green and yellow, respectively.

In accordance with **Fig. 9**, the underestimation of the actual vegetation height by the scattering center height is reflected. In general, the differences in height between leaf-on (yellow line) and leaf-off (dark green line) season are less in coniferous forest stands (**Fig. 11c** and **d**) compared to broadleaf forest stands (**Fig. 12c** and **d**). While the differences between leaf-on and leaf-off seasons in height are low in coniferous forest stands and rather caused by spatial variations due to inaccuracies of the data sets, the scattering center heights corresponding to leaf-on season are significantly higher compared to leaf-off season over broadleaf forest stands and imply significant deeper penetration into the canopy caused by the absence of leaves. Especially in case of HH polarization (**Fig. 12d**), the seasonal changes are reflected by the scattering center height.

#### 4.2. Forest Structure Classification

**Fig. 13** illustrates the results of the forest structure classification based on the scattering center heights corresponding to leaf-on season and VV (**Fig. 13a**) as well as HH (**Fig. 13b**) polarization and leaf-off season and VV (**Fig. 13c**) as well as HH (**Fig. 13d**) polarization. In accordance with **Fig. 8a-d**, the variations in scattering center height across the study area are represented by the forest structure classifications. Both, similarities as well as differences

between the height data sets are depicted. The large forest gaps in the south of the study area, the increase in height from southwest to northeast as well as the spatial distribution of rather homogeneous and heterogeneous parts are well reflected. In the central region of the study area, which is dominated by coniferous forest stands, the classification leads to almost the same result for the leaf-on (**Fig. 13a** and **b**) and leaf-off (**Fig. 13c** and **d**) season due to very similar scattering center heights (**Fig. 8**) independent of polarization. In contrast, the northeastern part of the study area, which is predominantly covered by broadleaf forest stands, shows significant differences between the leaf-on and leaf-off season in the forest structure classification results caused by the deviating phenological stages in this area.

To further illustrate the effect of phenology, **Fig. 14** and **Fig. 15** show two inventory plots located in a coniferous forest stand and broadleaf forest stand, respectively. **Fig. 14c** shows very similar height distributions for all acquisitions representing a rather homogenous forest stand with a canopy height around 18 m, while **Fig. 15c** depicts significantly different height distributions for the leaf-on and leaf-off acquisitions indicating different forest structure. Subsequently, the forest stand of **Fig. 14** is assigned to the same forest structure class “Closed Canopy One-Stratum III” for all acquisitions whereas the forest stand

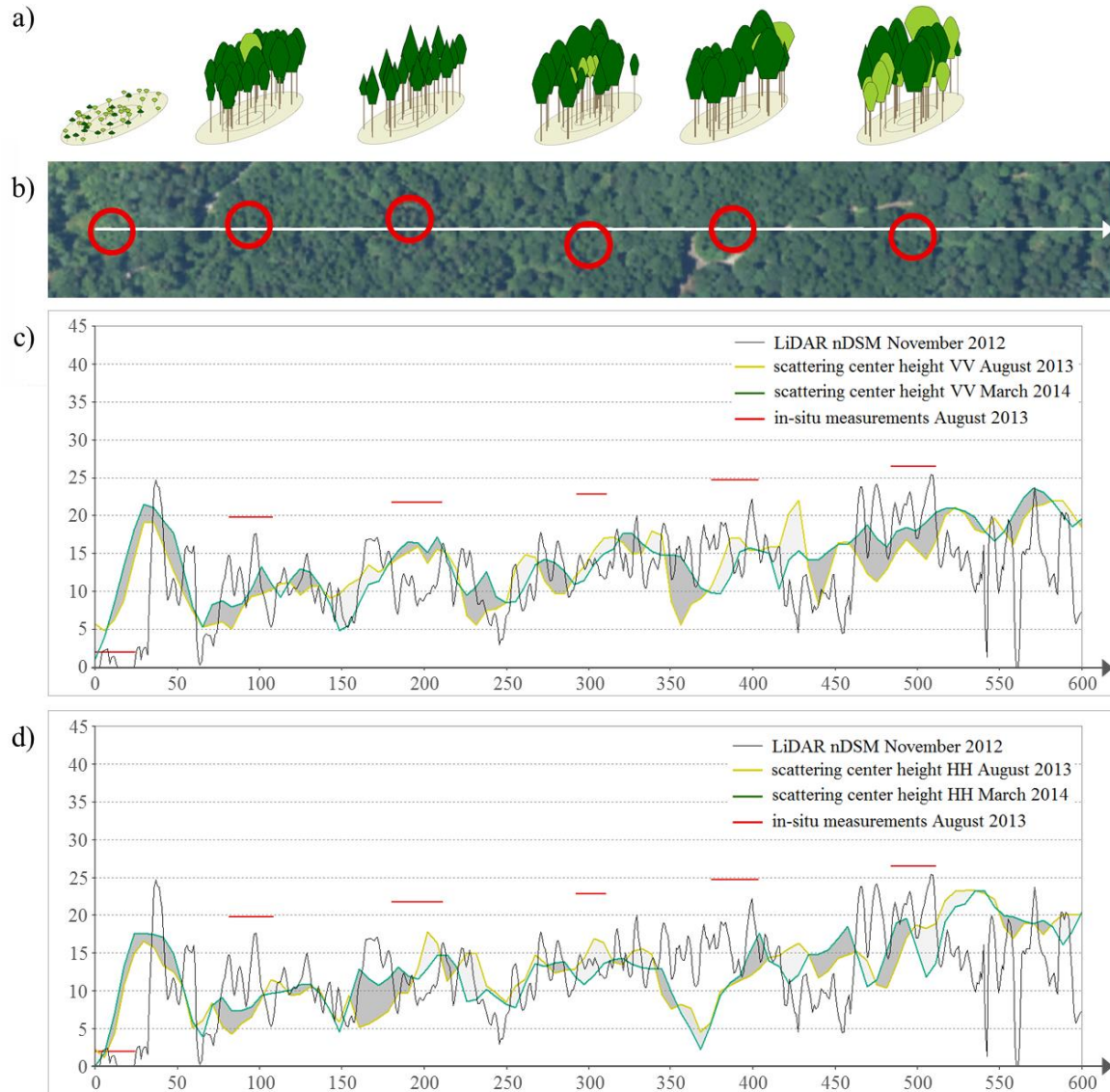


**Fig. 11:** A 600 m transect intersecting six inventory plots across the study area located in predominantly coniferous forest stands. **a)** 3-d illustrations of the inventory plots according to the field measurements, where coniferous tree species are colored dark green and broadleaf tree species are colored light green. **b)** Excerpt of the orthophoto showing the location of the transect and the inventory plots in a synoptic view. **c)** Height profiles of the scattering center height corresponding to VV polarization related to leaf-on season (yellow line) and leaf-off season (dark green line), LiDAR-based nDSM (black line) and averaged field measurements per inventory plot (red line). **d)** Height profiles of the scattering center height corresponding to HH polarization related to leaf-on season (yellow line) and leaf-off season (dark green line), LiDAR-based nDSM (black line) and averaged field measurements per inventory plot (red line).

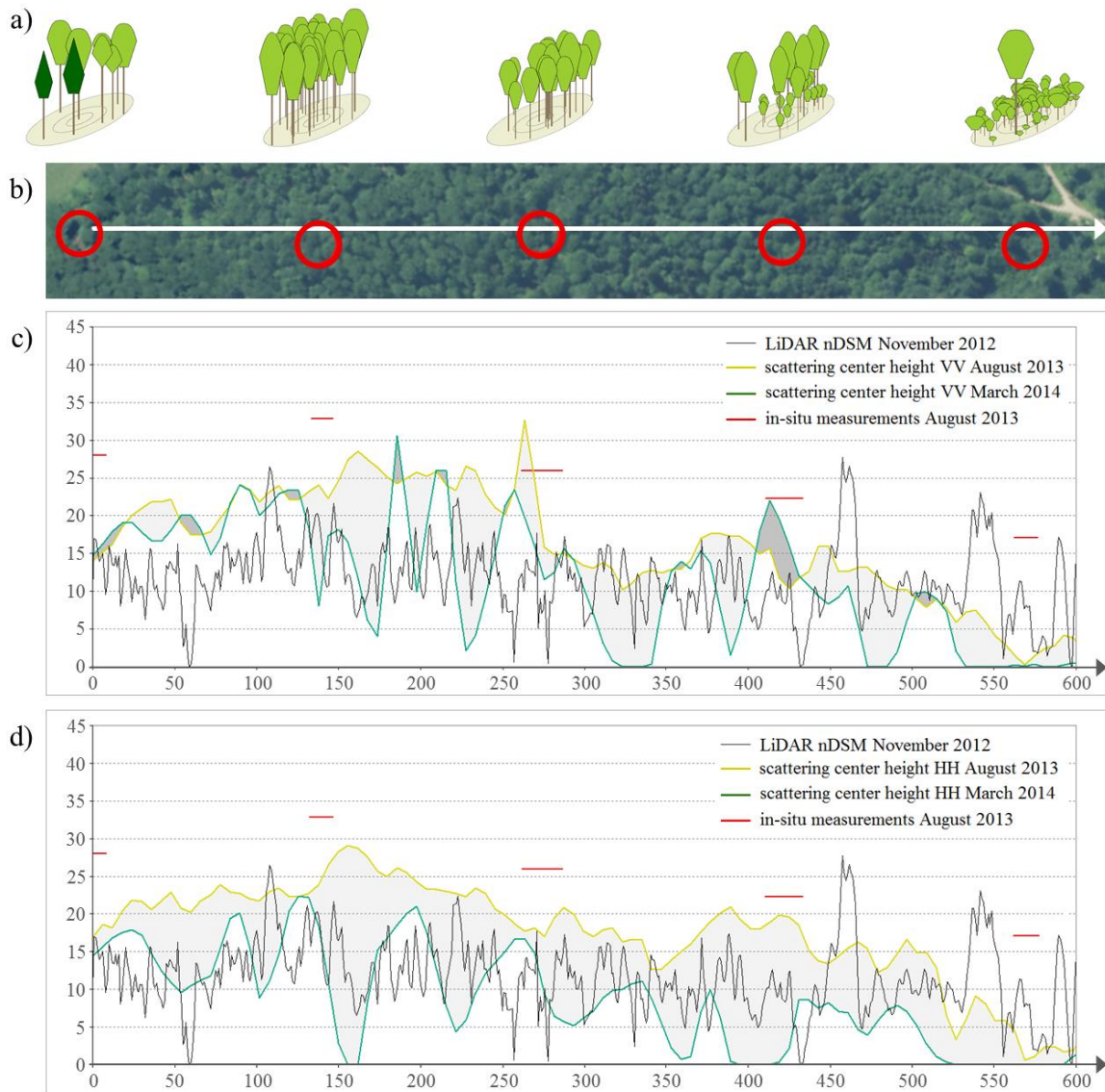


**Fig. 12:** A 600 m transect intersecting six inventory plots across the study area located in broadleaf forest stands. **a)** 3-d illustrations of the inventory plots according to the field measurements, where coniferous tree species are colored dark green and broadleaf tree species are colored light green. **b)** Excerpt of the orthophoto showing the location of the transect and the inventory plots in a synoptic view. **c)** Height profiles of the scattering center height corresponding to VV polarization related to leaf-on season (yellow line) and leaf-off season (dark green line), LiDAR-based nDSM (black line) and averaged field measurements per inventory plot (red line). **d)** Height profiles of the scattering center height corresponding to HH polarization related to leaf-on season (yellow line) and leaf-off season (dark green line), LiDAR-based nDSM (black line) and averaged field measurements per inventory plot (red line).

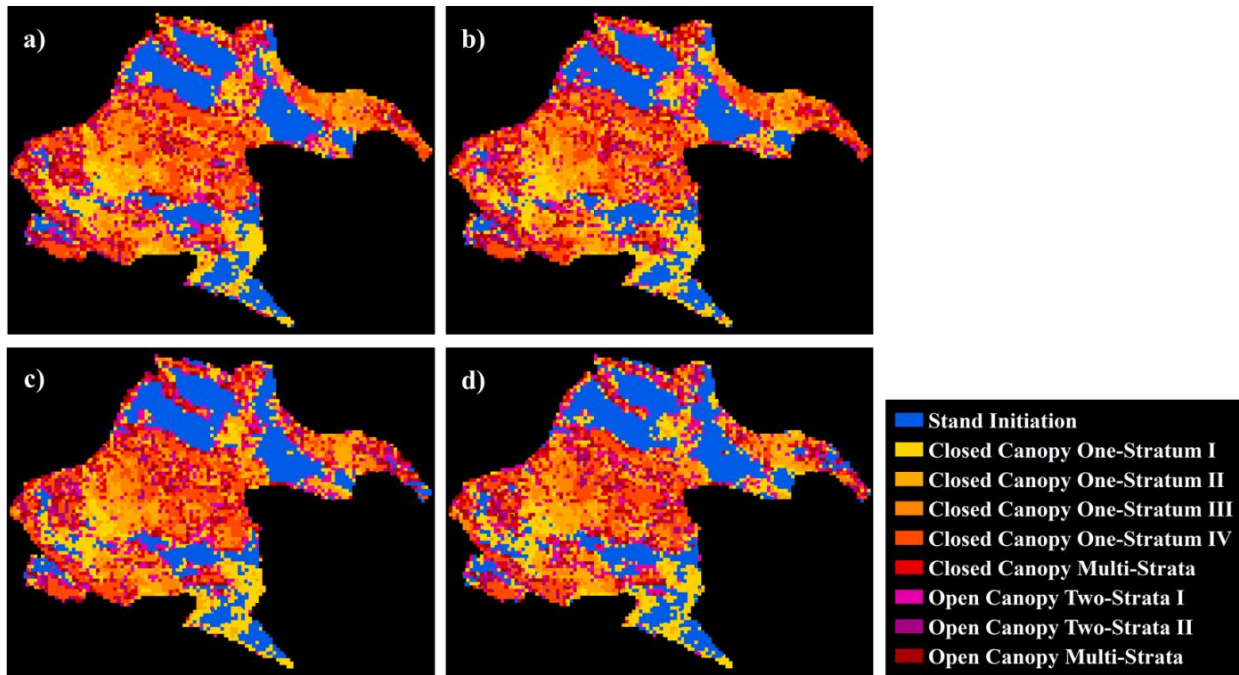


**Fig. 13:** Forest structure classification according to layering and closure of the canopy based on scattering center height derived from the interferometric TanDEM-X acquisitions of **a)** leaf-on season and VV polarization, **b)** leaf-on season and HH polarization, **c)** leaf-off season and VV polarization and **d)** leaf-off season and HH polarization.

according to **Fig. 15** is assigned to different forest structure classes for leaf-on (“Closed Canopy One-Stratum VI”) and leaf-off (“Closed Canopy Multi-Strata”) season. The deviating classification results of the forest stand of **Fig. 15** in the leaf-off season is caused by deeper penetration into the canopy due to the absence of leaves.

The forest stands within the study area are classified according to layering and closure of the canopy at spatial units of  $24 \times 24 \text{ m}^2$ . To assess the accuracy of each classification result, the assigned layering is validated according to the field measurements while the allocated canopy closure is evaluated using the LiDAR data. **Fig. 16** holds the confusion matrices for layering of the classification results related to leaf-on season and VV polarization, leaf-on season and HH polarization, leaf-off season and VV polarization as well as leaf-off season and HH polarization separated with respect to coniferous (dark green) and broadleaf (yellow) forest stands. It becomes obvious that the accuracy is significantly higher for coniferous compared to broadleaf forest stands due to misclassifications caused by phenological effects. In general, superior classification results can be achieved using scattering center heights corresponding to HH polarization. While in case of coniferous forest stands the data set related to

leaf-on season and HH polarization yield the best overall accuracy, the data set based on the leaf-off season and HH polarization achieved the best overall accuracy considering broadleaf forest stands. The producer’s accuracies for the class “one-layered” are high, whereas the producer’s accuracies for the other two classes are rather low. One main reason is the incapability of X-band to penetrate deep into the forest and thus it cannot provide information about the understory. Accordingly, the understory under dense canopies cannot be captured and thus leads to overestimation of one-layered forest stands and underestimation of two- and multi-layered forest stands. In addition, only few two- and multi-layered forest stands are present in the study area which emphasizes the effect of each individual misclassification. In general, all data sets lead to an overestimation of one-layered forest stands. For both, coniferous and broadleaf dominated forest stands, the greatest overestimation could be registered for the data sets corresponding to the leaf-on season. In case of coniferous forest stands, two-layered stands are underestimated and multi-layered stands are slightly overestimated. In contrast, for broadleaf forest stands, two-layered as well as multi-layered stands are underestimated.

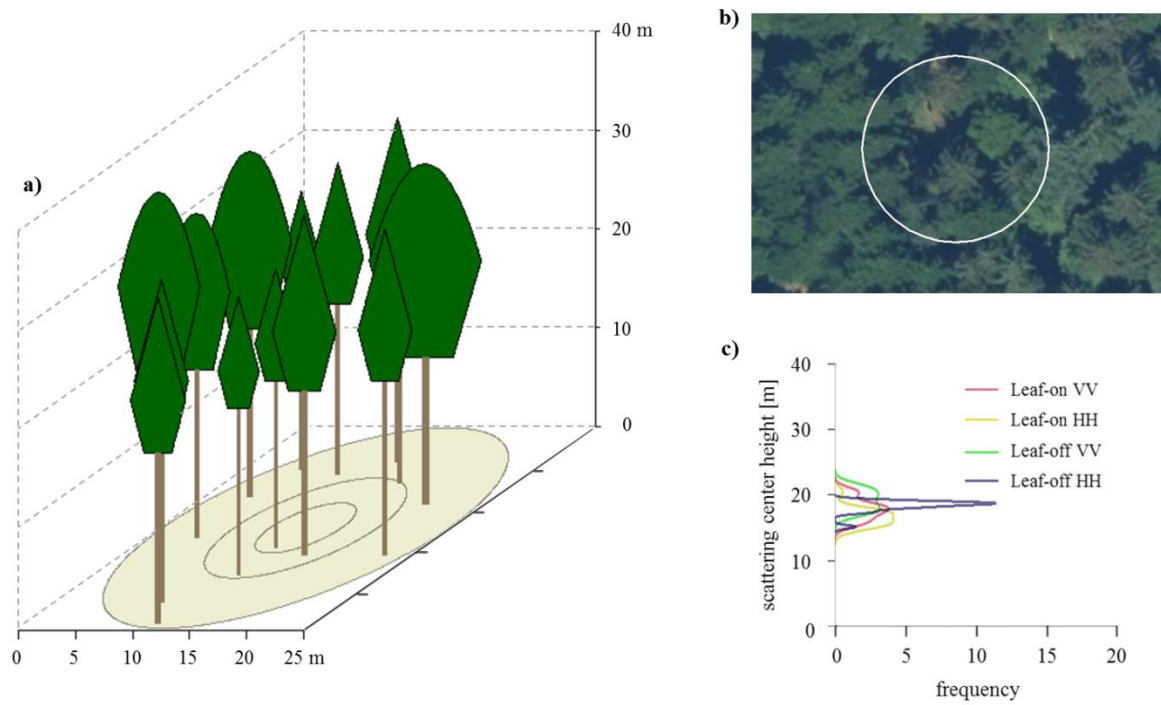


**Fig. 14:** **a)** Three-dimensional representation of an inventory plot based on in-situ measurements. **b)** Related detail of an orthophoto. **c)** Related height histograms based on the scattering center heights of leaf-on season and VV polarized InSAR data (red), leaf-on season and HH polarized InSAR data (yellow), leaf-off season and VV polarized InSAR data (green) and leaf-off season and HH polarized InSAR data (blue).

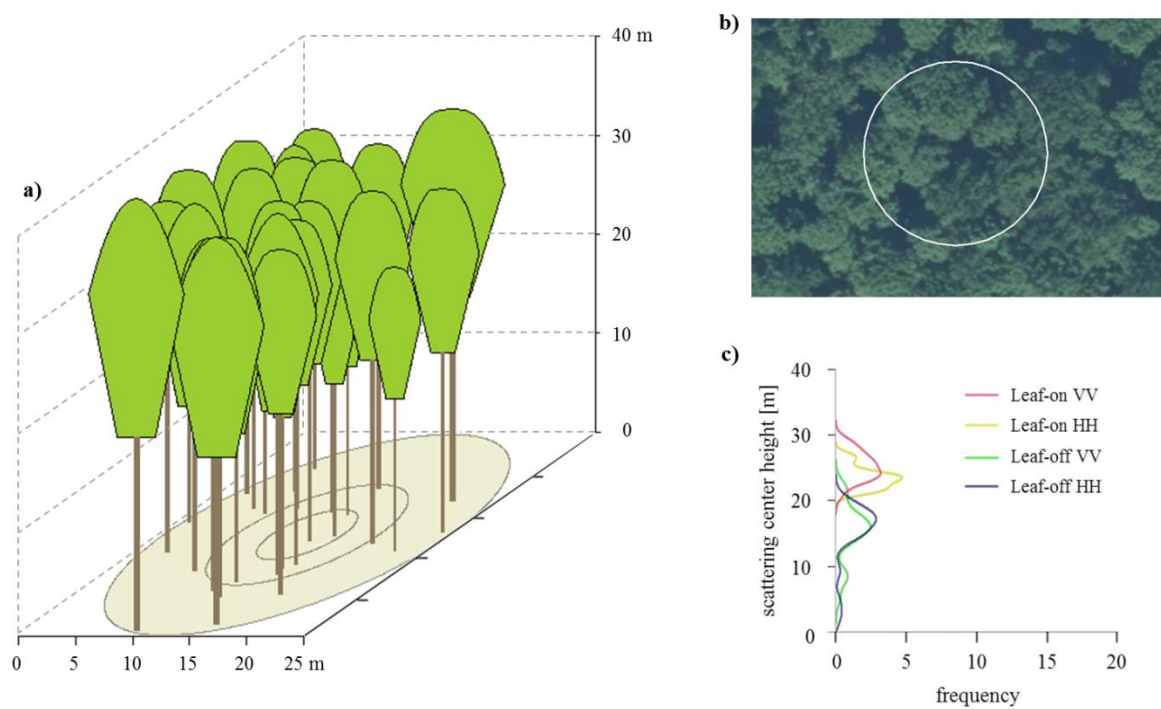


**Fig. 15:** **a)** Three-dimensional representation of an inventory plot based on in-situ measurements. **b)** Related detail of an orthophoto. **c)** Related height histograms based on the scattering center heights of leaf-on season and VV polarized InSAR data (red), leaf-on season and HH polarized InSAR data (yellow), leaf-off season and VV polarized InSAR data (green) and leaf-off season and HH polarized InSAR data (blue).

		Inventory				User's Accuracy
		one-layered	two-layered	multi-layered	total	
leaf-on VV	one-layered	27   12	19   16	6   9	52   37	51.9   32.4
	two-layered	2   1	5   2	0   5	7   8	71.4   25.0
	multi-layered	0   3	5   3	1   0	6   6	16.7   0.00
	<b>total</b>	<b>29   16</b>	<b>29   21</b>	<b>7   14</b>	<b>65   51</b>	
Producer's Accuracy		93.1   75.0	17.2   9.50	14.3   0.00		<b>50.8   27.5</b>

		Inventory				User's Accuracy
		one-layered	two-layered	multi-layered	total	
leaf-on HH	one-layered	26   14	20   15	2   10	48   39	54.2   35.9
	two-layered	3   1	5   1	0   3	8   5	62.5   20.0
	multi-layered	0   1	4   5	5   1	9   7	55.6   14.3
	<b>total</b>	<b>29   16</b>	<b>29   21</b>	<b>7   14</b>	<b>65   51</b>	
Producer's Accuracy		89.7   87.5	17.2   4.8	71.4   7.1		<b>55.4   31.4</b>

		Inventory				User's Accuracy
		one-layered	two-layered	multi-layered	total	
leaf-off VV	one-layered	23   12	15   15	4   10	42   37	54.8   32.4
	two-layered	4   2	7   2	0   1	11   5	63.6   40.0
	multi-layered	2   2	7   4	3   3	12   9	25.0   33.3
	<b>total</b>	<b>29   16</b>	<b>29   21</b>	<b>7   14</b>	<b>65   51</b>	
Producer's Accuracy		79.3   75.0	24.1   9.5	42.9   21.4		<b>50.8   33.3</b>

		Inventory				User's Accuracy
		one-layered	two-layered	multi-layered	total	
leaf-off HH	one-layered	28   13	14   12	5   10	47   35	59.6   37.1
	two-layered	1   1	6   5	1   4	8   10	75.0   50.0
	multi-layered	0   2	9   4	1   0	10   6	10.0   0.0
	<b>total</b>	<b>29   16</b>	<b>29   21</b>	<b>7   14</b>	<b>65   51</b>	
Producer's Accuracy		96.6   81.3	20.7   23.8	14.3   0.0		<b>53.9   35.3</b>

**Fig. 16:** Confusion matrices for the forest structure classification according to layering corresponding to **a)** leaf-on season and VV polarization, **b)** leaf-on season and HH polarization, **c)** leaf-off season and VV polarization and **d)** leaf-off season and HH polarization, where the dark green and yellow colored numbers are related to coniferous and broadleaf forest stands, respectively.

A two-layered forest stand, predominantly covered by coniferous tree species is chosen to illustrate the impact of the incapability of X-band to capture layers below the main canopy layer (Fig. 17). As depicted in Fig. 17b the main layer is rather dense and the canopy is almost closed. Due to the incapability of X-band to

capture the understory, the scattering center heights represent only the main layer of the forest stands (Fig. 17c).

Regarding canopy closure, the accuracies are significantly higher for all data sets compared to the

accuracies related to layering (**Fig. 18**). The results are consistently much better for coniferous (dark green) compared to broadleaf (yellow) forest stands. The best overall accuracy for coniferous dominated forest stands could be achieved using the data sets of leaf-on season in combination with VV polarization and leaf-off season in combination with HH polarization. In contrast, the data sets corresponding to leaf-on season and HH polarization yield the best overall accuracy for broadleaf forest stands. In case of the leaf-on as well as leaf-off season regardless polarization, openness of the canopy is overestimated and closeness of the canopy is underestimated for coniferous as well as broadleaf forest stands. This effect is more distinct in the leaf-off season compared to leaf-on season due to the absence of leaves and thus deeper penetration into the forest.

## 5. Discussion

The current study demonstrates the influence of phenology on forest structure classification by means of X-band InSAR data acquired in leaf-on and leaf-off season. In addition, the dependency on polarization mode is investigated. The complex temperate forest of Traunstein, composed of unevenly aged coniferous,

broadleaf and mixed forest stands, was used as study area. This forest is characterized by high species richness and different development stages, which reflect a “close-to-nature” silviculture (Pretzsch et al., 2015).

Few studies discussed the seasonal dependency on forest height estimation by means of X-band InSAR data over different forest biomes. Studies carried out in broadleaf and mixed forest stands (Olesk et al., 2015; Kugler et al., 2014) found less penetration into the forest in the leaf-on season compared to leaf-off season. In contrast, investigations carried out in coniferous forest stands (Sadeghi et al., 2017; Solberg et al., 2015) reported no significant difference between leaf-on and leaf-off season.

In accordance with these findings, the current study indicates that height estimations based on X-band InSAR over coniferous forest stands is not significantly affected by phenology, whereas over broadleaf forest stands it is essentially influenced by the phenological differences between leaf-on and leaf-off season (**Fig. 10**). In general, a lower scattering center height is detected in the leaf-off season. The absence of leaves yields a decrease of relevant scatterers in the upper part of the canopy and thus leads to deeper penetration of the RaDAR signal. Regarding polarization mode, the effect

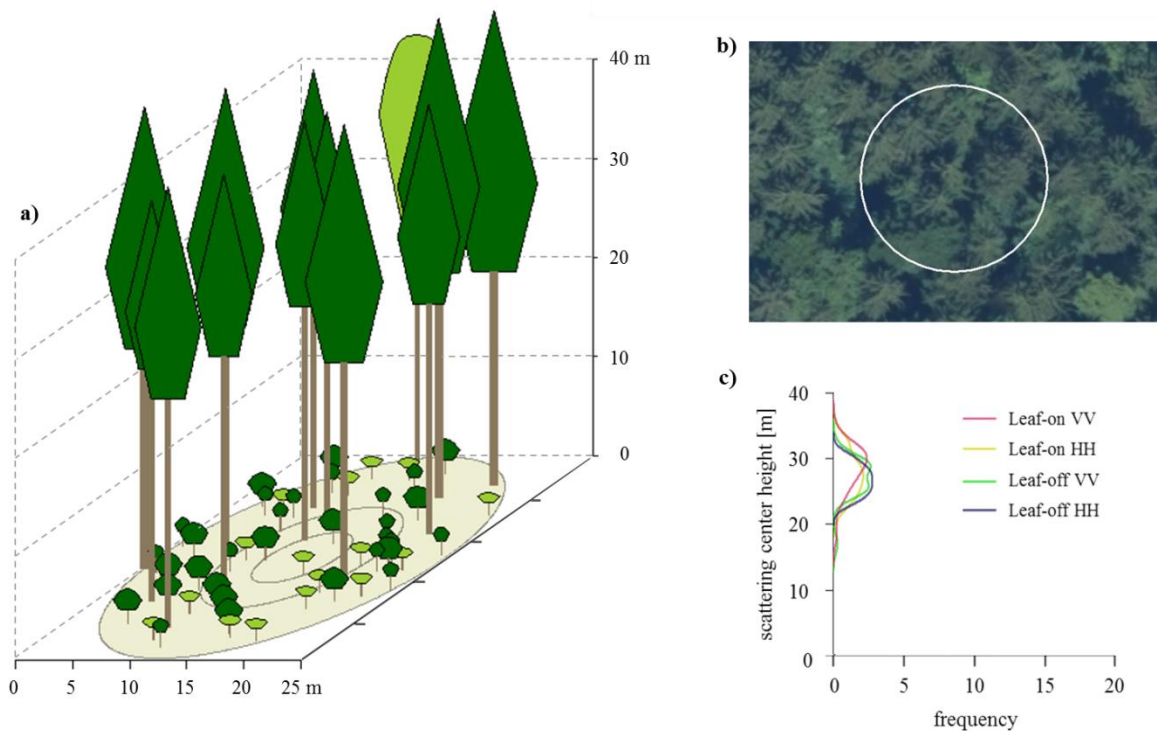


**Fig. 17:** a) Three-dimensional representation of an inventory plot based on in-situ measurements. b) Related detail of an orthophoto. c) Related height histograms based on the scattering center heights of leaf-on season based on VV polarized InSAR data (red), leaf-on season based on HH polarized InSAR data (yellow), leaf-off season based on VV polarized InSAR data (green) and leaf-off season based on HH polarized InSAR data (blue).



		LiDAR			User's Accuracy
		open	closed	total	
leaf-on VV	open	11   16	8   11	19   27	57.9   59.3
	closed	5   5	41   19	46   24	89.1   79.2
	<b>total</b>	<b>16   21</b>	<b>49   30</b>	<b>65   51</b>	
Producer's Accuracy		68.8   76.2	83.7   63.3		<b>80.0   68.6</b>

		LiDAR			User's Accuracy
		open	closed	total	
leaf-on HH	open	11   16	10   10	21   26	52.4   61.5
	closed	5   5	39   20	44   25	88.6   80.0
	<b>total</b>	<b>16   21</b>	<b>49   30</b>	<b>65   51</b>	
Producer's Accuracy		68.8   76.2	79.6   66.7		<b>76.9   70.6</b>

		LiDAR			User's Accuracy
		open	closed	total	
leaf-off VV	open	13   16	14   12	27   28	48.2   57.1
	closed	3   5	35   18	38   23	92.1   78.3
	<b>total</b>	<b>16   21</b>	<b>49   30</b>	<b>65   51</b>	
Producer's Accuracy		81.3   76.2	71.4   60.0		<b>73.9   66.7</b>

		LiDAR			User's Accuracy
		open	closed	total	
leaf-off HH	open	15   15	12   19	27   34	55.6   44.1
	closed	1   6	37   11	38   17	97.4   64.7
	<b>total</b>	<b>16   21</b>	<b>49   30</b>	<b>65   51</b>	
Producer's Accuracy		93.8   71.4	75.5   36.7		<b>80.0   51.0</b>

**Fig. 18:** Confusion matrices for the forest structure classification according to canopy closure corresponding to **a)** leaf-on season and VV polarization, **b)** leaf-on season and HH polarization, **c)** leaf-off season and VV polarization and **d)** leaf-off season and HH polarization, where the dark green and yellow colored numbers are related to coniferous and broadleaf forest stands, respectively.

of phenology on scattering center height is more significant based on HH polarization (**Fig. 10b**) compared to VV polarization (**Fig. 10a**). Admittedly, vegetation height is underestimated in the leaf-on as well as leaf-off season based on VV- as well as HH-polarized data, however the most accurate height estimations could be achieved using VV-polarized InSAR data corresponding to the leaf-on season.

Several studies investigated the potential of InSAR data for the detection of forest structure, while only a few studies performed the classification of forest structure types (e.g., De Grandi et al., 2015; Liesenberg & Gloaguen, 2013; Hoekman & Quiñones, 2002). Moreover, all mentioned studies disregarded the influence of phenology. However, the current study demonstrates that phenology considerably affects the assessment of forest structure. Especially regarding

forest stands which are predominantly covered by broadleaf tree species, the classification results differentiate significantly between leaf-on and leaf-off season. While forest structure classification yield similar overall accuracies independent of season and polarization in coniferous-dominated forest stands, it obtains varying accuracies dependent on season and polarization in broadleaf-dominated forest stands. Regarding layering, the classification accuracies are significantly higher for coniferous-dominated than for broadleaf-dominated forest stands. While the seasonality does not influence the classification with respect to layering for coniferous forest stands, obviously better classification results can be achieved using off-leaf data in broadleaf forest stands. Considering the polarization mode, HH-polarized data are more suitable to detect canopy layering. Also with respect to canopy closure, the classification results for coniferous forest stands are not significantly influenced by phenology. In this regard, InSAR data from leaf-on season demonstrates to be more suitable in case of broadleaf forest stands. Polarization mode has no significant influence on classification of canopy closure. Considering the best classification results in general, HH-polarized InSAR data from leaf-on season and HH-polarized data from leaf-off season should be preferred to estimate forest layering in coniferous and broadleaf forest stands, respectively. In addition, InSAR data from leaf-on season in HH polarization can be recommended to classify canopy closure. The comparison of the classification results corresponding to leaf-on and leaf-off season clarifies the high impact of the phenological development stage on capturing forest structure based on a synoptic view. Therefore it is advisable to cautiously select the time of image acquisition with respect to the forest parameter under investigation. Moreover, to monitor the development of the forest structure within a certain time frame, it is of high importance to select data sets corresponding to the same phenological stage in order to mitigate the erroneous detection of changes caused by phenology.

However for all data sets, the classification accuracies of layering are rather poor caused by a high overestimation of one-layered forest stands. The RaDAR signal in X-band possesses the ability to penetrate into the upper part of the canopy, but is incapable to detect the understory below a dense canopy. Consequently, the classification based on X-band InSAR data results in an overestimation of one-layered and underestimation of two- and multi-layered forest stands. To solve this problem, a combination of X-band with longer wavelengths (e.g., L-band) should be considered. The longer wavelengths would provide

complementary information on forest layers below the main canopy due to the capability to penetrate deeper into the forest. In contrast to layering, the classification accuracies of canopy closure are much better. However, the closure of the canopy is underestimated compared to the LiDAR-based measures, which indicates deeper penetration of the RaDAR signals compared to LiDAR. The underestimation of canopy closure increases in the leaf-off season caused by the absence of leaves and thus deeper penetration into the canopy.

Besides, the accuracy of the classification results also suffers more general restrictions due to limitations of the X-band InSAR data. First, spatial displacements caused by geometrical effects (e.g., foreshortening, shadowing, georeferencing) lead to inaccurate height estimations and thus erroneous classification. Especially at small spatial units of about 500 m<sup>2</sup>, geometrical effects significantly influence the classification results. However, forest succession processes in “close-to-nature” forest stands, which mainly affect forest structure, take place on patches at this scale (Bugmann, 2001; Pretzsch, 2009). These processes characterize the architecture of the canopy layer and thus regulate the amount of available sunlight in deeper forest layers, which in turn influences the vertical forest structure. Accordingly, information about forest structure at this spatial scale is highly relevant in terms of biodiversity assessment as well as sustainable forest management. Nevertheless, in order to increase the classification accuracies, also larger spatial units should be considered for further investigations. Second, the penetration capability of the signal is affected by the canopy architecture and thus, it spatially differs mostly dependent on tree species. Therefore, height information based on TanDEM-X InSAR data exhibits additional spatial variations as well as patterns that is independent from the actual forest height. Third, the processing of the DEM itself includes sources of error. Loss of accuracy can be caused by system noise, decorrelations to the different sensor positions during image acquisition as well as terrain roughness (Moreira et al., 2013; Rosen et al., 2000; Bamler & Hartl 1998).

Beyond, the detected differences between leaf-on and leaf-off season present the prospect of monitoring and detecting seasonal changes in the course of the year. Well-chosen time series of X-band InSAR data facilitate detection of spatiotemporal phenology-related information about the forest. Especially in the context of ongoing climatic changes, time series provide the possibility to explore the shifting temporal cycle of phenological development stages. Moreover, the differences in penetration of the RaDAR signal between

leaf-on and leaf-off season, which are mainly related to broadleaf-dominated forest stands, offer the opportunity to stratify forests according to coniferous and broadleaf tree species.

## 6. Conclusion

In this paper, the dependency of height estimation and forest structure classification on phenology and polarization by means of TanDEM-X acquisitions was investigated over complex temperate forest stands. The objectives were defined as i) assessment of phenology-based differences in height estimation dependent on polarization mode (i.e., VV-polarized and HH-polarized InSAR data) and ii) the consequent limitations in forest structure classification accuracy. The study has demonstrated that the phenological development stage of trees has a high impact on height estimation and forest structure classification by means of X-band InSAR data in broadleaf-dominated forest stands, while coniferous forest stands are largely unaffected. The differences between leaf-on and leaf-off season became clearly visible in HH polarization, while the differences were less distinct in VV polarization. The actual vegetation height was underestimated in the leaf-on as well as leaf-off season based on VV- as well as HH-polarized data due to penetration of the SAR signal, whereas the most accurate height estimations could be achieved using VV-polarized InSAR data corresponding to the leaf-on season. Regarding forest structure classification according to layering and closure of the canopy, the accuracies suffer limitations caused by general technical restrictions like geometrical effects (e.g. foreshortening, layover, georeferencing), penetration of the SAR signal and processing errors (e.g. phase unwrapping errors). Despite the penetration ability of the SAR signal, the understory could not be detected below a dense canopy in X-band due to the small wavelength, which leads to an overestimation of one-layered stands and an underestimation of two- and multi-layered forest stands. In general, the InSAR data set related to leaf-on season and HH polarization yielded the best classification result in coniferous forest stands, while in case of broadleaf forest stands the data set corresponding to leaf-off season and HH polarization achieved the best result. Concerning canopy closure, the InSAR data related to leaf-off season and HH polarization led to the superior results according to overall accuracy in coniferous forest stands, whereas the data based on leaf-on season and HH polarization achieved the best classification results in broadleaf forest stands. Summarizing, VV-polarized

InSAR data related to leaf-on season is preferable to estimate height, whereas HH polarization acquisitions are more suitable to capture forest structure.

## Acknowledgements

This study was supported by the Federal Ministry for Economic Affairs and Energy under Project 50EE1261. The authors would like to thank the German Aerospace Agency (DLR) for providing the TanDEM-X data. Further, the authors would like to thank Gerhard Fischer from the Municipal Forest Traunstein for providing the field measurements and supporting the field survey.

## References

- Abdullahi, S., Kugler, F. & Pretzsch, H., 2016. Prediction of stem volume in complex temperate forest stands using TanDEM-X SAR data. *Remote Sensing of Environment*, Volume 174, pp. 197-211.
- Abdullahi, S., Schardt, M. & Pretzsch, H., 2017. An unsupervised two-stage clustering approach for forest structure classification based on X-band InSAR data - A case study in complex temperate forest stands. *International Journal of Applied Earth Observation and Geoinformation*.
- Bamler, R. & Hartl, P., 1998. Synthetic aperture radar interferometry. *Inverse Problems*, Volume 14, pp. R1-R54.
- Bayerische Staatsforsten, 2011. *Richtlinie für die mittel- und langfristige Forstbetriebsplanung in den Bayerischen Staatsforsten (Forsteinrichtungsrichtlinie - FER 2011)*, Regensburg: s.n.
- Bayerische Vermessungsverwaltung, 2017. *Bayernbefliegung*. [Online] Available at: <http://www.ldbv.bayern.de/vermessung/luftbilder/bayernbefliegung.html> [Accessed 29 May 2017].
- Bonan, G. B., 2008. Forests and Climate Change: Forcings, Feedbacks, and the Climate Benefits of Forests. *Science*, 320(5882), pp. 1444-1449.
- Bugmann, H., 2001. A Review of Forest Gap Models. *Climatic Change*, Volume 51, pp. 259-305.
- Carey, A. & Wilson, S., 2001. Induced Spatial Heterogeneity in Forest Canopies: Responses of Small Mammals. *Journal of Wildlife Management*, 65(4), pp. 1014-1027.

- Congalton, R. G., 1991. A review of assessing the accuracy of classifications of remotely sensed data. *Remote Sensing of Environment*, 37(1), pp. 35-46.
- Cornelius, C., Estrella, N., Frenz, H. & Menzel, A., 2013. Linking altitudinal gradients and temperature responses of plant phenology in the Bavarian Alps. *Plant Biology*, 15(1), pp. 57-69.
- De Grandi, E. C., Mitchard, E. & Hoekman, D., 2016. Wavelet Based Analysis of TanDEM-X and LiDAR DEMs across a Tropical Vegetation Heterogeneity Gradient Driven by Fire Disturbance in Indonesia. *Remote Sensing*, 8(641).
- De Grandi, E. C., Mitchard, E. T. A., Woodhouse, I. H. & Verhegghen, A., 2015. Statistics of TanDEM-X DSM, coherence and backscatter for the characterization of tropical forest structure configuration. *IEEE International Geoscience and Remote Sensing Symposium (IGARSS)*. July, pp. 1805-1808.
- Definiens, 2009. *Definiens eCognition Developer 8 reference book*, Munich: Definiens AG.
- del Río, M. et al., 2015. Characterization of the structure, dynamics, and productivity of mixed-species stands: review and perspectives. *European Journal of Forest Research*.
- Dobson, M. C. et al., 1995. Dependence of Radar Backscatter on Coniferous Forest Biomass. *IEEE Transactions on Geoscience and Remote Sensing*, Volume 2, pp. 412-415.
- DWD, D. W., 2016. *Daten Deutschland*. [Online] Available at: [http://www.dwd.de/DE/klimaumwelt/klimaueberwachung/phaenologie/daten\\_deutschland/daten\\_deutschland\\_nod\\_e.html](http://www.dwd.de/DE/klimaumwelt/klimaueberwachung/phaenologie/daten_deutschland/daten_deutschland_nod_e.html) [Accessed 20 December 2016].
- Gama, F. F., Santos, J. R. & Mura, C. J., 2010. Eucalyptus Biomass and Volume Estimation Using Interferometric and Polarimetric SAR Data. *Remote Sensing*, 2(4), pp. 939-956.
- Gao, T., Hedblom, M., Emilsson, T. & Nielsen, A. B., 2014. The role of forest stand structure as biodiversity indicator. *Forest Ecology and Management*, Volume 330, pp. 82-93.
- Harding, D. J., Blair, J. B., Rodriguez, E. & Michel, T., 1995. Airborne laser altimetry and interferometric SAR measurements of canopy structure and sub-canopy topography in the Pacific Northwest. *Second Topical Symposium on Combined Optical-Microwave Earth and Atmosphere Sensing*, 3-6 April, Volume Conference Proceedings, pp. 22-24.
- Hoekman, D. H. & Quiñones, M. J., 2002. Biophysical Forest Type Characterization in the Colombian Amazon by Airborne Polarimetric SAR. *IEEE Transactions on Geoscience and Remote Sensing*, 40(6), pp. 1288-1300.
- IPPC, 2014. *Climate Change 2014: Impacts, Adaptation, and Vulnerability. Contribution of Working Group II to the Fifth Assessment Report of the Intergovernmental Panel on Climate Change*, Cambridge, United Kingdom and New York, NY, USA: Cambridge University Press.
- Kantardzic, M., 2011. *Data mining: Concepts, models, methods, and algorithms*. Hoboken, New Jersey: John Wiley & Sons.
- Kohonen, T., 1982. Self-organized formation of topologically correct feature maps. *Biological Cybernetics*, 43(1), pp. 59-69.
- Krieger, G. Z. M. et al., 2013. TanDEM-X: A radar interferometer with two formation-flying satellites. *Acta Astronautica*, Volume 89, pp. 83-98.
- Kugler, F. et al., 2014. TanDEM-X Pol-InSAR Performance for Forest Height Estimation. *IEEE Transactions on Geoscience and Remote Sensing*, 52(10), pp. 6404-6422 .
- Kuuluvainen, T., Penttinen, A., Leinonen, K. & Nygren, M., 1996. Statistical Opportunities for Comparing Stand Structural Heterogeneity in Managed and Primeval Forests: An Example from Boreal Spruce Forest in Southern Finland. *Silva Fennica*, 30(2-3), pp. 315-328.
- Le Toan, T., Beaudoin, A., Riou, J. & Guyon, D., 1992. Relating Forest Biomass to SAR Data. *IEEE Transactions on Geoscience and Remote Sensing*, Volume 2, pp. 403-411.
- Liesenberg, V. & Gloaguen, R., 2013. Evaluating SAR polarization modes at L-band for forest classification purposes in Eastern Amazon, Brazil. *International Journal of Applied Earth Observation and Geoinformation*, Volume 21, pp. 122-135.
- MacQueen, J., 1967. Some methods for classification and analysis of multivariate observations. *Proceedings of the Fifth Berkeley Symposium on Mathematical Statistics and Probability*, Volume 1: Statistics, pp. 281-297.
- Manning, C. D., Raghavan, P. & Schütze, H., 2008. *Introduction to Information Retrieval*. Cambridge: University Press.
- Moran, N., Nieland, S., Tintrup gen. Suntrup, G. & Kleinschmit, B., 2017. Combining machine learning and ontological data handling for multi-source classification of nature conservation areas. *International Journal of Applied Earth Observation and Geoinformation*, Volume 54, pp. 124-133.
- Moreira, A. et al., 2013. A Tutorial on Synthetic Aperture Radar. *IEEE Geoscience and Remote Sensing Magazine*, 1(1), pp. 6 - 43.

- Nilsson, M. & Holgren, J., 2003. Prediction of forest variables using LiDAR measurements with different footprint sizes and measurement densities. *Proceedings of the ScandLaser scientific workshop on airborne laser scanning of forests*, pp. 125-133.
- Olesk, A. V. K., Vain, A., Noorma, M. & Parks, J., 2015. Seasonal Differences in Forest Height Estimation From Interferometric TanDEM-X Coherence Data. *IEEE Journal of Selected Topics in Applied Earth Observation and Remote Sensing*, 12(8), pp. 5565-5572.
- Önal, H., 1997. Trade-off between Structural Diversity and Economic Objectives in Forest Management. *American Journal of Agricultural Economics*, 79(3), pp. 1001-1012.
- Pommerening, A., 2006. Evaluation structural indices by reversing forest structural analysis. *Forest Ecology and Management*, Volume 224, pp. 266-277.
- Pretzsch, H., 1996. Structural diversity as a result of silvicultural treatment. *Allgemeine Forst- und Jagdzeitung*, Volume 11, pp. 213-221.
- Pretzsch, H., 2005. Diversity and Productivity in Forests: Evidence from Long-Term Experimental Plots. In: M. Scherer-Lorenzen, C. Körner & E. Schulze, eds. *Forest diversity and function. Temperate and Boreal Systems*. Ecological Studies 176 ed. ed. Berlin Heidelberg: Springer-Verlag, pp. 41-64.
- Pretzsch, H., 2009. *Forest Dynamics, Growth and Yield*. Berlin Heidelberg: Springer-Verlag.
- Pretzsch, H., Biber, P. & Ďurský, J., 2002. The single tree-based stand simulator SILVA: construction, application and evaluation. *Forest Ecology and Management*, Volume 162, pp. 3-21.
- Pretzsch, H., Biber, P., Uhl, E. & Dauber, E., 2015. Long-term stand dynamics of managed spruce-fir-beech mountain forests in Central Europe: structure, productivity and regeneration success. *Forestry*, 88(4), pp. 407-428.
- Pulliainen, J., Engdahl, M. & Hallikainen, M., 2003. Feasibility of multi-temporal interferometric SAR data for stand-level estimation of boreal forest stem volume. *Remote Sensing of Environment*, 85(4), pp. 397-409.
- Rosen, P. A. et al., 2000. Synthetic Aperture Radar Interferometry. *Proceedings of the IEEE*, 88(3), pp. 333-382.
- Sadeghi, Y., St-Onge, B., Leblon, B. & Simard, M., 2017. Effects of TanDEM-X Acquisition Parameters on the Accuracy of Digital Surface Models of a Boreal Forest Canopy. *Canadian Journal of Remote Sensing*, 43(2), pp. 1-14.
- Schüler, S., Liesebach, M. & von Wühlisch, G., 2012. Genetische Variation und Plastizität des Blattaustriebs von Herkünften der Rot-Buche. *Applied Agricultural and Forestry Research*, 4(62), pp. 211-220.
- Solberg, S., Weydahl, D. J. & Astrup, R., 2015. Temporal Stability of X-Band Single-Pass InSAR Heights in a Spruce Forest: Effects of Acquisition Properties and Season. *IEEE Transactions on Geoscience and Remote Sensing*, 53(3), pp. 1607-1614.
- Townsend, P., 2002. Estimating forest structure in wetlands using multitemporal SAR. *Remote Sensing of Environment*, 79(2-3), pp. 288-304.
- Van Laar, A. & Akça, A., 2007. *Forest mensuration (managing forest ecosystems)*. Dordrecht, The Netherlands: Springer-Verlag.
- Varghese, A. O., Suryavanshi, A. & Joshi, A. K., 2016. Analysis of different polarimetric target decomposition methods in forest density classification using C band SAR data. *International Journal of Remote Sensing*, 37(3), pp. 694-709.
- Vesanto, J., Himberg, J., Alhoniemi, E. & Parhankangas, J., 2000. *SOM Toolbox for Matlab 5*, Finland: Helsinki University of Technology.
- Yang, H. et al., 2014. Simulation of Interferometric SAR Response for Characterizing Forest Successional Dynamics. *IEEE Geoscience and Remote Sensing Letters*, 11(9), pp. 1529-1533.

## D Eidesstattliche Erklärung

Ich erkläre an Eides statt, dass ich die bei der Fakultät Wissenschaftszentrum Weihenstephan für Ernährung, Landnutzung und Umwelt (promotionsführende Einrichtung) der TUM zur Promotionsprüfung vorgelegte Arbeit mit dem Titel:

### **Detection and definition of forest structure types by means of radar remote sensing (TanDEM-X)**

Am Lehrstuhl für Waldwachstumskunde

unter der Anleitung und Betreuung durch: Prof. Dr. Dr. hc. Hans Pretzsch ohne sonstige Hilfe erstellt und bei der Abfassung nur die gemäß § 6 Ab. 6 und 7 Satz 2 angebotenen Hilfsmittel benutzt habe.

Ich habe keine Organisation eingeschaltet, die gegen Entgelt Betreuerinnen und Betreuer für die Anfertigung von Dissertationen sucht, oder die mir obliegenden Pflichten hinsichtlich der Prüfungsleistungen für mich ganz oder teilweise erledigt.

Ich habe die Dissertation in dieser oder ähnlicher Form in keinem anderen Prüfungsverfahren als Prüfungsleistung vorgelegt.

Die vollständige Dissertation wurde in

\_\_\_\_\_ veröffentlicht. Die promotionsführende  
Einrichtung \_\_\_\_\_  
hat der Veröffentlichung zugestimmt.

Ich habe den angestrebten Doktorgrad noch nicht erworben und bin nicht in einem früheren Promotionsverfahren für den angestrebten Doktorgrad endgültig gescheitert.

Ich habe bereits am \_\_\_\_\_ bei der Fakultät für \_\_\_\_\_  
\_\_\_\_\_ der  
Hochschule \_\_\_\_\_ unter  
Vorlage einer Dissertation mit dem Thema \_\_\_\_\_ die Zulassung  
zur Promotion beantragt mit dem Ergebnis: \_\_\_\_\_  
\_\_\_\_\_

Die öffentlich zugängliche Promotionsordnung der TUM ist mir bekannt, insbesondere habe ich die Bedeutung von § 28 (Nichtigkeit der Promotion) und § 29 (Entzug des Doktorgrades) zur Kenntnis genommen. Ich bin mir der Konsequenzen einer falschen Eidesstattlichen Erklärung bewusst.

Mit der Aufnahme meiner personenbezogenen Daten in die Alumni-Datei bei der TUM bin ich

einverstanden  nicht einverstanden.

\_\_\_\_\_  
Ort, Datum, Unterschrift

## E Lebenslauf

### Sahra Abdullahi

#### Angaben zur Person

---

Adresse Burghausener Straße 2, 80634 München  
E-Mail [sahraabdullahi@web.de](mailto:sahraabdullahi@web.de)  
Staatsangehörigkeit deutsch  
Geburtsdatum 28.12.1984 in Dachau

---

#### Berufserfahrung

---

- 04/2013 – 03/2016 **Wissenschaftliche Mitarbeiterin**  
Projekt “Forstinventurparameter- und Waldstrukturerfassung durch neuartige Fernerkundungsprodukte”  
Lehrstuhl für Waldwachstumskunde (Prof. Dr. Dr. h.c. Hans Pretzsch),  
Wissenschaftszentrum Weihenstephan, Technische Universität München  
Tätigkeitsbereiche: Radarfernerkundung, Forstwissenschaften
- 07/2010 – 09/2010 **Praktikum**  
Projekt GITEWS (German Indonesian Tsunami Early Warning System)  
Abteilung Zivile Kriseninformation und Georisiken (Dr. Harald Mehl, Betreuer Dr.  
Joachim Post), Deutsches Fernerkundungsdatenzentrum, Deutsches Zentrum für  
Luft- und Raumfahrt  
Tätigkeitsbereich: Geoinformatik (Risikomodellierung)
- 06/2009 – 08/2009 **Hilfswissenschaftlerin**  
Projekt SMOSHYD (Integrative Analysis of SMOS Soil Moisture Products)  
Lehrstuhl für Geographie und Geographische Fernerkundung (Prof. Dr. Wolfram  
Mauser), Ludwig-Maximilians-Universität München  
Tätigkeitsbereiche: Feldmethoden, Fernerkundung
- 12/2007 – 03/2008 **Hilfswissenschaftlerin**  
Projekt GLOWA-Danube (Global Change and the Hydrological Cycle at the Upper  
Danube)  
Lehrstuhl für Geographie und Geographische Fernerkundung (Prof. Dr. Wolfram  
Mauser), Ludwig-Maximilians-Universität München  
Tätigkeitsbereich: Umweltmodellierung, Statistik

---

## Ausbildung

---

- seit 04/2013                    **Promotion** (Dr. rer. nat.)  
Titel der Dissertation: „Erfassung und Typisierung von Waldstrukturen über Radarfernerkundung (TanDEM-X)“  
04/2013 – 06/2013 Gastwissenschaftlerin am Institut für Hochfrequenztechnik und Radarsysteme des Deutschen Zentrums für Luft- und Raumfahrt  
seit 04/2016 Förderung im Rahmen des Laura Bassi-Preises  
Technische Universität München
- 10/2009 – 10/2012           **Master of Science in Geospatial Technologies** (Abschluss mit Auszeichnung)  
Titel der Masterarbeit: „Development of a generic algorithm for population modeling and application in a test area in Western Africa“ (am Deutschen Zentrum für Luft- und Raumfahrt)  
Karl-Franzens-Universität Graz, Technische Universität Graz
- 10/2006 – 09/2009           **Bachelor of Science in Geographie** (Vertiefungsrichtung Physische Geographie, Nebenfach Informatik)  
Titel der Bachelorarbeit: „Bestimmung der Grenze zwischen feuchtem und trockenem Schnee auf der Antarktischen Halbinsel aus LANDSAT ETM+ Daten“  
Ludwig-Maximilians-Universität München
- 2006                                **Abitur**  
Ignaz-Taschner Gymnasium Dachau

---

## Publikationen

---

- Fachzeitschriften              Abdullahi, S., Schardt, M. & Pretzsch, H. (2017) An unsupervised two-stage clustering approach for forest structure classification based on X-band InSAR data — A case study in complex temperate forest stands. *International Journal of Applied Earth Observation and Geoinformation* 57, 36-48.
- Abdullahi, S., Kugler, F. & Pretzsch, H. (2016) Prediction of stem volume in complex temperate forest stands using TanDEM-X SAR data. *Remote Sensing of Environment* 174, 197-211.
- Konferenzbeiträge              Abdullahi, S., Biber, P. & Poschenrieder, W. (2015) TanDEM-X – Forstinventurparameter- und Waldstrukturerfassung durch neuartige Fernerkundungsprodukte. Workshop des DLR Raumfahrtmanagement „Nutzung der Sentinels und nationalen Erdbeobachtungs-Missionen“, 21.-22. Januar 2015, Bonn, Deutschland.
- Schneider, T., Abdullahi, S., Elatawneh, A., Stepper, C. & Poschenrieder, W. (2014) Integration of S2 type RS Data and Forest Growth Modelling as Cost Effective Option for Interim Forest Inventories. SENTINEL-2 for Science Workshop, 20.-22. Mai 2014, ESA-ESRIN, Frascati (Rom), Italien.



Abdullahi, S., Elatawneh, A., Stepper, C. & Schneider, T. (2014) A-priori change assessment of inventory points by means of Remote Sensing – a cost effective option for interim inventories. Conference on Forest Change, 2.-4. April 2014, Freising, Deutschland.

---

## **Persönliche Fähigkeiten**

---

Sprachen	<b>Deutsch</b> (Muttersprache) <b>Englisch</b> (verhandlungssicher in Wort und Schrift) <b>Französisch</b> (Grundkenntnisse in Wort und Schrift)
Softwarekenntnisse und Programmiersprachen	<b>Sehr gute Kenntnisse:</b> R, ESRI ArcGIS, ERDAS Imagine, MS Office <b>Fortgeschrittene Kenntnisse:</b> MATLAB, Python, eCognition Developer, HTML, XML <b>Grundkenntnisse:</b> IDL, C, SQL, Java, UML, RSG (Remote Sensing Software Graz), VNS (Virtual Nature Studio), GfK Regiograph

---